Genome-wide mapping of chromatin landscape and regulatory networks in decidualizing human endometrial stromal cells and cultured mesenchymal stem cells

Raffaella Lucciola

A thesis submitted to the University of Warwick for the degree of Doctor of Philosophy
Joint PhD with Monash University

Warwick Medical School
University of Warwick

December 2017

Table of Contents

Chapter 2: MATERIALS AND METHODS

List of Figures

Chapter 1: INTRODUCTION

Chapter 3: CHROMATIN PROFILING IN DECIDUALIZING HUMAN ENDOMETRIAL STROMAL CELLS

Chapter 4: CHARACTERIZATION OF ENDOMETRIAL MESENCHYMAL STEM CELLS EXPANDED IN CULTURE IN RESPONSE TO TGF-β-RECEPTOR BLOCKADE

Chapter 5: ANALYSIS OF DYNAMIC CHROMATIN CHANGES IN CULTURED eMSCs UPON TGF-β-R INHIBITION

Acknowledgments

I have always been taught to pursue my dreams: if ‘you can dream it, you can do it’ (Walt Disney). Today, I can say that is true! I have dedicated the majority of my life to study and one of my dreams was to do research in the field of reproduction and to do this around the world. This PhD perfectly fitted with my dream and one of the reasons I was able to pursue it, was my English supervisor, Professor Jan Brosens. He trusted me the first time ‘I knocked his office door to ask for this PhD’ and he gave me the privilege of embarking on this professional adventure with him. As strict as supportive, he has always pushed me to reach the highest levels. He has been a great supervisor and a big brother. As a joint PhD student, I had the opportunity to be supervised by another leading researcher, Professor Caroline Gargett, in Australia. She made me feel at home when I was on the other side of the world. She led me to successfully carry out my research in a short period of time. In light of Australian culture, she encouraged me to actively interact with other researchers, to further build my skills.

During my PhD, I joined two big international groups which opened my mind and enabled me to adopt different approaches to work. In my English lab, I would like to thank Dr Paul Brighton, who has been a reference for me in the lab; Dr Joanne Muter who is a great example of professionality and speed; Dr Emma Lucas, a researcher who can answer any question presented to her; Dr Flavio Barros, Dr Scarlett Salter, Dr Ruban Durairaj, Dr Maru Yojiro and Dr Risa Fujihara who, with their kindness, helped me to settle in the lab; Dr Andy Blanks and Professor Sascha Ott for their extensive knowledge, and last but not least, Dr Pavle Vrjilack who has been a great ‘teacher’ and a fantastic friend.

On the other side, I would like also to thank my ‘Australian’ group, particularly Dr Fiona Cousins, a highly qualified colleague and really good friend; Dr Shayanti Mukherjee, a friend of adventures; Dr Shanti Gurung who helped me to settle in the lab; Dr James Dean, a real example of Australian culture, such as healthy and practical; Dr Lisa Xiao and Xiaqing Yang, two real hard workers; and Stuart and Saehadah for their friendship.

An immeasurable gratitude is for my family and friends. My parents who gave me the example of how to live a successful and healthy life. They taught me to work hard, be dedicated in everything that I do and to enjoy the beauty of the world. My brother, Giuseppe, the reflection of happiness, has been supportive, always providing me with the right perspective for my work. To all of my relatives, for being close even if we were miles apart; my ‘tremendous little old mum’ for the energy she always provides, encouraging me to make the right decisions; my wonderful English friend, Sarah, who has become my little sister, for providing a ‘home’ away from home; and my oldest friends, Lia who has been able to understand you without even having to say anything, and Rachele, my talking cricket. Thank you to all the people who, in their own ways, contributed to making this time of my life unique.

Finally, I wish to thank the University of Warwick for the Chancellor’s scholarship award and the women who trusted science and donated their tissue samples, it’s thanks to them that my research was possible.

Declaration

This thesis is submitted to the University of Warwick in support of my application for the degree of Doctor of Philosophy. It has been composed by myself and has not been submitted in any previous application for any degree.

The work presented (including data generated and data analysis) was carried out by the author except in the cases outlined below:

i) analysis of RNA-seq and ATAC-seq datasets in collaboration with Pavle Vrljicak, PhD (Tommy's national Centre for Miscarrigae Research, Warwick Medical School) and Associate Professor (A/P) Sascha Ott (Tommy's National Centre for Miscarriage Research, Department of Computer Science).

ii) generation of RNA-seq data from undifferentiated and decidualizing EnSCs in collaboration with Dr Joanne Muter.

Parts of this thesis have been published by the author:

Pavle Vrljicak*, Emma S. Lucas*, Lauren Lansdowne*, **Raffaella Lucciola***, Joanne Muter, Nigel P. Dyer, Jan J. Brosens, Sascha Ott (2017). Analysis of chromatin accessibility in decidualizing human endometrial stromal cells. In press *The FASEB Journal*.

* These authors contributed equally to this work.

Raffaella Lucciola, Pavle Vrljicak, Sascha Ott, Jan J Brosens, Caroline Gargett (2017). Genome-wide mapping of regulatory transcriptional networks in human

endometrial mesenchymal stem/stromal cells by ATAC-seq and RNA-seq. Abstract in press *Gene Medicine*.

Paul J. Brighton, Yojiro Maruyama, Katherine Fishwick, Pavle Vrljicak, Shreeya Tewary, Risa Fujihara, Joanne Muter, Emma S. Lucas, Taihei Yamada, Laura Woods, **Raffaella Lucciola**, Yie Hou Lee, Satoru Takeda, Sascha Ott, Myriam Hemberger, Siobhan Quenby, Jan J. Brosens (2017). Clearance of senescent decidual cells by uterine natural killer cells drives endometrial remodeling during the window of implantation. In press *eLife.*

Abstract

Decidualization denotes the differentiation of endometrial stromal cells (EnSCs) into specialized decidual cells that control embryo implantation. This process can be recapitulated in culture upon treatment of primary EnSCs with cyclic AMP analogue and progesterone. In this work, I subjected undifferentiated and decidualizing human EnSCs to Assay for Transposase Accessible Chromatin with sequencing (ATAC-seq) to map the underlying chromatin changes.

ATAC-seq is a newly developed technique that utilizes the highly active transposase Tn5 to interrogate accessibility of the genome and map open chromatin regions. These putative *cis*-regulatory DNA regions can be further explored for “footprints” of transcription factor (TF) binding. In this study, I optimized ATAC-seq and used this technique first to investigate the regulatory mechanisms underlying decidualization of the human endometrial cells. A total of 185,084 open DNA loci were mapped accurately in EnSCs. Altered chromatin accessibility within 10 kb of transcription start sites upon was strongly associated with differential gene expression in decidualizing EnSCs. Analysis of 1,533 opening as well as closing chromatin regions revealed overrepresentation of DNA binding motifs for known decidual TFs and identified putative new regulators, including RAR related orphan receptor A (RORA), aryl hydrocarbon receptor nuclear translocator like (ARNTL) and Meis homeobox 1 (MEIS1). Conversely, downregulation of runt related transcription factor 1 and 2 (RUNX1/RUNX2), SRY-box 12 (SOX12), transcription factor 3 (TCF3), and ETS Proto-Oncogene 1 (ETS1) upon decidualization corresponded to loss of corresponding high-affinity binding sites differentiating EnSCs.

Because of its dynamic nature, cyclic human endometrium is a rich source of adult stem cells that could be exploited for clinical purposes. However, clinical use of eMSCs is hampered by differentiation and loss of proliferative capacity of cells in prolonged cultures. As part of my Monash-Warwick alliance studentship, I joined the laboratory of Professor Gargett in Melbourne, Australia, and applied integrated ATAC-seq and RNA-seq analyses to study the impact of TGF-β receptor inhibition on endometrial mesenchymal stem cells (eMSCs) maintained in prolonged culture. I demonstrated that culturing of eMSCs in the presence A83-01, a small molecule inhibitor the of TGF-β receptor, maintains the proliferative capacity and attenuates the loss of stemness features of eMSCs in extended cultures. Furthermore, integrated ATAC-seq and RNA-seq revealed that A83-01 modifies the chromatin accessibility of 5,967 loci and alters the expression 1,463 genes. Mining and cross-referencing of these data sets revealed that A83-01 not only maintains selected stemness-associated genes but also that it represses multiple genes involved in extracellular matrix (ECM) deposition and metabolism. Furthermore, my analysis indicated that induction nuclear receptor subfamily 4 group A member 1 (*NR4A1*, also known as *NUR77*) may be an important TF that mediate the repression of ECM genes in response to A83-01 treatment.

In summary, by integrating advanced genome-wide expression and DNA accessibility profiling techniques, my work has advanced our understanding of the dynamic changes in the *cis*-regulatory DNA landscape underpinning decidualization of EnSCs and in the maintenance of a stem-like phenotype of eMSCs in prolonged cultures. Analyses of these two large data sets revealed

novel transcriptional regulators in cycling endometrium and putative new targets that could be exploited to accelerate clinical translation of autologous eMSC therapies for a variety of reproductive disorders. Furthermore, the data sets generated during the course of my investigations constitute an important resource to interrogate fundamental molecular questions pertaining to human endometrial cell biology.

List of Abbreviations

ATAC-seq	Assay for Transposase-Accessible Chromatin through high-throughput sequencing
bZIP	Basic Leucine Zipper Domain
8-br-cAMP	8-Bromoadenosine-3', 5'-cyclic monophosphate
CD90	Cluster of differentiation 90
CD140b	Cluster of differentiation 140b
CEBP/β	CCAAT/ enhancer binding protein β
ChIP-seq	chromatin immunoprecipitation followed by sequencing
DAVID	Database for Annotation, Visualization and Integrated Discovery
DESeq	Differential expression analysis for sequence count data
DHSs	DNase I hypersensitivity sites
DiffM	Differentiated Motifs
DNA	Deoxyribonucleic acid
DNase-seq	DNase I hypersensitive sites sequencing
ECM	Extracellular matrix
eMSCs	Endometrial mesenchymal stromal cells
ENCODE	Encyclopedia of DNA Elements
EnSCs	Endometrial stromal cells
FAIRE-seq	Formaldehyde-Assisted Isolation of Regulatory Elements through high-throughput sequencing
FOXO	Forkhead box transcription factor O
GEO	Gene Expression Omnibus
GO	Gene ontology
GSK3-β	Glycogen synthase kinase 3 beta
HOMER	Hypergeometric Optimization of Motif EnRichment
HOX	Homeobox
IGFBP1	Insulin-like growth factor binding protein-1

Kb	kilobase
KEGG	Kyoto Encyclopedia of Genes and Genomes
MEK/MAP2K/ MAPKK	Mitogen-activated protein kinase kinase
MFI	Mean fluorescence intensity
MPA	medroxyprogesterone actetate
NHMRC	National Health and Medical Research Council
P	Passage
PCA	Principal component analysis
PD	Population doubling
PGR	Progesteron receptor
POP	Pelvic organ prolapse
PRL	Prolactin
RIN	RNA integrity number
rlog	regularized log
RNA	Ribonucleic acid
SUSD2	sushi domain containing 2
TF	Transcription factor
TGF-β	Transforming growth factor beta
TGF-β-R	Transforming growth factor beta receptor
TPM	Transcript per million
TSS	Transcription start site
UndiffM	Undifferentiated Motifs

Chapter 1

Introduction

1.1 Human endometrium

The endometrium is the mucosa that lines the uterine cavity. It is composed of two major compartments: the basalis, a basal layer lying on the myometrium, contains the bases of the endometrial glands immerged in a rich stroma, and the functionalis, a functional layer containing the glands extending from surface epithelium and a loose stroma (Figure 1.1) (Gargett *et al.*, 2012; Padykula, 1991).

It consists of surface and glandular epithelial cells and a rich stroma. The latter comprises a heterogeneous population of cells, such as stem/progenitor cells, including mesenchymal stem cells (MSCs) and transit amplifying (TA) cells, mature fibroblasts and decidual cells (Table 1.1) (Gargett, 2007; Gellersen *et al.*, 2007; Gellersen & Brosens, 2014; Masuda *et al.*, 2012; Schwab & Gargett, 2007). Both epithelial and stromal cellular compartments are exquisitely responsive to ovarian hormone signalling. During the proliferative phase of the menstrual cycle, rising estrogen levels from the growing ovarian follicle induce proliferation of the tissue (Brosens *et al.*, 2002; Gray *et al.*, 2001). Increasing levels of estrogen positively regulates luteinising hormone (LH) through a positive feedback, resulting in a LH surge that controls ovulation and stimulates progesterone production. By contrast, the post-ovulatory increase in progesterone inhibits the proliferative activity and drives the differentiation of the endometrium, which renders this tissue transiently receptive to blastocyst implantation during the mid-luteal phase of the cycle (Gellersen & Brosens, 2003). Acquisition of a receptive phenotype coincides with profound changes in the stromal compartment, characterised by influx of specialized immune cells (predominantly uterine natural killer cells, uNK cells) (Brighton *et al*., 2017), vascular remodelling, and transformation of endometrial fibroblasts into specialized decidual cells (Table 1.1). In the absence of pregnancy, the corpus luteum will atrophy and progesterone production ceases.

The fall in circulating progesterone levels then triggers breakdown of the functional endometrial layer and menstrual shedding. The underlying basal layer

remains intact and from it a new functional layer regenerates in the following menstrual cycle (Gellersen & Brosens, 2014).

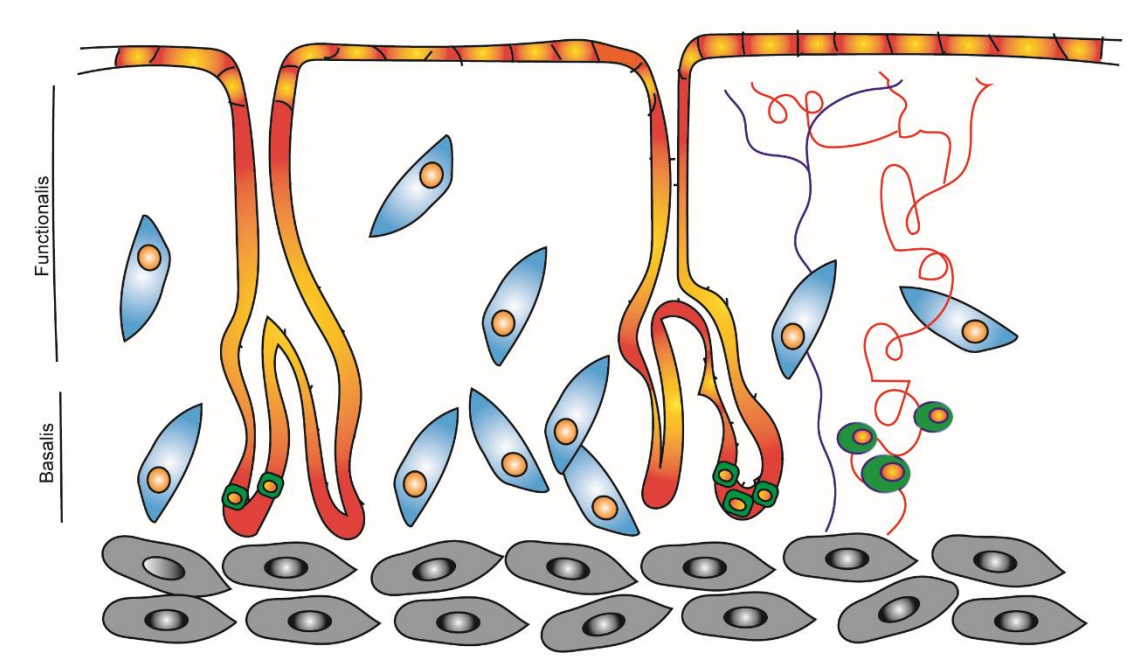

Figure 1.1. Human endometrium. The endometrium lies on myometrium (grey cells). It consists into two compartments: a basal layer, basalis, that persists in each cycle and the functional layer, functionalis, which cyclically originates from the basalis each month. Blue cells represent endometrial fibroblasts; green cells represent stem progenitor cells located around the spiral arterioles (red vessels) and into the glandular epithelium. Blue vessels are the veins; orange tubular structures represent the glands.

Table 1.1 Endometrial stromal cell populations

Cell types	Markers/Properties	References
MSCs	CD146+PDGFRβ+	Schwab & Gargett, 2007; Masuda *et al*., 2012
	SUSD2+ (W5C5+)	
	clonogenic	
	high proliferative/self-renewing/multipotent	
	self-renewing	
	multipotent	
Transit amplyfing (TA) cells	SUSD2- (W5C5-)	Gargett, 2007
	clonogenic	
Side population (SP) cells	Low Hoechst 33342 fluorescence	Masuda *et al*., 2010
Mature fibroblasts	SUSD2- (W5C5-)	Gellersen *et al*., 2007
	non-clonogenic	
	fibrobalst-like appearance	
	higly responsive to decidual cues	
Decidual cells	scretory, epithelioid-like stromal cells	Gellersen & Brosens, 2014
	high expression of decidual markers	
	responsive to embryonic cues	
uterine natural killer (uNK) cells	immune cells	Brighton *et al*., 2017
	CD56+ CD16-	
	clearence of decidual cells as decidual process unfolds	

1.2 Decidualization of the human endometrium

Decidualization, the process of transformation of endometrial stromal cells (EnSCs), is initiated in response to elevated progesterone levels and local rise in cyclic adenosine monophosphate (cAMP) levels, which in turn trigger sustained activation of the protein kinase A (PKA) pathway (Gellersen *et al.*, 2007). Decidualization consists of a dramatic transformation of EnSCs into specialised secretory cells, which undergo integrated changes in morphology and at transcriptome and proteome levels (Gellersen & Brosens, 2014). In most placental mammals, decidualization of the endometrium is the maternal response to pregnancy and occurs only upon implantation of the blastocyst. The latter attaches and penetrates the epithelium by invading the endometrial connective tissue. However, in humans and a handful of other mammals, decidualization does not require the implantation of the blastocyst but is initiated 'spontaneously' in each ovulatory cycle. In the absence of pregnancy, falling circulating progesterone levels result in breakdown of the decidual superficial endometrial layer, menstrual shedding and tissue regeneration (Evers, 2002). Decidual reprogramming of the endometrium is critical in all placental species for pregnancy. It underpins the acquisition of specialized cell functions, such as the ability to deal with increased levels of reactive oxygen species, to modulate trophoblast invasion, to regulate vascular and immune responses, and hence tolerance to fetal antigens. On the other side, a growing body of evidence suggests that an impaired remodelling of the endometrium may cause a multitude of pregnancy complications, such as miscarriage, abruption, fetal growth restriction and pre-eclampsia (Brosens & Gellersen, 2006).

1.3 Morphological and biochemical reprogramming of EnSCs

During the menstrual cycle, the endometrium exhibits a unique ability to re-build itself in response to hormonal signals in order to be ready to accommodate a future pregnancy. Both in the proliferative phase of the cycle and in culture,

EnSCs are mesenchymal cells with a fibroblast-like appearance (Cornillie *et al.*, 1985). On the other hand, upon decidualization, endometrial cells undergo huge changes in morphology, consisting of a shift from an elongated, spindle shape to rounded, enlarged cells with abundant cytoplasm. Further changes include a well-expanded rough endoplasmic reticulum and Golgi apparatus, accumulation of glycogen and lipid droplets in the cytoplasm, a more rounded nucleus and an increase in numbers of nucleoli. Furthermore, multiple cytoplasmic processes from cell surface to engulf the extracellular matrix (ECM), or extend into the cytoplasm of adjacent cells. Decidualized cells also produce ECM proteins, such as laminin, decorin, type IV collagen, fibronectin and heparin sulphate proteoglycans (Aplin *et al.*, 1988).

EnSCs provide a nutritive matrix that is essential for embryo implantation and placental development and hence critical for successful pregnancy. In order to facilitate this intercellular communication, cadherin-11, a protein belonging to the cadherin family, is upregulated in decidualizing cells, especially in stromal cells located around spiral arteries. Another highly expressed protein in endometrial stromal compartment is protein connexion 43 (CX43), which forms gap junctions, between decidualizing stromal cells. In patients with recurrent early pregnancy loss, a decrease in the expression of CX43 has been observed, a finding that underscores the importance of gap junction-mediated communication (Nair *et al.*, 2011).

Decidualization also denotes a biochemical reprogramming of the proliferative EnSCs into specialized secretory cells. The major products highly secreted by decidualizing cells are prolactin (PRL) and insulin-like growth factor binding protein-1 (IGFBP1), two proteins widely used as phenotypic markers of decidual EnSCs and to establish the differentiation status of human EnSCs in culture (Gellersen & Brosens, 2003). In pregnancy, multiple functions have been ascribed to decidual PRL, including stimulating trophoblast growth and invasion in the utero-placental interface, regulating uNK cell survival, immune-suppression, promoting angiogenesis, and modulating the transport of water from the amnion towards the maternal compartment. Decidual secretion of IGFBP1, also known as placental protein 12, reaches its peak around 16 weeks of gestation. However, decidualized stromal cells also produce other secretory

products, including a huge number of cytokines (for instance, interleukin-11 [IL-11]), growth factors (e.g., epidermal growth factor [EGF]), heparin-binding (HB-) EGF, Lefty-A, activin A and several neuropeptides. It is thought that these secretory products play a role in amplifying the decidual process in an autocrine or paracrine way (Dimitriadis *et al.*, 2005).

This morphologic and biochemical reprogramming of endometrial stromal fibroblasts into decidual cells is underpinned by integrated changes observed at transcriptome level. In particular, genes encoding superoxide dismutase-2 (SOD2), growth arrest- and DNA damage-inducible protein of 45kd (GADD45), CCAAT enhancer-binding protein b (C/EBPβ), and forkhead transcription factors are highly expressed upon differentiation of the endometrial stromal compartment in the mid- to late-secretory phase of the cycle, and induced upon decidualization of primary stromal cells in vitro. Microarray studies confirmed that decidualization involves profound transcriptional changes, which in turn have enabled a molecular definition of this differentiation process based on reprogramming of gene families that are functionally associated and involved in ECM organization, cell adhesion, organization of cytoskeleton, signal transduction, stress response, metabolic pathways, differentiation and apoptosis (Giudice, 2004).

1.4 Decidualizing hormonal cues

The physiology of the uterus is regulated by the steroid hormones estrogen and progesterone produced by the ovary (Figure 1.2). Luteinizing granulosa cells within the ovary produce progesterone, whose levels increase during the postovulatory phase of the cycle and play a central role in driving the differentiation process of the endometrium.

Differentiation of the stromal compartment, which starts in cells near the terminal spiral arteries and under the luminal epithelium, only becomes apparent approximately 10 days after the postovulatory rise in progesterone levels. This suggests that the cells require additional signals to initiate this reprogramming process. Similarly, treatment of cells in culture with progesterone, alone or with

estradiol, induces decidualization, but requires 8 to 10 days to be effective (Bra *et al.,* 1997).

The initiating trigger for decidualization is a rise in the cellular levels of cAMP, a ubiquitous second messenger molecule produced by adenylate cyclase. The binding of extracellular ligands to G_s protein-coupled receptors activate G_s protein and the subsequent activation of adenylate cyclase generates cAMP from adenosine triphosphate (ATP). cAMP modifies the gene expression of EnSCs, acting through the protein kinase A (PKA) pathway. PKA phosphorylates and hence activates target molecules such as cAMP response element binding protein (CREB) and cAMP response element modulator (CREM). Consequently, CREB and CREM form a dimer and bind to cAMP response elements (CRE) in target DNA and also allow the binding of CREB-binding protein (CBP), a histone acteyltransferase, to promoter regions of target genes (Maruyama & Yoshimura, 2008).

Primary cultures treated with a cAMP analogue express PRL and IGFBP1, the phenotypic markers of decidualized cells, within hours, but levels decrease after 6 to 8 days of culture, suggesting decidualization is not sustained in response to cAMP signalling alone. Addition of a progestin not only enhances the cAMP response but also maintains the induction of decidual markers in long-term cultures. Progesterone acts through the activation of the progesterone receptor (PR), a member of the human superfamily of nuclear receptors. It is a receptor with multiple functional domains which allow ligand-mediated activation and signalling to bind DNA and modulate transcription. PR is present as two major isoforms, PR-A and PR-B, which are encoded by a different use of promoter in a single gene (Gellersen & Brosens, 2014). The two variants of the receptor differ from each other in amino acid content, and in particular PR-B has additional 164 amino acids at the N-terminal compared to PR-A. However, PR-A is thought to be predominant isoform in decidualizing human EnSCs. In female mice, the selective ablation of PR-A causes sterility and negatively affects the decidualization process, in response to an artificial stimulus (Mulac-Jericevic & Conneely, 2004; Richer *et al.*, 2002).

Cross-talk between cAMP and progesterone signalling pathways drives the decidualization process, inducing changes in both transcriptional and proteomic

landscape (Gellersen & Brosens, 2003). The mechanisms underlying the synergy between cAMP and progesterone signalling in human EnSCs has been studied intensely. PR is a nuclear receptor and, in common with other nuclear receptors, induces or represses the expression of target genes, depending on its interaction with co-activators and corepressors, respectively. In other cell systems, cAMP has been shown to disrupt the recruitment of co-repressors in favour of the interaction with coactivators. Furthermore, a wide range of transcriptor factors, such as SP1, FOXO1, signal transducers and activators of transcription (STAT) -3 and -5, and C/EBPβ, are induced by cAMP and have the ability to interact directly with the progesterone receptor. (Lynch *et al.*, 2011) found that, in placental mammals, some genes expressed in the endometrium that were located within transposable elements of the genome. These transposons function as enhancers, repressors and insulators and, in response to cAMP and progesterone, they interact directly with transcription factors indispensable for pregnancy outcome, co-operating in the modulation of gene expression (Lynch et *al.* 2011).

The transcriptional activity of PR is also tightly regulated by post-translational modifications, including phosphorylation, ubiquitination and sumoylation. Sumoylation is a process whereby small ubiquitin-related modifier (SUMO) family proteins, in an enzymatic reaction similar to the ubiquitin pathway, covalently attach a small peptide to target proteins, mainly transcription factors. This covalent attachment profoundly modifies the subnuclear position and functions of transcription factors. PR-A and PR-B are regulated by SUMO-1 and in particular the binding of small ubiquitin modifiers confers the PR-A repressive properties. Experimental data demonstrated that the mutation of the single SUMO binding site in PR-A changes this isoform into a strong transcriptional activator. It has been observed that cAMP second messenger pathway affects the expression of several conjugating and deconjugating SUMO enzymes. A consequent loss of PR-A sumoylation and increase in receptor activity seems to be related to the cAMP pathway (Jones *et al.*, 2006).

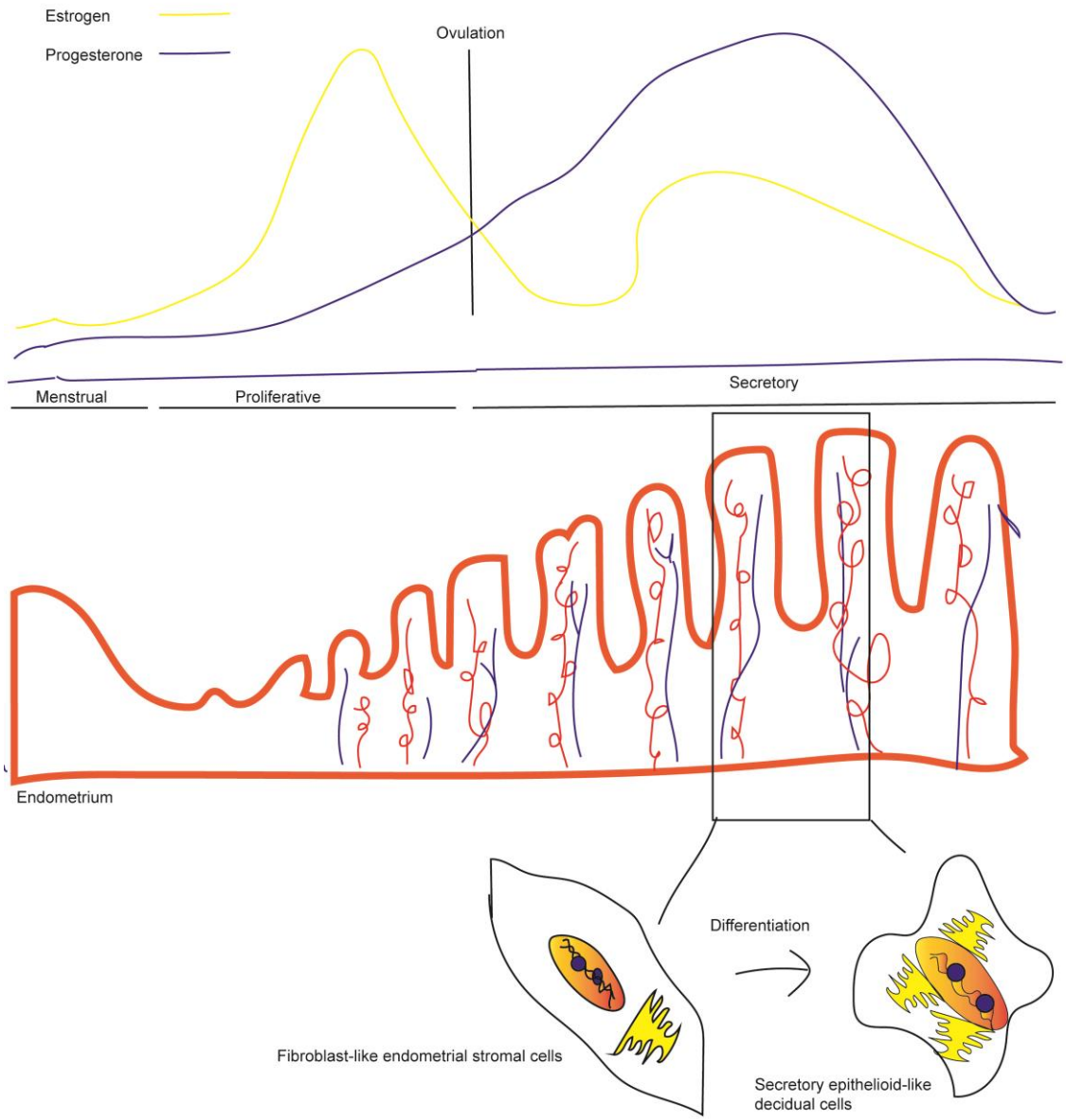

Figure 1.2. Circulating steroid hormones regulate the human menstrual cycle. Schematic representation of the menstrual cycle, which is divided into three main parts, such as menstrual, proliferative and secretory phase, regulated by the steroid hormones estrogen and progesterone. The postovulatory increase in the progesterone levels and cAMP production initiate the decidual transformation of EnSCs during the mid-secretory phase of the cycle.

1.5 Regulation of decidual gene expression

Decidualization is featured by a profound reprogramming in the transcriptome. Changes in gene expression are finely regulated at transcriptional and epigenetic level (Gellersen & Brosens, 2014).

Transposable elements

PRL human gene is expressed in anterior pituitary and stromal cells of the endometrium, and in human B-lymphoblastoid cell line IM-9-P3 (Gellersen *et al*., 1989). Scientific evidence shows that decidual and lymphoid cells use an alternative promoter of human *PRL* gene compared to pituitary cells. This regulatory region is located 5.9 kilobase (Kb) upstream the pituitary promoter. Selective activation of this promoter results in transcription of a longer PRL transcript. However the resulting protein coding region remains unchanged (Gellersen *et al*., 1989; Di Mattia *et al*., 1990). Further studies identified CRE-like element in the decidual promoter, regulated by cAMP signalling, but resulting in a modest transcriptional regulation. Further, a new regulatory region was mapped to -332/-270 upstream the transcriptional start site (TSS) (Telgmann *et al*., 1997). This enhancer resulted in a consistent increase in *PRL* expression in response to cAMP signalling (Telgmann *et al*., 1989; Al-Sabbagh *et al*., 2011). Interestingly, this enhancer is part of a transposable element, named MER20. Transposable elements are DNA sequences that can move within the genome. Insertion of transposable elements within the chromatin landscape results in addition of active regulatory elements, for example promoters, enhancers, repressors, that alter gene expression (Fedoroff, 2012). Interestingly, MER20 transposons map near genes differentially regulated during decidualization in response to cAMP and progestin signalling, for example *PRL*, Wnt family member 5A (*WNT5A*), hydroxysteroid 11-beta dehydrogenase 1 (*HSD11B1*). Further, MER20 transposons contain short sequence binding motifs for transcription factors (TFs), essential during decidual transformation, such as progesterone receptor (PGR), forkhead box transcription factors of the O subclass (FOXOs), homeobox (HOX) proteins and CCAAT/enhancer-binding proteins (C/EBPβ) (Lynch, 2011).

Taken together, these observations highlight the role of transposable elements in the transcriptional regulation of decidual genes.

Key decidual TFs for decidualization

Several TFs have been implicated in driving changes in gene expression of decidual genes. In this section, I will describe the core decidual TFs implicated in decidualization of human EnSCs.

CEBPs

During early phase of decidualization, EnSCs express increased level of C/EBPs. The latter are members of basic leucine-zipper (bZIP) superfamily of TFs that bind DNA sequences (Lekstrom and Xanthopoulos, 1998). C/EBP β-isoform, C/EBPβ, has been shown to bind to an enhancer located within MER20 transposon (Pohnke *et al*., 1999). Subsequently, C/EBPβ enables binding of other TFs, such as FOXO1 and PGR-A (Christian *et al*., 2002; Christian *et al.,* 2002). Immunochemistry shows high levels of C/EBPβ in the nuclei of decidual cells during the midsecretory phase of the menstrual cycle (Christian *et al*., 2002; Plante *et al*., 2009). Several lines of evidence indicate that C/EBPβ is implicated in interleukin 11 (IL-11) and in cell cycle during decidualization (Wang *et al*., 2012). Further, deficiency in C/EBPβ levels in female mice impairs decidual transformation of EnSCs and results in infertility (Mantena *et al*., 2006). Finally, absence of C/EBPβ correlates with decreased expression of bone morphogenetic protein 2 (BMP2), a morphogen playing a critical role in mouse and human decidual EnSCs, and in the regulation of WNT4 (Wang *et al*., 2012).

FOXOs

FOXOs are proteins belonging to subfamily of forkhead TFs. FOXOs play a role in increase accessibility of genomic regions within chromatin, thereby enabling recruitment of other TF binding (Lalmansingh *et al*., 2012). FOXOs regulate expression of genes involved in cell growth, differentiation, apoptosis and

senescence (Accili & Arden, 2004). cAMP and progesterone signalling positively regulate *FOXO1* expression upon decidualization. Activation of FOXO1 results in cell cycle exit of EnSCs and induce expression, amongst others, of decidual markers, *PRL* and *IGFBP-1* (Takano *et al*., 2007). In response to progesterone withdraw, FOXO1 translocate into the nucleus of decidual stromal cells and promote apoptosis (Labied *et al*., 2006). In addition, recent evidence has highlighted the role of FOXO1 in driving senescence of EnSCs in an IL-8 dependent manner (Brighton *et al*., 2017). Hence, FOXO1 is central role in orchestrating cell cycle exit, differentiation and senescence of EnSCs during decidualization.

HOX proteins

HOX proteins are a family of TFs controlling body plan along the anterior-posterior axis. They are featured by conserved sequence, the homeobox (Favier & Dolle, 1997). In the human endometrium, HOXA10 and HOXA11 are markedly upregulated in the midluteal phase of the menstrual cycle (Taylor *et al*., 1999). Silencing of *HOXA10* in vitro negatively impact on *PRL* and *IGFBP1* gene expression and result in higher expression of IL-11 and IL-15 (Godbole & Modi, 2010). Interestingly, a combination between HOXA10 and FOXO1 seem to modulate transition from proliferation to differentiation of stromal compartment, through differential regulation of the same target genes (Lu *et al.,* 2008). Finally, HOXA11 and FOXO1 converge to regulate *PRL* expression. Specifically, HOXA11 binds MER20 transposon within *PRL* promoter and negatively regulate gene expression. Conversely, in the presence of FOXO1, HOXA11 acts an activator (Lynch *et al*., 2009).

Genome-wide chromatin remodelling governs decidual gene expression

Different cellular phenotypes result from distinct gene expression profiles. Chromatin organization and a dynamic epigenetic code regulate gene transcription. Epigenetic modifications, including nucleosome positioning, DNA modifications, TF binding and chromatin regulators, alter genomic structure,

thereby sequestering some DNA regions and leaving others open or accessible to TF binding (Chen & Dent, 2014).

Gene expression profiling study revealed that genes coding for epigenetic modulators are up-regulated during decidualization, and they include histone-modifiers and binding proteins, DNA methyltransferases and CpG-binding proteins. This suggests that a dynamic epigenetic code operates on the chromatin landscape of the EnSCs during decidualization and is responsible of the acquisition of the decidual identity (Grimaldi *et al*., 2012). Specifically, an example is provided by declining expression level for the histone methyltransferase enhancer of Zeste homolog 2 (EZH2) during decidualization. This results in a gradual loss of trimethylation of histone 3 on lysine 27 (H3K27me3) within the proximal promoters *PRL* and *IGFBP1*. A coordinated loss of methylation and gain of acetylation at the same loci results in increased accessibility of the chromatin, which is indicative of a positive regulation of the transcription. This chromatin remodelling underpins the acquisition of decidual phenotype (Grimaldi *et al*., 2011).

Also, another study indicates that the use of the DNA methylation inhibitor 5-aza-2'-deoxycytidine in human EnSCs alters genomic conformation and results, amongst others, in the up-regulation fo decidual genes involved in cellular properties that feature decidual cells, for example ECM organization and cell adhesion (Logan *et al*., 2010). Conversely, inhibition of methylation prior to and after implantation in the mouse impairs decidualization and correlates with pregnancy failure (Gao *et al.,* 2012).

These observations suggest that a dynamic epigenetic code operates on the chromatin structure as decidualization unfolds. This results in wholesale chromatin remodelling underpinning profound changes occurring in the transcriptome of the endometrial decidual cells.

1.6 Endometrial regeneration requires stem/progenitor cells

The human endometrium exhibits an extraordinary ability to cyclically regenerate during each menstrual cycle. As mentioned, endometrial tissue undergoes menstrual shedding in response to estrogen and progesterone withdrawal in the absence of pregnancy (Gellersen & Brosens, 2014). Menstruation is a rare event occurring only in a few species all characterised by spontaneous decidualization, such as higher primates, elephant shrews, fruit bats and the common (Cairo) spiny mouse (Bellofiore *et al*., 2017; Emera *et al*., 2012). One of the theories about the evolutionary purpose of menstruation infers its unique role in restarting the next reproductive cycle (Emera *et al*., 2012), through cyclic activation of stem/progenitor cells (Evans *et al*., 2016).

Human endometrium harbours two stem cell populations, such as epithelial stem/progenitor cells and mesenchymal stem cells (MSCs) (Chan *et al*., 2004; Garget *et al*., 2009; Masuda *et al*., 2012). The latter represents the major fraction of stem cells within the endometrial cell population (about 1-5%) (Gargett *et al*., 2009). Endometrial MSCs (eMSCs) exhibit high proliferative potential, self-renewal capacity *in vitro*, and ability to differentiate into more mature progeny *in vivo* (Gargett *et al*., 2016; Miyazaki *et al*., 2012; Wolff *et al*., 2007). Bone marrow-derived cells have been shown to migrate into the endometrium of both human and mice, although at low levels. These observations suggest that human endometrium regeneration mainly depends on the endogenous stem cell population (Gargett *et al*., 2012).

Several approaches have been employed to isolate endometrial stromal populations enriched in MSCs, including flow activated cell sorting of cells that co-express cluster of differentiation 140b (CD140b), also known as platelet-derived growth factor receptor β (PDGFRβ) and CD146 (also known as melanoma cell adhesion molecule, MCAM) (Schwab & Gargett, 2007). Recently, a monoclonal antibody (W5C5) has been identified to selectively isolate clonogenic perivascular eMSCs using magnetic-activated cell sorting (Masuda et al., 2012). Subsequent studies demonstrated that W5C5 antibody binds the type 1 integral membrane protein Sushi domain containing 2 (SUSD2)

(Sivasubramaniyan *et al*., 2013). This method makes it possible to overcome damaging effects on cell viability associated with the use of flow cytometry (Schwab & Gargett, 2007).

Identity and gene profile of eMSCs

eMSCs exhibit the ability to both self-renew and differentiate. Cell fate decisions are determined by signals emanating from the cellular niche (Li & Xie, 2005). Understanding of the gene signature defining eMSC identity provides insights into their role in the endometrial regeneration. A recent genome-wide expression profiling study compared freshly isolated CD146+ PDGFR-β+ eMSCs to endometrial fibroblasts and endothelial cells. The study showed increased expression in eMSCs of genes associated with Notch, insulin-like growth factor (IGF), epidermal growth factor (EGF), Hedgehog, transforming growth factor β (TGF-β), WNT and G-protein-coupled receptor signalling pathways, which have been associated with both self-renewal and differentiation, highlighting the role of eMSCs in endometrial regeneration and remodelling (Spitzer *et al*., 2012). CD146+ PDGFR-β+ eMSCs express high levels of *SUSD2*, the integral protein used as single marker for eMSC prospective isolation (Spitzer *et al*., 2012; Masuda *et al*., 2012).

eMSCs locate in the perivascular niche of the endometrium and express pericyte markers, genes associated with angiogenesis, immunomodulation and responses to hypoxia (Spitzer *et al*, 2012). A gene profiling study comparing SUSD2+ and SUSD- cells showed that cells derived from SUSD2+ cells are characterised by a perivascular gene signature. Interestingly, SUSD2+ cells become the major source of cytokines and chemokine production during decidualization. This suggests a role for eMSCs in promoting trophoblast migration towards maternal vessels and mediating maternal immune response in pregnancy (Murakami *et al*., 2014).

eMSCs in regenerative medicine

eMSCs hold great promise for cell-based therapy for women with reproductive disorders. eMSCs are clonogenic, self-renewing, highly proliferative, immunomodulatory and multipotent, hence they are attractive candidates of cell-based therapy in regenerative medicine (Darzi *et al*., 2016).

eMSCs represent an easily accessible source of cells. They can be selectively isolated from endometrial biopsy, which can be obtained in a routine office procedure without anaesthesia (Garget *et al*., 2016). They have been detected also in post-menopausal endometrium. This enables an autologous use of eMSCs for reproductive disorders, including pelvic organ prolapse (POP) in post-menopausal women (Ulrich *et al*., 2014). Synthetic polypropylene meshes have mainly been used for POP treatment. However, adverse side effects, including contraction and pain, raised warnings on their clinical use (Darzi *et al.*, 2016). Ulrich *et al.* (2012) developed a new kind of mesh, composed of polyamide and gelatin, with enhanced mechanical properties. eMSCs seeded with these new meshes promoted angiogenesis and collagen deposition, compared with mesh alone, when implanted into an immunocompromised rat model. Furthermore, an early inflammatory response was observed and characterized by an influx of M1 macrophages, that switched to M2 would healing phenotype and then gradually decreased (Edwards *et al.*, 2015). *In vitro,* eMSCs seeded with polyamide/gelatin meshes have been shown to differentiate into smooth muscle cells and fibroblasts, suitable to regenerate vaginal tissue structure and ultimately restore its function. Further studies have been undertaken to determine if delivered eMSCs function through paracrine effect or they differentiate themselves and reconstitute the vaginal wall (Gargett *et al*., 2016).

Altered endometrial stem/progenitor cell function may potentially hinder endometrial regeneration and ultimately compromise the ability of the endometrium to support embryo implantation (Yu *et al.,* 2008). Women with a thin endometrial layer unable to respond to estrogen stimulation are particularly challaging in IVF treatment. Asherman's syndrome is a reproductive disorder characterized by a thin dysfunctional endometrium and it has been hypothesized

that it might be related to lack of eMSCs or compromised eMSC function (Gargett et al., 2016). In a rat model of Asherman's syndrome, adipose-derived MSCs administrated in the uterine horn promoted angiogenesis and cell proliferation, and together with estrogen, reduced fibrosis. Even though, a local delivery of MSCs resulted in an apparent improved endometrial regeneration, results in terms of endometrial receptivity were not assessed (Kilic *et al*., 2014; Gargett *et al*., 2016). In several case studies, cultured autologous bone-marrow cells were injected into the uterine cavity or the sub-endometrial zone, together with estrogen administration. This cell-based approach resulted in a modest increase of thickness of the endometrium, no sufficient to guarantee a successful pregnancy outcome. However, because of lack of controls, data need to be interpreated with caution (Singh *et al.,* 2014; Gargett & Healy, 2011).

Endometrium is a promising, alternative source of MSCs for autologous and allogenic cell-based therapy, that might be exploited to treating gynaecological disorders, including POP and Asherman's syndrome. However, because of their rarity the use of eMSCs for clinical trials first requires their expansion in culture (Ulrich *et al*., 2013). As in the case of MSCs from other cell systems (Baxter *et al*., 2004), cultured eMSCs undergo spontaneous differentiation (Gurung *et al*., 2015). Further, the telomeres of eMSCs become shortened due to replicative stress. Consequently, eMSCs lose their proliferative capacity as well as the ability to reconstitute tissue *in vivo* (Baxter *et al*., 2004; Banfi *et al*., 2002). These observations predate the realization that prolonged culture of eMSCs results in reduced clinical efficacy (Darzi *et al*., 2016). Gurung *et al*., (2015) showed that culturing eMSCs in medium containing TGF-β Receptor (TGF-β-R) inhibitor, A83-01, in serum free conditions, maintains eMSCs in an undifferentiated state in prolonged culture. Their findings describe the use of small molecules, to selectively inhibit signalling pathways associated to differentiation and improve the purity of cells during culture expansion for therapeutical applications.

Nevertheless, for clinical trials it is of paramount importance to understand molecular 'programming' underlying pharmacological approaches. Development of novel techniques, such as Assay for Transposase-Accessible Chromatin with High-Throughput Sequencing (ATAC-seq), for fast and sensitive epigenomic

profiling of chromatin structure of defined cell populations provides a powerful strategy to address this question (Buenrostro *et al*., 2013).

1.7 ATAC-seq

The human genome contains approximately two metres of DNA, which is hierarchically packed into chromatin within a five-micron nucleus. DNA is wrapped around a core of proteins, called histones, to form nucleosomes, and nucleosomes are compacted into chromatin (Figure 1.3) (Kornberg, 1974; Sha & Boyer, 2009). This hierarchical packaging plays a central role in the regulation of gene expression (Gross & Grarrard, 1988; Bell *et al*., 2011). In the genome, two different varieties of chromatin are distinguishable, heterochromatin and euchromatin. The former identifies inactive genomic regions, whereas the latter refers to regions where DNA is lightly packed and hence accessible to transcription factors, and therefore is potentially biologically active (Buenrostro *et al.,* 2015). Chromatin states are regulated by a dynamic epigenetic code which include DNA methylation, histone modification, chromatin remodellers, nucleosome positioning, non-coding RNAs, as well as changes due to the interaction with transcriptions factors (Kouzarides, 2007). Epigenetic mechanisms manipulate chromatin structure and its compaction level, regulating chromatin accessibility. Hence, their role in determining cellular phenotypes is obvious (Chen & Dent, 2014).

Open chromatin profiling methods are highly effective means to understand the epigenetic code governing chromatin remodelling. They interrogate chromatin accessibility and probe regions of nucleosome positioning and TF binding. Mapping of differential chromatin opening enables identification of the *cis*-regulatory landscape responsible for different cellular functions, including cell proliferation and differentiation (Tsompana & Buck, 2014). ATAC-seq is a recently developed method for genome-wide analysis of the chromatin structure. By contrast to earlier techniques, including DNase-seq (Song & Crawford, 2010), ATAC-seq does not require many cells as starting material. The number of cells

required to successfully map chromatin accessibility by ATAC-seq ranges between 500 and 50,000. Hence, ATAC-seq provides a powerful new method for genome-wide chromatin analysis of rare cell types, including stem cells (Buenrostro *et al.*, 2013). It uses hyperactive Tn5 transposase to probe DNA accessibility by inserting sequencing adapters into relatively open regions of chromatin (Figure 1.4).

ATAC-seq simultaneously reveals information on chromatin compaction, allows mapping of nucleosome positions and genomic locations of transcription-factor binding. Finally, the whole assay requires less complex and time-consuming protocols when compared to previous genome-wide analysis methods (Buenrostro *et al*., 2013).

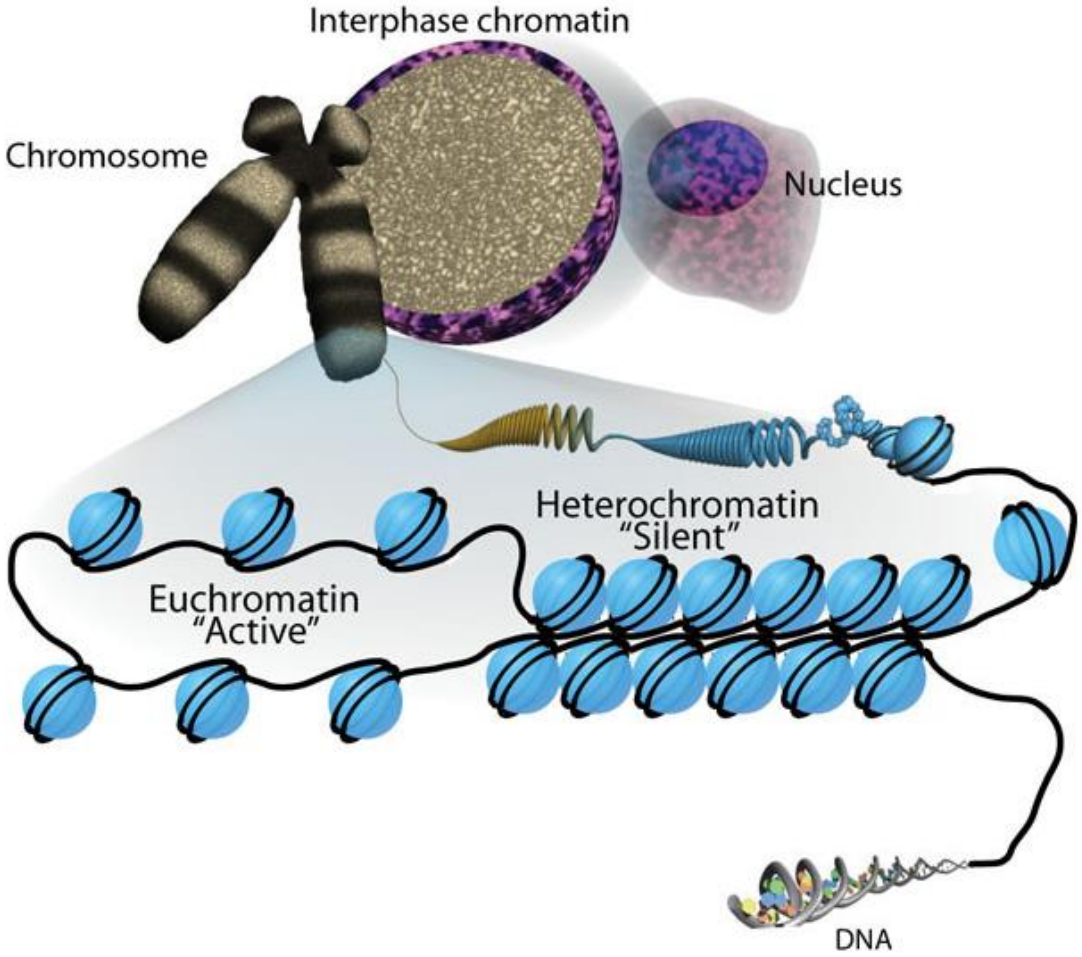

Sha and Boyer, StemBook 2009

Figure 1.3. Chromatin organization. The DNA is wrapped around a core of eight proteins, called histones, to form nucleosome (light blue). The latter is the basic unit in which the chromatin is organized. Nucleosome packaging into higher order structures generates two varieties of chromatin organization, such as euchromatin and heterchromatin. The level of the packaging regulates chromatin accessibility and consequently gene expression.

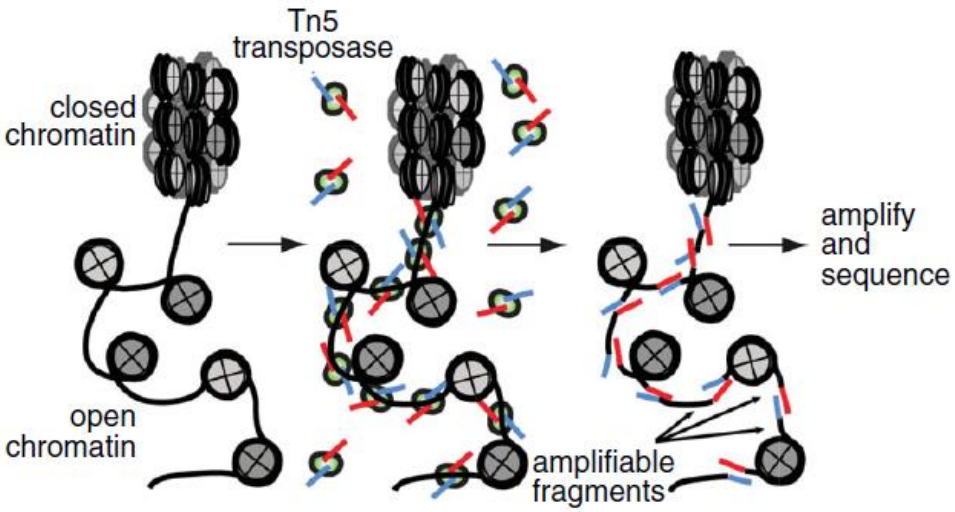

Buenrostro JD *et. al,* Nat Methods 2013

Figure 1.4. Schematic representation of ATAC-seq reaction. Tn5 transposase (green) simultaneously cuts and tagments accessible genomic regions (mapped between nucleosomes, in gray) with unique sequencing adapters (blue and red). This reaction generates genomic fragments that can be amplified via PCR and subjected to high-throughput sequencing.

Nucleosome positions

ATAC-seq discloses detailed genome-wide information on chromatin compaction. In particular, paired-end reads generated by high-throughput sequencing reveal nucleosome positioning in regulatory elements.

Specifically, the DNA winds 1.7 turns around the nucleosome wrapping a total length of 147 bp (McGinty & Tan, 2015). Buenrostro *et al*., (2013) showed that the fragment size distribution of sequenced paired-end reads from human chromatin has a periodicity of 200 bp, suggesting that some regions in the DNA are protected by steric hindrance which makes the transposition less probable (Buenrostro *et al.,* 2013). Hence, fragments with a length of 200 bp may include a single nucleosome and larger fragments may be protected by multiple nucleosomes. Therefore, high molecular weight fragments may contain chromatin in a more compact state compared to short fragments, hence refractory to the transcription machinery that drives differential gene expression.

Buenrostro *et al.* (2013) also demonstrated that ATAC-seq provides information about the different functional states of chromatin, showing that short fragments of DNA were enriched in CCCTC-binding factor (CTCF)-bound regions, whereas transcription start sites (TSSs) were differentially reduced to fragments associated with one, two and three nucleosomes. Furthermore, this study showed that transcribed sequences of DNA and regions mapped to promoters had longer multi-nucleosomal fragments, and were hence less accessible compared to TSSs. These large fragments of the DNA were enriched in heterochromatin that is inaccessible to nuclease digestion (Ghirlando *et al.,* 2004). This body of evidence suggests that ATAC-seq reveals functional states of chromatin that are differentially accessible.

In order to show the efficacy of ATAC-seq to map nucleosomes within the genome, Buenrostro *et al*. (2013) separated sequencing datasets into shorter reads generated from nucleosome-free regions and reads generated by nucleosome-associated chromatin, based on the observations related the periodicity of the insert size distributions (about 200 bp). Then, a data track was calculated and used to map nucleosomes within accessible regions of chromatin

using a simple heuristic model, which measures positively nucleosome-associated fragments and negatively weights nucleosome-free fragments. The nucleosome-free regions were massively enriched in TSSs when compared to distant elements, which tended to be enriched in nucleosomes.

Thus, ATAC-seq allows high-resolution readouts of regions protected by nucleosomes and nucleosome-free regions in the regulatory chromatin landscape (Buenrostro *et al.,* 2013).

ATAC-seq discloses the position of DNA-binding proteins and the interplay between their genomic location and nucleosome positioning

According to Buenostro *et al.* (2013), transposition is less probable in chromatin regions bound by DNA-binding proteins. Footprints generated from ATAC-seq inferred the presence of DNA-binding proteins at specific sites in the genome, similar to data obtained from DNase digestion footprints; thus providing information on transcription factor occupancy. In other words, ATAC-seq promises to be a powerful technique to delineate genome regulatory frameworks (Hesselberth *et al.,* 2009).

As aforementioned, ATAC-seq allows detailed mapping of nucleosome positions. With respect to the nucleosome locations mapped through ATAC-seq data, Buenrostro *et al*. (2013) identified the position of four major classes of DNA-binding proteins. A class of proteins has been shown to strongly avoid nucleosomes, with binding sites approximately at 180 nucleotides from the closest nucleosome positions (NFYA, C-FOS and IRF3 included). A gradation of different behaviours, resulting in avoiding or overlapping nucleosome, has been mainly ascribed to transcription factors (TFs). The other two groups include cohesin-complex subunits RAD21 and SMC3 and chromatin looping factors, which belong to a group of factors whose binding sites locate next to nucleosome boundary, and proteins which tend to bind DNA associated to nucleosomes (Buenrostro *et al.,* 2013).

Epigenomic profiling on clinical timescales

ATAC-seq is a rapid and information-rich genome-wide analysis method and thus might provide a powerful tool to generate epigenomic analysis on a diagnostic timescale. In order to show that clinically remarkable information might be inferred by ATAC-seq, Buenrostro *et al.* (2013) applied the assay to a healthy volunteer's T cells to profile their regulatory chromatin landscape. In particular, IL2 locus was the subject of this study. IL-2 is a cytokine which plays a key role in autoimmune and inflammatory diseases and is responsible of T-cell growth (Fraser *et al.,* 1991). ATAC-seq data revealed the drug target involved in the therapeutic IL-2 inhibition in proband T cells. Through footprints the method enabled the profiling of personalised gene regulatory networks and demonstrated that ATAC-seq might be compatible with future diagnostic applications.

Taken together, ATAC-seq might have a wide applicability to understand genome regulatory networks and thus gene expression and offer the possibility to be applicable to the translational research for mapping an individual's epigenome. It may potentially be applied to rare, relevant cellular subtypes during the different stages of differentiation to improve the understanding of the development of human diseases (Buenrostro *et al.,* 2013).

1.8 Research Justification and Aims

ATAC-seq is a newly developed technique that utilizes the highly active transposase Tn5 to interrogate accessibility of the genome and map open chromatin regions. These putative cis-regulatory DNA regions can be further explored for “footprints” of transcription factor (TF) binding (Buenrostro *et al*., 2013). In the first part of this study, I applied ATAC-seq to investigate the regulatory mechanisms underlying decidualization of the human endometrial cells, an obligatory transformation for embryo implantation (Gellersen & Brosens, 2013). As part of my Monash-Warwick alliance studentship, I joined the laboratory of Professor Gargett in Melbourne, Australia, where I studied the impact of TGF-β receptor inhibition on endometrial mesenchymal stem cells (eMSCs) maintained in prolonged culture.

To address these questions:

1. I established ATAC-seq on EnSCs and mapped dynamic changes in the *cis*-regulatory DNA landscape underpinning decidualization of EnSCs.
2. I integrated ATAC-seq and RNA-seq analyses to probe changes in the chromatin landscape and the transcriptome of cultured eMSCs in response to TGF-β inhibition.

Chapter 2

Materials and Methods

2.1 Materials and Methods Part 1

The first part of this work has been carried out in the laboratory of Professor Jan J Brosens, at the Universtity of Warwick, UK.

2.1.1 Human endometrium tissue sampling

These studies were conducted on endometrial biopsies obtained from women undergoing uterine Natural Killer cell test, in the Implantation Clinic, at University Hospitals Coventry and Warwickshire (UHCW) National Health Service Trust. Pipelle biopsies, timed from mid-secretory phase of the cycle, were obtained from patients who gave written informed consent in according with the guidelines in The Declaration of Helsinki 2000. Experiments were performed on undifferentiated and decidualizing EnSC cultures, established from one patient awaiting IVF treatment and 2 recurrent miscarriage (n = 3). None of the patients received hormonal therapy for at least 2 cycles prior the biospsy cycle. The study was approved by the NHS National Research Ethics-Hammersmith and Queen Charlotte's & Chelsea Research Ethics Committee (1997/5065).

2.1.2 Primary cell culture

2.1.2.1 Isolation of EnSCs

Endometrial biopsies were collected individually in DMEM-F12 medium (Invitrogen) supplemented with 10% dextran coated charcoal (DCC) fetal bovine serum and processed for primary culture as previously described (Barros *et al*., 2016). Briefly, after removing the excess media, biopsies were cut into small pieces using sterile scalpels in a Petri dish and enzymatically dissociated in

phenol-free DMEM-F12 (Invitrogen) containing 0.5mg/ml collagenase (Sigma Aldrich) and 0.1mg/ml deoxyribonuclease type I (DNAse I, Roche) for 1 hour at 37°C, with vigorous shaking every 20 minutes to aid digestion. DNase and collagenase were inactivated by 10% DCC supplemented DMEM-F12 followed by centrifugation at 200*g* for 5 minutes. After centrifuge, cell pellets were re-suspended in DMEM-F12 containing 10% DCC, 1nM estradiol (Sigma-Aldrich), 2mg/ml insulin (Sigma-Aldrich), 100 IU/mL penicillin (Gibco), 100g/mL streptomycin (Gibco) and 2mM L-glutamine (Gibco), and then transferred to tissue culture flasks, mixed gently to ensure distribution of cells and incubated in a humidified environment at 37°C and 5% CO_2 overnight. Media was changed the following day. EnSCs were separated from epithelial cells by attachment timings. Here, any suspended cells (epithelial and blood cells), were removed by washing attached cells with fresh 10% supplemented media, which was subsequently changed every other day. Confluent monolayers of EnSCs were passaged by washing with Dulbecco's Phosphate Buffered Saline (PBS) and lifted with 1ml trypsin-EDTA (0.25%, Gibco) for 5 min at 37°C. Any remaining attached cells were dislodged by gentle agitation. Subsequently, trypsin activity was inhibited by the addition of 9ml 10% DCC supplemented media. Cells were collected by centrifugation for 5 min at 200g and seeded into 6-well plates and 35mm dishes, as required, and cultured in 10% DCC-supplemented media.

2.1.2.2 Decidual timecourse

Confluent monolayers of EnSCs were placed in phenol red-free DMEM/F-12 containing, L-glutamine, antibiotic/antimycotic and 2% DCC overnight at 37°C. In order to induce the differentiated phenotype, human EnSCs were treated with 0.5 mM 8-bromo-cAMP (Sigma-Aldrich) and 1μM medroxyprogesterone acetate (MPA, Sigma-Aldrich) in DMEM-F12 containing 2% DCC, for the indicated time-points. All experimental treatments were carried out before the third cell passage.

2.1.3 ATAC-seq

Decidualized and control EnSC monolayers were subjected to ATAC-seq as previously described (Buenrostro *et al*., 2013; Buenrostro *et al*., 2015), albeit with some modifications.

2.1.3.1 ATAC-seq Nuclei Harvest and Library Preparation

Extract nuclei

Nuclei EZ prep kit (Sigma-Aldrich) was used to harvest nuclei from undifferentiated and decidualizing human EnSC cultures. Confluent cell monolayers were washed with ice cold PBS and then lysed using ice cold lysis buffer (10mM Tris-HCl, pH 7.4, 10 mM NaCl, 3 mM $MgCl_2$ and 0.1% IGEPAL CA-630, Sigma-Aldrich).The cells were scraped and then transferred to pre-labelled cold RNase/DNase free 1.5ml eppendorfs. The tubes were vortexed, left on ice for 5 min and then pelleted in a fixed-angle refrigerated benchtop centrifuge. The latter was used to avoid losing nuclei and the supernatant was carefully discarded by pipetting away from the pellet.

Transposase reaction (tagmentation)

Following the nuclei preparation, the pellet was re-suspended in the transposase reaction mix, containing 25µl Tagment DNA Buffer, 5µl Tagment DNA Enzyme and 20µl nuclease free water (Nextera DNA sample preparation kit – Illumina). In order to optimize the time of incubation, the transposition reaction was carried out for 30, 45, 60, 90 and 120 min at 37°C. Directly after incubation, samples were

pulse-spun to collect reaction and purified using a Zymo DNA Clean and Concentrator-5 Purification kit.

Purify DNA

Transposome may bind tightly to DNA ends and interfere with the subsequent steps. It is therefore critical to purify tagmented DNA from transposome. Zymo DNA binding buffer was added to the 50µl sample which was vortexed and transferred to the column. Samples were then spun at 17g for 30 seconds (s) at room temperature (RT). The resulting flow through was discarded and 200µl DNA wash buffer (Zymo DNA Clean and Concentrator-5 Purification kit, Zymo Research) added, which was centrifuged as described previously. The wash and centrifugation steps were repeated twice. After removing the residual liquid, the columns were changed to clean tubes and 23µl pre-warmed elution buffer (Zymo DNA Clean and Concentrator-5 Purification kit) added to the columns. The samples were incubated for 2 min at RT. To elute the DNA, columns were centrifuged for 2 min.

PCR

Following purification, library fragments were re-suspended 20µl sample in a 0.2mL PCR tube containing the following reagents (Nextera DNA preparation kit and Nextera DNA sample preparation index kit, Illumina):

- 5µl Primer Cocktail (PPC)
- 15 µl Master mix (NPM)
- 5µ index 1
- 5µ index 2

Subsequently, they were amplified in a traditional PCR machine (AB Applied Biosystem, Vetri 96 Well Thermal Cycler, Foster City, CA, USA), using the following PCR conditions:

- 1 cycle: 72°C for 3 min
  98°C for 30 s
- 15 cycles: 98°C for 10 s
  63°C for 30 s
  72°C for 1 min

PCR clean up

The libraries were purified using AMPure XP, as recommended on the Illumina Nextera kit protocol. Each sample was added to 1.5mL Eppendorf lobind tubes and then re-suspended in 30µl AMPure beads. The samples were first incubated for 5 min at RT and then placed on the magnetic stand. The supernatant was carefully aspirated and 200µl of freshly prepared 80% EtOH was added to wash the pellet. After 30 s, the supernatant was aspirated and the washing step was repeated. All supernatant was then removed and the beads were allowed to air dry for 15 min at RT. The samples were removed from the magnetic stand and 23µl Resuspension Buffer (RSB) (Nextera DNA preparation kit – Illumina) was added. The beads were re-suspended, incubated for 2 min at RT and then placed on magnet for 2 min. The supernatant was carefully collected into clean tubes.

2.1.3.2 Quantification of amplified DNA library

The amplified libraries were quantified by using Qubit HS DNA Assay, according to the manufacturer's instructions. Briefly, Qubit dsDNA HS dye and Buffer (Qubit Assays kit, Invitrogen by life technology Qubit 2.0 Fluorometer) at a ratio 1:200

were used to prepare working solution. Qubit dsDNA HS Standard 1 and Standard 2 (Qubit Assays kit, Invitrogen by life technology Qubit 2.0 Fluorometer) were re-suspended separately in 190µl working solution. They were vortexed and left to stand at RT for 2 min. 1µl of the sample was added to 199µl of working solution, vortexed and incubated for 2 min at RT. Qubit 2.0 Fluorometer machine was used to measure both standards and samples, according to the manufacturer's instructions.

2.1.3.3 Quality Control

Library sizes were assessed on an Agilent Technologies 2100 Bioanalyzer and the High Sensitivity DNA chip was used.

2.1.3.4 Sequencing

ATAC-seq library samples were sequenced on an Illumina HiSeq 2500 at Source Bioscience. A depth of thirty million paired end reads were sequenced per sample, with a read length of 100 bp.

2.1.3.5 Sequencing data analysis

Sequencing data and bioinformatics analysis have been performed in collaboration with Pavle Vrljicak, PhD (Tommy's national Centre for Miscarrigae Research, Warwick Medical School) and Associate Professor (A/P) Sascha Ott (Tommy's National Centre for Miscarriage Research, Department of Computer Science). Sequenced paired-end reads were aligned to the University of California Santa Cruz (UCSC) human genome 19 (hg19) assembly using bowtie2-2.2.6 (Langmead and Salzberg, 2012) and samtools-1.2.0 (Li *et al*.,

2009) and peak calling performed using MACS-2.1.0 (Zhang *et al*., 2008). 185,087 out of 202,169 identified peaks were significant ($q < 1 \times 10^{-4}$).

HTSeq-0.6.1 (Anders et al., 2015) was used to count the reads overlapping the peaks and differential expression analysis of sequencing data 2 (DESeq2) (Anders and Huber, 2010) was used to determine opening and closing regions of the chromatin. Significant ATAC-seq peaks were ranked based on their *p*-value *(p)* and their fold change, so that opening and closing peaks correspond to lower and higher values, respectively. Data have been submitted to Gene Expression Omnibus (GEO) (accession number GSE104720).

2.1.3.6 Comparison between ATAC-seq data and other sequencing datasets

ATAC-seq data were cross-referenced with other sequencing data. The analysis was performed in collaboration with Pavle Vrljicak, PhD (Tommy's national Centre for Miscarrigae Research, Warwick Medical School) and A/Professor Sascha Ott (Tommy's National Centre for Miscarriage Research, Department of Computer Science). More accurately, chromatin immunoprecipitation followed by sequencing (ChIP-seq) data obtained from decidualizing EnSCs from GEO, for FOSL2 (GSM1703568), PGR (GSM1703567) and FOXO1 (GSM1703607). Also, Formaldehyde-Assisted Isolation of Regulatory Elements through high-throughput sequencing (FAIRE-seq) data from whole endometrial tissue from GEO, GSM1011119, and DNase I hypersensitivity (HS) data obtained from decidualized EnSCs from GEO, GSE61793. Finally, ATAC-seq data were compared to ENCODE DNaseI HS dataset from other cell systems, from the UCSC genome browser (The Encyclopedia of DNA Elements (ENCODE) Project Consortium, 2012; Thurman *et al*., 2012; Karolchic *et al*., 2004).

2.1.3.7 Mapping of differential ATAC-seq peaks to proximal genes

Differential open chromatin regions were mapped to *cis*-regulatory elements of their proximal genes using ENCODE DNaseI hypersensitivity data (Thurman *et al.*, 2012). Physical interaction and distance no greater than 10 kb were used as criteria to assess association between ATAC-seq peak and proximal gene regulatory element. The analysis was carried out in collaboration with Pavle Vrljicak, PhD (Tommy's national Centre for Miscarrigae Research, Warwick Medical School) and A/Professor Sascha Ott (Tommy's National Centre for Miscarriage Research, Department of Computer Science).

2.1.3.8 Binding Motif Discovery

Hypergeometric Optimization of Motif EnRichment (HOMER) v.4.8 was used to determine enrichment and depletion of TF short sequence binding motifs in the differential ATAC-seq peaks. Footprint analysis was performed using Wellington (Piper *et al*., 2013). TFs associated to high affinity binding motifs were cross-referenced with RNA-seq data obtained from three independent undifferentiated and decidualizing primary EnSC cultures. The analysis was performed in collaboration with Pavle Vrljicak, PhD (Tommy's national Centre for Miscarrigae Research, Warwick Medical School) and A/Professor Sascha Ott (Tommy's National Centre for Miscarriage Research, Department of Computer Science).

2.1.4 RNA Sequencing

2.1.4.1 RNA Extraction

To reduce the risk of RNA degradation, RNase and DNase free 1.5 mL eppendorfs and nuclease-free water were used. Supernatant was collected from the cells and frozen at -80°C for further future studies. Total RNA was extracted from EnSCs cultures using 200µl RNA Stat-60 reagent per well in a 6 well plate ensuring all cells were covered. The cells were scraped thoroughly with appropriate cell scraper, transferred to pre-labelled RNase-free 1.5ml eppendorfs, left at room temperature for 5 mins and then placed on ice. Subsequently, 40µl of 100% chloroform was added to the Stat-60 solution. The samples were mixed vigorously, left to stand at room temperature for 3 mins and then centrifuged. This step separates the samples into three distinct phases, such as, an aqueous phase, a white layer and a pink phase. RNA remains exclusively in the colourless upper aqueous phase. The aqueous phase was carefully transferred into ½ a volume of 100% isopropanol, vortexed and centrifuged at 12,000 g at 4°C for 15 minutes, washed twice with 1ml 75% ice cold ethanol and dried at RT and dissolved in an appropriate volume of nuclease free water. RNA concentration and quality assessed by nanodrop. Satisfactory values were considered equal to or greater than 1.80 on the 260/280 absorbance scale, indicating pure RNA without contamination of protein. Samples were stored at -80°C.

2.1.4.2 RNA Quality Control and RNA Libraries

RNA quality control was assessed on an Agilent Technologies 2100 Bioanalyzer according to the manufacturer's instructions RNA samples with RNA Integrity Number (RIN) > 8 were used to generate RNA libraries. High quality RNA

samples were used to generate RNA libraries according to the Illumina Stranded mRNA protocol at Source Bioscience. Library size was assessed on an Agilent Technologies 2100 Bioanalyzer and quantified by Qubit and quantitative polymerase chain reaction (qPCR).

2.1.4.3 RNA Sequencing

RNA libraries were sequenced on the Illumina HiSeq3000 at Source Bioscience. Fifty million single end reads were sequenced per sample with a read length of 100 bp.

2.1.4.4 Sequencing data analysis

RNA-seq data analysis was performed in collaboration with Pavle Vrljicak, PhD (Tommy's National Centre for Miscarriage Research, Warwick Medical School) and Associate Professor Sascha Ott (Tommy's National Centre for Miscarriage Research, Department of Computer Science, University of Warwick). Transcriptomic maps were identified using bowtie-2.2.3, samtools-0.1.19 and tophat-2.0.12 against the UCSC hg19 transcriptome reference from the Illumina iGenomes resource (2014). Counts were assessed using HTSeq -0.6.1 and transcripts per million (TPM) were calculated. Three different methods for detection of differentially expressed genes were used to analyse count data, such as DESeq2, baySeq and edgeR. To characterize differentially expressed genes, the latter were subjected to Gene Ontology (GO) enrichment analysis using the Database for Annotation, Visualization and Integrated Discovery (DAVID) version 6.8.

2.2 Materials and Methods Part 2

The second part of this work has been carried out in the laboratory of Professor Caroline Gargett, at Monash University, The Ritchie Centre, Hudson Institute, Australia.

2.2.1 Human endometrium tissue sampling

The study was approved by the Monash Health and Monash University Human Research Ethics committees. Endometrial biopsies were obtained from pre-menopausal women (n = 3), without endometrial pathologies, who gave written informed consent according to The Declaration of Helsinki (2000) guidelines. Women were excluded if they had taken any hormonal treatment for the preceding three months.

2.2.2 Primary cell culture

2.2.2.1 Isolation and magnetic-activated cell sorting of eMSCs

Endometrial biopsies were processed and single-cell suspension of eMSCs obtained as previously described (Masuda *et al*., 2012). Briefly, endometrial tissue was finely minced and enzymatically digested in Dulbecco's modified Eagle's medium (DMEM-F12) supplemented with 0.5 collagenase type I (Worthington Biochemical Corporation) and 40 µg/ml DNase I (Worthington Biochemical Corporation) at 37°C on a rotating MACSmix (Miltenyi Biotech) for 60 min. The digested tissue was filtered through 40 µm nylon mesh cell strainer (BD Bioscience) to remove epithelial glandular cells then centrifuged at 1100rpm for 5 min. Supernatant was carefully aspirated and red blood cells removed using

Ficoll-Paque (GE healthcare Bio-science), a density gradient media. After centrifuge at 1500 rpm for 15 min, the interface containing EnSCs was carefully aspirated and washed in DMEM/F12 containing 10% fetal calf serum (FCS, Thermo Fisher) (Invitrogen), 1% antibiotic/antimycotic (Life Technologies) and 2mM glutamine (Invitrogen). EnSC single-cell suspension were re-suspended in separation buffer, such as 0.5% FCS/PBS, and 10 µg/ml phycoerythrin (PE)-conjugated anti-human SUSD2 (BioLegend) added. Cells were incubated for in the dark at 4°C for 30 min. After incubation, the cells were washed to remove unbound primary antibody in separation buffer and centrifuged at 1100rpm for 5 min. The supernatant was then carefully aspirated and the pellet was re-suspended in separation buffer (80 µl/10^7 total cells, according to the manifacturer's instructions) and 20 µl of anti-PE magnetic active cell sorting (MACS) microbeads (Miltenyi Biotec) in the dark at 4°C for 30 min. The cells were washed in separation buffer and centrifuged at 1100rpm for 5 min. The conjugated pellet was re-suspended in separation buffer (500 µl/10^7) and applied to a Miltenyi column (Myltenyi Biotec) in the magnetic field (MACS separator). Columns were flushed three times with buffer and unlabelled cells that passed through were collected in a sterile tube. Magnetically labelled cells, such as SUSD2+ eMSCs, were eluted with buffer away from the magnetic field and cell number was determined using glasstic slide 10 with grids according to the manufacturer's instructions.

2.2.2.2 Cell culture

SUSD2+ eMSCs yielded from MACS separation were cultured in DMEM-F12 medium containing 10% FCS (Invitrogen), 1% antibiotic/antimycotic (Life Technology) and 2mM glutamine (Invitrogen), supplemented with 10 ng/ml basic fibroblast growth factor (bFGF) and slowly scaled-down to an in-house DMEM/F12 serum free medium (SFM) at 37 °C, 5% CO_2, as previously described (Rajaraman et al., 2013) in the presence or absence of 1 µM TGF-β-R inhibitor, A83-01) (Tocris Bioscience). Cells were seeded at conventional density (5,000 cells/cm^2) and media was changed every 48h. Both untreated and A83-01 treated

eMSC cultures were passaged on day 15, 22, 29 and 36 in fibronectin-coated T25 culture flasks (10 µg/ml; Becton Dickinson, BD, Bioscience) as previously described (Gurung *et al*., 2015). At each passage, cells were counted as described above and cumulative cell population (total cell number) was calculated by multiplying total number of cells yielded at the current passage by total number of cells yielded at the previous passage, and then divided by the number of cells seeded at the current passage, as previously described (Gargett *et al*., 2009). Cell proliferation at each passage was also assessed by calculating the number of population doublings (PDs) using the following formula: PD = 3.322logN/N0, where N is the total cumulative cell number calculated at each passage and N0 represents the initial number of seeded primary cells (Pellegrini *et al.*, 1999). At day 36, untreated and A83-01 treated eMSC cultures were subjected to flow cytometry, RNA-seq and ATAC-seq.

2.2.3 Flow cytometry

Surface phenotype for untreated and A83-01 treated eMSCs was assessed by flow cytometry for three stem cell markers, such as SUSD2, CD140b and CD90, as previously described, albeit with some modifications (Gurung *et al*., 2015). eMSCs were incubated with 1:20 allophycocyanin (APC)- and PE- conjugated primary antibodies or matched isotype control antibodies, in PBS containing 2% FCS for 1h at 4°C in dark. The primary antibodies used were APC-conjugated SUSD2 (Biolegend), PE- conjugated CD140b (R&D) and APC- conjugated CD90 (BD Pharmingen). After incubation, cells were washed with PBS containing 2% FCS to remove unbound cells and then fixed with 4% paraformaldehyde (PFA) in PBS containing 2% FBC. Untreated and A83-01 treated eMSCs were analysed using BD FACSCanto II (BD Bioscience) (10,000 events captured/sample per flow) and software FlowJo v.10.

2.2.4 RNA Sequencing

2.2.4.1 RNA Extraction

Total RNA was extracted from untreated and A83-01 treated eMSCs using RNeasy Mini kit (Qiagen) according to the manifacturer's instructions, albeit with some variations. Briefly, eMSC monolayers were washed with PBS and trypsinised using TryLE^{TM} (Life Technologies). DMEM/F12 containing 5% heat-inactivated newborn calf serum was added to cell-suspension to inactivate trypsin and cells were transferred to an RNase-free centrifuge tube to minimize risk of RNA degradation. Cell suspensions were then centrifuged at 300g for 5 min. To disrupt the cells, RNeasy Lysis (RLT) Buffer, containing β-mercaptoethanol, was added to cell pellets (600 µl up to 10^7 cells) and mixed by pipetting/vortexing. After adding 1 volume of 70% ethanol, cell suspensions were transferred to an RNeasy spin column placed in a 2 ml collection tube. Samples were centrifuged at maximum speed (≥ 8000 g) for 15 sec. Flow-through was discarded. To minimize genomic DNA contamination, the optional four steps were performed. 350 µl RNA wash (RW1) Buffer was added to the RNeasy spin column to wash column membrane. Samples were centrifuged at maximum speed for 15 sec and flow-through discarded. 80 µl DNase I incubation mix, prepared according to the manufacturer's instructions, were added carefully on the membrane of the RNeasy spin column and left at room temperature for 15 min. To wash the membrane, 350 µl Buffer RW1 were added to the RNeasy spin column and samples were centrifuged and flow-through discarded. To further wash the column membrane, 500 µl Buffer RPE were added to tube. Samples were centrifuged at maximum speed for 15 sec. The washing step was repeated again, but this time samples were centrifuged for 2 min to further wash the column membrane. Flow-through was discarded and, to eliminate Buffer RPE completely, the RNeasy spin column was placed in another 2 ml collection tube and centrifuged at maximum speed for 1 min. To elute the RNA, the RNeasy spin column was transferred to a new collection tube and 30 to 50 µl RNase-free water

was added carefully to the membrane of the column.

2.2.4.2 RNA Quality Control and RNA Libraries

RNA quality control and RNA libraries were performed at the Monash Health Translation Precinct (MHTP) Medical Genomic Facility. The former was assessed on an Agilent Technologies 2100 Bioanalyzer according to the manufacturer's instructions RNA samples with RNA Integrity Number (RIN) > 8 were used to generate RNA libraries. The latter were produced according to the Illumina Stranded mRNA protocol. Library size was assessed on an Agilent Technologies 2100 Bioanalyzer and quantified by Qubit and quantitative polymerase chain reaction (qPCR).

2.2.4.3 RNA Sequencing

RNA libraries were sequenced on the Illumina HiSeq3000 at MHTP Medical Genomic Facility. Fifty million single end reads were sequenced per sample with a read length of 50 bp.

2.2.4.4 Sequencing data analysis

RNA-seq data analysis was performed as described in 2.1.4.4 in collaboration with Pavle Vrljicak, PhD (Tommy's National Centre for Miscarriage Research, Warwick Medical School) and Associate Professor Sascha Ott (Tommy's National Centre for Miscarriage Research, Department of Computer Science, University of Warwick).

2.2.5 ATAC-seq

Freshly isolated MSCs were treated with or without TGF-β-R inhibitor for 36 days and then subjected to ATAC-seq. ATAC-seq libraries were processed as described in 2.2.3 and data analysed in collaboration with Pavle Vrljicak, PhD (Tommy's National Centre for Miscarriage Research, Warwick Medical School) and Associate Professor Sascha Ott (Tommy's National Centre for Miscarriage Research, Department of Computer Science, University of Warwick).

2.2.6 *in vitro* colony-forming unit-fibroblast (CFU-F) assay

eMSCs were cultured with or without A83-01 for 2 passages (29 days) and then seeded at a low density (50 cells/cm^2) to assess colony efficiency as previously described, albeit with some modifications (Gurung *et al*., 2015). Briefly, untreated and A83-01 treated eMSCs were seeded on fibronectin (10 µg/ml) pre-coated 10 mm culture dishes (BD Falcon) and cultured in SFM, supplemented with bFGF (1 µl/ml, Peprotech) and EGF (1ul/ml; Invitrogen), in the presence or absence of A83-01 (0.1 µl/ml, Tocris Bioscience) at 37°C 5% CO_2, further for 2 weeks. Media was changed every 48h. Untreated and treated eMSC cultures were fixed in 10% formalin for 10 min and stained with haematoxylin (Amber Scientific). Samples were washed twice with distilled water and the Scott's tap water was used to enhance blue colour of the colonies stained. The number of colonies was counted and colony efficiency percentage estimated by dividing total number of colonies yielded by number of cells seeded x 100.

2.2.7 Statistical Analysis

Statistical analyses were performed with GraphPad Prism 6. Where appropriate, two-way analysis of variance (ANOVA) or paired non parametric Wilcoxon test was applied. Data represent mean ± standard error of the mean (S.E.M). Values of *p*-value (*p*) < 0.05 were considered statistically significant.

For RNA-seq data analysis, statistical significance was assessed on a large number of variables (i.e. genes). Benjamini-Hochberg procedure was applied to control the false discovery rate. Changes in gene expression were deemed statistically significant if the adjusted *p*-value (*q*-value) was less than 0.05.

Chapter 3

Chromatin profiling in decidualizing human endometrial stromal cells

3.1 Introduction

Decidualization is a profound transformation of EnSCs from fibroblast-like to secretory decidual cells that occurs 'spontaneously' in menstruating species (Brosens *et al*., 2006). Decidual transformation involves large-scale gene expression changes (Gellersen & Brosens, 2014; Takano *et al*., 2007). Genome-wide remodeling of the chromatin architecture underlies the wholesale transcriptomic reprogramming upon decidualization (Munro *et al*., 2010; Zelenko *et al*., 2012). Gene expression profiling studies revealed that genes coding for epigenetic modulators are up-regulated during decidualization, and they include histone-modifiers and binding proteins, DNA methyltransferases and CpG-binding proteins. This suggests that a dynamic epigenetic code operates on the chromatin landscape of the EnSCs during decidualization and is responsible of the acquisition of the decidual identity (Grimaldi *et al*., 2012). Specifically, an example is provided by declining expression level for the histone methyltransferase enhancer of Zeste homolog 2 (EZH2) during decidualization. This results in a gradual loss of trimethylation of histone 3 on lysine 27 (H3K27me3) within the proximal promoters *PRL* and *IGFBP1*. A coordinated loss of methylation and gain of acetylation at the same loci results in increased accessibility of the chromatin, which is indicative of a positive regulation fo the transcription. This chromatin remodelling underpins the acquisition of decidual phenotype (Grimaldi *et al*., 2011). Also, another study indicates that the use of the DNA methylation inhibitor 5-aza-2'-deoxycytidine in human EnSCs alters genomic conformation and results, amongst others, in the up-regulation fo decidual genes involved in cellular properties that feature decidual cells, for example ECM organization and cell adhesion (Logan *et al*., 2010). Conversely, inhibition of methylation prior to and after implantation in the mouse impairs decidualization and correlates with pregnancy failure (Gao *et al.,* 2012). These observations suggest that a dynamic epigenetic code operates on the chromatin structure as decidualization unfolds.

Recent technological advances have enabled the rapid profiling of open chromatin landscapes using genome-wide analysis techniques, such as ATAC-

seq. This assay probes regions of increased accessibility and further interrogates them for “footprints” of TF binding (Buenrostro *et al*., 2013). Footprints are sequences of tens of basepairs (bp) that infer the presence of DNA-binding proteins (Hesselberth *et al*., 2009). The latter makes the chromatin less accessible and hence refractory to transposase activity (Buenrostro *et al*., 2013). Previous work has characterized whole endometrial open chromatin signatures by Formaldehyde-Assisted Isolation of Regulatory Elements through high-throughput sequencing (FAIRE-seq) and DNase-seq in decidualized EnSCs (Lynch *et al*., 2015; Thurman *et al*., 2012). This provided genome-wide views of open chromatin regions, but did not show what changes occur in decidualization.

In this chapter, I performed ATAC-seq to map global changes in the chromatin landscape of EnSCs upon decidualization. The most enriched short sequence binding motifs were determined in opening and closing genomic regions. To examine factor occupancy, footprint analysis was performed and resulting footprints inferring DNA-binding proteins were interrogated. Finally, ATAC-seq data were integrated with RNA-seq data to examine gene expression of potential binding TFs and ultimately identify novel transcriptional regulators implicated in decidualization.

3.2 Results

3.2.1 Optimization of incubation time for transposase reaction

ATAC-seq uses hyperactive Tn5 that simultaneously cuts and probes accessible regions of chromatin. This process generates genomic libraries that can be subjected to high-throughput sequencing (Buenrostro *et al*., 2013). High quality library size distribution varies between 250 and 1000 bp (Illumina guidelines). To successfully perform ATAC-seq, I optimized incubation time for transposase reaction on undifferentiating and decidualizing human EnSCs.

Briefly, primary human EnSCs were decidualized in response to 8-br-cAMP and MPA for 4 days. Paired undifferentiated and decidualizing cultures were subjected to ATAC-seq. Buenrostro *et al*. (2015), optimized 30 min as incubation time for transposase reaction on lymphoblastoid cells. To determine the optimal reaction time for primary endometrial cells, the transposase reactions were run for either 120, 90, 60, 45 or 30 min. To determine the fragment length distribution of the genomic libraries, samples were subjected to quality control on Agilent Technologies 2100 Bioanalyzer using the High Sensitivity DNA chip. As shown in Figure 3.1, subjecting cultures to a transposase reaction lasting 120 min resulted genomic libraries with a fragment lenght distribution with a predominant peak at lower range (200-300 bp). Short fragments can map to inaccessible regions of the genome, generating noise during sequencing. A 90 min reaction yielded larger fragments (average ~500 bp) and a modest increase in fragment length was observed when the transposase reaction was stopped after 60 and 45 min. For the latter, as the sample was too concentrated the software was not able to assign the bp scale to the x-axis, but measured the detection of fluorescence intensity over time (seconds). The ladder was used to manually calculate the approximate fragment size (e.g. fragments 200 bp long were detected at 60 seconds). Finally, the 30 min reaction resulted in the largest fragment size, suggesting insufficient transposition. The 30 min incubation time

generated too large molecular fragments, that can result in a reduced clustering efficiency during sequencing (Figure 3.1).

Considering the length of DNA wrapped around a nucleosome (~200 bp), I inferred that fragments containing a single nucleosome were likely to be present in the genomic library of the 120 min. On the other hand, 90, 60 and 45 min incubation times were all likely to yield similar library size distributions. However, Bioanalyzer traces were not really indicative of the average fragment size generated. Hence, I arbitrarily chose 90 min and 45 min (half of the former) as incubation times and make the data more informative by sequencing.

Taken together, data suggested that subjecting cell cultures to a transposase reaction lasting 120 and 30 min results in average library fragment size as small as 250 bp and as big as 1000 bp. On the other hand, incubation times in between seemed to be all equivalent and Bionalyzer traces not to be predictive of successfully sequenced genomic libraries. Hence, to infer if 45 and 90 min incubation time could generate libraries with high clustering efficiency, I proceeded with sequencing.

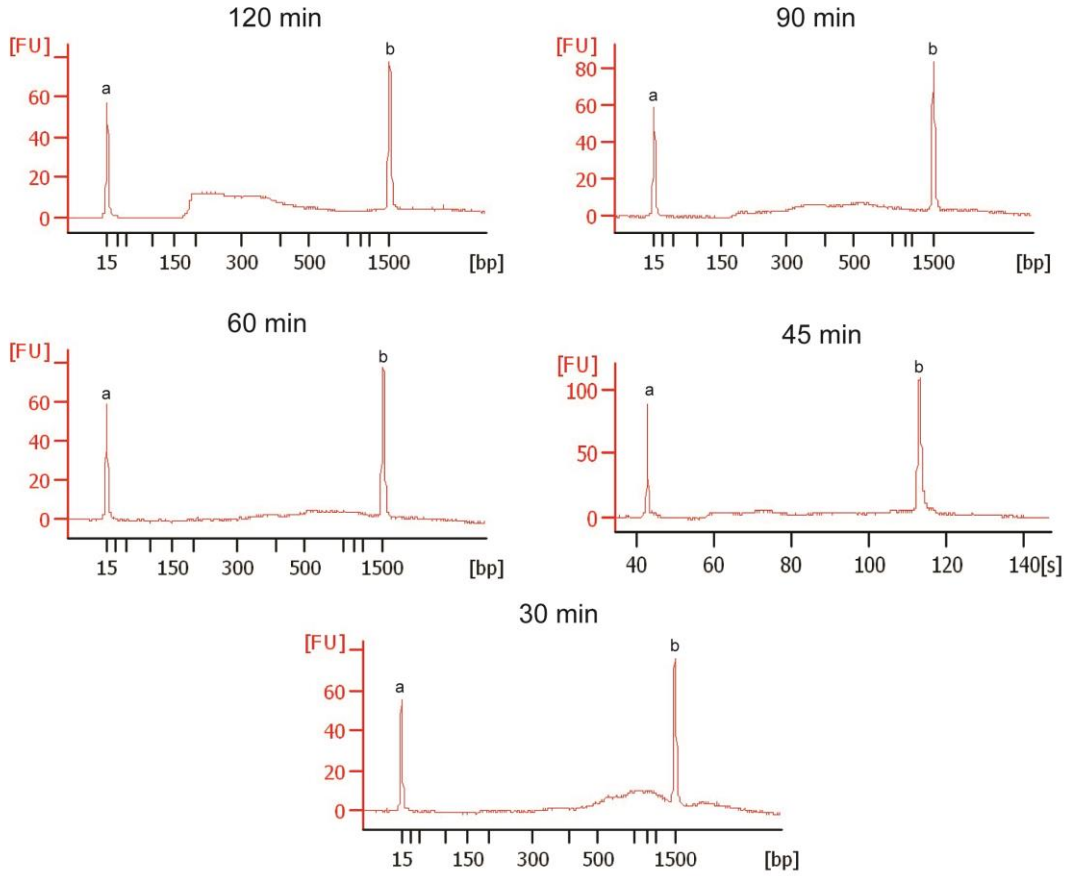

Figure 3.1 Different times of incubation for transposase reaction generated different library size distributions. EnSCs were seeded in 35 mm dishes, nuclei were harvested and subjected to ATAC-seq. Representative genomic library size distribution generated from 120, 90, 60, 45 and 30 min incubation time was assessed on Agilent Technologies 2100 Bioanalyzer. The graphs show detection of fluorescence by the genomic fragments. The Y-axis shows fluorescent intensity (FU). The X-axis represents the size (bp) of the fragments or time of detection, for samples that were too concentrated. The standard in each experimental sample is shown as two peaks labelled as the lower (a) and upper (b) marker.

3.2.2 Chromatin profiling in primary human EnSCs

To map genome-wide dynamic changes in the chromatin landscape upon decidualization, undifferentiated and decidualizing human EnSCs were subjected to ATAC-seq.

Briefly, primary human EnSCs were decidualized in response to 8-br-cAMP and MPA for 4 days. ATAC-seq libraries were sequenced on the Illumina HiSeq1500. Thirty million paired end reads were sequenced per sample, with a read length of 100 bp. Surprisingly, data revealed that despite Bioanalyzer data were not convincing, subjecting genomic libraries to transposase reaction lasting either 45 or 90 min, results in high clustering efficiency. As both incubation times generated the same sequencing data, they could be equally chosen for future experiments and I chose 45 min to further optimize the time of the whole procedure.

More accurately, ATAC-seq analysis identified a total of 185,087 significant differential ATAC-seq peaks, revealing profound chromatin remodelling in response to decidual cues. The resulting ATAC-peaks were ranked from the most strongly opening to the most strongly closing peak. Transition of closed to open chromatin at major differentiation genes, such as *PRL* and *IGFBP1* (Figure 3.2A-B), confirmed ATAC-seq as powerful tool to accurately probe genomic regions that change dynamically upon decidualization.

Previous work had interrogated the chromatin landscape of the decidualized EnSCs and the whole endometrium, using DNase-seq and FAIRE-Seq, respectively (Lynch *et al*, 2015). Therefore, the profile of the chromatin architecture resulting from the ATAC-seq analysis was compared to the previous data to investigate if the use of ATAC-seq provided additional enrichment in the description of genome-wide landscape of chromatin of EnSCs. Results showed that less than 20% of the genomic regions of the decidual cells and of the whole endometrium were previously identified showed that compared to the proportion of the ATAC-seq data. Furthermore, a comparison with Encyclopedia of DNA Elements (ENCODE) project's DNase-seq data from 125 human cells and tissue

types (Thurman *et al.,* 2015) confirmed that more than 90% of the ATAC-seq peaks represent true regions of differential opening (Figure 3.3). More accurately, when DNase I hypersensitivity sites (DHSs) identified by DNase-seq were compared to the ATAC-seq peaks, they overlapped with the closing ATAC-seq peaks rather than with the opening peaks (Figure 3.4).

Even though, prediction of gene expression cannot exclusively be based on opening or closing chromatin because it likely results from a combination of different TFs at different genomic locations, analysis of 100 genes associated with the most open and closed ATAC-seq peaks revealed that genes with opening ATAC-seq peaks were also upregulated during decidualization, whereas closing ATAC-seq peaks were associated to genes that were down-regulated upon decidualization ($p = 2.65\ 10^{-9}$, *t*-test) (Figure 3.5).

Taken together the data revealed that ATAC-seq strongly contributes to increase our knowledge of the chromatin architecture of EnSCs before and after decidualization.

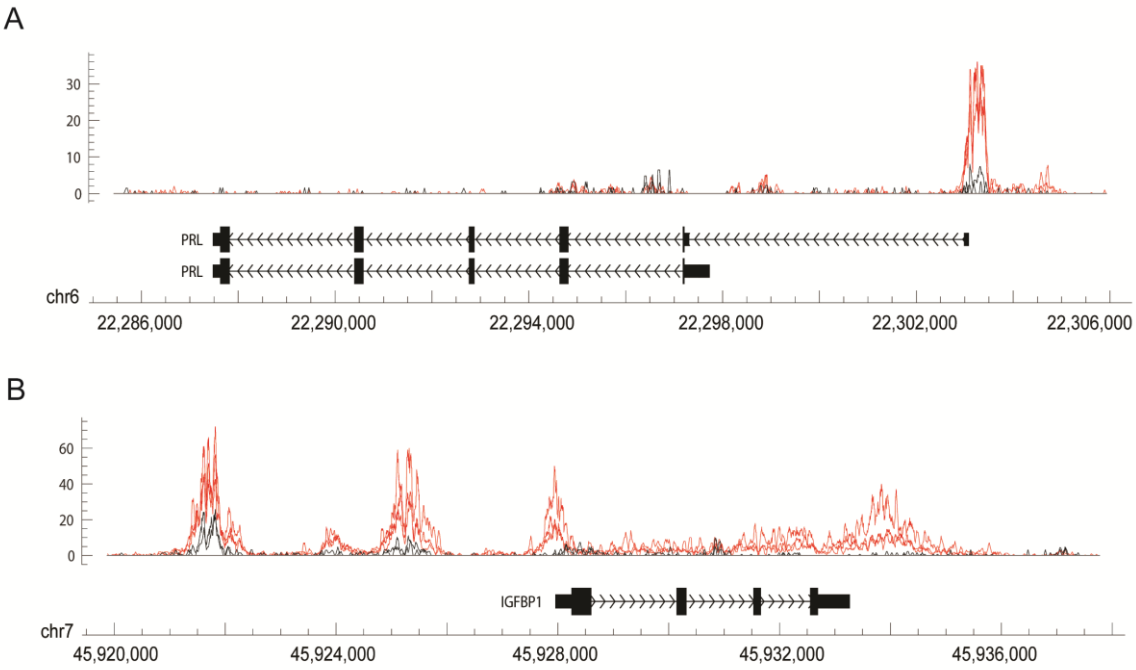

Figure 3.2. Transition of closed to open chromatin exemplified by ATAC-seq peaks. Examples of ATAC-seq peaks showing significant opening and closing in the chromatin landscape at major decidual markers, such as *PRL* (A) and *IGFBP1* (B). Black and red traces represent ATAC-seq signal in the undifferentiated and differentiated cells, respectively. For both *PRL* and *IGFBP1,* ATAC-seq peaks preferentially localize around the promoters. Additionally, IGFBP1 has differential opening peaks upstream of the transcription start site and downstream of the termination site.

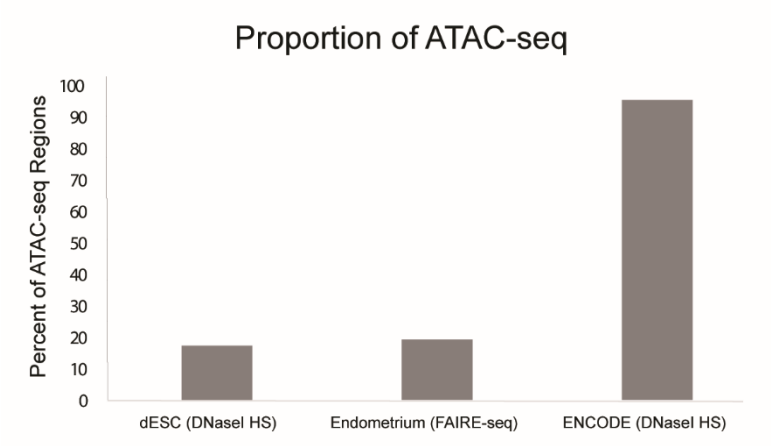

Figure 3.3. Decidualized EnSC chromatin landscape profiled by ATAC-seq in comparison to other endometrium assays. DNase I hypersensitivity (HS) sites and FAIRE-seq in decidualized EnSCs and in the whole endometrium, respectively, identified less than 20% of the open chromatin regions described by ATAC-seq. More than 90% of the ATAC-seq regions have been identified in other cell systems.

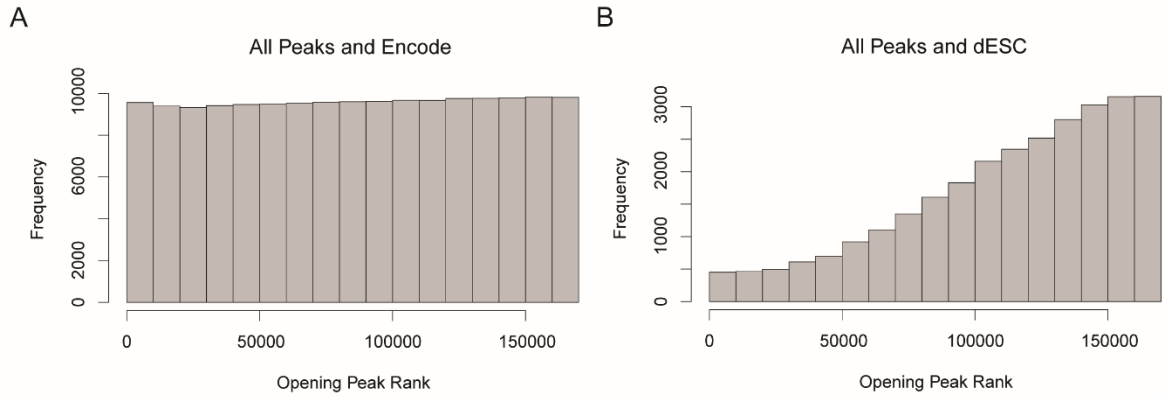

Figure 3.4. Previous DNase I HS sites in decidualizaed EnSCs described chromatin regions overlapping with closing genomic regions. ATAC-seq peaks were ranked from the ones that strongly open down to the ones that strongly close during decidualization and grouped according to this ranking; then, the number of peaks that overlapped with previously identified genomic regions was calculated. A cross-referencing with ENCODE showed a uniform distribution of the overlapping regions across this ranking (A). Previously identified DNase I HS sites in decidualized EnSCs mainly overlapped with closing ATAC-seq peaks (B).

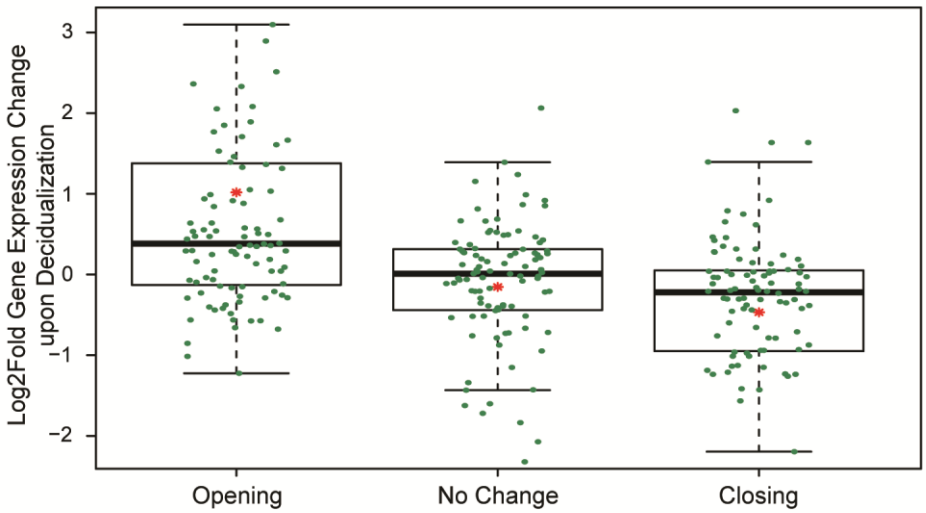

Figure 3.5. Correlation between differential organized chromatin and differential gene expression in decidualizing EnSCs. Opening and closing of chromatin correlate to changes in gene expression during decidualization. Box plots showing increase or decrease in transcript levels of 100 genes (within 10 kb of the TSS) associated with the most open and closed ATAC-seq peaks. Y-axis shows relative changes in transcript levels, expressed as log2-fold change: +ve and –ve values relate to up- and down-regulated genes, respectively. X-axis shows ATAC-seq peaks clustered in opening, no changing (N/C) and closing peaks. Green dots represent the genes and the red asterisk represents mean log2-fold change (p = 2.65 10^{-9}, t-test).

3.2.3 Binding Motif Enrichment in decidualizing EnSCs

Differential chromatin opening makes the chromatin more accessible in some genomic regions rather than in others and therefore more accessible to the binding of specific TFs, likely involved in the regulation of nearby gene expression. Hence, *de novo* binding motif enrichment analysis, using Hypergeometric Optimization of Motif EnRichment (HOMER), was performed on statistically significant opening and closing ATAC-seq peaks (Bonferroni adjusted $p < 0.05$) to identify the overepresented binding motifs and putative TFs that underly changes in gene expression upon decidualization.

A total of 17 motifs, named differentiated motifs 1-17 (DiffM1-17), were significantly enriched in 1,225 differential ATAC-seq peaks that significantly open upon decidualization and 7 motifs, named undifferentiated motifs 1-7 (UndiffM1-7), were significantly overepresented in 278 closing ATAC-seq peaks (Figure 3.6). Data showed that closing or opening of genomic regions could also be predicted by the occurrence of the motifs (Figure 3.7). Within regions of chromatin opening, TF occupancy should result in a footprint. To investigate if the identified motifs were indicative of TF binding, ATAC-seq signal was averaged over all expected locations of the identified conserved motif sequences. Average ATAC-seq signal profile centered at each motif revealed sequence footprint reflecting factor occupancy (Figure 3.8). DNA-protein binding makes the occupied genomic region refractory to transposition, causing enrichment of positive strand reads 5’ of the binding motif paired with excess of negative strand reads 3’ of the motifs. Evidence of footprints revealed the presence of DNA-binding protein in all the conserved motifs except for Opening motif 10 and Closing motif 2. Absence of footprint at these genomic sites suggested that there was no evidence of TF occupancy. However, these chromatin regions might still play a role in the regulation of gene expression. For example, they might be involved in the folding of the chromatin to facilitate interactions between functionally related genes spatially separated along the genome.

Next, to identify the putative TFs that might bind at these genomic locations, the short sequence motifs were matched against known TF datasets and their expression level was examined. HOMER motif analysis revealed overepresentation of binding sites representing high affinity binding motifs for known decidual TFs, including CCAAT/enhancer binding protein beta and delta (CEBPB/CEBPD), Fos-like antigen (FOSL2 or FRA2), forkhead box O1 (FOXO1), progesterone receptor (PGR), and signal transducer and activator of transcription 3 and 5 (STAT3/STAT5) (Mazur *et al*., 2015; Kaya *et al*., 2015; Jiang *et al*., 2015; Kim *et al*., 2005). Depletion of TEA domain transcription factor 1 (TEAD1) binding motif was dectected upon decidualization (Figure 3.9). Interestingly, TEAD1 was previously shown to negatively regulate the expression of *PRL*, a well-established decidual marker (Kessler *et al*., 2008). A full list of the best match of TFs for all of the binding motifs enriched in the opening and closing motifs are shown in Appendix 1 and 2, respectively.

Cross-referencing the resulting ATAC-seq regions with available chromatin immunoprecipitation followed by sequencing (ChIP-seq) data (e.g. ENCODE database), for PGR, FOXO1 and FOSL2 in EnSCs, provided confidence in the identified binding domains (Vasquez *et al*., 2015). In agreement with their key role in decidualization, ChIP-seq data revealed that FOXO1 and PGR binding sites were overepresented in open chromatin regions. Particularly, chromatin regions enriched with both PGR and FOSL2 binding motifs were associated to open chromatin in decidualized EnSCs, whereas in absence of PGR binding site, FOSL2 binding domain was enriched in closing chromatin regions (Figure 3.10).

Taken together, data showed that ATAC-seq accurately mapped dynamic changes upon decidual transformation. It identified binding sites for TFs known to play an essential role in promoting decidualization. However, ATAC-seq yielded novel candidate TFs likely to be involved in licensing genomic regions for remodelling in response *to* decidual transformation. The role of these putative novel transcriptional regulators in decidual transformation of EnSCs requires further investigations. Experimentally, RNA-seq or RT-qPCR and western blot could be applied to validate the induction of TFs of interest at a transcript and protein level. ChIP-qRT-PCR or cross-referencing with available ChIP-seq data

(e.g. ENCODE database) would provide confidence in the transcriptional regulation of genes of interest by specific TFs. Furthermore, silencing of the most highly ranked conserved TFs by siRNA-mediated gene silencing could be performed to validate their role during the decidual process. In this work, RNA-seq was performed to examine gene expression of new putative decidual TFs. However, time limitations prevented me of persuing this line of investigation even further.

Figure 3.6. Enriched TF binding motifs in opening and closing chromatin regions. *De novo* short sequence binding motif enrichment analysis revealed overrepresentation of 17 and 7 binding sites in statistically significant opening

and closing ATAC-seq, respectively. The frequency (%) of peaks (blue bars) containing a given motif is shown relative to genomic regions randomly selected from the genome (orange bars) (±50 Kb from TSS, matching size, and GC/CpG content).

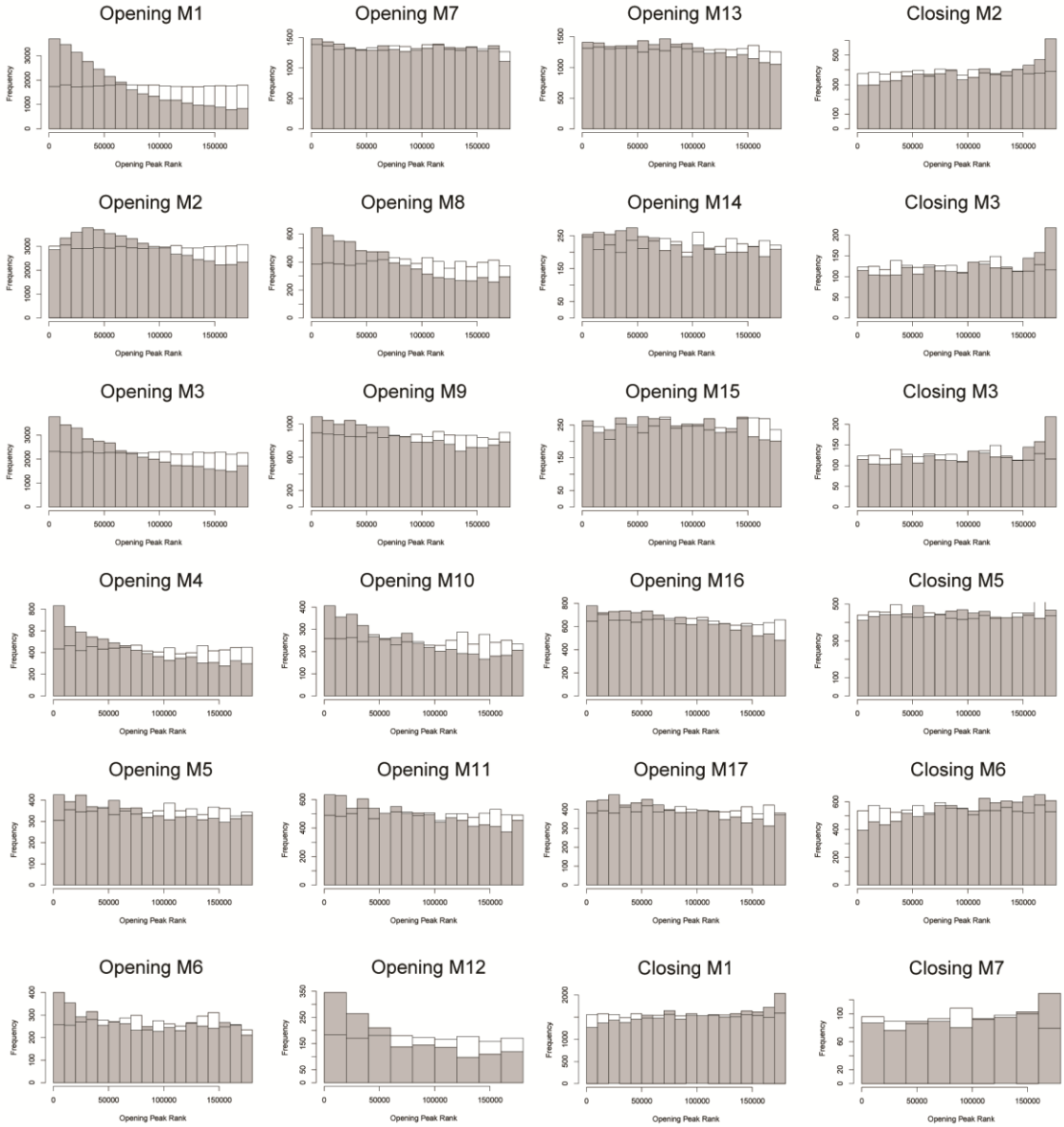

Figure 3.7. Occurrence of TF binding motifs correlates to differential chromatin opening. The short sequence binding motifs resulted from HOMER motif analysis were associated with chromatin opening and closing over the whole ATAC-seq dataset. The frequency of opening and closing motifs (Y-axis) was identified in all ATAC-seq peaks. Peaks were sorted from most opening to most closing peak and ranks of peaks containing motifs were plotted as histograms (X-axis). ATAC-seq peaks containing Opening Motifs 1-17 are most frequently opening, whereas ATAC-seq peaks containing Closing Motifs 1-7 are more frequently closing. Empty bars indicate random expectation based on genomic background frequency.

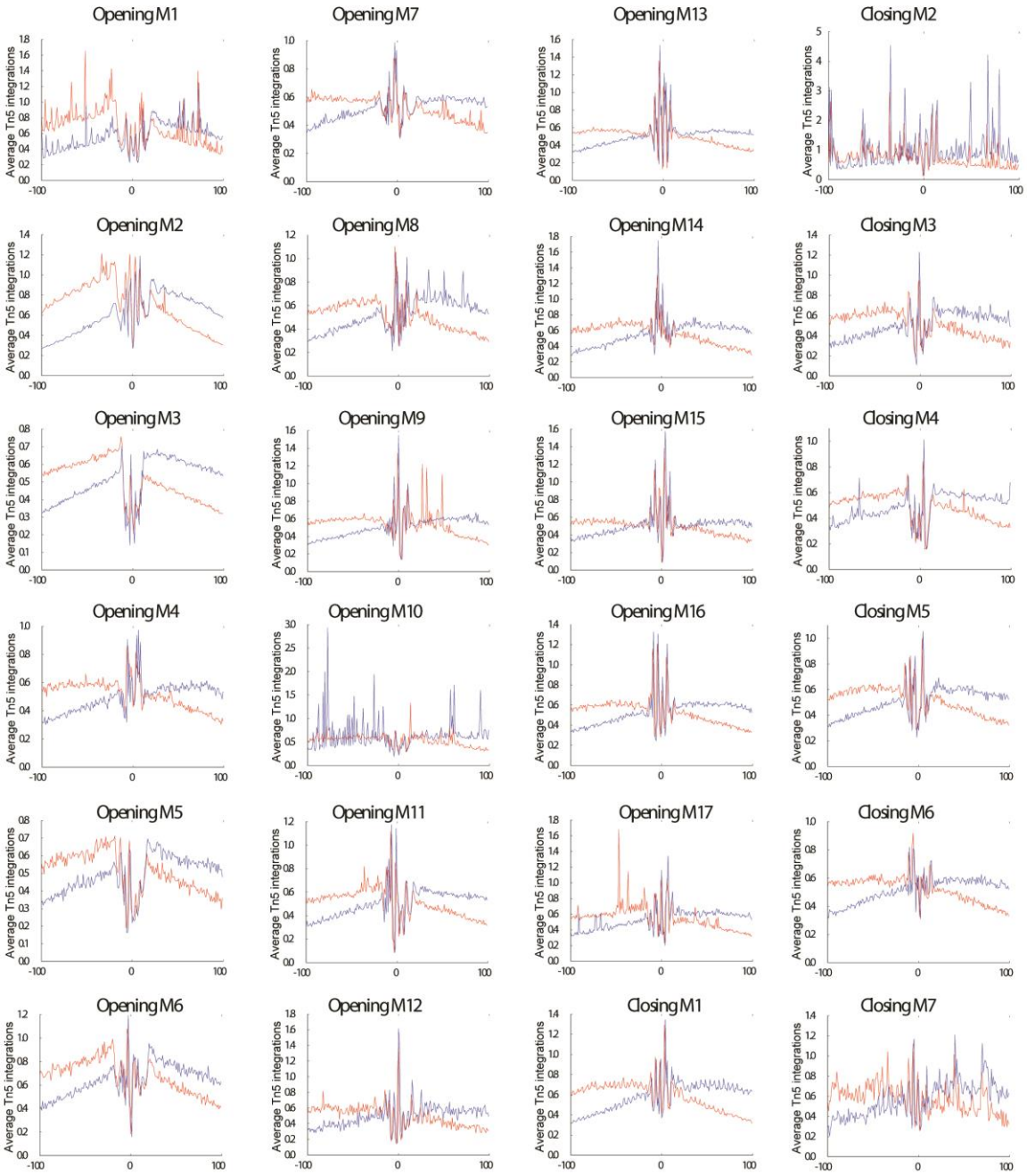

Figure 3.8. Footprint analysis. Footprint at the enriched motifs indicating evidence of TF occupancy. Graphs show average ATAC-seq signal profile centred at the opening (A) and closing (B) binding motifs, calculated within ±200 bp on enriched motif. Red and blue represent positive and negative strand cuts, respectively. Reduced read numbers in the region of the motif together with increase in positive and negative strand reads at 5' and 3' of the motif indicate enrichment of fragments that span the uncut (protected) region of DNA binding.

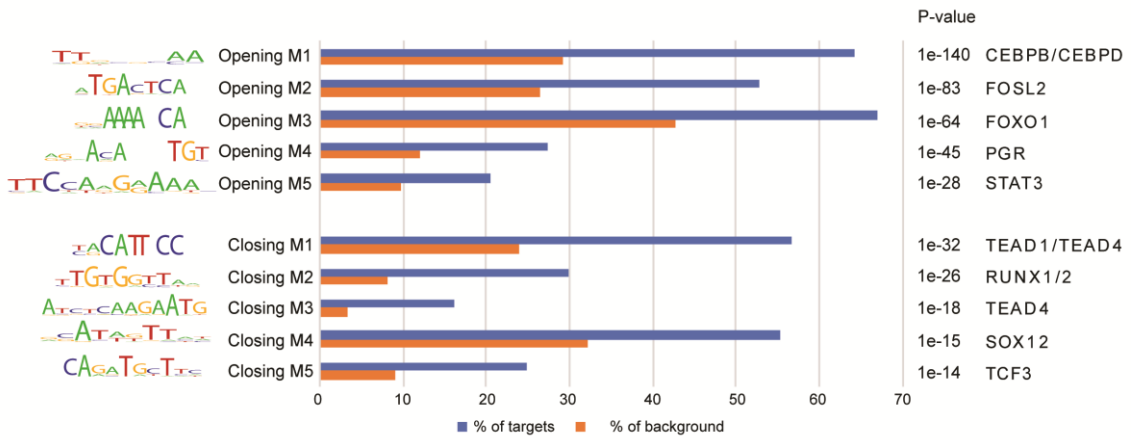

Figure 3.9. Top 5 enriched and depleted binding motifs and coupled high binding affinity TFs. Bar graphs showing top 5 binding motifs, enriched in the opening and closing ATAC-seq peaks, matched with the most plausible differentially expressed TFs, based on motif specificity. In the bar graphs, the frequency (%) of peaks (blue bars) containing the motif is shown relative to genomic regions randomly selected from the genome (orange bars) (±50 Kb from TSS, matching size, and GC/CpG content). *P* indicates the *p* of the short sequence binding motifs.

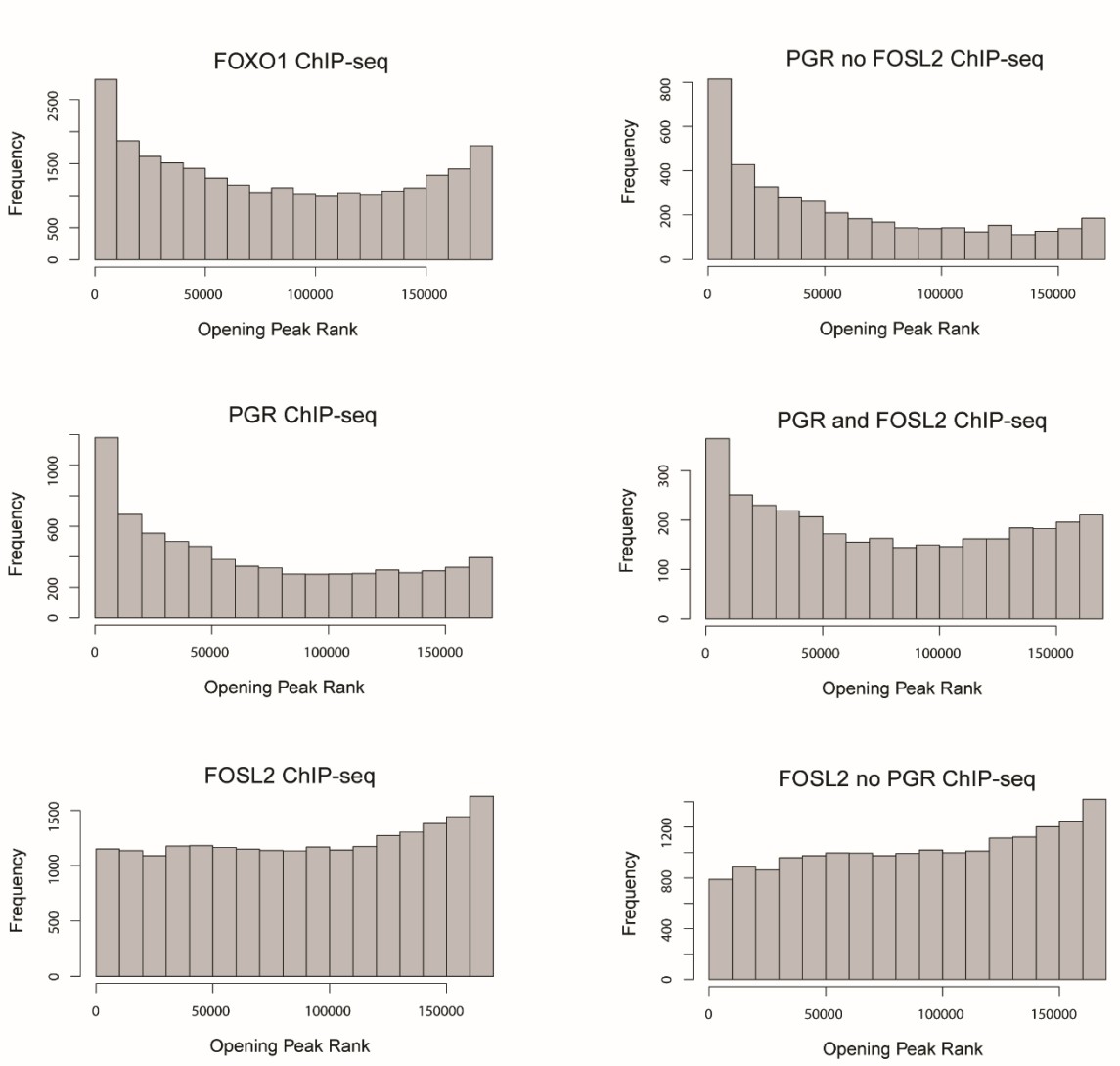

Figure 3.10. Mapping of known FOXO1, PGR and FOSL2 binding domains in the differential ATAC-seq peaks in decidualized EnSCs. Cross-reference of ATAC-seq data with public ChIP-seq data for the indicated key transcription factors during decidualization, revealed enrichment of FOXO1 and PGR binding motifs in the opening genomic regions; FOSL2 binding motif was enriched in closing chromatin regions, whereas FOSL2 in the presence of PGR binding domain was associated to opening chromatin regions. Again, ATAC-seq peaks were ranked from the most strongly opening to the most strongly closing peak.

3.2.4 Transcriptomic profile of human undifferentiated and decidualizing EnSCs

Microarray studies described profound changes in the transcriptome of EnSCs as the decidual transformation unfolds (Gellersen & Brosens, 2014; Giudice, 2004; Clock *et al*., 2008; Takano *et al*., 2007). Compelling lines of evidence indicate the presence of a dynamic epigenetic code governing differential gene expression upon decidualization (Munro *et al*., 2010; Zelenko *et al*., 2012). For the first time, ATAC-seq accurately mapped changes in chromatin accessibility in undifferentiated and decidualizing human EnSCs upon decidualization. Binding motif discovery confirmed enrichment in *cis*-regulatory regions of the genome for short sequence binding motifs with high affinity for TFs known as key decidual core TFs. However, ATAC-seq data potentially revealed novel candidate TFs that might play a role in the acquisition of the decidual phenotype. To examine gene expression of TFs likely to bind high specificity short sequence motifs, EnSCs decidualized in response to 8-br-cAMP and MPA for 4 days were subjected to RNA-seq.

RNA libraries, generated using high integrity samples with a RIN > 8.0, were sequenced on the Illumina HiSeq3000. Fifty million single end reads were sequenced per sample, with a read length of 50 base pairs (bp). Principal Component Analysis (PCA), a multivariate analysis, was performed on the regularized log (rlog) transformation of the counts from differential expression analysis of sequencing data (DESeq) to explore how the samples clustered or segregate. In this work, PCA was perfomed in an unsupervised manner, i.e. undifferentiated and decidualizing samples were not ‘labeled’ as such. PC1, which accounted for 83% of variation in gene expression segregated undifferentiated from decidualizing EnSCs, thus reflecting the cellular response to deciduogenic cues. PC2, which accounted for 12% of variation, clustered the undifferentiated samples 198 and 200, apart from the 208; and the decidualizing samples 208, apart from 200 and 198, thus reflecting intrinsic interpatient variability (Figure 3.11).

Based on Benjamini adjusted *p* (*q)* < 0.05, DESeq identified a robust list of 2,931 differentially expressed genes between undifferentiated and decidualizing cultures (Figure 3.12). Out of 2,931 differentially expressed genes, 1,432 (49%) were up-regulated and 1,499 (51%) were down-regulated upon decidualization. Amongst the most highly enriched genes, data confirmed up-regulation of key decidual markers, such as *PRL* ($q = 2.60 \times 10^{-93}$) and *IGFBP1* ($q = 5.32 \times 10^{-98}$) (Gellersen & Brosens, 2003). A full list of differentially up- and down- regulated genes is shown in Appendix 3 and 4, respectively.

Mining of RNA-seq data to infer gene expression of putative candidate TFs likely to bind short sequence motifs mapped in opening and closing motifs confirmed gene expression for known key decidual TFs, including CEBPB/CEBPB, FOSL2 (or FRA2), FOXO1, PGR and STAT3/STAT5. However, data revealed differential gene regulation for several candidates (Figure 3.13). For example RAR related orphan receptor A (RORA), aryl hydrocarbon receptor nuclear translocator like (ARNTL) and Meis homeobox 1 (MEIS1). Conversely, combined RNA-seq and ATAC-seq revealed downregulation of runt related transcription factor 1 and 2 (RUNX1/RUNX2), SRY-box 12 (SOX12), transcription factor 3 (TCF3), and ETS Proto-Oncogene 1 (ETS1) in parallel with depletion of genome-wide depletion of high affinity binding sites in decidualized EnSCs.

Gene Ontology (GO) enrichment analysis was performed using DAVID version 6.8 to characterize differentially expressed genes in EnSCs upon decidualization and infer associated biological functions, cellular components and molecular functions and ultimately confirm if the EnSC cultures were properly decidualized. Amongst the most up-regulated GO categories, data showed enrichment for extracellular matrix organization ($p = 3.30 \times 10^{-7}$), inflammatory response ($p = 1.29 \times 10^{-6}$) and angiogenesis ($p = 5.85 \times 10\text{-}6$). Down-regulated genes were enriched for cell division ($p = 3.99 \times 10^{-21}$), DNA replication ($p = 1.08 \times 10\text{-}19$) and mitotic nuclear division ($p = 5.34 \times 10^{-18}$) (Figure 3.14A-B). Enrichment and depletion of the identified GO categories were consistent with the known spectrum of functions differentially regulated upon decidualization, confirming what was already broadly studied (Gellersen & Brosens, 2014).

Taken together, data confirmed a broadly wholesale reprogramming of gene expression upon decidualization and captured expression of novel putative modulators that might be implicated in promoting the acquisition of the decidual phenotype.

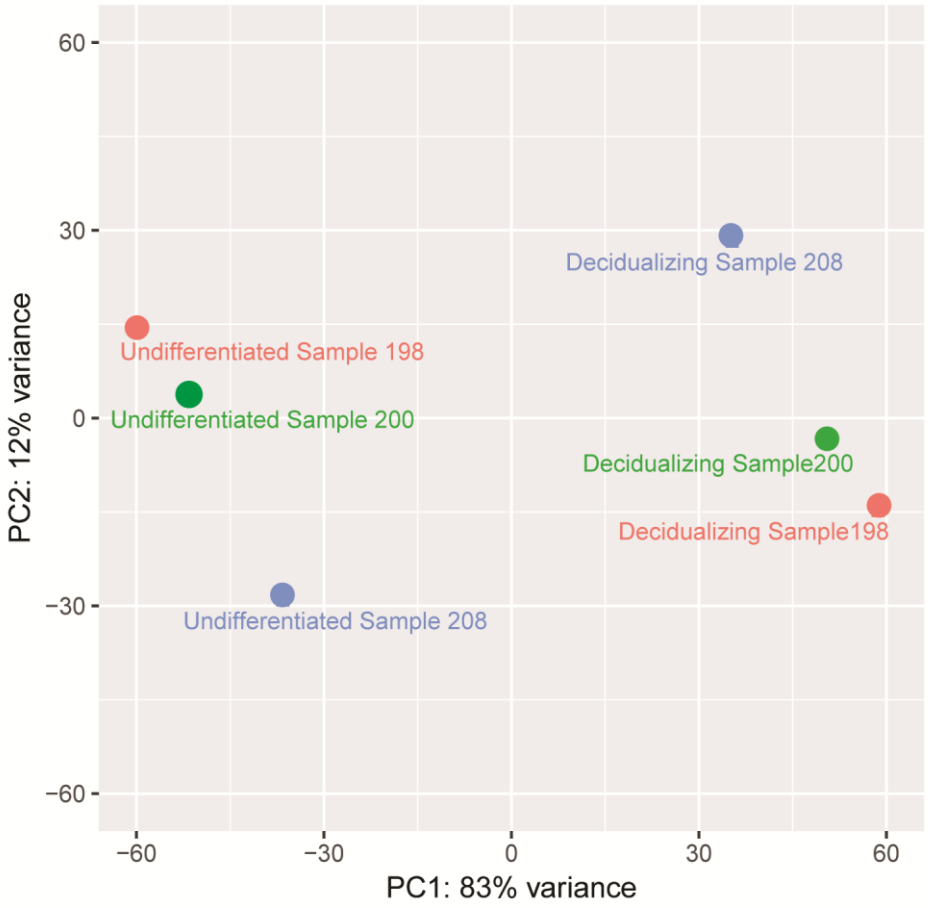

Figure 3.11. PCA of undifferentiated and decidualizing EnSCs. PCA of RNA-sequencing data from three independent EnSC cultures, decidualized in response to 8-br-cAMP and MPA for 4 days. PC1 distinguished between undifferentiated and decidualizing samples, whereas PC2 segregated different primary cultures.

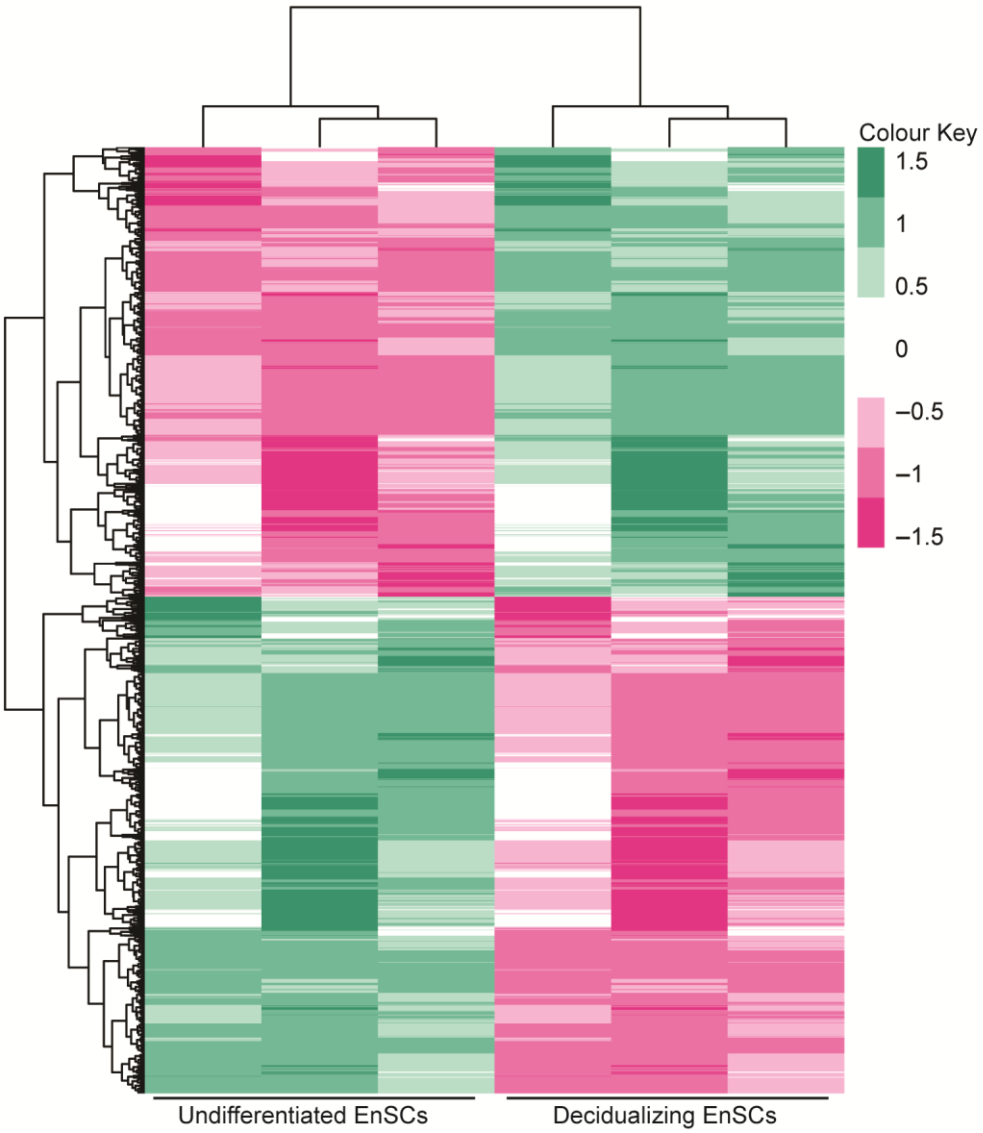

Figure 3.12. Differential gene expression profile upon decidualization. Clustered heatmap representing differential gene expression pattern in EnSCs decidualized in response to 8-br-cAMP and MPA for 4 days**.** The colour key is represented on the right side of the heatmap, with the most highly enriched genes indicated in green.

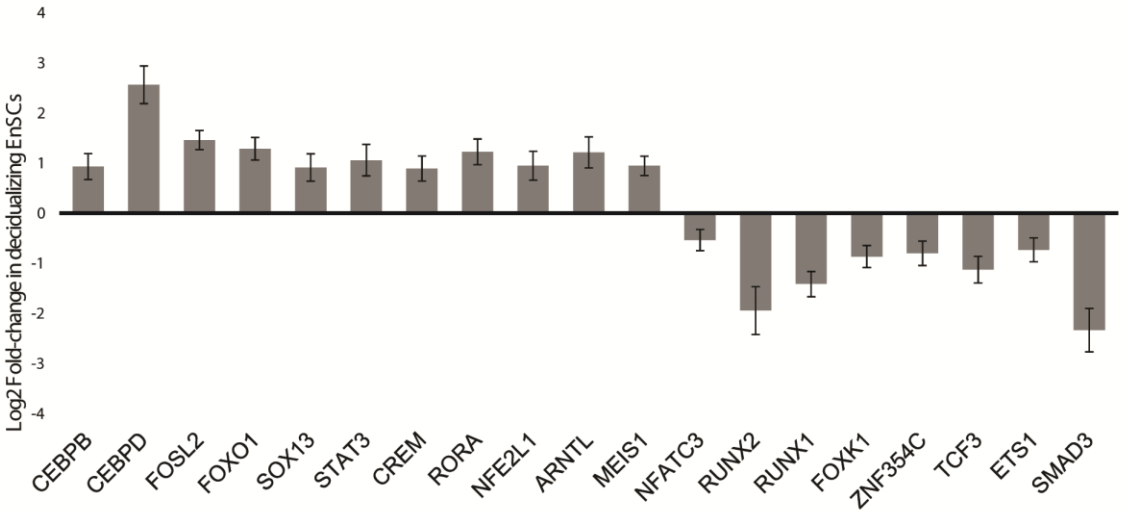

Figure 3.13. Differential expression of candidate TFs upon decidualization. Graph showing changes in the transcript levels of selected significantly up- and down-regulated TFs, expressed as log2-fold change. +ve and -ve values indicate increase and decrease in gene expression, respectively.

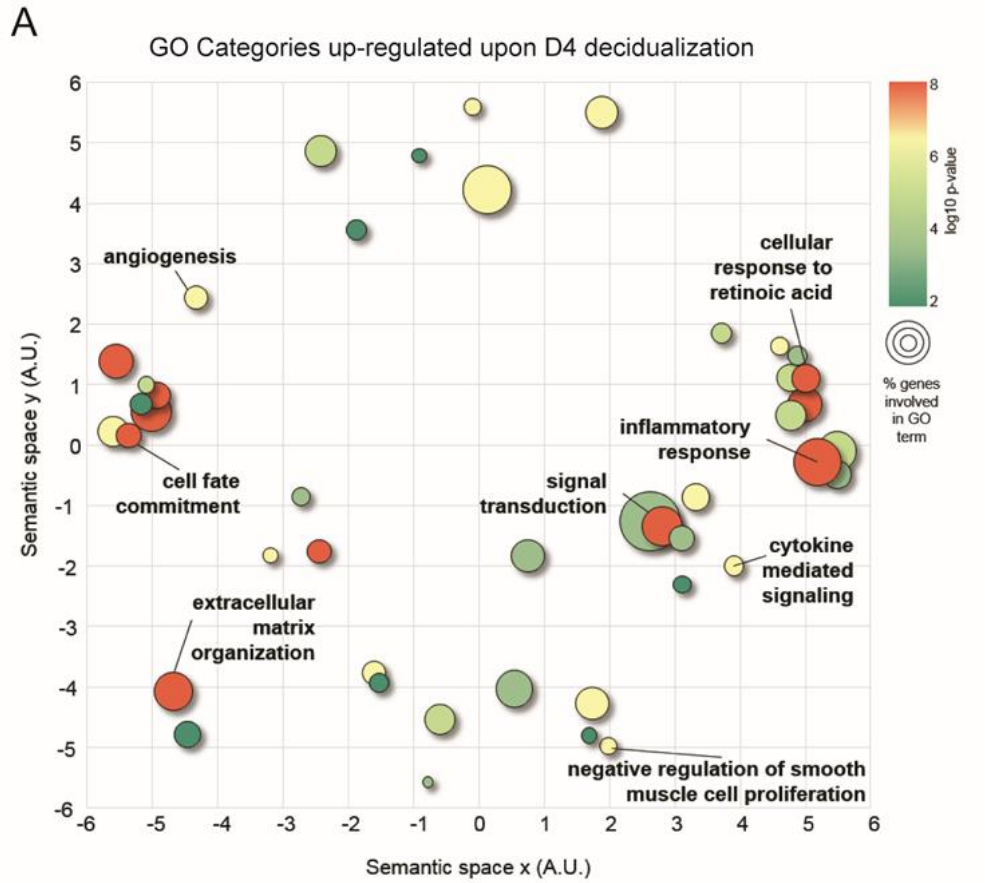
A
GO Categories up-regulated upon D4 decidualization
angiogenesis
cellular response to retinoic acid
inflammatory response
cell fate commitment
signal transduction
cytokine mediated signaling
extracellular matrix organization
negative regulation of smooth muscle cell proliferation
Semantic space y (A.U.)
Semantic space x (A.U.)
log10 p-value
% genes involved in GO term

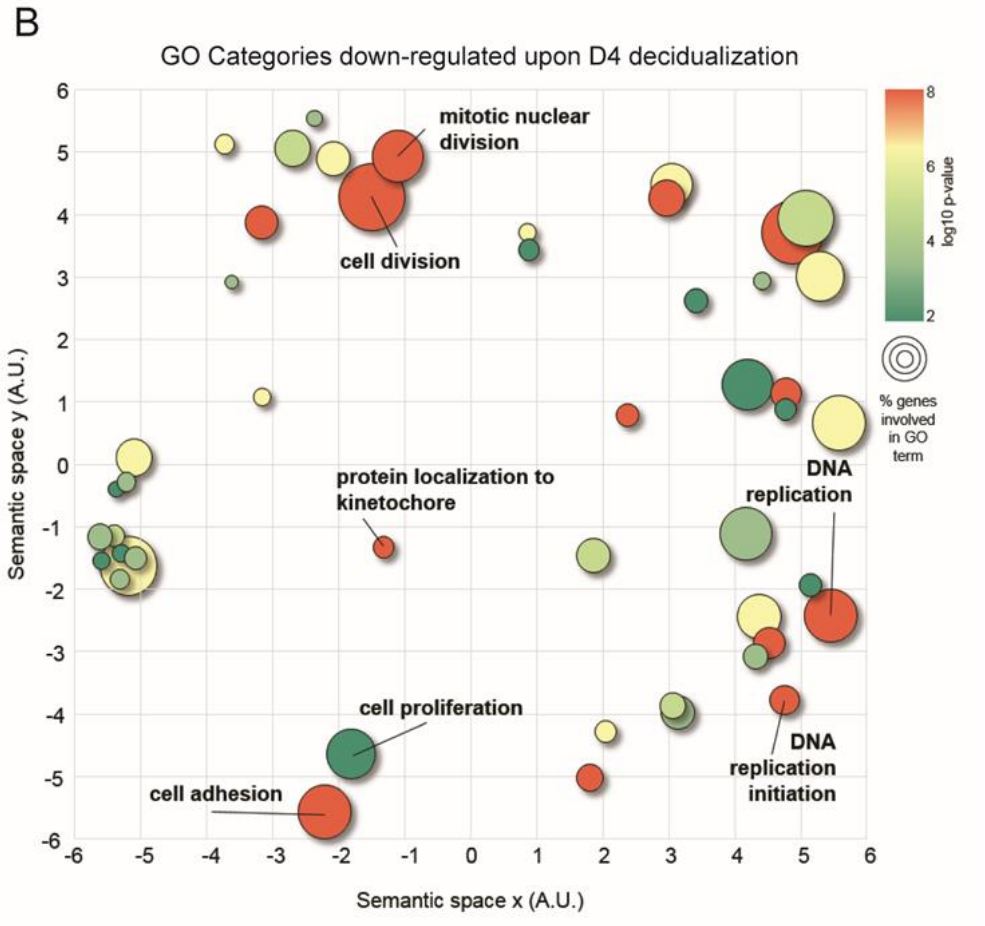
B
GO Categories down-regulated upon D4 decidualization
mitotic nuclear division
cell division
protein localization to kinetochore
DNA replication
cell proliferation
cell adhesion
DNA replication initiation
Semantic space y (A.U.)
Semantic space x (A.U.)
log10 p-value
% genes involved in GO term

Figure 3.14 Enrichment and depletion of GO categories in primary EnSCs upon decidualization. GO enrichment analysis was applied to differentially expressed genes and the significant GO annotations ($p < 0.05$) summarized using REVIGO and clustered based on semantic similarities, which means that if they are described by a common ontology they cluster close in the graph. (A) GO categories associated to the up-regulated genes. (B) GO categories enriched for down-regulated genes. The colour key is represented on the right. The most highly enriched GO categories are indicated in green. The size of the circles indicates the number of genes in the GO term and reflects the frequency of the GO term. The results were consistent with the known spectrum of biological processes differentially regulated upon decidualization and hence validated previous findings.

3.3 Discussion

Cyclic decidualization of the endometrium is a coordinated process essential for embryo implantation and placental development, and hence is critical for successful reproductive outcome (Gellersen & Brosens, 2014; Salker *et al*., 2011). Several lines of evidence show that a dynamic epigenetic code operates atop the *cis*-regulatory landscape of the genome and governs decidual cell identity (Grimaldi *et al*., 2012; Zelenko *et al*., 2010; Munro *et al*., 2010).

In this work, I used ATAC-seq to accurately probe regions of differential chromatin opening in undifferentiated and decidualizing human EnSCs. ATAC-seq data showed wholesale remodelling of the chromatin structure. A total of 185,084 open DNA loci were accurately mapped in EnSC. Changes in genomic accessibility at major decidual genes, such as *PRL* and *IGFBP1* confirmed the ability of ATAC-seq to accurately map changes in the *cis-regulatory* elements of the chromatin. Combined ATAC-seq and RNA-seq revealed a strong association between changes in DNA accessibility and in gene expression.

De novo binding motif discovery using HOMER revealed enrichment and depletion of 17 and 7 short sequence motifs, respectively. Analysis of footprints confirmed factor occupancy in 22 out of 24 binding motifs, highlighting the presence of DNA-binding proteins in the majority of the biding sites. Highly enriched motifs in the opening ATAC-seq peaks showed high binding affinity for known decidual TFs, including CEBPB/CEBPD, FOSL2, FOXO1, PGR, and STAT3/STAT5 (Gellersen & Brosens, 2014; Mazur *et al*., 2015). Previous studies reported that interactions between TFs can differently modify chromatin accessibility (Christian *et al*., 2002; Christian *et al*., 2002; Lynch *et al*., 2009). More accurately, cross-referencing of ATAC-seq data with ChIP-seq data showed that enrichment for both FOXO1 and PGR binding sites correlated to opening chromatin (Mazur *et al*., 2015; Vasquet *et al*., 2015). Additionally, FOSL2 is a putative PGR co-regulator (Mazur *et al*., 2015). Interestingly, the presence of both FOSL2 and PGR binding sites correlated with opening chromatin. However, binding sites with high affinity for FOSL2 in the absence of PGR were enriched in closing chromatin regions.

Cross-referencing the identified binding motifs with RNA-seq data revealed induction of novel putative TFs not yet implicated in decidualization, in parallel with genome-wide enrichment for high affinity binding sites, for example RORA, ARNTL, and MEIS1. Conversely, down-regulation of other TFs, including RUNX1/RUNX2, SOX12, TCF3 and ETS1 upon decidualization correlated with depletion of high affinity binding sites.

The role of these putative transcriptional regulators in decidual transformation of EnSCs requires further investigation. Experimentally, Real Time quantitative PCR (RT-qPCR) and western blot could be applied to validate the induction of TFs of interest at a transcript and protein level. ChIP-qRT-PCR or cross-referencing with available ChIP-seq data (e.g. ENCODE database), would provide confidence in the transcriptional regulation of genes of interest by specific TFs. Furthermore, silencing of the most highly ranked conserved TFs by siRNA-mediated gene silencing could be performed to validate their role upon decidualization. Time limitations prevented me of persuing this line of investigation even further, although a graduate student subsequently demonstrated that siRNA-mediated knockdown of *ARNTL*, *NFE2L1* and *TFC3* perturbated the induction of *PRL* and *IGFBP1* in decidualizing cultures.

The ATAC-seq analysis of undifferentiated and decidualizing EnSCs is important on multiple levels. First, it provides an important resource to analyse chromatin changes associated with differential gene expression at specific loci. The footprint analysis provides insight into the transcriptional drivers of genes of interests, although confirmation still requires ChIP-PCR or cross-referencing with existing ChIP-seq data sets. Nevertheless, the ATAC-seq data will greatly facilitate mechanistic analysis of the pathways and downstream TFs that regulate specific genes or gene networks. Finally, my analysis provided proof of principle that ATAC-seq is a powerful tool to screen rapidly for dynamic chromatin changes in human endometrial cells. I envisage that applying this technique to various reproductive disorders associated with aberrant endometrial function, such as endometriosis, endometrial cancer, infertility and recurrent miscarriage, will yield important mechanistic insights into the underlying pathological pathways.

Chapter 4

Characterization of endometrial mesenchymal stem cells expanded in culture in response to TGF-β-Receptor blockade

4.1 Introduction

The endometrium is a highly dynamic tissue that undergoes cyclic waves of proliferation, differentiation (decidualization) and menstruation. Its extraordinary ability to adapt to changes, physiological or otherwise, depends on eMSCs (Gargett *et al*., 2016).

eMSCs are a rare group of cells (around 1-4%) recently identified in the perivascular niche of the endometrium (Masuda *et al*., 2012; Schwab & Gargett, 2007) from where they can be selectively isolated on basis of co-expression of two cell surface markers, CD140b and CD146 (Schwab & Gargett, 2007), or with a single marker, SUSD2. By using a single marker, eMSCs can be isolated using magnetic-activated cell sorting, which results in a higher yield of viable cells when compared to flow cytometry and cell sorting (Masuda *et al*., 2012).

eMSCs are immune-privileged, clonogenic and self-renewing cells. eMSCs also exhibit high proliferative potential and have the ability to differentiate into more mature progeny and regenerate tissue (Gargett *et al*., 2016; Miyazaki *et al*., 2012; Wolff *et al*., 2007). The perivascular niche is a privileged site for eMSCs to contribute to cyclic endometrial regeneration and formation of the placenta during pregnancy (Murakami *et al*., 2014). eMSCs are also promising candidates for cell-based therapy for women's reproductive health disorders, including pelvic organ prolapse, urinary incontinence and regeneration of scarring endometrium in women affected by Asherman's syndrome (Darzi *et al.*, 2016; Emmerson & Gargett, 2016; Gargett & Healy, 2011).

Because of their rarity, the use of eMSCs for clinical trials first requires their expansion in culture (Ulrich *et al*., 2013). As in the case of MSCs from other cell systems (Baxter *et al*., 2004), eMSCs spontaneously differentiate over several passages (Zhu *et al*., 2011; Ulrich *et al*., 2014; Barragan *et al*., 2016; Gargett *et al*., 2016). During prolonged expansion in culture, the telomeres of eMSCs become shortened due to replicative stress. Consequently, eMSCs lose their proliferative capacity as well as the ability to reconstitute tissue *in vivo* (Baxter *et*

al., 2004; Banfi *et al*., 2002). Therefore, the effectiveness of eMSCs in cell-based therapies is curtailed by the need for extended cultures.

The use of small molecules that modulates stem cell specification and function offers significant opportunities to study the cell biology and enhance our knowledge of the therapeutic potential of stem cells (Yu *et al*., 2014; Li *et al*., 2013). Small molecules can act as activators or repressors of signalling pathways. In this way, they regulate downstream gene transcription (Yun *et al*., 2014). The use of a TGF-β type I receptor ALK4, 5 and 7 kinase inhibitor, A83-01, to maintain self-renewal of induced pluripotent stem (iPS) cells in prolonged culture exemplified such approach (Li *et al*., 2009). A recent study showed that the use of a small molecule, A83-01, a selective inhibitor of TGF-β type I receptor ALK4, 5 and 7 kinase, increases eMSC proliferation and prevents senescence, thereby maintaining the functional properties of eMSCs (Gurung *et al*., 2015). The use of small molecules, such as A83-01, which are purported to control self-renewal and proliferative ability of eMSCs, might be an effective strategy to maintain eMSCs in a stem cell-like state during prolonged culture.

For clinical application, it is of paramount importance to understand the mechanisms underlying pharmacological expansion of eMSCs in culture. In this chapter, I validated the effect of A83-01-induced TGF-β-Receptor (TGF-β-R) blockade on the proliferative capacity of cultured eMSCs and the expression of stem cell markers. Furthermore, I combined RNA-sequencing with ATAC-sequencing to define the impact of TGF-β-R inhibition on the transcriptome and chromatin landscape of cultured eMSCs.

4.2 Results

4.2.1 TGF-β-R signalling pathway negatively regulates eMSC expansion in prolonged culture.

To assess the effect of the TGF-β-R inhibitor A83-01 on proliferation, eMSCs isolated from three independent human endometrial biopsies using SUSD2-magnetic bead sorting were expanded in culture in the presence or absence of 1 µM A83-01 for 36 days. The cells were seeded at low density (10,000 cells/well in 24-well plate) and passaged on day 15, 22, 29 and 36. The plating density at passaging was 5,000 cells/cm^2. At each passage, the cells were counted using glasstic slide 10 with grids and cumulative cell population calculated as an indicator of proliferative potential.

As shown in Figure 4.1A, the effect of A83-01 on eMSC proliferation was consistent between different primary cultures (Figure 4.1A). Cumulative cell population was comparable between A83-01 treated and untreated cells up to 22 days in culture, after which cells treated with A83-01 exhibited a clear proliferation advantage (Figure 4.1B; $p < 0.05$). The relative difference in cumulative cell population in 3 paired treated and untreated primary cultures at day 36 was 400%, 500%, and 1,800% (Figure 4.1C).

The effect of the TGF-β-R inhibitor on cell proliferation was evaluated further by calculating the number of population doublings (PDs) using the following formula: PD = 3.322logN/N0, where N is the total cumulative cell number calculated at each passage and N0 represents the initial number of seeded primary cells (Pellegrini *et al.*, 1999). The effect of A83-01 on the number of population doublings was consistent between different samples (Figure 4.2A). Figure 2B shows that, after the first 15 days of culture, A83-01 treatment progressively increased the number of PDs, confirming that A83-01 positively regulates the proliferative potential of eMSCs. A83-01 treatment consistently resulted in increased population doubling, although statistical significance, as determined by ANOVA, was not reached ($p > 0.05$).

Taken together, the data suggest that TGF-β-R signalling plays a role in limiting the proliferative potential of eMSCs maintained in continuous cultures. As the proliferative capacity of freshly isolated eMSCs is very high, A83-01 treatment conferred proliferation advantage only after 3 weeks in culture.

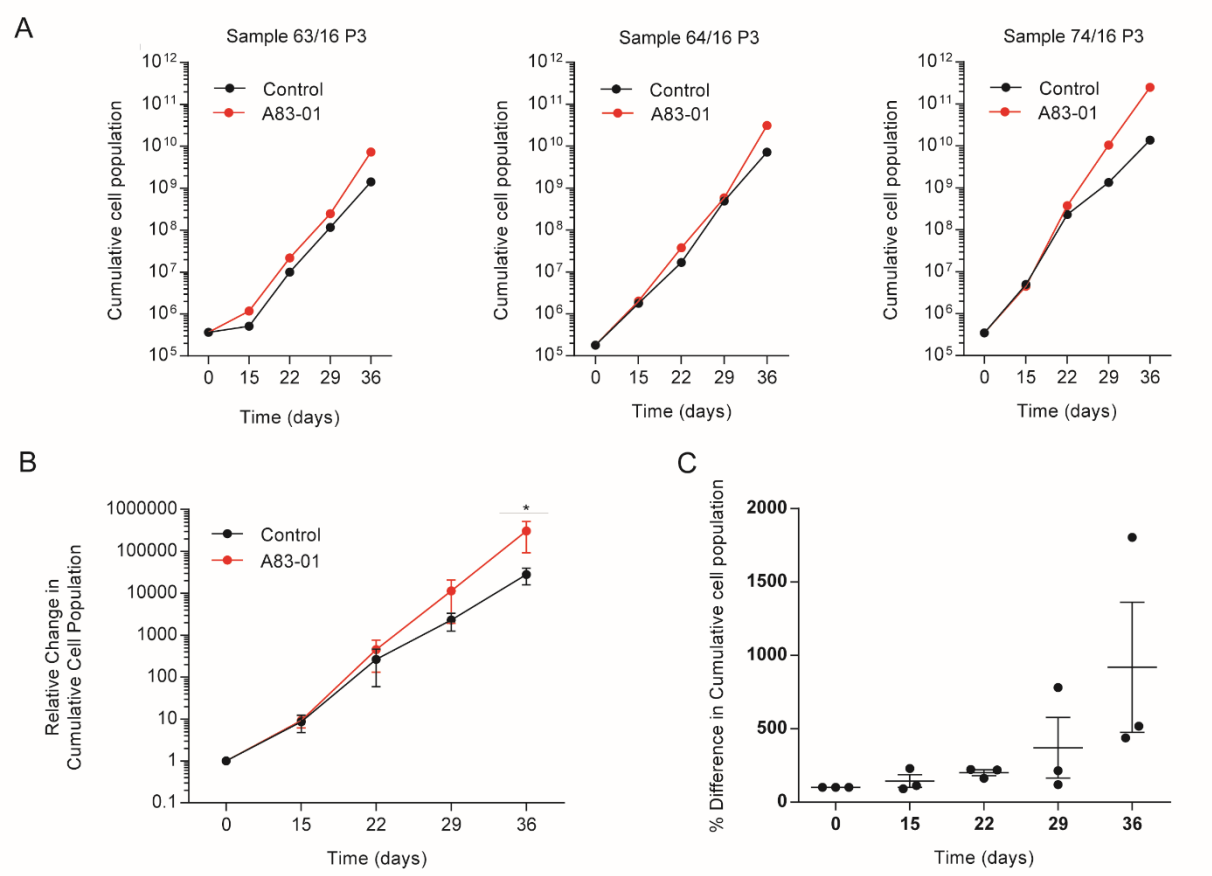

Figure 4.1. TGF-β-R inhibitor improves expansion of eMSCs in culture. Primary human eMSCs, isolated using SUSD2 magnetic bead sorting, were cultured with or without 1 µM A83-01 for 5 weeks. (A) Individual biological replicates. (B) Relative change in cumulative cell population in 3 independent cultures. Data represent mean ± SEM; * indicates $p < 0.05$. Note the logarithmic scale of the Y-axis. (C) Percentage change in cumulative cell population in eMSC cultures treated with A83-01 compared to untreated cultures at the indicated time-points.

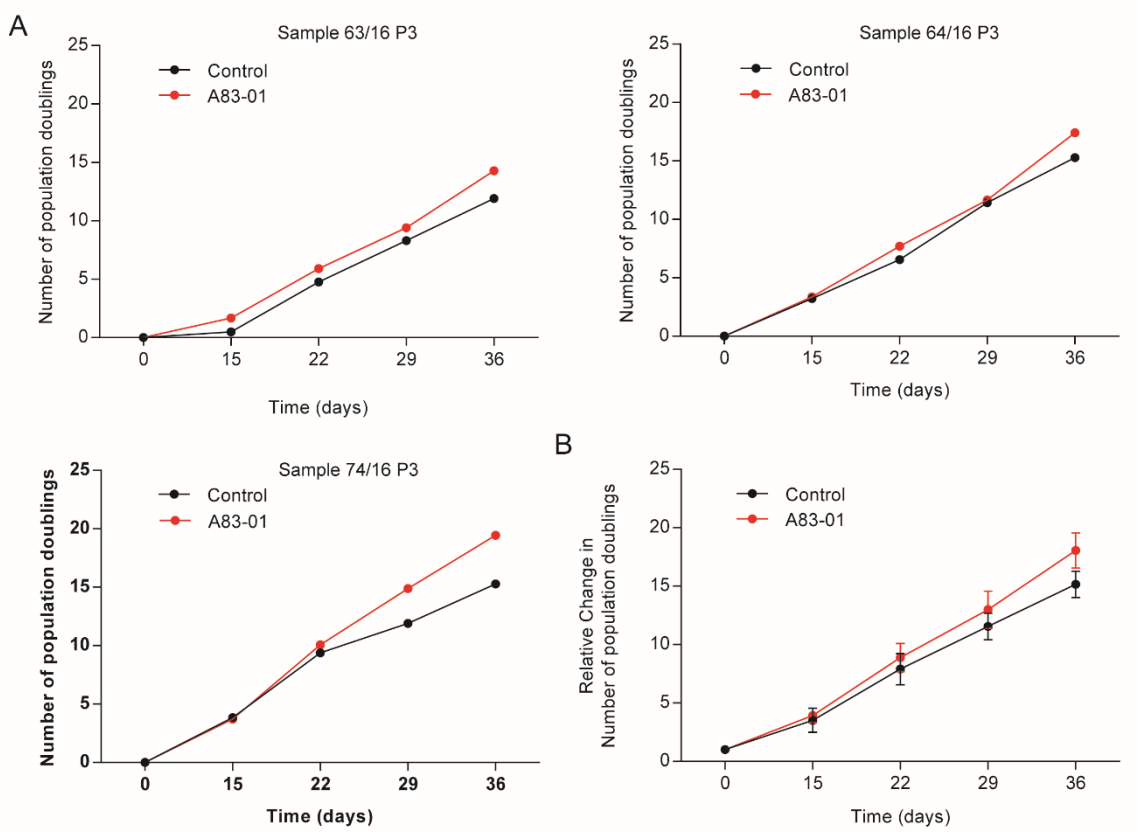

Figure 4.2. A83-01 increases population doubling (PD) in eMSCs. Proliferative activity was assessed by calculating the number of PDs according to the formula: PD = 3.322logN/N0, where N is the total cumulative cell number calculated at each passage and N0 represents the initial number of seeded primary cells. (A) Impact of A83-01 on PD of 3 individual primary cultures at the indicated time-points. (B) Relative change in population doublings. Data represent mean ± SEM of three independent samples.

4.2.2 Phenotyping of A83-01 treated eMSCs

eMSCs express specific surface markers that are widely used to define cell identity and stemness, including CD146, CD140b, SUSD2 and CD90 (Gargett & Masuda, 2010). Co-expression of CD146 and CD140b (Schwab & Gargett, 2007), or single marker SUSD2 (Masuda *et al.,* 2012) can be used to selectively isolate eMSCs, using magnetic flow cytometry and magnetic bead sorting, respectively. However, magnetic isolation of clonogenic eMSCs increases the number of viable cells compared with flow cytometry, as it is less damaging to the cells (Schwab & Gargett, 2007; Masuda *et al.,* 2012). The percentage of CD146+ cells has been already previously shown not to change upon A83-01 treatment (Gurung *et al.,* 2015), hence it was excluded for this analysis. CD90 is a marker of endometrial stromal cells, but not epithelial cells and it has been shown that SUSD2+ cells are predominantely CD90+ perivascular cells (Schwab *et al.,* 2008; Gargett *et al.,* 2016). Hence, it is been included in this study. To assess the effect of TGF-β-R inhibition on the expression of these phenotypic markers, A83-01 treated and untreated primary eMSCs were subjected to flow cytometry at day 36. This time-point was chosen as the impact of A83-01 on cell proliferation was apparent.

The effect of A83-01 on the expression of these surface markers was consistent between different eMSC cultures (Figure 4.3aA). The percentage of CD90 positive cells did not change upon TGF-β-R blockade. By contrast, A83-01 treatment resulted in an increase in the percentage of CD140b- and SUSD2-positive cells when compared to untreated eMSCs, although statistical significance was not reached ($p > 0.05$) (Figure 4.3aB-C; 43b).

Mean Fluorescence Intensity (MFI) was also calculated to evaluate if there was an increase in the abundance of cell surface molecules per cell. Again, A83-01 cellular effects were consistent between different primary cultures (Figure 4.4A, 4.5A and 4.6A). The MFI for CD90 expression did not change significantly upon A83-01 treatment, although the response was variable between cultures (Figure 4.4A-B). By contrast, the MFI of CD140b consistently increased in response to

A83-01treatment (Figure 4.5B) although statistical significance was not reached ($p > 0.05$). For SUSD2 expression, the MFI increased markedly in 2 out of 3 primary cultures (Figure 4.6A). This induction was not statistically significant when paired non parametric Wilcoxon test was applied (Figure 4.6B).

Altogether, these results confirm that A83-01 has a positive effect on the percentage of CD140b- and SUSD2-positive cells in prolonged culture. However, the data also reveal marked variation in the responsiveness of primary cultured eMSCs to A83-01. This intrinsic variability between primary cultures accounted for the lack of statistically significance.

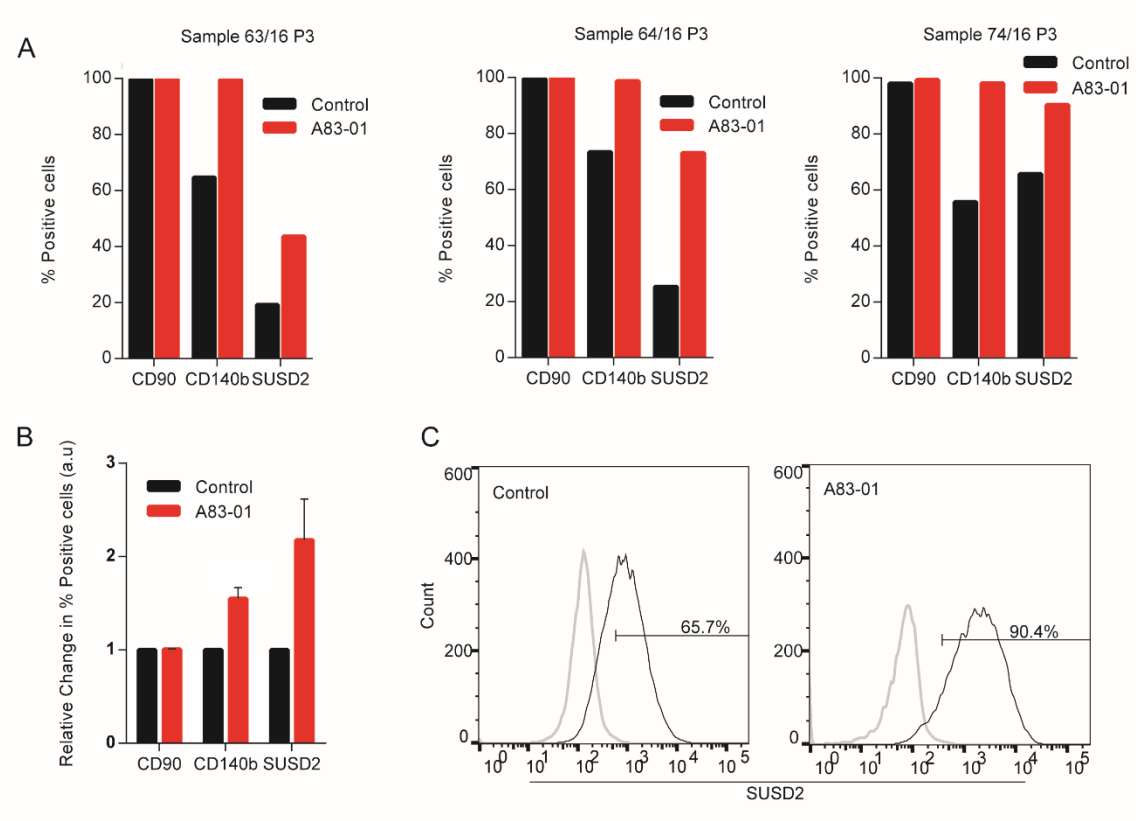

Figure 4.3a. Surface phenotype of eMSCs cultured with or without A83-01. A83-01 cellular effects were consistent on different eMSC primary cultures (A). Flow cytometry analysis for three eMSC surface markers in 3 independent eMSC culture (B). Mean change (± SEM) in positive cells for the indicated cell surface markers. (C) Representative flow cytometry histograms of SUSD2 positive cells in eMSC cultures, treated with or without A83-01. The X-axis shows the fluorescence intensity and the Y-axis the number of cells (count); the grey curves represent the isotype control IgG.

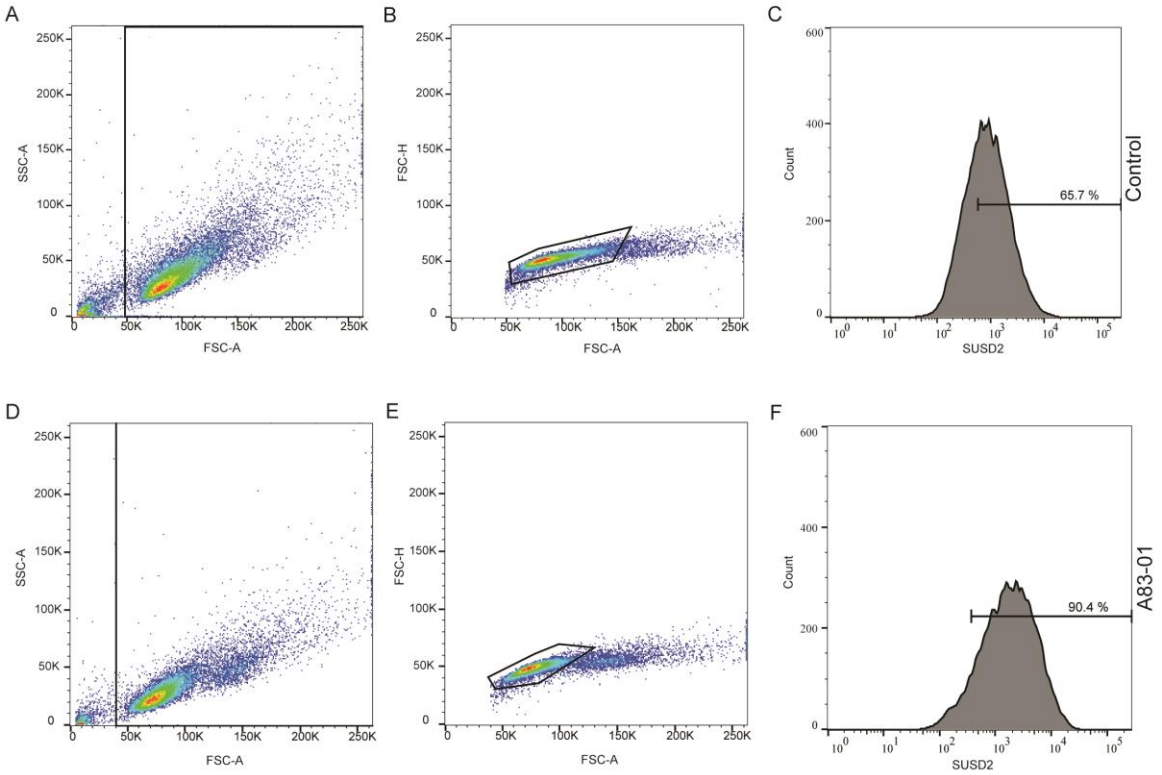

Figure 4.3b. Representative flow cytometry representation. These graphs show representative flow cytometry figures for SUSD2 marker in untreated (A-B-C) and A83-01 treated eMSC (D-E-F) cultures, showing serial gating strategies. (A) Forward versus side scatter density plot used to gate cells of interest based on size and granularity. Based on light refraction, forward scatter area (FSC-A) indicates cell size and side scatter area (SSC-A) relates to granularity of the cells. (B). Forward scatter height (FSC-H) versus FSC-A density plot is used to exclude doublets. (C). Single paramenter histogram for identifying cells expressing SUSD2 marker. Similar gating strategies were used for flow cytometry analysis in A83-01 treated eMSC cultures.

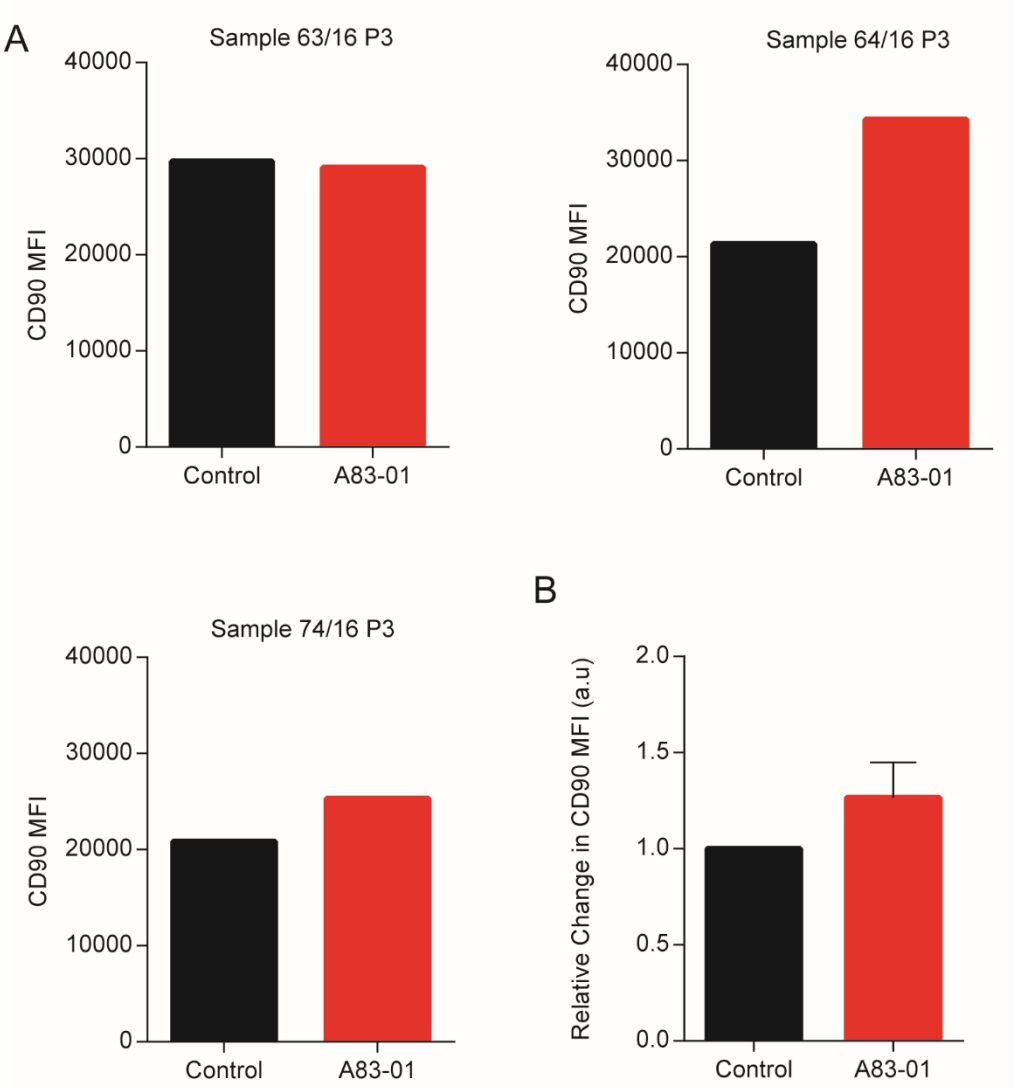

Figure 4.4. Mean Fluorescence Intensity (MFI) of CD90 in A83-01 treated eMSCs. (A) MFI for CD90 in 3 independent eMSC cultures cultured for 36 days in the presence or absence of A83-01. Each graph represents an individual culture. (B) Relative change (mean ± SEM) in CD90 MFI.

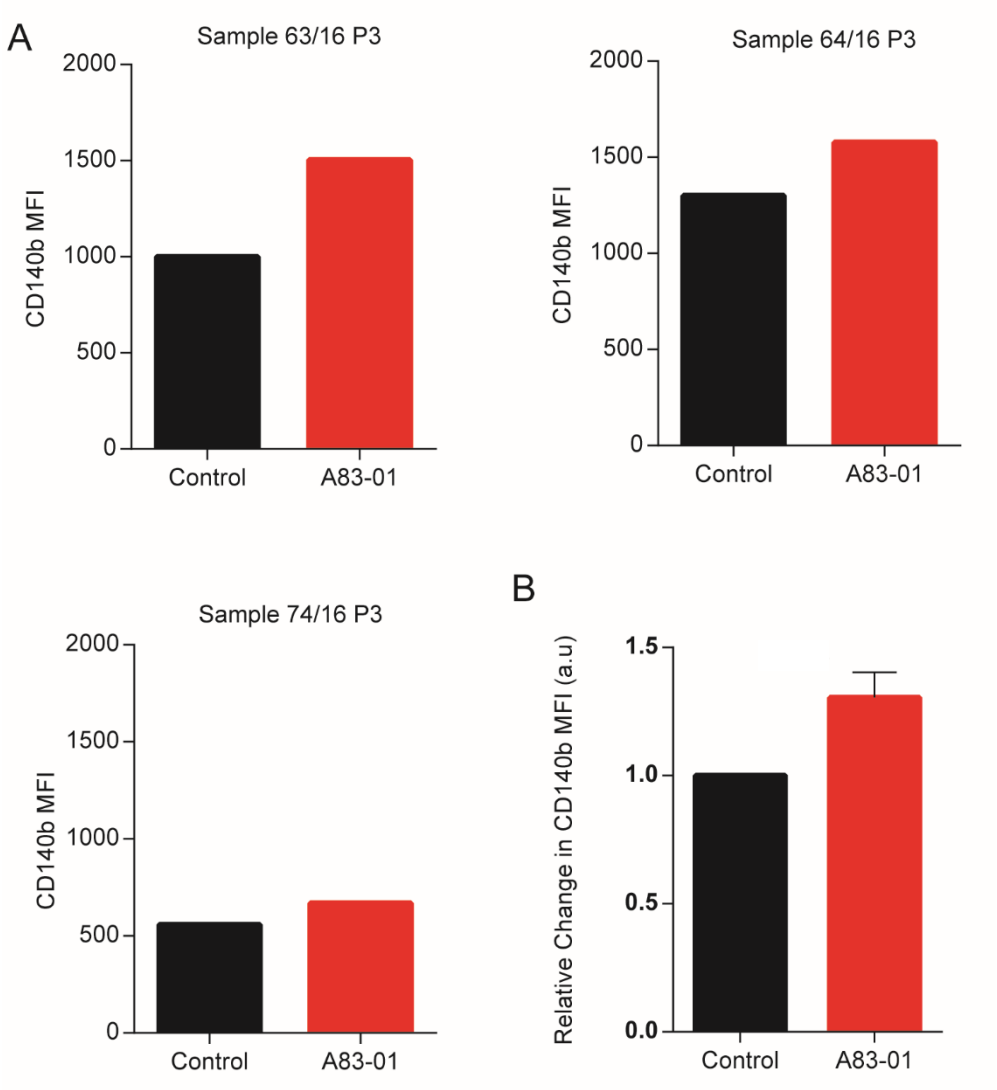

Figure 4.5. CD140b MFI in response to A83-01 treatment of primary eMSCs cultured for 36 days. (A) MFI for CD140b in 3 independent eMSC cultures cultured in the presence or absence of A83-01. Each graph represents an individual culture. (B) Relative change (mean ± SEM) in CD140b MFI.

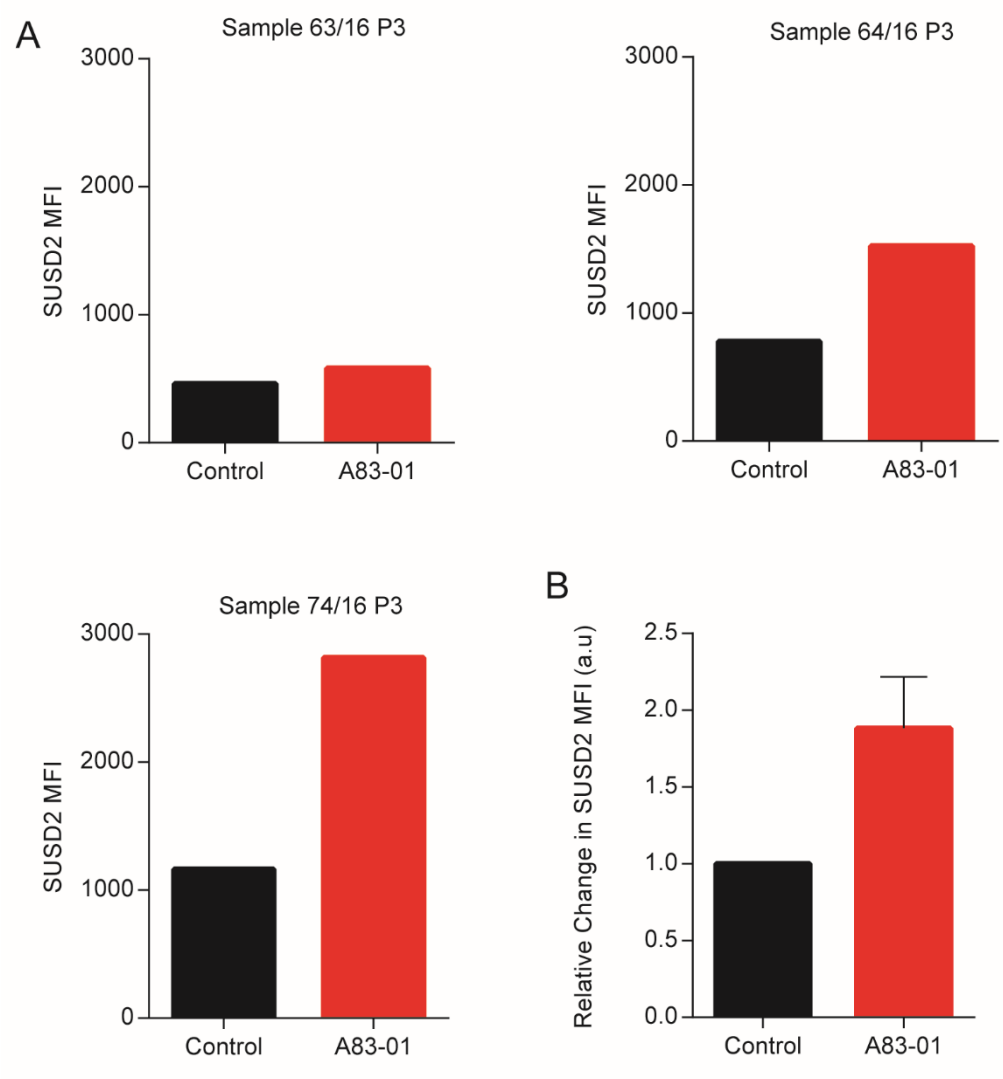

Figure 4.6. SUSD2 MFI in response to A83-01 treatment of primary eMSCs cultured for 36 days. (A) MFI for SUSD2 in 3 independent eMSC cultures cultured in the presence or absence of A83-01. Each graph represents an individual culture. (B) Relative change (mean ± SEM) in SUSD2 MFI.

4.2.3 Impact of A83-01 treatment on clonogenicity of cultured eMSCs

Inhibition of TGF-β-R signalling pathway has been purported to increase eMSC colony efficiency in late passage (Gurung *et al*., 2015). To validate this observation, *in vitro* colony-forming unit-fibroblast (CFU-F) assay was performed to investigate the impact of A83-01 treatment on colony formation.

eMSCs were cultured with or without A83-01 for 2 passages (29 days) and then seeded at a low density (50 cells/cm^2) to allow colony formation and treated further for 2 weeks. Again, the response to A83-01 treatment was consistent between primary cultures, although the magnitude of the response markedly varied (Figure 4.7A). Blockade of TGF-β-R signalling increased the ability of eMSCs to form colonies when compared to control cultures (Figure 4.7B), although statistical significance was not reached ($p > 0.05$). Haematoxylin stained representative colonies of three independent cultures are shown in Figure 4.7C. In addition, colonies generated by A83-01 treated eMSCs were smaller and more rounded (Figure 4.7C, bottom right panel), compared to more elongated clonal cells resulting from control (untreated) cultures (Figure 4.7C, top right panel).

Data showed that TGF-β-R signalling blockade increases the ability of eMSCs to form colonies, although the magnitude of the A83-01 effect differs between primary cultures.

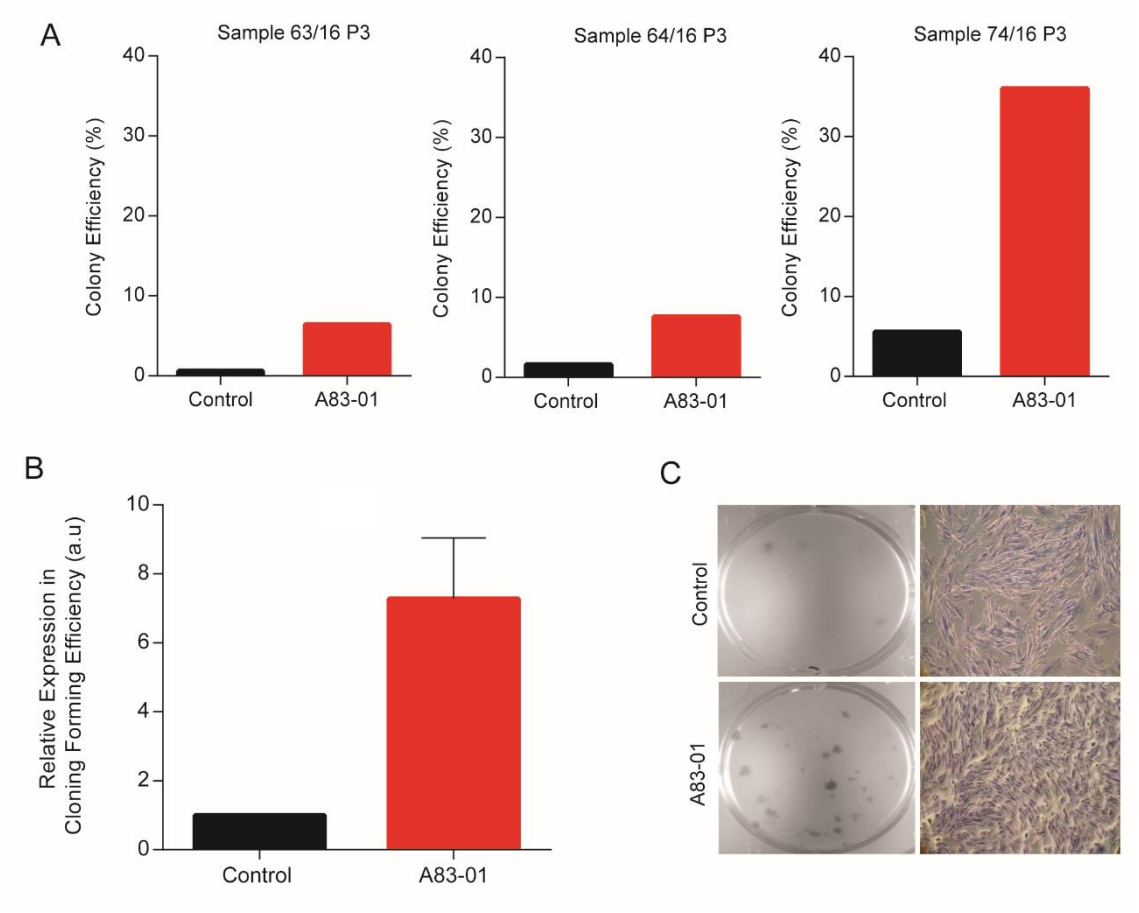

Figure 4.7. A83-01 positively regulates eMSC clonal efficiency. (A). Colony forming unit efficiency was determined in 3 primary eMSC cultures treated with or without A83-01. Each graph represents an individual culture. (B) Mean change (± SEM) in colony forming capacity upon A83-01 treatment compared to untreated cultures.. (C) Representative images of eMSC colonies established from untreated (control) and A83-01 treated cultures. The right panel shows higher magnification (10X) images of colonies. Typically, clonal cells following A83-01 were smaller and lacked the elongated fibroblast-like morphology of untreated cells

4.2.4 Changes in gene expression as result of A83-01 treatment

My next aim was to define the molecular mechanisms through which A83-01 maintains cells in a more undifferentiated state upon prolonged culture. Hence, total RNA obtained from three paired eMSC cultures, treated with or without of the TGF-β-R inhibitor for 36 days, was subjected to RNA-sequencing. This time-point was chosen because it clearly showed the proliferation advantage of A83-01 treated compared to control cultures (Figure 4.1).

Briefly, eMSCs were selectively isolated from 3 independent endometrial biopsies using magnetic bead sorting and treated with or without TGF-β-R inhibitor for 36 days. RNA libraries, generated using RNA samples with a RIN > 8.0, were sequenced on the Illumina HiSeq3000. Fifty million single end reads were sequenced per sample, with a read length of 50 bp. PCA was performed on the rlog transformation of the counts from DESeq to explore how the samples clustered or segregated. In this analysis, Principal Component 1 (PC1), which accounted for 48.10% of variation in gene expression, reflected intrinsic differences in primary cultures. It clustered the treated samples 63 and 64 apart from the 74; and the control samples 64 and 74 apart from 63. As aforementioned, intrinsic variation in the responsiveness of primary cultures was also observed in the functional assays (Figure 4.2-4.7). PC2, which accounted for 28.44% of variation in gene expression, separated control from A83-01 treated cultures, thus reflecting the effect of TGF-β-R blockade on gene expression (Figure 4.8). Based on $q < 0.05$, DESeq identified a robust list of 1,463 differentially expressed genes between control and treated cultures (Figure 4.9). Out of 1,463 differentially expressed genes, 759 (52%) were up-regulated and 704 (48%) were down-regulated following A83-01 treatment. All the differentially up- and down- regulated genes are listed in Appendix 5 and 6, respectively.

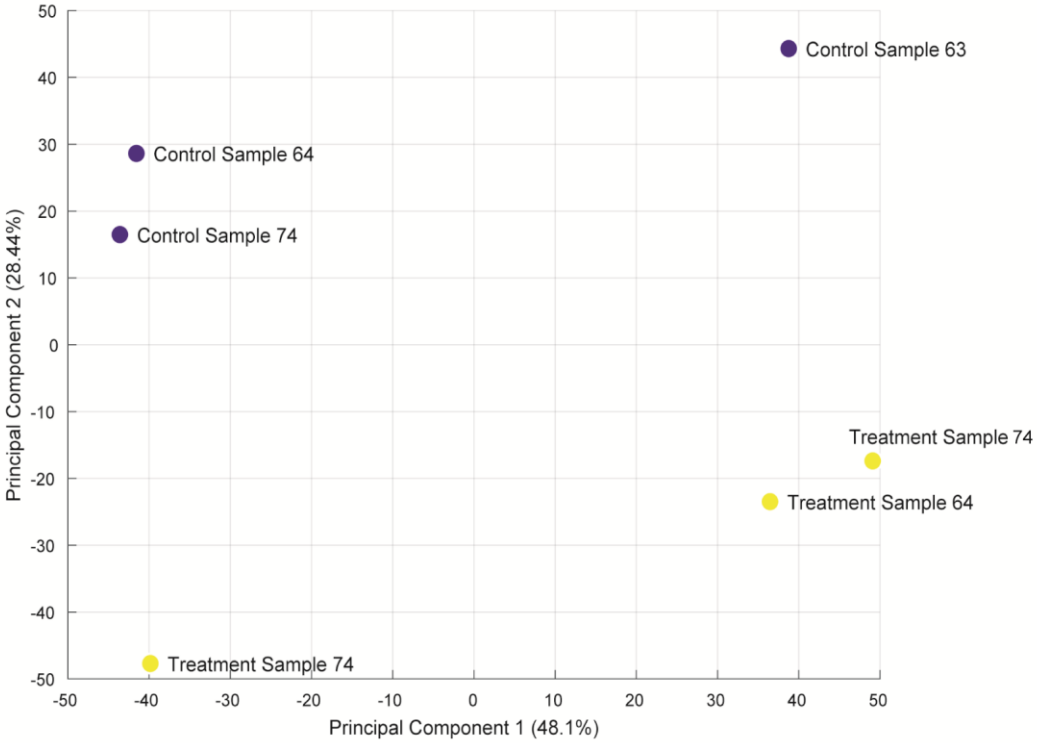

Figure 4.8. PCA of A83-01 treated and untreated eMSCs. PCA of RNA-sequencing data from three independent eMSC cultures, treated with or without A83-01 for 36 days. PC1 segregated different primary cultures, whereas PC2 reflects the response to treatment.

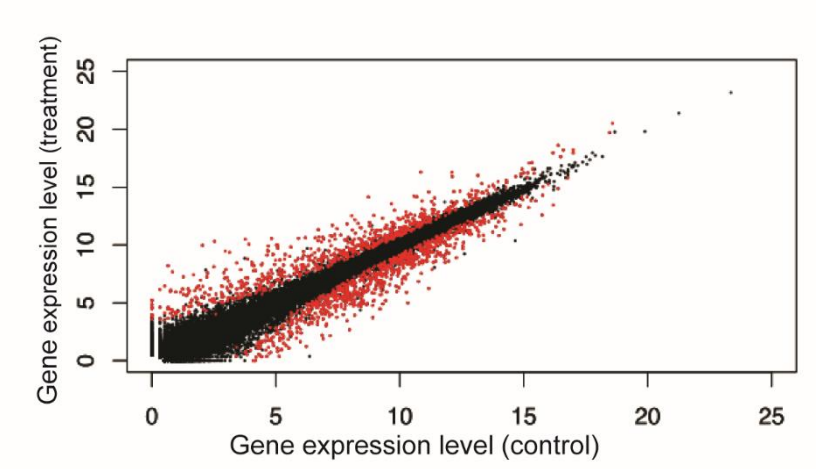

Figure 4.9. Average gene expression levels between A83-01 treated and untreated eMSC cultures. The scatter plot shows the average expression of differentially expressed genes between control and A83-01 treated libraries. Red dots represent significantly differentially expressed genes ($q < 0.05$), whereas black dots are no differentially expressed genes. The axes show the average gene expression levels expressed as log2 transformed counts normalized to library size.

Identification of the most A83-01 responsive genes

To identify genes most enriched or depleted upon A83-01 treatment, differentially expressed genes were ranked according to the log2-fold change. The top three most up-regulated genes were *DMKN* (q = 8.28 x 10^{-28}), *DPP6* (q = 1.35 x 10^{-19}) and *CPVL* (q = 4.09 x 10^{-18}). *DMKN* encodes for dermokine, a protein up-regulated in inflammatory diseases (Naso *et al*., 2007); *DPP6* encodes for dipeptidyl-peptidase 6, a transmembrane protein (Van Es et al., 2008); and *CPVL* encodes a carboxypeptidase that cleaves a single amino acid from the carboxyl termini of peptides (Mahoney *et al*., 2001).

The top three most down-regulated genes were *CST1* (q =2.80 x 10^{-64}), *PMEPA1* (q = *1.67 x* 10^{-57}) *and LINC00643* (q = 7.08 x 10^{-37}). *CST1* encodes for cystatin SN, a cysteine protease inhibitor (Cao *et al*., 2015); *PMEPA1* encodes for prostate transmembrane protein androgen induced 1, a transmembrane protein with a SMAD interacting motif (Koido *et al*., 2016); and *LINC00643* encodes for long intergenic non-protein coding RNA 643 (Figure 4.10).

Next, I ranked all genes differentially regulated by A83-01 in prolonged cultures on basis of the abundance of transcript levels, i.e. transcripts per million (TPMs). Out of the top 50 most abundantly expressed genes in prolonged eMSC cultures, 7 were up-regulated in response to A83-01 treatment and 43 were down-regulated. Interestingly, 20 out of the 43 down-regulated genes encode ECM proteins or factors involved in ECM turn-over. Figure 4.11 shows the repression of these genes in response to A83-01 treatment. The TPMS of these genes ranged between 342.33 to 14,586.59. Notable examples of A83-01 repressed ECM genes include *COL1A1* (collagen type I alpha chain; q = 1.37 x 10^{-9}), *COL1A2* (collagen type I alpha 2 chain; q = 1.44 x 10^{-3}) and *SPARC* (secreted protein acidic and cysteine rich; q = 8.43 x 10^{-4}).

ECM production by fibroblasts is a well characterized response to injury. In the case of tissue damage, fibroblasts transit from a quiescent to an activated state, where TGF-β signalling, amongst others signalling pathways, activates genes

encoding for ECM proteins and cytoskeletal remodelling (Nakerakanti & Trojanowska, 2012; Biernacka *et al,* 2011).

Taken together, the results suggest that inhibition of TGF-β-R signalling maintains eMSCs in a less differentiated state by preventing fibroblast activation in prolonged culture.

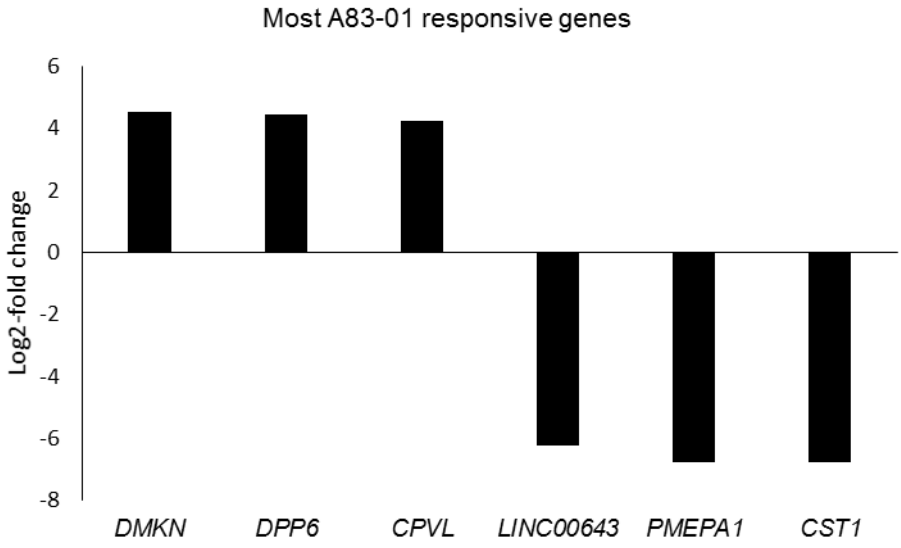

Figure 4.10. Top A83-01 responsive genes. The data show relative changes in gene expression, shown as log2-fold change, of the most A83-01 responsive genes in eMSC cultures treated with A83-01 compared to control.

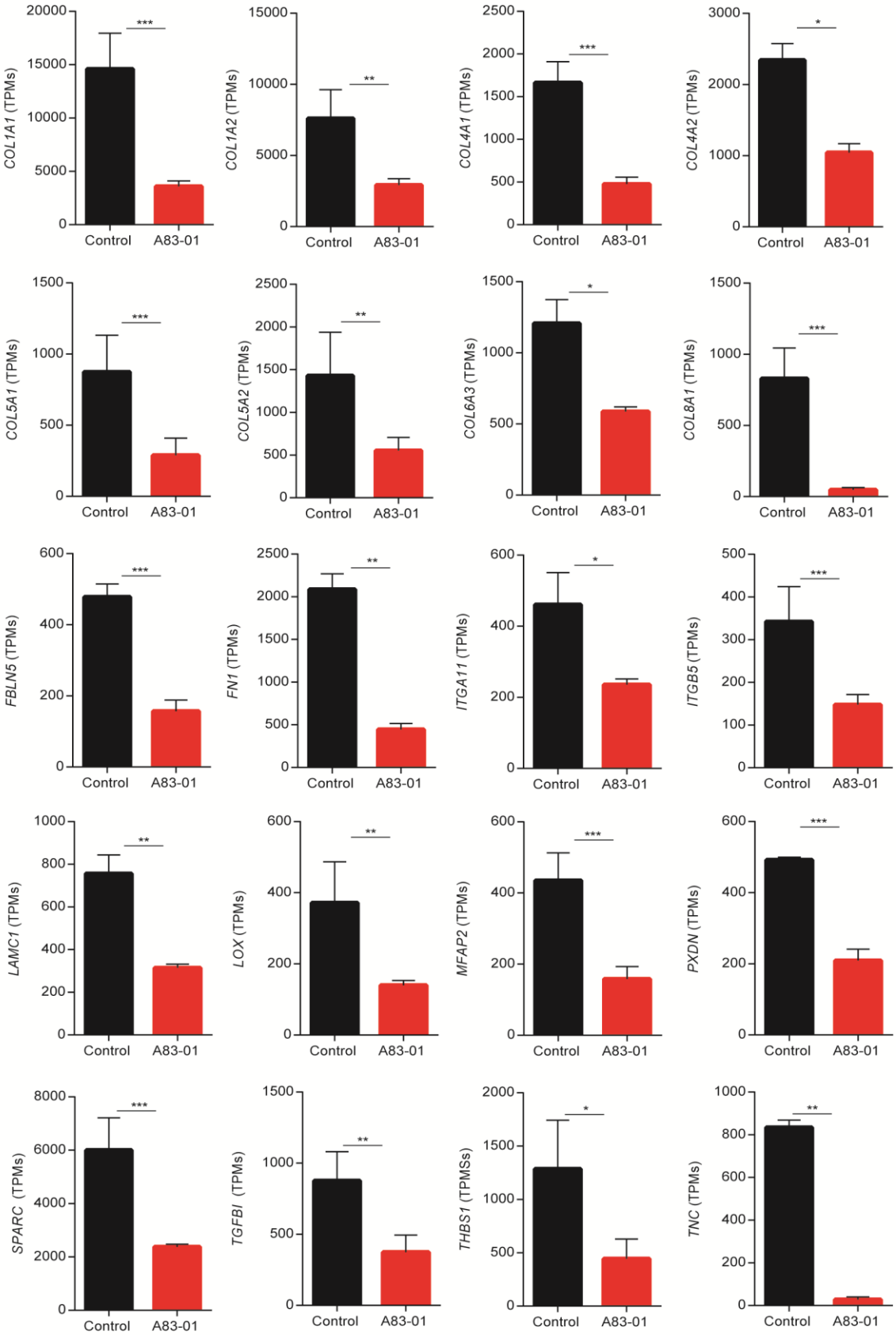

Figure 4.11. ECM genes down-regulated in response to A83-01 treatment. Graphs showings changes in level of gene expression of ECM genes negatively

regulated by TGF-β-R inhibitor, represented as changes in TPMs. Data represent mean ± SEM; Y-axis shows TPMs; * indicates $q < 0.05$, ** $q < 0.01$ and *** $q < 0.001$.

4.2.5 Gene ontology analysis and genes of interest

GO analysis

GO enrichment analysis was performed using the Database for Annotation, DAVID v. 6.8 to characterize differentially expressed genes in eMSC A83-01 treated compared to untreated cultures. Based on $p < 0.05$, GO analysis revealed that up- and down- regulated genes in response to A83-01 treatment were enriched for 61 and 72 categories, respectively, encompassing biological processes, cellular components, and molecular functions (Appendix 7 and 8, respectively). As shown in Figure 4.12A, up-regulated genes were enriched for intracellular receptor signalling pathways ($p = 4.54 \times 10^{-4}$) and regulation of cell growth ($p = 7.76 \times 10^{-4}$). Collagen catabolism ($p = 1.73 \times 10^{-13}$) and cell fate commitment ($p = 4.29 \times 10^{-3}$) were GO terms enriched in genes negatively regulated upon A83-01 treatment. Significantly enriched GO terms for both up- and down-regulated genes were visualized using Reduce and Visualize Gene Ontology (REVIGO) server (Figure 4.12).

A

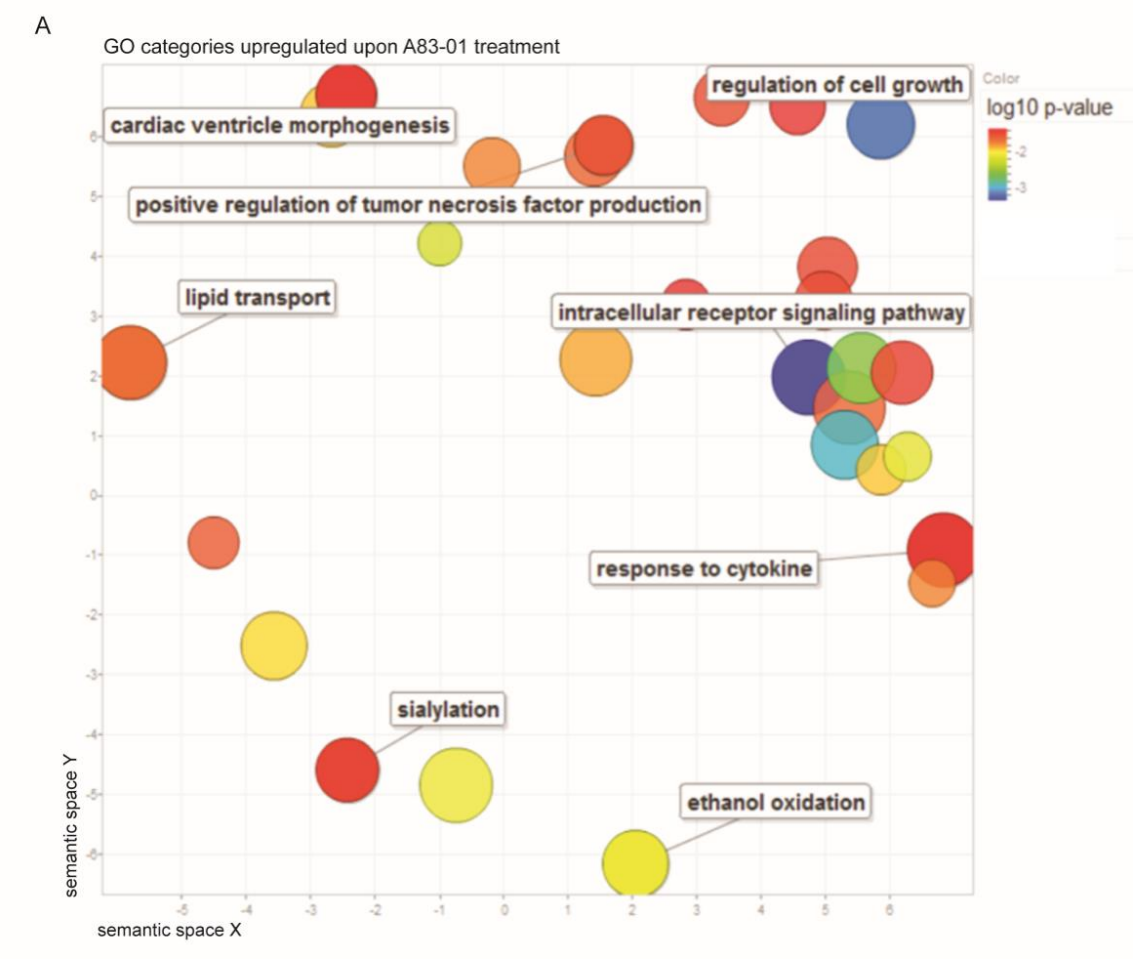
GO categories upregulated upon A83-01 treatment
regulation of cell growth
cardiac ventricle morphogenesis
positive regulation of tumor necrosis factor production
lipid transport
intracellular receptor signaling pathway
response to cytokine
sialylation
ethanol oxidation
Color
log10 p-value
semantic space Y
semantic space X

B

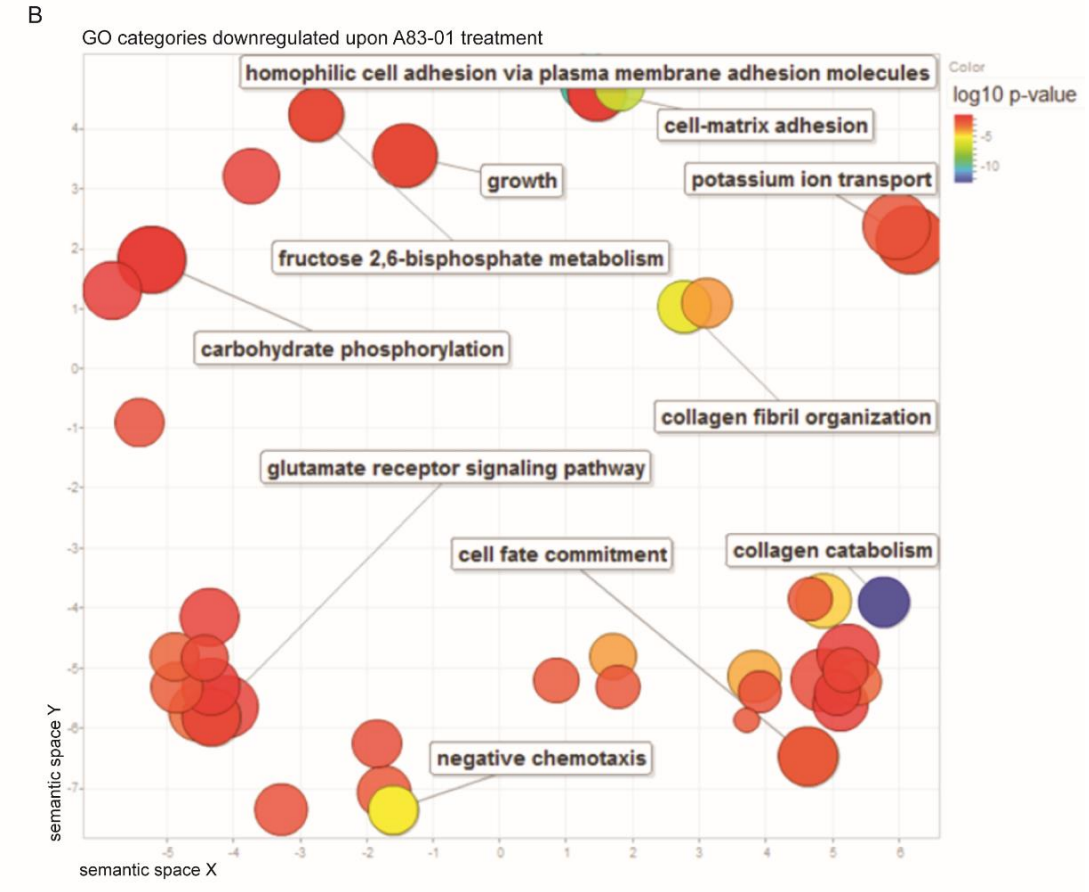
GO categories downregulated upon A83-01 treatment
homophilic cell adhesion via plasma membrane adhesion molecules
cell-matrix adhesion
growth
potassium ion transport
fructose 2,6-bisphosphate metabolism
carbohydrate phosphorylation
collagen fibril organization
glutamate receptor signaling pathway
cell fate commitment
collagen catabolism
negative chemotaxis
Color
log10 p-value
semantic space Y
semantic space X

Figure 4.12. Enrichment and depletion of biological processes upon A83-01 treatment. GO enrichment analysis was applied to differentially expressed genes and the significant GO annotations ($p < 0.05$) summarized using REVIGO and clustered based on semantic similarities, which means that if they are described by a common ontology they cluster close in the graph. (A) GO categories associated to the up-regulated genes. (B) GO categories enriched for down-regulated genes. The colour key is represented on the right. The most highly enriched GO categories are indicated in blue. The size of the circles reflects the frequency of the GO term.

eMSC and perivascular markers

Mining of the RNA-seq sequencing data for established eMSC markers revealed that A83-01-induced TGF-β-R blockade markedly upregulated the expression of *SUSD2*, consistent with increase in the SUSD2- positive cells and MFI for the same marker shown by flow cytometry (Figure 3.3 and 3.6). However, manual mining of the RNA-seq data also revealed that A83-01 treatment resulted in the downregulation of other notable perivascular markers (Murakami *et al*., 2014, including *MCAM* (q = 3.97 x 10^{-2}), *ELN* (q = 7.83 x 10^{-15}) and *MYH11* (q = 4.43 x 10^{-2}) (Figure 4.13).

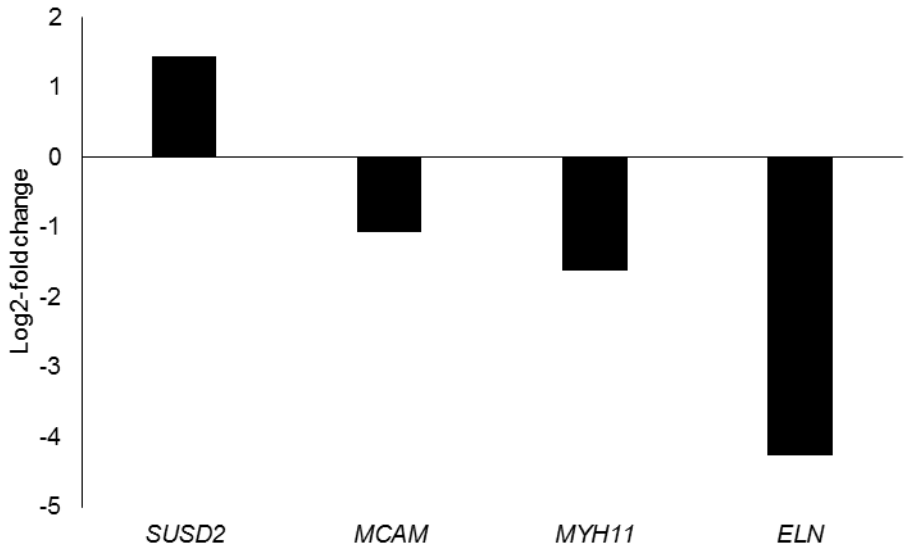

Figure 4.13. eMSC and perivascular markers. Selected eMSC and perviscular markers. The data show relative change, expressed as log2-fold change, in gene expression in cultures treated with A83-01 compared to control.

4.2.6 Identification of eMSC-associated genes regulated by A83-01

In a previous study in our laboratory, RNA-sequencing was used to determine the transcriptome profiles of clonal eMSCs and time-matched unselected perivascular cells (PVCs). Briefly, total mRNA was isolated of eMSCs subjected to clonal assay for 12 days and matched to primary PVCs also cultured for 12 days. To determine if A83-01 maintains cultured eMSCs in a less differentiated state, I examined the overlap in differentially expressed genes in both datasets. Figure 4.14 shows a graphic representation of the two datasets compared in this part of the study.

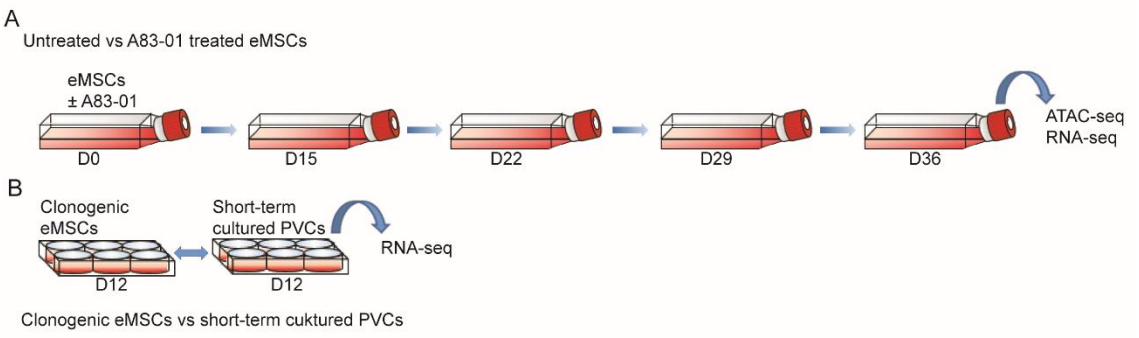

Figure 4.14. 'Untreated vs A83-01 treated eMSCs' vs 'Clonal eMSCs vs short-term cultured PVCs'. Graphic representation of the two datasets compared. (A) shows dataset one where freshly isolated eMSCs were cultured in the presence or absence of TGF-β-R inhibitor for 36 days and then subjected to ATAC-seq and RNA-seq. (B) represent dataset two where clonal eMSCs were subjected to CFU assay for 12 days and compared to primary PVCs cultured for 12 days. At day 12 clonal eMSCs and PVCs were subjected to RNA-seq.

Comparison between the two dataset showed that A83-01 treated cells and clonal eMSCs share 38 commonly upregulated genes, including *SUSD3* (q = 1.36 x 10^{-11}), *LPAR3* (q = 2.67 x 10^{-5}) and *ITGA8* (q = 7.07 x 10^{-6}) (Figure 4.15A-B). The Human Protein Atlas was used to determine the spatial expression of these genes in the endometrial tissue (Uhlén *et al*, 2015), particularly in the perivascular niche. As shown in Figure 4.16 (left panel), immunohistochemistry analysis revealed that SUSD3 (sushi domain containing 3), LPAR3 (lysophosphatidic acid receptor 3), and ITGA8 (integrin subunit alpha 8) are indeed expressed in cells surrounding the terminal spiral arteries, in keeping that eMSCs reside predominantly in the perivascular niche (Masuda *et al*., 2012).

A total of 120 genes were commonly down-regulated in both A83-01 and clonal eMSCs and included several genes coding for extracellular matrix (ECM) proteins such as *MFAP5* (q = 1.07 x 10^{-5}), *FN1* (q = 2.35 x 10^{-8}), and *VCAN* (q = 2.72 x 10^{-7}) (Figure 4.17). Again, the Human Protein Atlas was used to annotate the cellular distribution of these genes in the perivascular regions of the endometrial tissue. As shown in Figure 4.16B, *MFAP5* (microfibrillar associated protein 5), *FN1* (fibronectin) and *VCAN* (versican) were abundantly expressed in the stromal compartment but less prominently in perivascular cells around the terminal spiral arteries.

Taken together, these results suggest that A83-01-induced TGF-β-R blockade upon prolonged eMSC culture only partly recapitulates the gene signature of clonal eMSCs. In keeping with the known role of TGF-β in regulating ECM (Verrecchia & Mauviel, 2002), the effect of A83-01 on eMSCs in prolonged culture may equally relate to the inhibition of ECM components in prolonged cultures.

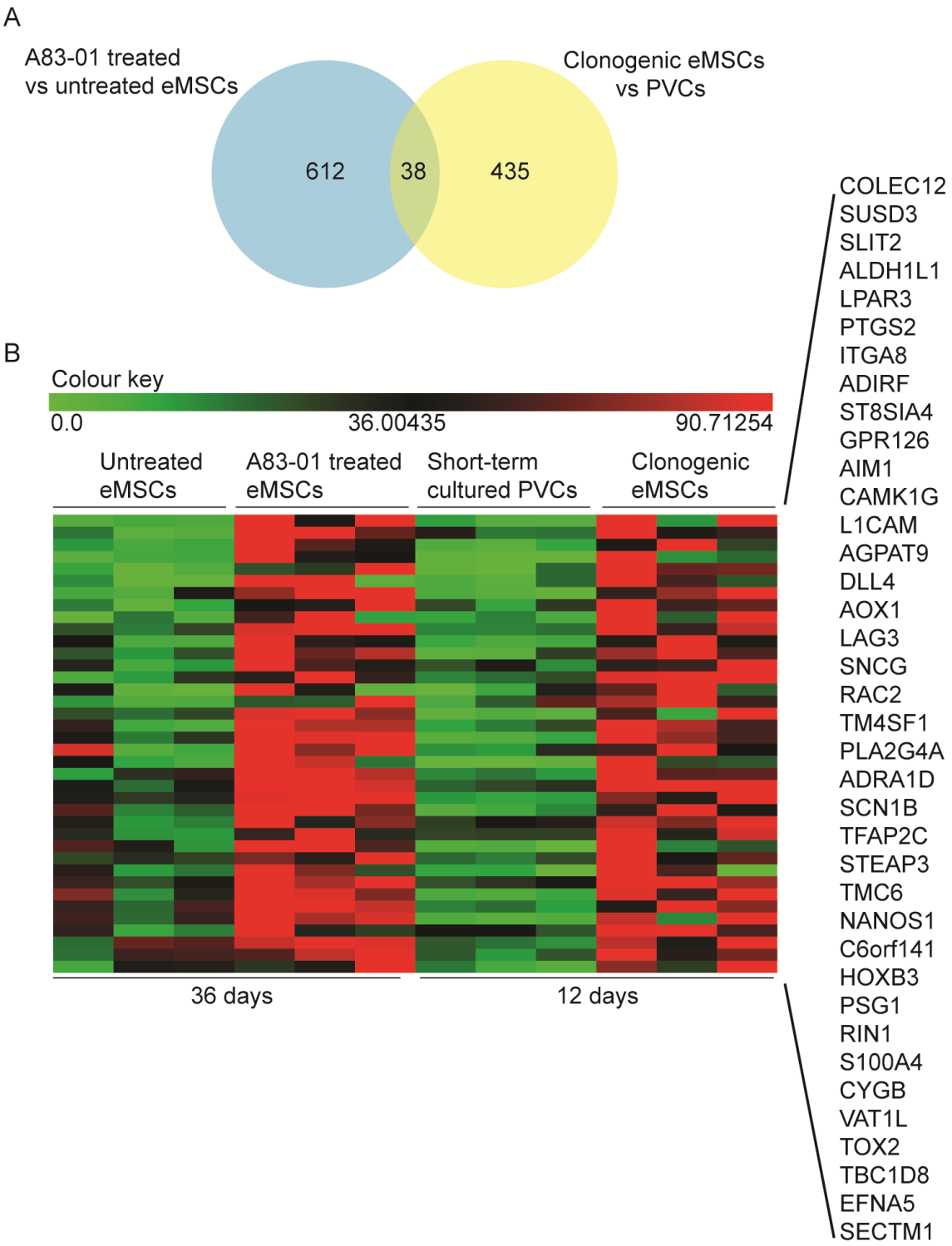

Figure 4.15. A83-01 treated and clonogenic eMSCs share a set of commonly upregulated genes. (A) Venn diagram showing overlap of 38 genes commonly upregulated both in A83-01 treated and clonogenic eMSCs (Log2-fold change ≥ 1; $q < 0.05$). (B) Heatmap representing the gene expression level of the 38 commonly upregulated genes, which are listed on the right. The colour key is represented above the heat map, the most highly enriched genes are indicated in red.

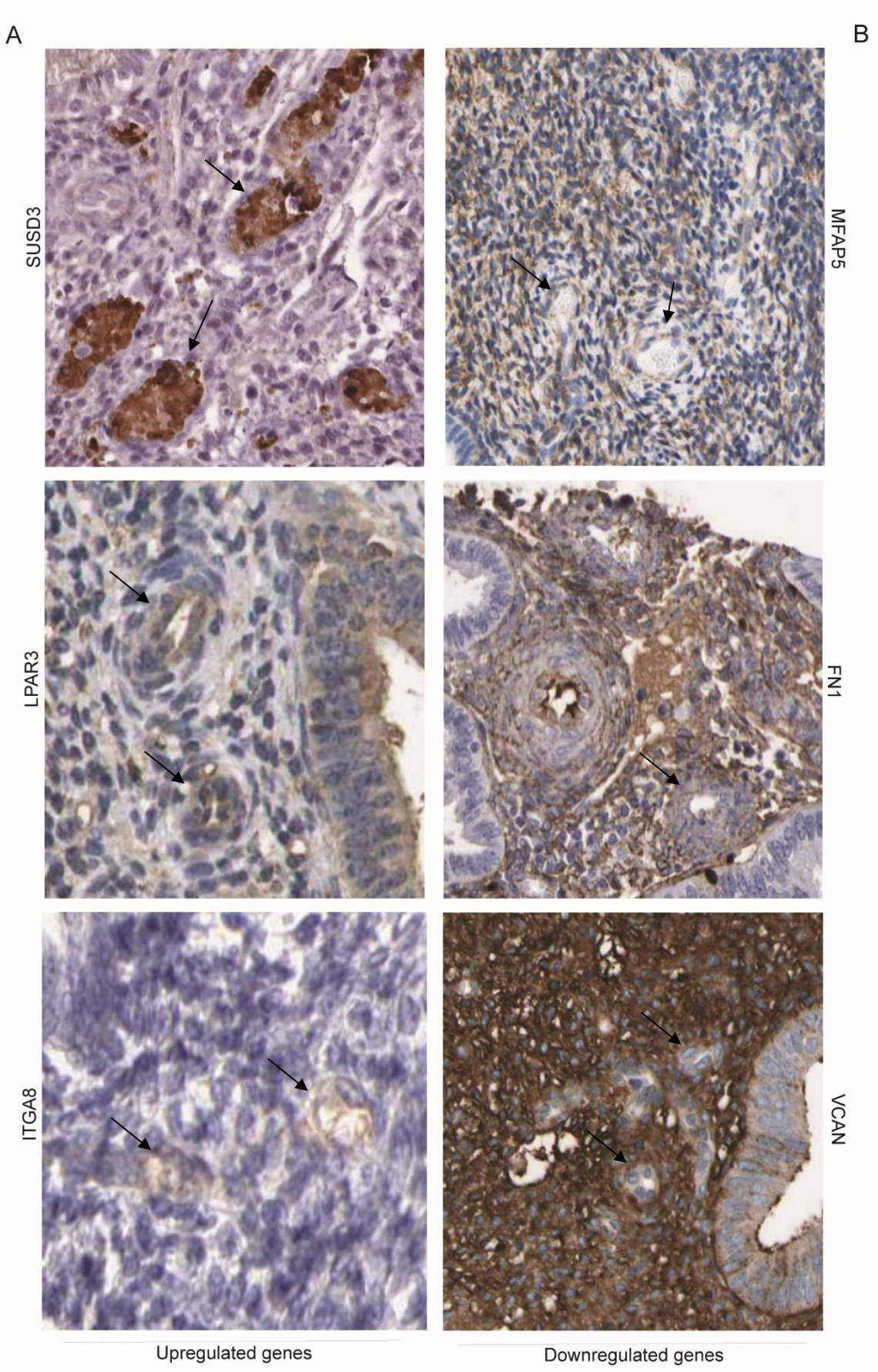
A
B
SUSD3
MFAP5
LPAR3
FN1
ITGA8
VCAN
Upregulated genes
Downregulated genes

Figure 4.16. Cellular distribution of A83-01 responsive genes in cycling human endometrium. (A) The Human Protein Atlas was mined to determine the tissue distribution of 3 proteins (SUSD3, LPAR3, and ITGA8) associated with clonal eMSCs and induced at mRNA level in prolonged cultures in response to A83-01. (B) The same resource was also mined to determine the tissue distribution of 3 proteins (MFAP5, FN1, and VCAN) down-regulated in clonal eMSCs as well as in response to A83-01 treatment of prolonged eMSC cultures. Overall, the selected A83-01 induced genes were more prominent expressed at protein level around the terminal spiral arteries whereas the opposite pattern of expression was apparent for A83-01 repressed genes.

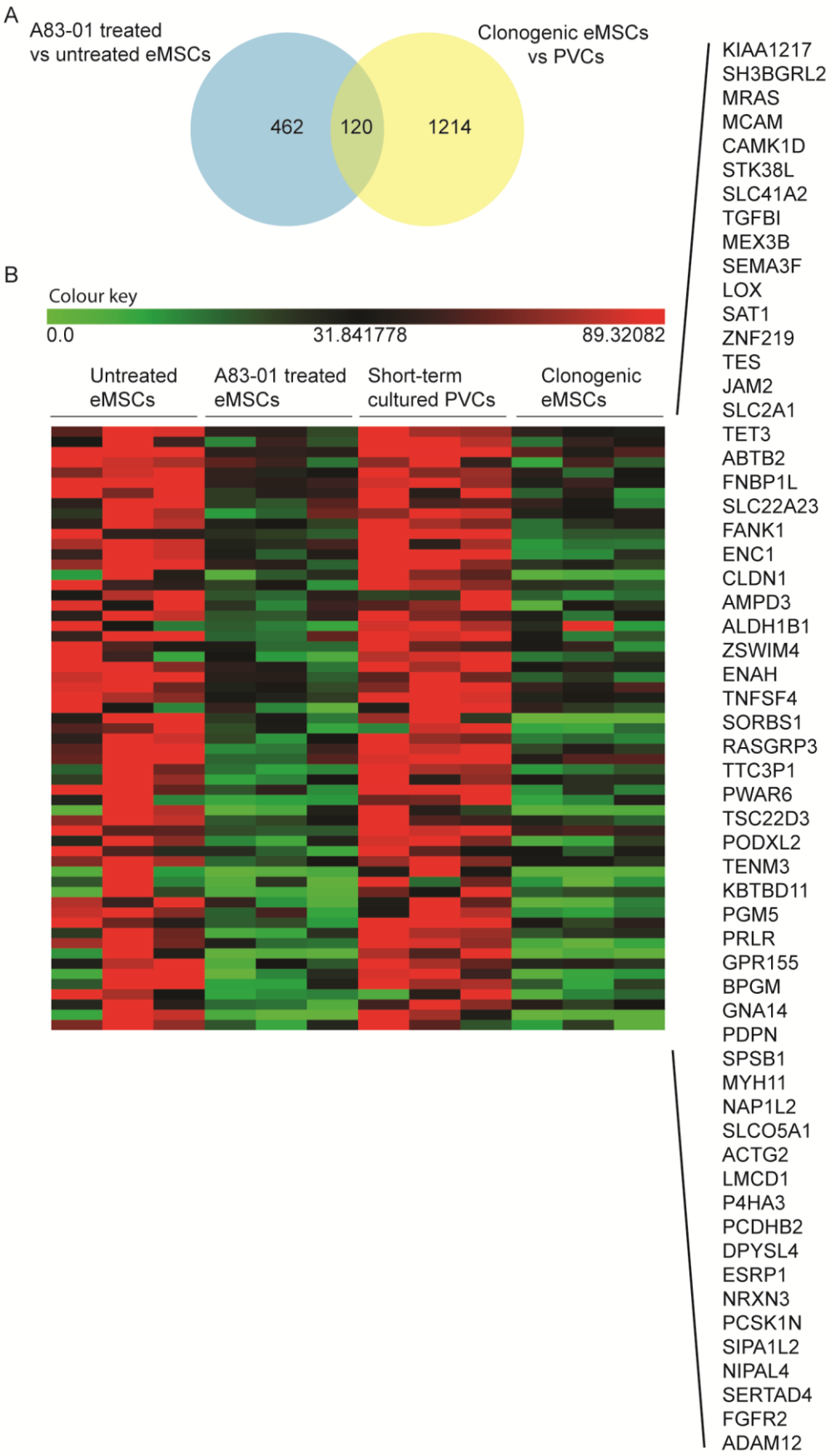
A
A83-01 treated
vs untreated eMSCs
Clonogenic eMSCs
vs PVCs
462
120
1214
B
Colour key
0.0
31.841778
89.32082
Untreated
eMSCs
A83-01 treated
eMSCs
Short-term
cultured PVCs
Clonogenic
eMSCs
KIAA1217
SH3BGRL2
MRAS
MCAM
CAMK1D
STK38L
SLC41A2
TGFBI
MEX3B
SEMA3F
LOX
SAT1
ZNF219
TES
JAM2
SLC2A1
TET3
ABTB2
FNBP1L
SLC22A23
FANK1
ENC1
CLDN1
AMPD3
ALDH1B1
ZSWIM4
ENAH
TNFSF4
SORBS1
RASGRP3
TTC3P1
PWAR6
TSC22D3
PODXL2
TENM3
KBTBD11
PGM5
PRLR
GPR155
BPGM
GNA14
PDPN
SPSB1
MYH11
NAP1L2
SLCO5A1
ACTG2
LMCD1
P4HA3
PCDHB2
DPYSL4
ESRP1
NRXN3
PCSK1N
SIPA1L2
NIPAL4
SERTAD4
FGFR2
ADAM12

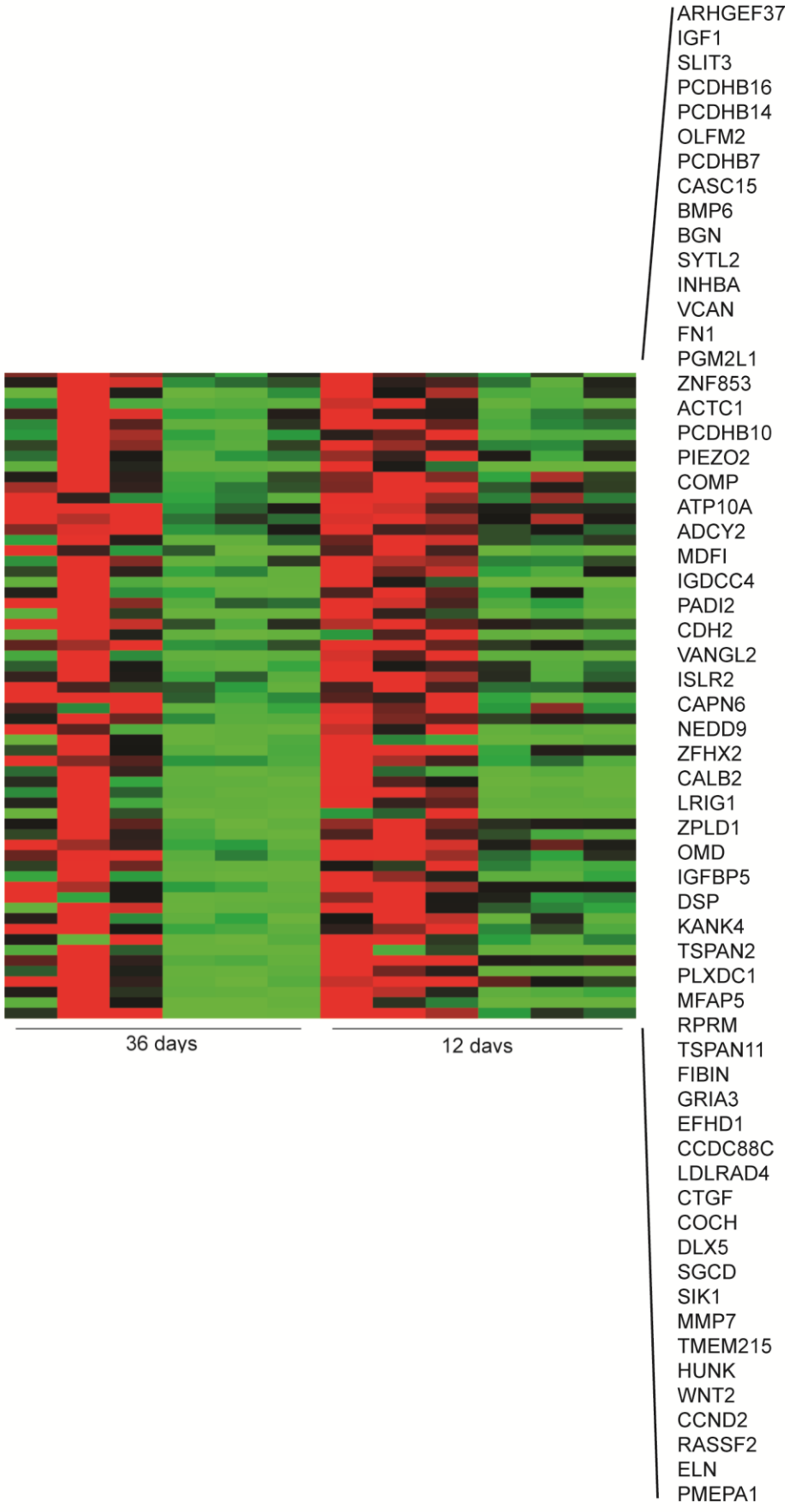
ARHGEF37
IGF1
SLIT3
PCDHB16
PCDHB14
OLFM2
PCDHB7
CASC15
BMP6
BGN
SYTL2
INHBA
VCAN
FN1
PGM2L1
ZNF853
ACTC1
PCDHB10
PIEZO2
COMP
ATP10A
ADCY2
MDFI
IGDCC4
PADI2
CDH2
VANGL2
ISLR2
CAPN6
NEDD9
ZFHX2
CALB2
LRIG1
ZPLD1
OMD
IGFBP5
DSP
KANK4
TSPAN2
PLXDC1
MFAP5
RPRM
TSPAN11
FIBIN
GRIA3
EFHD1
CCDC88C
LDLRAD4
CTGF
COCH
DLX5
SGCD
SIK1
MMP7
TMEM215
HUNK
WNT2
CCND2
RASSF2
ELN
PMEPA1
36 days
12 days

Figure 4.17. A83-01 treated and clonogenic eMSCs share a set of commonly downregulated genes. (A) Venn diagram showing overlap of 120 genes commonly downregulated both in A83-01 treated and clonogenic eMSCs (log2-fold change ≤ -1; $q < 0.05$). (B) Heatmap showing gene expression level of 120 commonly downregulated genes, which are listed on the right. The colour key is represented above the heat map, the most highly enriched genes are indicated in red. The heatmap was divided into two parts because of the size.

GO analysis of eMSC-associated genes induced by A83-01

GO enrichment analysis of the 38 commonly upregulated genes, i.e. eMSCs versus PVCs and A83-01 treated versus untreated cultures, was performed to identify relevant biological processes.

Based on $p < 0.05$, GO analysis showed enrichment for eight GO terms, including 'positive regulation of collateral sprouting' ($p = 1.56 \times 10^{-2}$), 'oxidation-reduction process' ($p = 2.79 \times 10^{-2}$) and 'negative regulation of endothelial cell migration' ($p = 3.48 \times 10^{-2}$). GO term associated to 'positive regulation of collateral sprouting' included *EFNA5* (ephrin A5) and *LPAR3* (lysophosphatidic acid receptor 3); 'oxidation-reduction process' included *PTGS2* (prostaglandin-endoperoxide synthase 2; also known as cyclooxygenase-2 or COX-2) and *VATL1* (vesicle amine transport 1 like); and 'negative regulation of endothelial cell migration' included *DLL4* (delta-like canonical Notch ligand 4) and *SLIT2* (slit guidance ligand 2). Interestingly, enrichment analysis of the 38 commonly up-regulated genes for Kyoto Encyclopedia of Genes and Genomes (KEGG) pathways revealed enrichment of the 'vascular endothelial growth factor (VEGF) signalling pathway' ($p = 9.57 \times 10^{-3}$), that included *RAC2* (Rac family small GTPase 2), *PTGS2* (prostaglandin-endoperoxide synthase 2) and *PLA2G4A* (phospholipase A2 group IVA) (Figure 4.18A).

GO analysis of the 120 commonly downregulated genes showed depletion of ten biological processes. The most significantly ($p < 0.05$) down-regulated were 'ECM organization' ($p = 2.95 \times 10^{-5}$) and 'cell adhesion' ($p = 1.28 \times 10^{-4}$). 'ECM organization' category included *ELN* (elastin) and *FN1*; 'cell adhesion' included *TGFBI* (transforming growth factor beta induced) and *CDH2* (cadherin 2). Enrichment analysis of KEGG pathway showed depletion for seven categories, for example 'signalling pathways regulating pluripotency of stem cells' ($p = 1.17 \times 10^{-2}$) and 'cell adhesion molecules (CAMs)' ($p = 1.23 \times 10^{-2}$) (Figure 18B). 'Signalling pathways regulating pluripotency stem cells' included *FGFR2* (fibroblast growth factor receptor 2) and *WNT2* (Wnt family member 2); and 'cell

adhesion molecules (CAMs)' included *JAM2* (junctional adhesion molecule 2) and *CLDN1* (claudin 1).

A

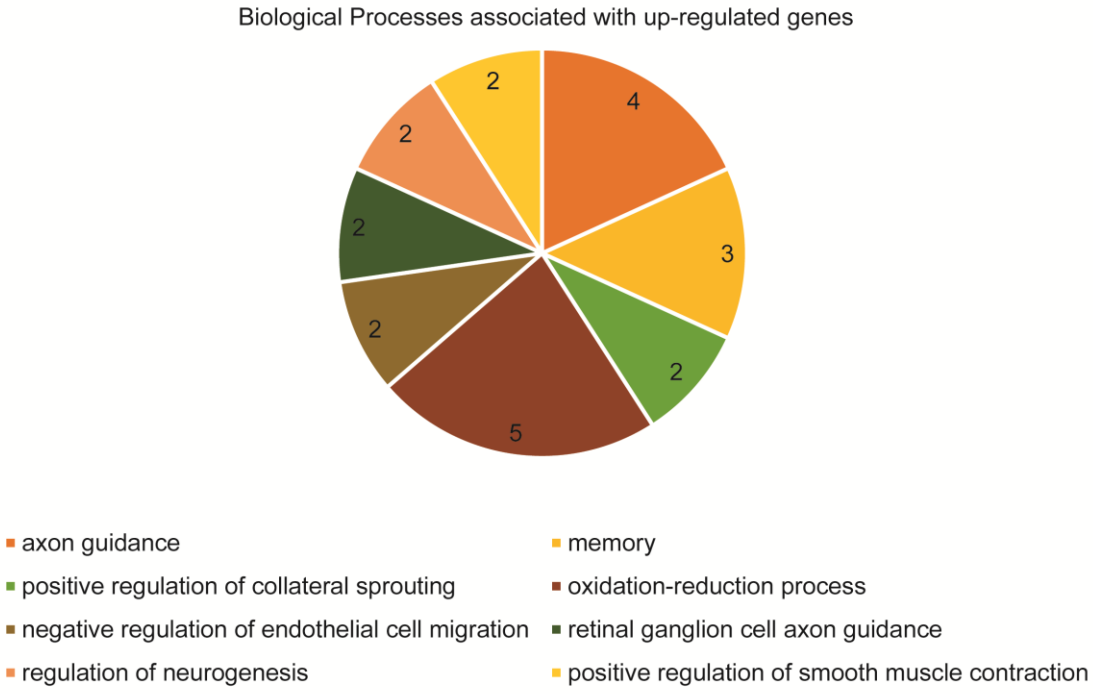
Biological Processes associated with up-regulated genes
4
3
2
5
2
2
2
2
axon guidance
memory
positive regulation of collateral sprouting
oxidation-reduction process
negative regulation of endothelial cell migration
retinal ganglion cell axon guidance
regulation of neurogenesis
positive regulation of smooth muscle contraction

B

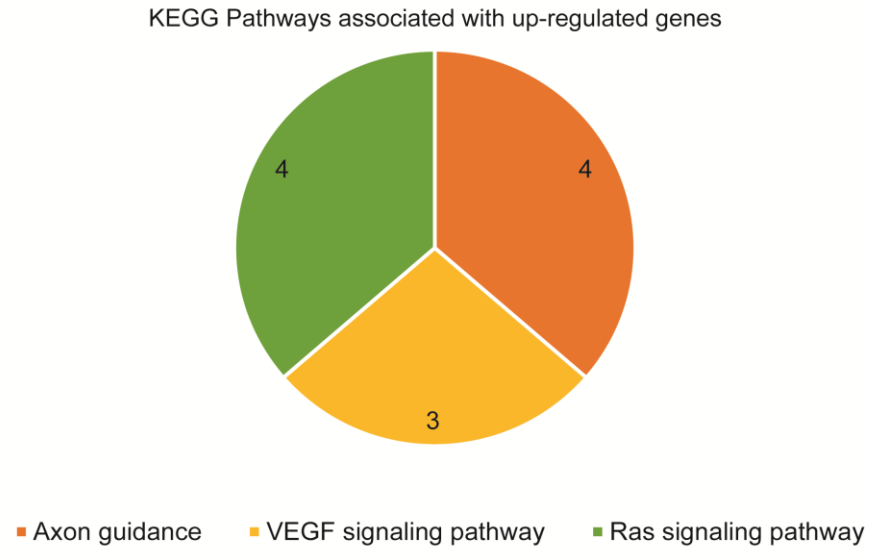
KEGG Pathways associated with up-regulated genes
4
3
4
Axon guidance
VEGF signaling pathway
Ras signaling pathway

C

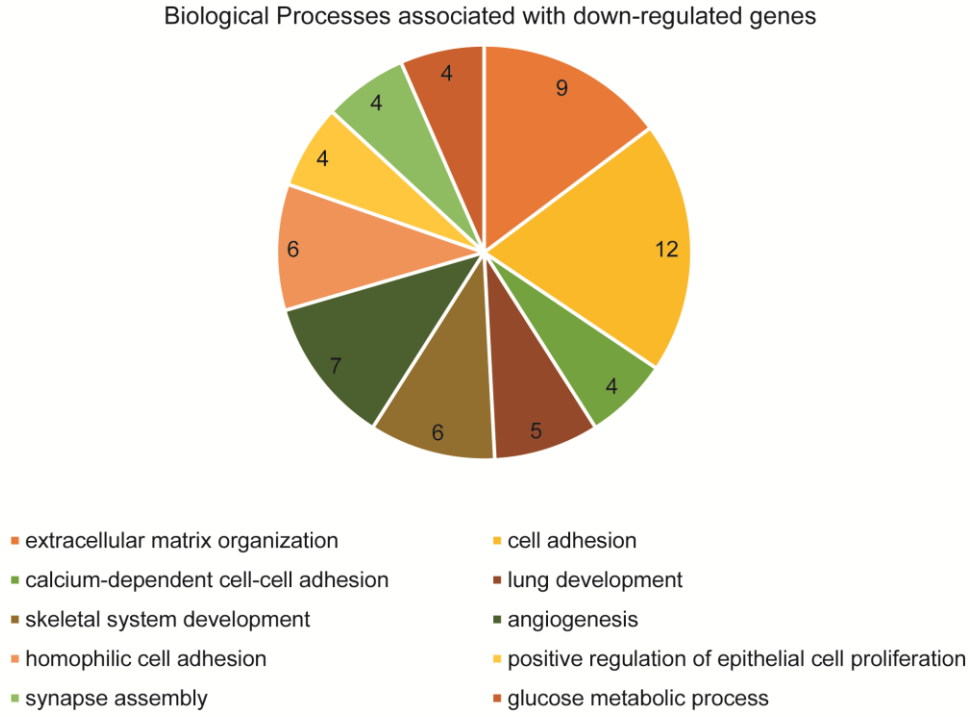

D

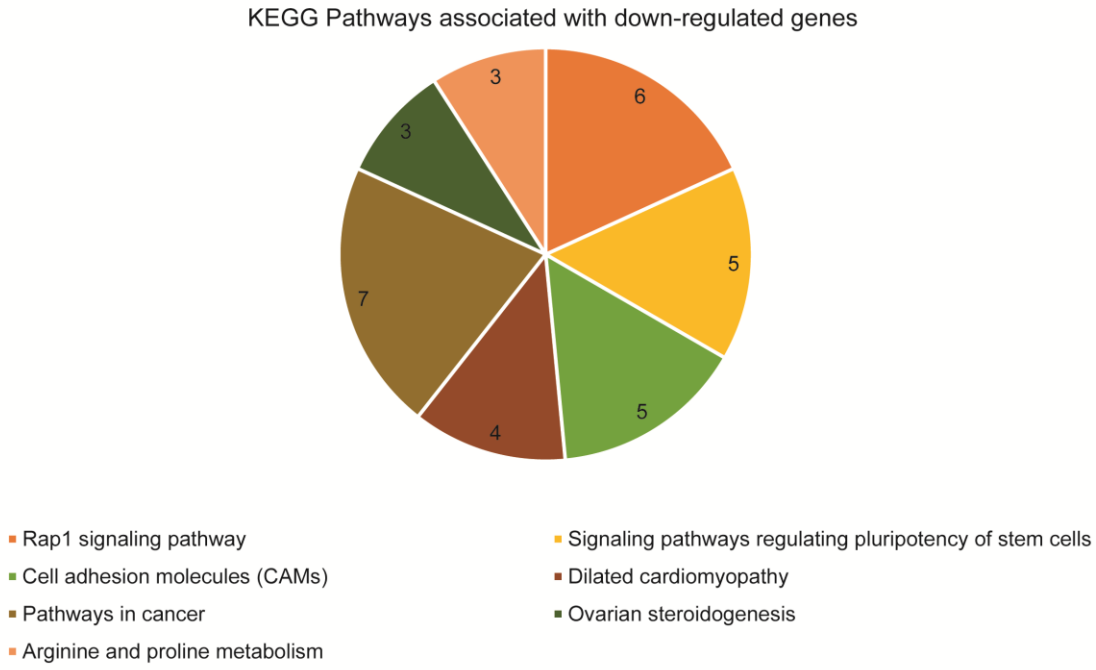

Figure 4.18. A83-01 treatment partly recapitulates stem cell features. Enrichment analysis of biological processes and KEGG pathways associated with the 38 and 120 commonly up- (A-B) and down-regulated (C-D) genes, respectively, in both RNA-sequencing datasets: A83-01 treated versus untreated cultured eMSCs and clonal eMSCs versus PVCs. The pie charts showed the

significantly enriched (A-B) or depleted categories (C-D), and the numbers indicate the number of genes contained in each identified biological process or KEGG pathway.

Divergent transcriptomic profiles between clonal and A83-01 treated eMSCs in prolonged culture

Inhibition of TGF-β-R signalling differentially regulated genes that partly recapitulated gene signature of clonal eMSCs, but also resulted in a unique gene signature. Specifically, A83-01 treatment induced 160 genes that were downregulated in the clonal eMSCs when compared to PVCs (Figure 4.19). Also, TGF-β-R blockade negatively regulated 58 genes, which were enriched in clonal eMSCs when compared to PVCs (Figure 4.20). To identify biological processes associated with these discordant genes, I performed further GO analysis. The top three most significant ($p < 0.05$) GO terms uniquely induced in the A83-01 treated eMSCs were 'negative regulation of substrate adhesion-dependent cell spreading' ($p = 1.43 \times 10^{-4}$), 'response to retinoic acid' ($p = 3.4 \times 10^{-4}$) and 'regulation of systemic arterial blood pressure by renin-angiotensin' ($p = 9.07 \times 10^{-4}$). The top three most negatively downregulated by A83-01 whereas were 'collagen catabolic process' ($p = 7.13 \times 10^{-4}$), 'extracellular matrix disassembly' ($p = 0.02$), and 'cellular response to vitamin D' ($p = 0.02$). It is notable that GO terms related to ECM were down-regulated in prolonged eMSC cultures treated with A83-01.

Taken together, the comparison of the two RNA-seq data sets revealed that TGF-β-R blockade upon prolonged culturing of eMSCs partly recapitulates the identity of clonal eMSCs, but also modulates a distinct gene network, consisting of 218 genes. A preponderance of genes selectively inhibited by A83-01 in prolonged eMSC culture relate to ECM proteins and ECM turnover.

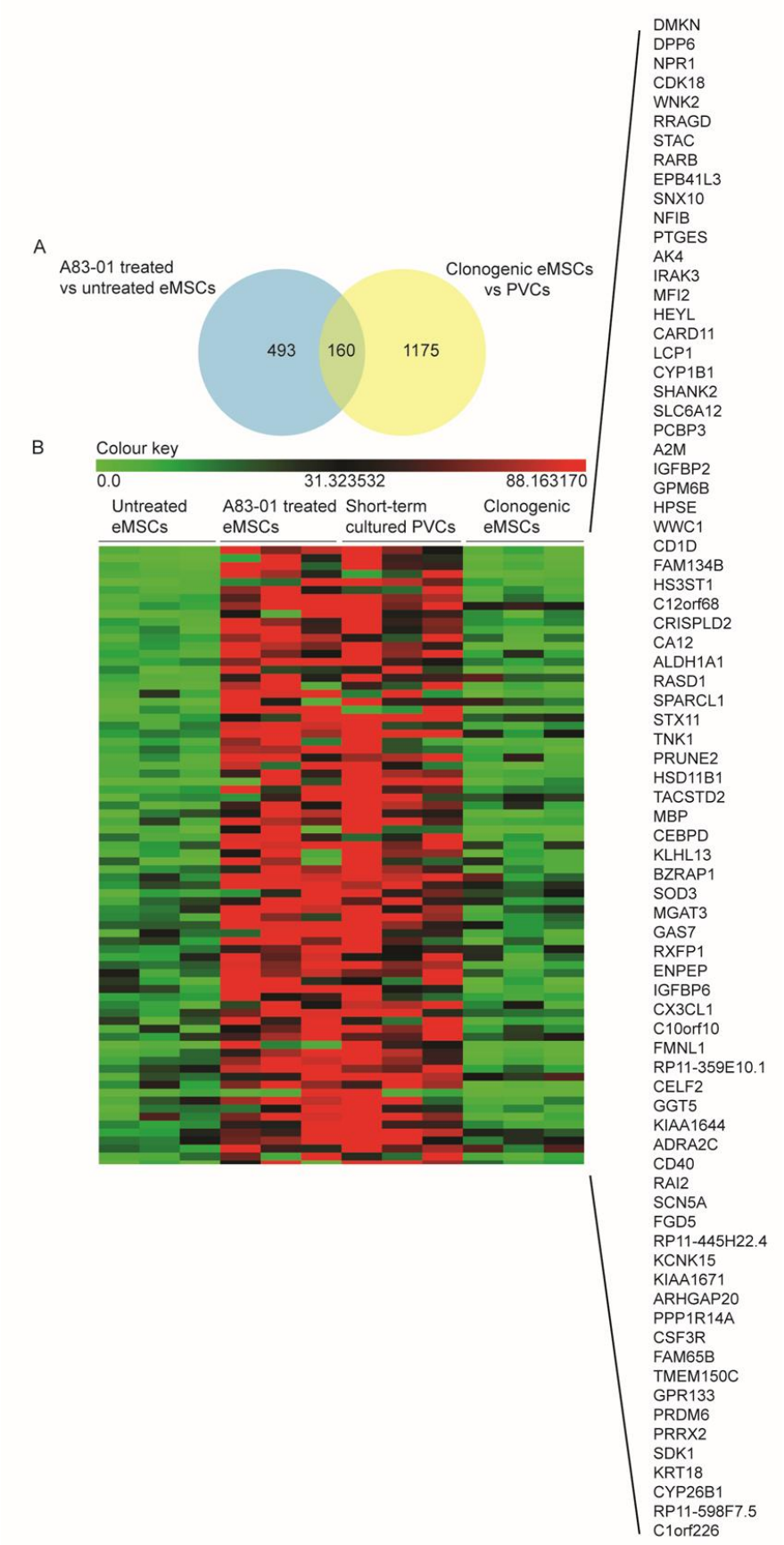
A
A83-01 treated
vs untreated eMSCs
Clonogenic eMSCs
vs PVCs
493
160
1175
B
Colour key
0.0
31.323532
88.163170
Untreated
eMSCs
A83-01 treated
eMSCs
Short-term
cultured PVCs
Clonogenic
eMSCs
DMKN
DPP6
NPR1
CDK18
WNK2
RRAGD
STAC
RARB
EPB41L3
SNX10
NFIB
PTGES
AK4
IRAK3
MFI2
HEYL
CARD11
LCP1
CYP1B1
SHANK2
SLC6A12
PCBP3
A2M
IGFBP2
GPM6B
HPSE
WWC1
CD1D
FAM134B
HS3ST1
C12orf68
CRISPLD2
CA12
ALDH1A1
RASD1
SPARCL1
STX11
TNK1
PRUNE2
HSD11B1
TACSTD2
MBP
CEBPD
KLHL13
BZRAP1
SOD3
MGAT3
GAS7
RXFP1
ENPEP
IGFBP6
CX3CL1
C10orf10
FMNL1
RP11-359E10.1
CELF2
GGT5
KIAA1644
ADRA2C
CD40
RAI2
SCN5A
FGD5
RP11-445H22.4
KCNK15
KIAA1671
ARHGAP20
PPP1R14A
CSF3R
FAM65B
TMEM150C
GPR133
PRDM6
PRRX2
SDK1
KRT18
CYP26B1
RP11-598F7.5
C1orf226

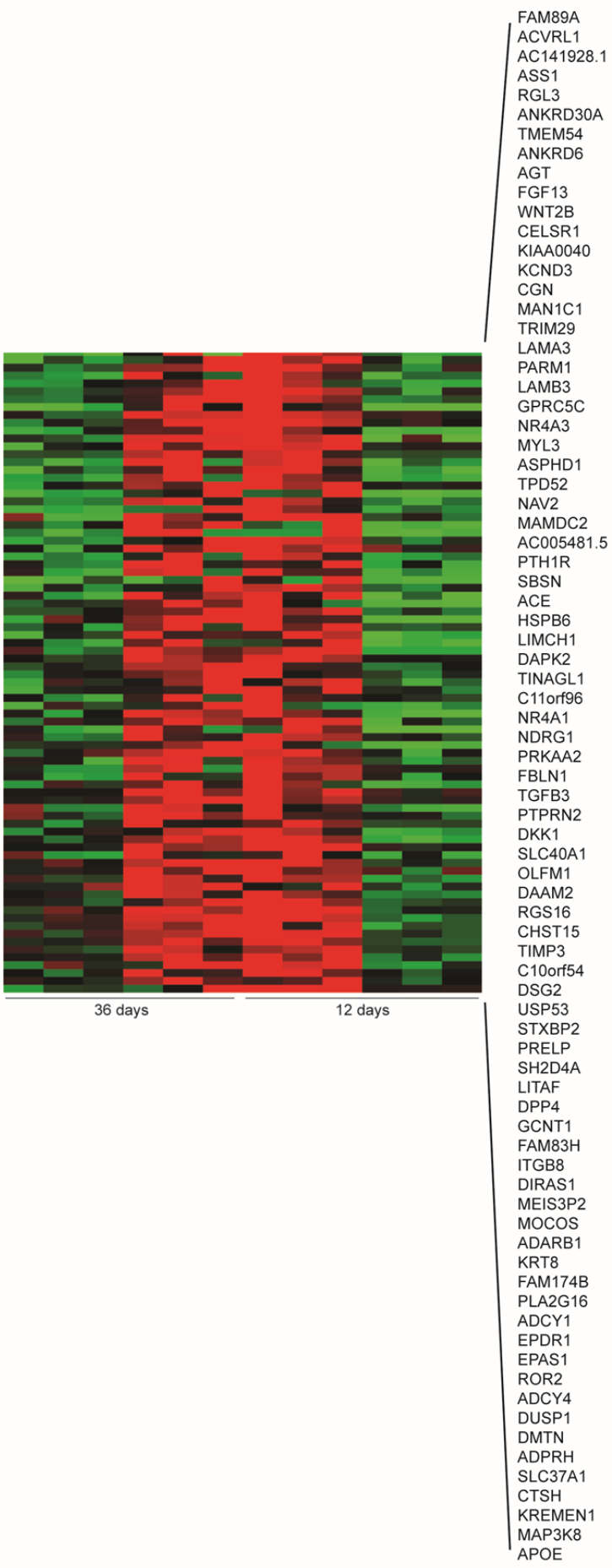
FAM89A
ACVRL1
AC141928.1
ASS1
RGL3
ANKRD30A
TMEM54
ANKRD6
AGT
FGF13
WNT2B
CELSR1
KIAA0040
KCND3
CGN
MAN1C1
TRIM29
LAMA3
PARM1
LAMB3
GPRC5C
NR4A3
MYL3
ASPHD1
TPD52
NAV2
MAMDC2
AC005481.5
PTH1R
SBSN
ACE
HSPB6
LIMCH1
DAPK2
TINAGL1
C11orf96
NR4A1
NDRG1
PRKAA2
FBLN1
TGFB3
PTPRN2
DKK1
SLC40A1
OLFM1
DAAM2
RGS16
CHST15
TIMP3
C10orf54
DSG2
USP53
STXBP2
PRELP
SH2D4A
LITAF
DPP4
GCNT1
FAM83H
ITGB8
DIRAS1
MEIS3P2
MOCOS
ADARB1
KRT8
FAM174B
PLA2G16
ADCY1
EPDR1
EPAS1
ROR2
ADCY4
DUSP1
DMTN
ADPRH
SLC37A1
CTSH
KREMEN1
MAP3K8
APOE
36 days
12 days

Figure 4.19. Discordant genes between A83-01 treated and clonogenic eMSCs. (A) Venn diagram showing overlap of 160 genes differentially regulated in A83-01 treated and clonogenic eMSCs ($q < 0.05$). (B) Heatmap representing expression level of the 160 discordant genes, which are listed on the right. Again, the heatmap was divided into two parts because of its size.

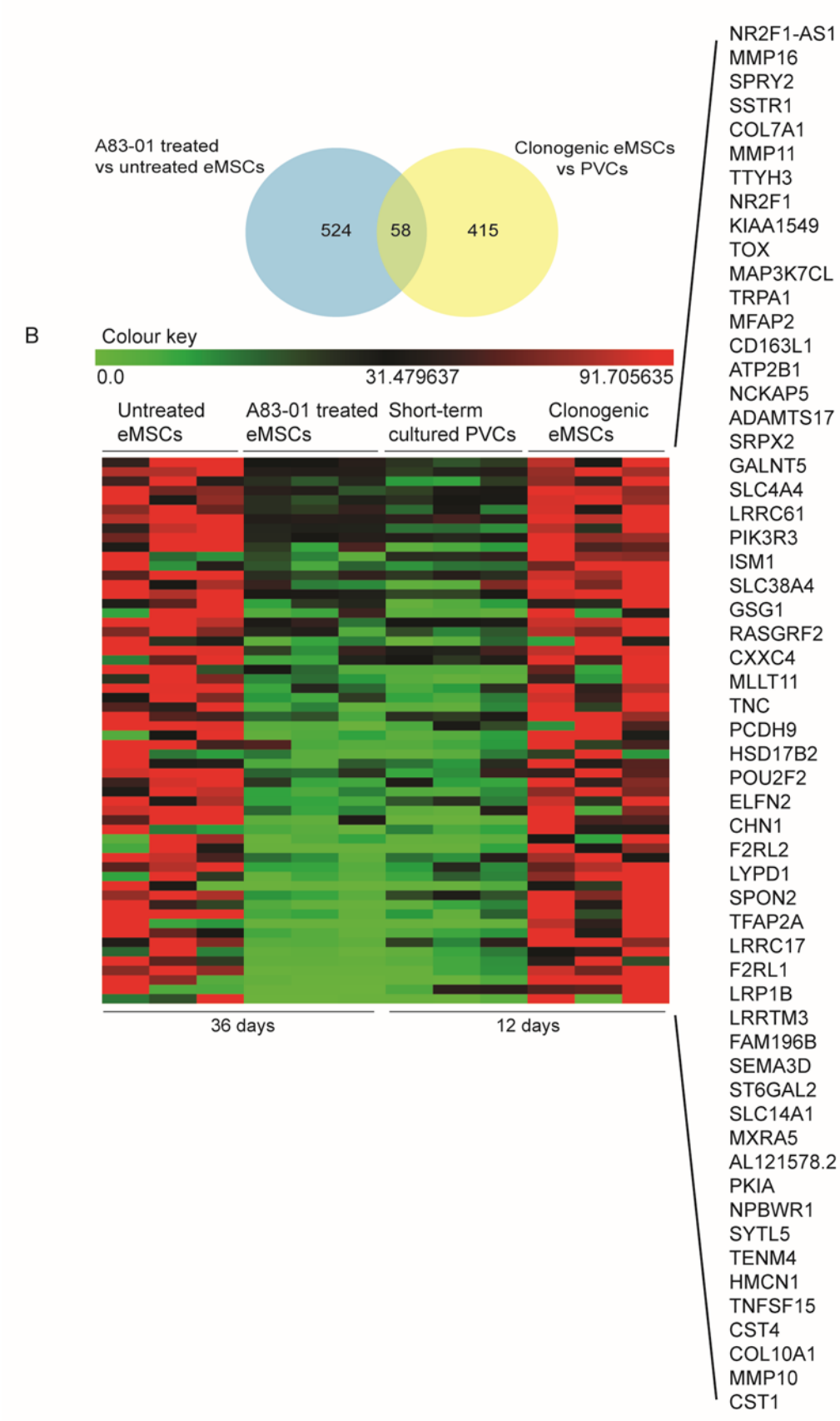
A83-01 treated
vs untreated eMSCs
Clonogenic eMSCs
vs PVCs
524
58
415
B
Colour key
0.0
31.479637
91.705635
Untreated
eMSCs
A83-01 treated
eMSCs
Short-term
cultured PVCs
Clonogenic
eMSCs
36 days
12 days
NR2F1-AS1
MMP16
SPRY2
SSTR1
COL7A1
MMP11
TTYH3
NR2F1
KIAA1549
TOX
MAP3K7CL
TRPA1
MFAP2
CD163L1
ATP2B1
NCKAP5
ADAMTS17
SRPX2
GALNT5
SLC4A4
LRRC61
PIK3R3
ISM1
SLC38A4
GSG1
RASGRF2
CXXC4
MLLT11
TNC
PCDH9
HSD17B2
POU2F2
ELFN2
CHN1
F2RL2
LYPD1
SPON2
TFAP2A
LRRC17
F2RL1
LRP1B
LRRTM3
FAM196B
SEMA3D
ST6GAL2
SLC14A1
MXRA5
AL121578.2
PKIA
NPBWR1
SYTL5
TENM4
HMCN1
TNFSF15
CST4
COL10A1
MMP10
CST1

Figure 4.20. Discordant genes between A83-01 treated and clonogenic eMSCs. (A) Venn diagram showing overlap of 58 genes differentially regulated in A83-01 treated and clonogenic eMSCs ($q < 0.05$). (B) Heatmap representing expression level of 58 discordant genes, which are listed on the right.

4.2.7 Disease state associated to A83-01-responsive genes

Next, DAVID v6.8 was used to determine the association between A83-01 responsive genes in prolonged eMSC cultures and disease states.

Interestingly, a conspicuous association was apparent between genes upregulated upon A83-01 treatment of eMSCs and metabolic and vascular disorders (Figure 4.21), especially 'carotid artery diseases' (fold enrichment = 23) and 'diabetes mellitus type 2' (fold enrichment = 23). Term related to 'carotid artery diseases' included three genes encoding *APOE* (apolipoprotein E), *AGT* (angiotensin) and *ACE* (angiotensin I converting enzyme); and 'diabetes mellitus type 2' included *NOS3* (nitric oxide synthase 3), *APOE* and *ACE*.

Interestingly, 'endometrial neoplasms' (fold enrichment = 13) and 'breast and prostate cancer' (fold enrichment = 4) were depleted upon A83-01 treatment (Figure 4.22). 'Endometrial neoplasm' included *MMP2* (matrix metallopeptidase 2), *MMP7* (matrix metallopeptidase 7) and *ESR1* (estrogen receptor 1); and 'breast and prostate cancer' included *HSD17B2* (hydroxysteroid 17-beta dehydrogenase 2), *IGF2* (insulin like growth factor 2) and *PRL* (prolactin receptor).

This analysis revealed a potential association between genes differentially regulated upon A83-01 and disease state. However, this does not necesserarly mean that induction or depletion of a particulary set of genes, related to a specific disease, is translated in a disorder. However, alterations of these genes might increase the risk. As the number of genes in each enriched GO term was limited, the data should be interpreted with caution.

Figure 4.21. Selected disease states associated to upregulated genes upon A83-01 treatment. Enrichment analysis of the significantly upregulated genes and their correlation with disease states. The size of the words describing the identified disorders is directly proportional to their fold enrichment (fold change values between 10 and 23).

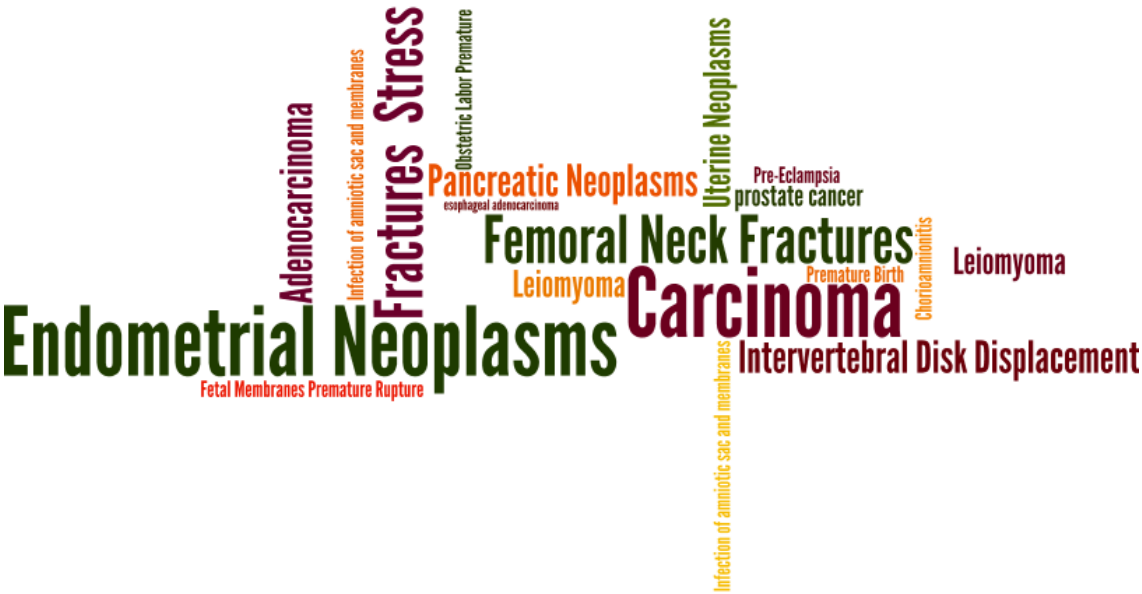

Figure 4.22. Selected disease states associated to downregulated genes upon A83-01 treatment. Enrichment analysis of the significantly downregulated genes and their correlation with disease states. The size of the words describing the identified disorders is directly proportional to their fold enrichment (fold change values between 3 and 13).

4.2.8 Differential regulation of transcription factors upon A83-01 treatment

Differentially expressed genes in A83-01 treated and untreated cultures were further interrogated to identify transcription factors (TFs) regulated in response to TGF-β-R inhibition.

Based on $q < 0.05$, a robust list of 104 differentially expressed TFs in response to A83-01 treatment was identified. *RARB* (retinoic acid receptor beta; $q = 1.06 \times 10^{-33}$); *WT1* (Wilms tumor 1; $q = 4.94 \times 10^{-16}$), and *HEYL* (hes related family bHLH transcription factor with YRPW motif-like; $q = 2.21 \times 10^{-10}$) were amongst the most highly enriched TFs. Highly repressed TFs included *MEOX1* (mesenchyme homeobox 1; $q = 1.06 \times 10^{-12}$), *ESR1* (estrogen receptor 1; $q = 7.04 \times 10^{-29}$), and *EGR2* (early growth response 2; $q = 6.59 \times 10^{-11}$) (Figure 4.23).

Out of the 104 A83-01 responsive TFs, only 8 were concordantly regulated between clonal eMSCs and matched PVSCs. A83-01-responsive TFs enriched in clonal eMSCs included *TFAP2C* (transcription factor AP-2 gamma), *HOXB3* (homeobox B3) and *TOX2* (TOX high mobility group box family member 2). Conversely, A83-01-responsive TFs downregulated upon differentiation of clonal to PVSCs included *DLX5* (distal-less homeobox 5), *ZFHX2* (zinc finger homeobox 2) and *ZNF853* (zinc finger protein 853).

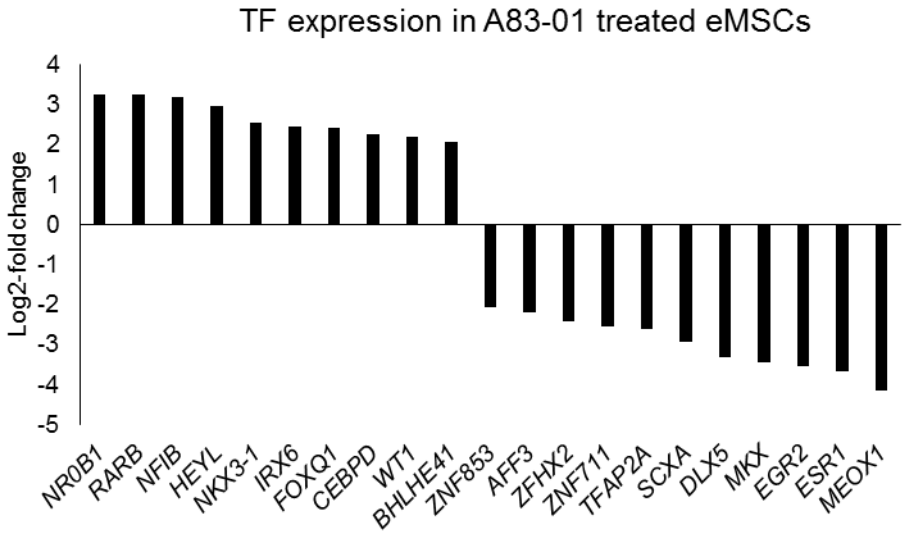

Figure 4.23. Changes in TF expression upon A83-01 treatment. Inhibition of TGF-β-R signalling pathways alters expression of genes encoding TFs. Graph shows expression of selected significantly up- and down-regulated TFs (log2-fold change ≥ 1 and ≤ -1).

4.3 Discussion

Cell reprogramming via the use of small molecules that modulates stem cell specification and function offers significant opportunities to study the cell biology and enhance our knowledge of the therapeutic potential of stem cells (Yu *et al*., 2014; Li *et al*., 2013). Compared to genetic tools, the use of small molecules for cell reprogramming provide several advantages, for example their effect is reversible, that means that they can temporally regulate cellular function. This allows to yield sufficient amounts of homogeneous cells for clinical applications. Also, small molecules can be used in synergy with other factors, and this may improve their efficacy (Li *et al*., 2012). Small molecules can act as activators or repressors of signalling pathways. In this way, they regulate downstream gene transcription (Yun *et al*., 2014). The use of a glycogen synthase kinase (GSK) 3 inhibitor to maintains the pluripotency of induced pluripotent stem (iPS) cells exemplified such approach (Takahashi & Yamanaka, 2006; Li *et al*., 2009; Ying *et al*., 2008; Silva *et al*., 2008).

A recent study showed that inhibition of TGF-β-R signalling, through TGF-β-R inhibitor A83-01, promotes eMSC proliferation, maintaining their clonogenic phenotype and preventing spontaneous differentiation (Gurung *et al*., 2015). The use of A83-01 as a signalling pathway modulator has provided a robust tool to generate amount in the large scale manufacture of homogenous eMSC populations for clinical applications. Understanding gene expression programs and mapping of altered chromatin accessibility in response to A83-01 treatment is required to realize regulatory mechanisms that maintains eMSCs in an undifferentiated state.

Data confirmed that TGF-β-R inhibition enhances proliferative ability of eMSCs as shown by increased cumulative cell population and number of PDs upon treatment. Furthermore, data revealed that TGF-β-R blockade maintains clonogenic phenotype of MSCs. Specifically, A83-01 positively regulated the number of CD140b- and SUSD2- positive cells in prolonged culture and increase for the same markers. Also, results confirmed that TGF-β-R blockade improves

the ability of cultured eMSCs to form colonies, preventing loss of clonogenicity. Notably, results showed marked variation in the responsiveness of primary cultured eMSCs to treatment, underlying the intrinsic variability between primary cultures.

Gene profiling of cultured eMSCs upon A83-01 treatment revealed that TGF-β-R blockade involves wholesale reprograming of the transcriptome. The resulting differentially expressed genes are implicated a broad range of functions. For example, A83-01 treatment resulted in upregulation of genes involved in intracellular receptor signalling pathways and regulation of growth, and downregulation of genes encoded for collagen catabolism and cell fate commitment. Notably, RNA-seq revealed upregulation of SUSD2, consistent with flow cytometry data showing increase in the percentage of SUSD2- positive cells and MFI for the same marker. Conversely, transcriptomic profiling revealed depletion of perivascular markers, such as *MCAM*, *MYH11* and *ELN*.

Mining of the data revealed that TGF-β-R inhibition repressed the expression of numerous genes encoding for ECM components, including *COL1A1*, *COL1A2* and *SPARC*. ECM production is a well characterized response to injury and TGF-β signalling is master regulator. More accurately, in the case of tissue damage, fibroblasts transit from a quiescent to an activated state, where TGF-β signalling, amongst others signalling pathways, activates genes encoding for ECM proteins and cytoskeletal remodelling (Nakerakanti and Trojanowska, 2012; Biernacka, A., *et al,* 2011). This suggests that the effect of TGF-β-R blockade in maintaining eMSCs in a less differentiated state might be mediated by preventing fibroblast activation and limiting ECM deposition in prolonged culture. Hence, it would be interesting to validate the induction of ECM genes at a mRNA and protein level through RT-qPCR and western blot, although time limitations prevented me of pursuing this line of investigation any further.

To determine if A83-01 induces a stem cell signature, I compared the transcriptome profile of A83-01 treated and untreated eMSCs with the RNA-seq data obtained from another dataset, comparing clonal eMSCs to time-matched unselected PVCs.

This analysis revealed a dataset of shared genes accounting for 38 concordant up- and 120 concordant down- regulated loci. Interestingly, functional annotation of the commonly down-regulated genes highlighted an abundance of genes encoding for ECM components or associated to ECM organization.

For therapeutic application, it is of paramount importance to ensure that A83-01 treatment does not alter expression level of transcripts associated to clinical disorders. Functional annotation revealed a majority to be associated with metabolic and vascular disorders, which might alert in terms of clinical use. On the other hand, analysis of the data showed that TGF-β-R blockade correlates with downregulation of genes associated to cancer, reassuring for a safe use of these cells in regenerative medicine.

Taken together, the current findings suggest that A83-01 effect might be related to prevention of fibroblast activation.

Chapter 5

Analysis of dynamic chromatin changes in cultured eMSCs upon TGF-β-R inhibition

5.1 Introduction

eMSCs are a rare and promising source of cells for cell-based therapy for women with reproductive disorders, largely because of their self-renewal and differentiation properties (Darzi *et al*., 2016). As in the case for other cell types, eMSC identity results from a specific gene expression pattern. Chromatin organization and a dynamic epigenetic code govern differential expression of the transcripts. Epigenetic modifications, including nucleosome positioning, TF binding and chromatin regulators, DNA modifications (e.g. acetylation, methylation, sumoylation etc.) alter genomic structure, thereby sequestering some DNA regions and leaving others open or accessible to TF binding (Chen & Dent, 2014).

Chromatin profiling of bone-marrow MSCs in prolonged culture revealed that changes in acetylation level of histone 3 (H3) negatively regulated the expression of pluripotency factors, such as octamer-binding transcription factor 4 (OCT4) and SRY-box 2 (SOX2) (Li *et al*., 2011). Other studies also showed that during MSC differentiation, changes in gene expression pattern correlate, amongst others, with dynamic changes in histone modifications (Herlofsen *et al*., 2013). Understanding of the interplay between genomic modifications and TFs regulating chromatin remodelling is a prerequisite for clinical applications of MSCs.

Gurung *et al*. (2015) provided a promising approach to promote eMSC proliferation in prolonged culture while preventing differentiation. In the previous chapter, I examined the impact of TGF-β-R blockade on the transcriptome of cultured eMSCs. Transcriptomic analysis of the differentially expressed genes revealed a wholesale transcriptomic reprogramming in cultured eMSCs treated with A83-01 compared to untreated cultures.

These changes in gene expression pattern must be underpinned by a dynamic genomic remodelling. I postulated that TF binding sites enriched or depleted in opening or closing chromatin loci, respectively, will provide further insights into

the mechanisms of A83-01 action. To test this hypothesis, in this chapter I used ATAC-seq as a robust method to accurately probe regions of differential chromatin opening effective also on rare group of cells.

5.2 Results

5.2.1 Analysis of chromatin landscape in cultured eMSCs

To map the changes in chromatin accessibility, primary eMSCs were treated with or without TGF-β-R inhibitor for 36 days. The nuclei were harvested and processed for ATAC-seq. ATAC-seq libraries, with a size distribution between 150 and 600 bp, were sequenced on the Illumina HiSeq1500. Twenty-five million paired end reads were sequenced per sample, with a read length of 50 bp. As for the RNA-sequencing, PCA was performed to assess the effect of TGF-β-R inhibition on chromatin landscape of cultured eMSC. In this analysis, PC1, which accounted for 43.26% of variation in chromatin opening, separated A83-01 treated and untreated cultures, reflecting the effect of TGF-β-R inhibition on chromatin accessibility. PC2, which accounted for 27.01% of variation in chromatin opening, reflected intrinsic differences in primary cultures. It separated the control samples 63 and 64 from 74; and treated samples 63 and 64 from 74 (Figure 5.1).

DESeq was used to identify differential ATAC-seq peaks, reflecting genomic regions of active chromatin opening or closing. Based on $q < 0.05$, DESeq revealed a total of 5,967 differential ATAC-seq peaks. Specifically, 3,555 (60%) and 2,412 (40%) genomic regions significantly opened or closed following A83-01 treatment over 36 days, respectively. Out of 5,967 peaks, 31% and 29% of the opening and closing ATAC-seq peaks, respectively, fell within - 10 to + 1 kilobases (kb) around TSSs. For example, *RARB*, *TGFBR3* (transforming growth

factor beta receptor 3) and *SUSD2* showed increased chromatin accessibility at and upstream of their proximal promoters upon inhibition of TGF-β-R signalling (Figure 5.2A-C). Cross-referencing with RNA-seq data showed a significant increase in *RARB*, *TGFBR3* and *SUSD2* transcript levels in response to A83-01 treatment ($q < 1.1 \times 10^{-32}$, $q < 1.23 \times 10^{-21}$ and $q < 2.72 \times 10^{-4}$, respectively). Conversely, *CADM1*, *WNT5A* and *COL1A1* are three examples of genes repressed upon TGF-β-R inhibition. As shown in Figure 5.3, downregulation of *CADM1* and *COL1A1* is associated with closure of their proximal promoters whereas silencing of *WNT5A* is mediated by closure of a distal enhancer. Again, cross-referencing of the ATAC-seq data with transcriptomic analysis data revealed an association between chromatin remodelling and differential gene expression. Specifically, TGF-β-R inhibition negatively regulated the expression levels of *CADM1* ($q < 1.93 \times 10^{-46}$), *COL1A1* ($q < 1.37 \times 10^{-9}$) and *WNT5A* ($q < 5.0 \times 10^{-30}$).

Dynamic chromatin changes at specific loci alter binding of TFs and thus gene expression. Because TFs can both activate and repress transcription, the correlation between dynamic changes in chromatin landscape and gene expression is not necessarily linear. Nevertheless, analysis of 200 loci associated with the most dynamic ATAC-seq peaks revealed that opening and closing loci (within 10 kb of the TSS) correlate with increased and decreased expression of nearby genes, respectively ($p = 1.0 \times 10^{-6}$) (Figure 5.4).

Taken together, the ATAC-seq data provided a genome-wide map of chromatin remodelling in response to TGF-β-R inhibition in prolonged eMSC cultures. Next, I interrogated the informative ATAC-seq peaks to gain insight into the *cis*-regulatory landscape that underpins the transcriptional reprogramming of eMSCs upon A83-01 treatment.

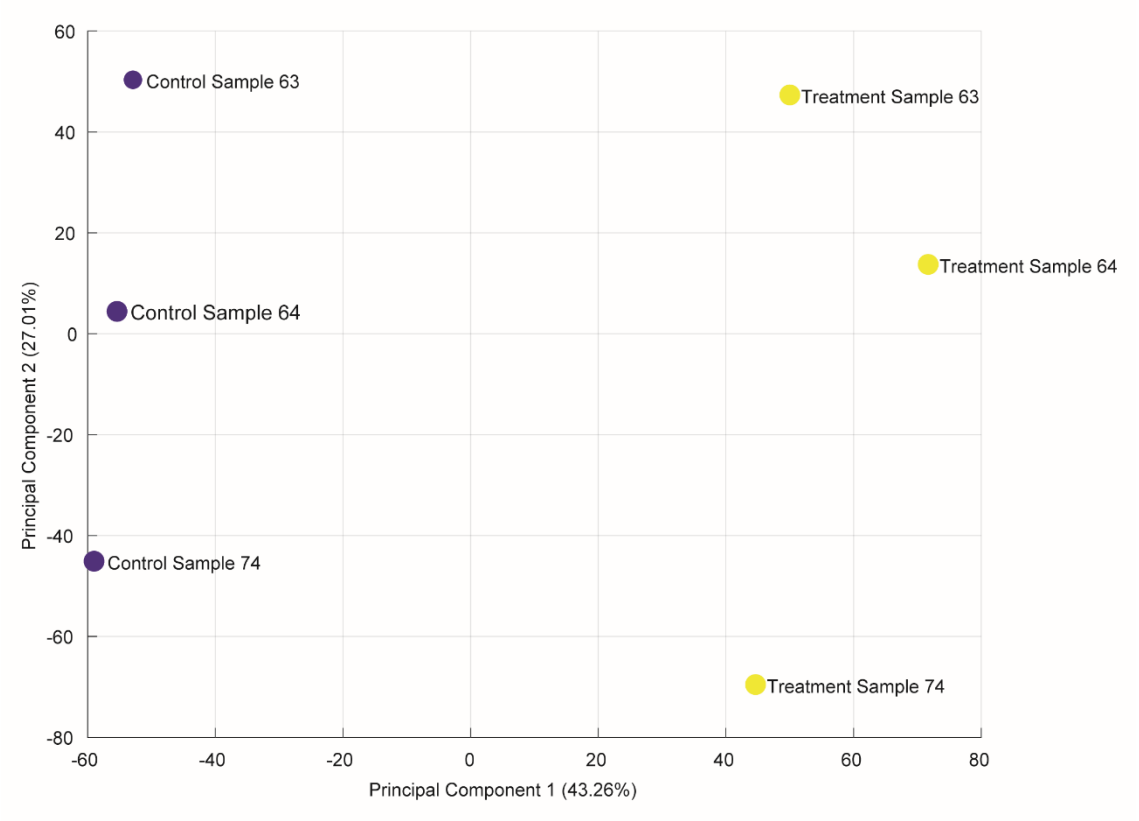

Figure 5.1. PCA of A83-01 treated and untretaed eMSCs. PCA of ATAC-seq data from three paired eMSC cultures, treated in the presence or absence of TGF-β-R inhibitor for 36 days. PC1 explains variation due to A83-01 treatment, whereas PC2 explians variability due to different primary cultures.

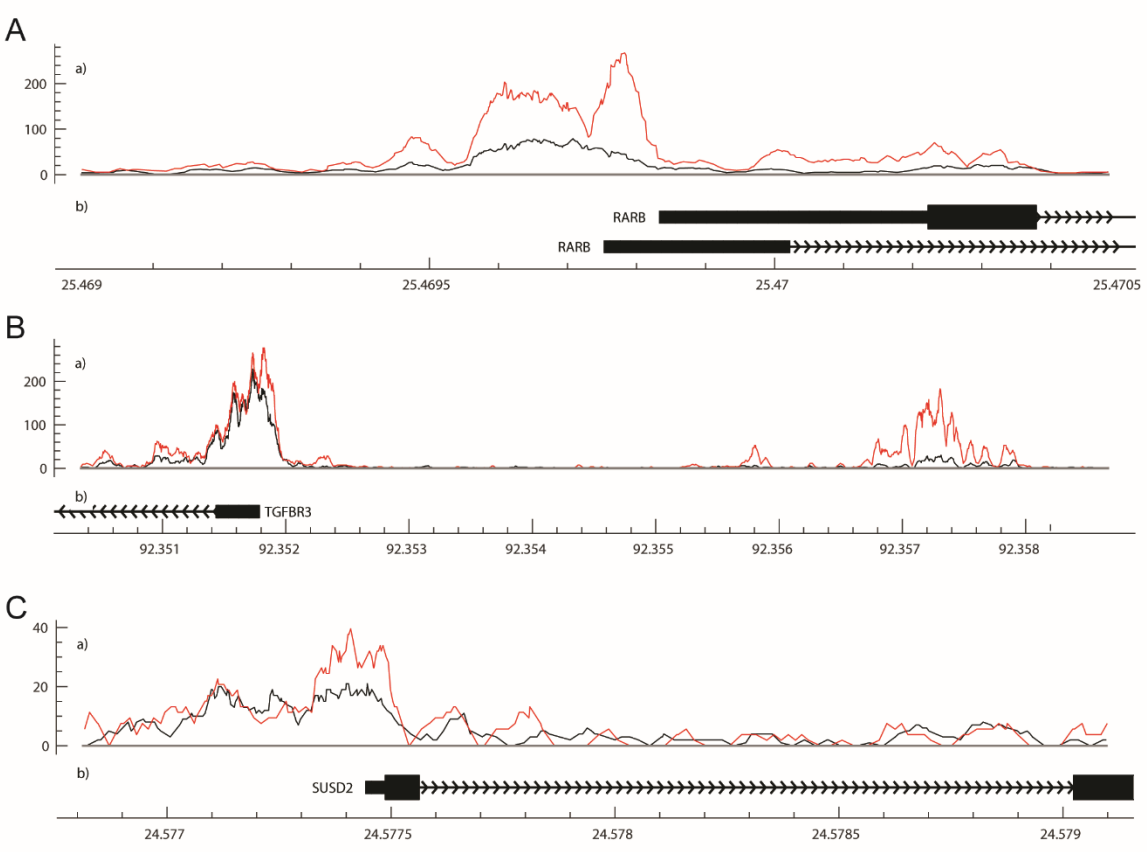

Figure 5.2. Representative opening ATAC-seq peaks. Representative ATAC-seq peaks showing transition from closing to opening chromatin upstream the promoter of *RARB* (A), *TGFBR3* (B) and *SUSD2* (C). Black and red traces represent untreated and A83-01 treated eMSC cultures. The X-axis shows the genomic location of the ATAC-seq peaks and genes. The Y-axis shows the frequency of Tn5 cutting.

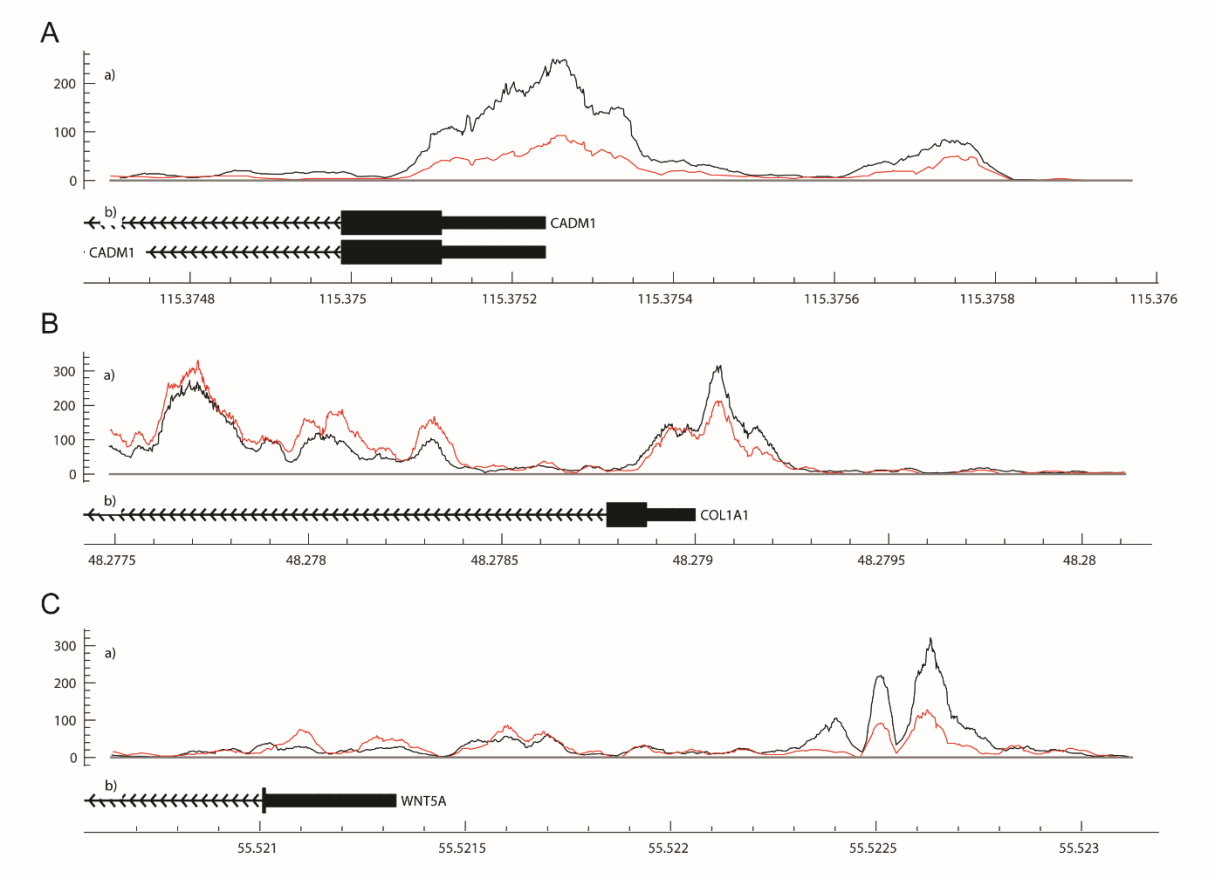

Figure 5.3. Representative closing ATAC-seq peaks. Differential ATAC-seq peaks showing closing transition from opening to closing chromatin of the proximal promoter of CADM1 (A) and COL1A1 (B) and of a distal enhancer of WNT5A (C) in response to A83-01. Black and red traces represent untreated and A83-01 treated eMSC cultures. The X-axis shows the genomic location of the ATAC-seq peaks and genes. The Y-axis shows the frequency of Tn5 cutting.

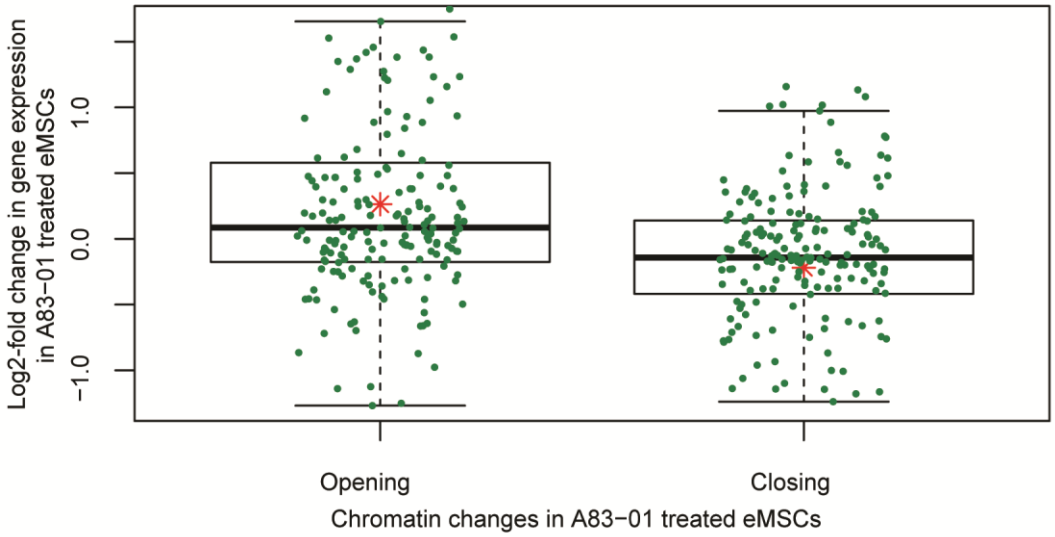

Figure 5.4. Differential chromatin opening correlates with gene expression changes in A83-01 treated eMSCs. Changes in chromatin landscape of eMSCs in response to TGF-β-R inhibition correlate with differential regulation of gene expression. Box plots showing increase or decrease in transcript levels of 200 genes (within 10 kb of the TSS) associated with the most open and closed ATAC-seq peaks. Y-axis shows relative changes in transcript levels, expressed as log2-fold change: +ve and –ve values relate to up- and down-regulated genes, respectively. X-axis shows ATAC-seq peaks clustered in opening and closing peaks. Green dots represent the genes and the red asterisk represents mean log2-fold change (p = 1.0 x 10^{-6}, t-test).

5.2.2 TF Binding Motif Discovery

To gain insights into *cis*-regulatory landscape underpinning differential gene expression in response to TGF-β-R inhibition, *de novo* short sequence motif enrichment analysis using HOMER was performed on 3,555 opening and 2,412 closing ATAC-seq peaks.

A total of 19 motifs (Opening M1-19) were significantly enriched in opening ATAC-seq peaks and 17 motifs (Closing M1-17) were significantly overrepresented in closing ATAC-seq peaks (Figure 5.5). To identify putative TFs likely to be involved in the binding of the identified motifs, I integrated the short sequence motifs with known TF databases and further examined the expression level of the presumable binding TFs. This analysis revealed a number of motifs enriched in opening and closing ATAC-seq peaks corresponded to high affinity binding sites for TFs enriched or depleted in response to A83-01 treatment, respectively. CEBPB, CEBPD, nuclear receptor subfamily 4 group A member 1 (NR4A1; also known as NUR77), RAR related orphan receptor A (RORA) and forkhead box P2 (FOXP2) were amongst the most plausible differentially induced TFs with high binding affinity for motifs enriched in opening ATAC-seq peaks. Conversely, downregulation of transcription factor 21 (TCF21), TGFβ induced factor homeobox 2 (TGIF2) and nuclear transcription factor Y subunit alpha (NFYA) in response to A83-01 treatment corresponded to loss of accessibility of their respective high affinity binding sites (Figure 5.6).

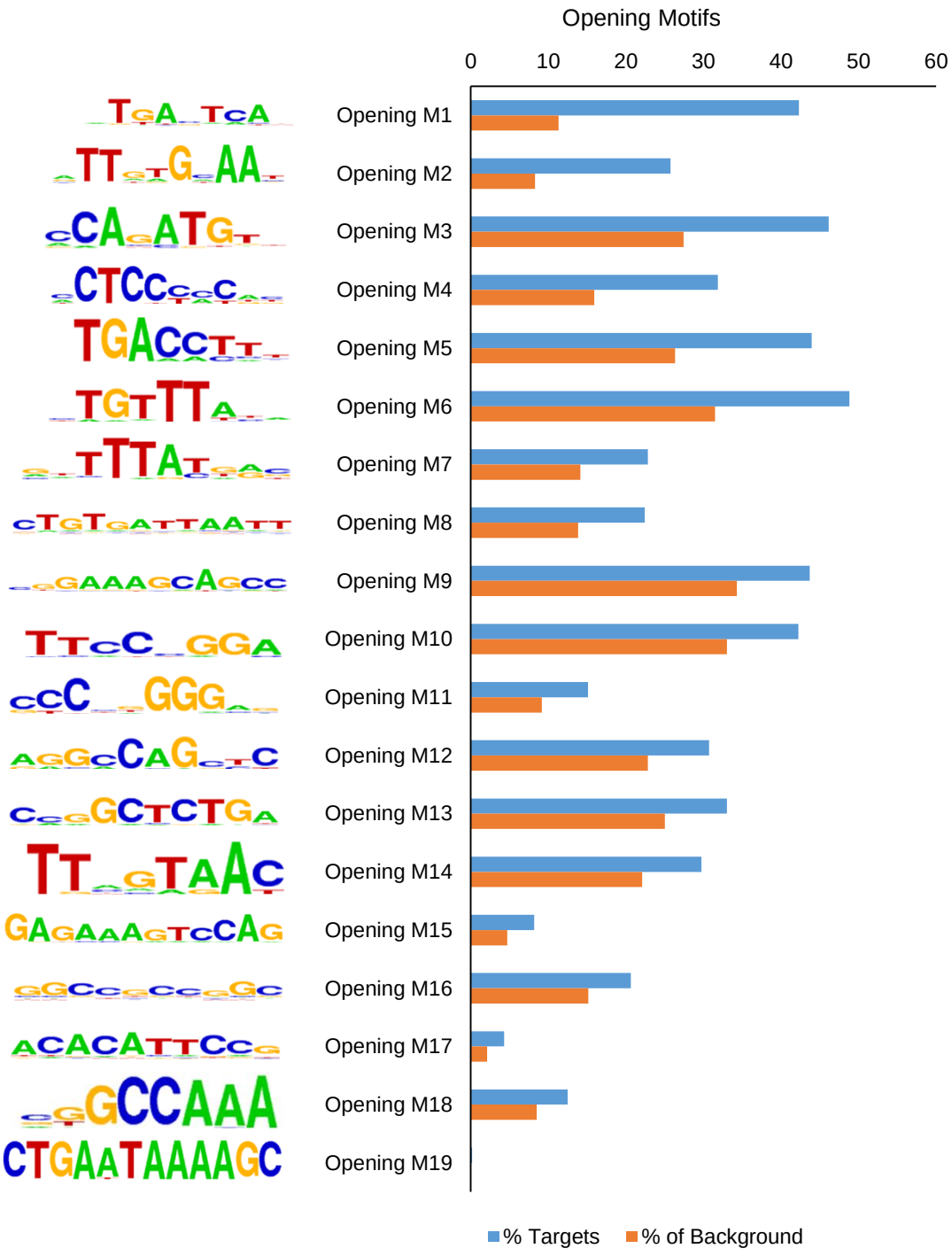
Opening Motifs
0
10
20
30
40
50
60
Opening M1
Opening M2
Opening M3
Opening M4
Opening M5
Opening M6
Opening M7
Opening M8
Opening M9
Opening M10
Opening M11
Opening M12
Opening M13
Opening M14
Opening M15
Opening M16
Opening M17
Opening M18
Opening M19
% Targets
% of Background

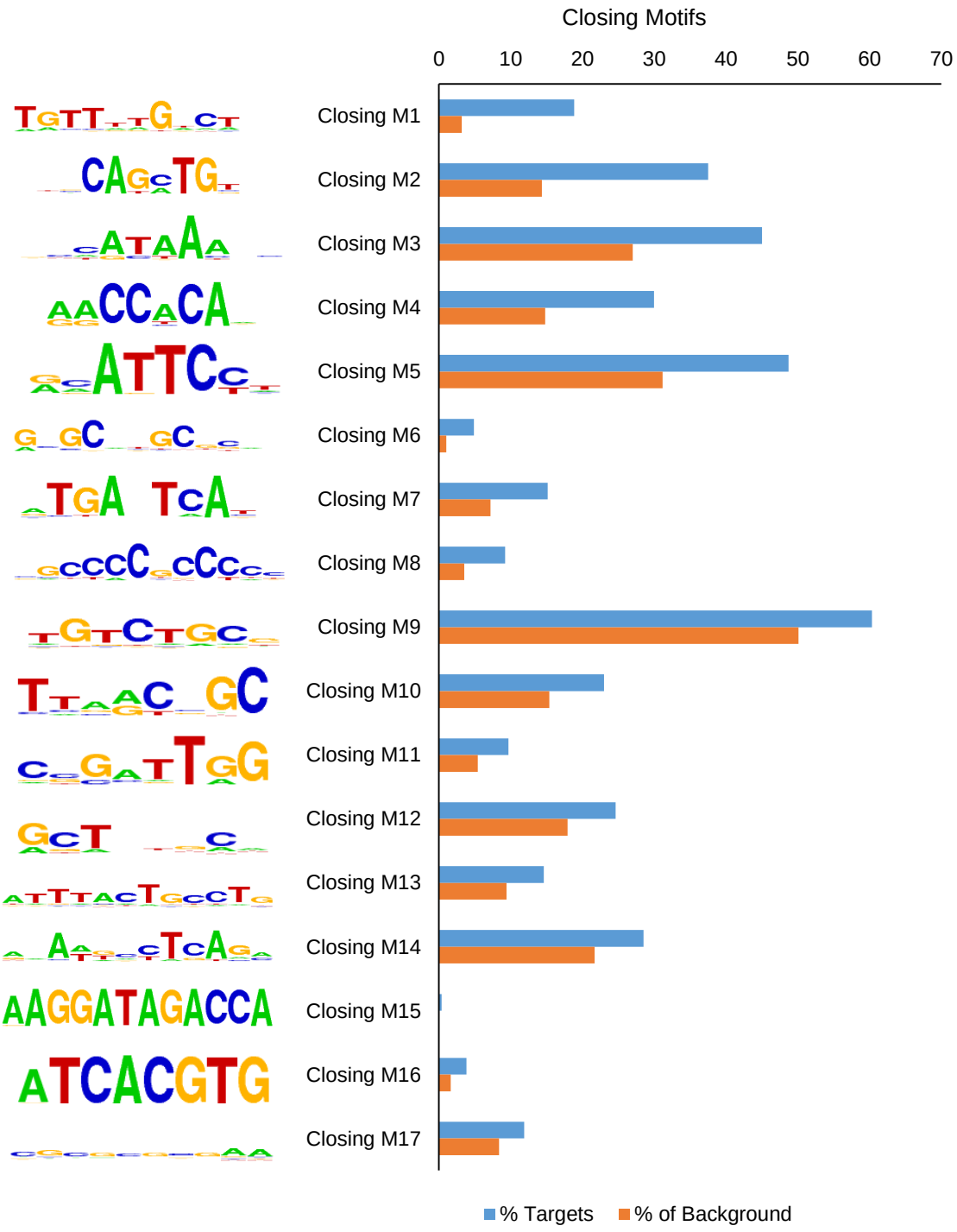

Figure 5.5. Enrichment of TF binding motifs in opening and closing genomic regions. Total of 19 and 17 TF binding motifs enriched in the opening and closing ATAC-seq peaks, respectively. The frequency (%) of peaks (blue bars) containing a given motif is shown relative to genomic regions randomly selected from the genome (orange bars) (±50 Kb from TSS, matching size, and GC/CpG content.

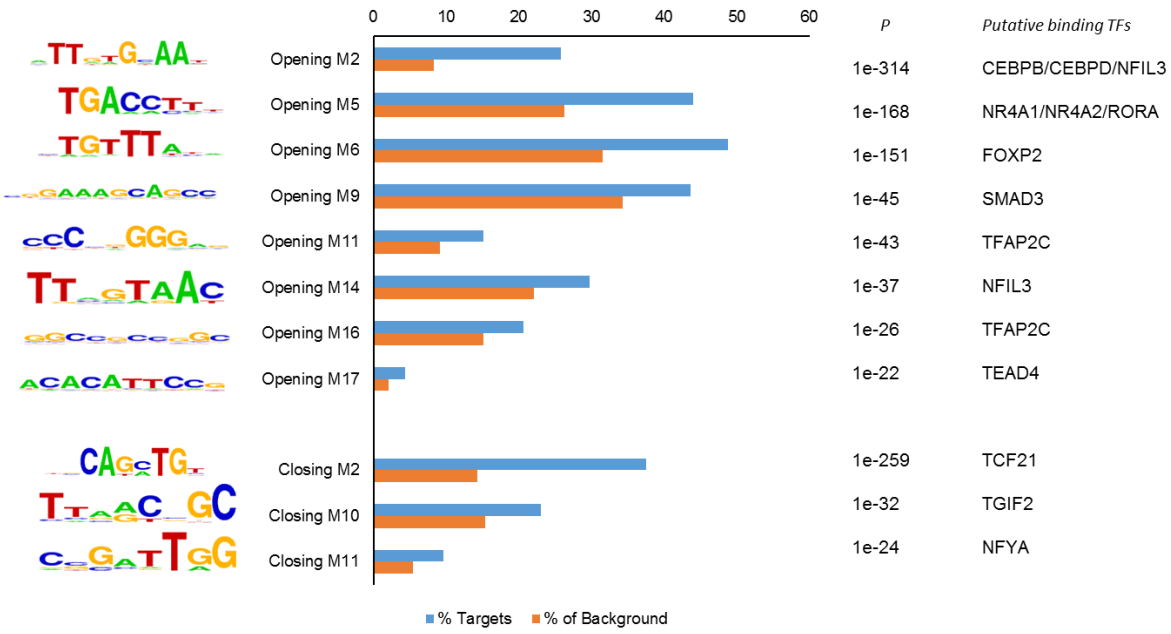

Figure 5.6. Differentially regulated TFs matched to enriched and depleted short sequence binding motifs. Bar graph showing enriched and depleted binding motifs coupled with the most plausible differentially expressed TFs, based on motif specificity. In the bar graph, the frequency (%) of peaks (blu bars) containing the motif is shown relative to genomic regions randomly selected from the genome (orange bars) (±50 Kb from TSS, matching size, and GC/CpG content). *P* indicates the *p*-value of the short sequence binding motifs.

5.3 Discussion

In this chapter, I examined the interplay between gene expression pattern and dynamic epigenetic code that govern the identity and function of eMSCs in extended culture. Because of their scarcity in tissues, it is challenging to investigate chromatin state of adult MSCs in general. ATAC-seq enables to overcome this limitation. It provides a robust method for genome-wide analysis of the chromatin structure of rare cellular types.

It is quite apparent that A83-01-induced TGF-β-R blockade provides a powerful approach for eMSC expansion in prolonged culture. In Chapter 4, I provided evidence that TGF-β-R blockade prevents loss of proliferative capacity of eMSCs in prolonged culture. Transcriptional profiling indicated that A83-01 partly maintains the expression of genes associated with stemness and, importantly, inhibits genes associated with fibroblast activation. ATAC-seq analysis provided unbiased analysis of the changes in the *cis*-regulatory landscape that underpin the cellular responses to A83-01 treatment.

By integrating the transcriptomic and ATAC-seq analysis, I was able to assign 12 A83-01 induced TFs to high-affinity binding motifs enriched in opening chromatin loci. Conversely, 3 TFs repressed in response to A83-01 corresponded loss of high affinity binding sites. Some of the most highly enriched *cis*-regulatory motifs showed high affinity for TFs implicated in eMSC differentiation, for example CEBPB and RORA (Frith & Genever, 2008; Myamoto *et al*., 2012). Hence, their role in maintaining cultured eMSCs in an undifferentiated state needs further investigation. However, this analysis also revealed some interesting new pharmacological targets to enhance *in vitro* expansion of eMSCs even further. For example, induction of *NR4A1* transcript levels in A83-01 treated cells corresponded to enrichment in putative NR4A1 binding sites. NR4A1, also known as NUR77, is an orphan nuclear receptor that belongs to steroid-thyroid hormone-retinoid receptor superfamily. NR4A1 was recently identified as an endogenous inhibitor of TGF-β signalling (Palumbo-Zerr *et al*., 2015). Nr4a1-null mice exhibit pronounced dermal thickening, massive deposition of collagen, and higher

myofibroblast counts when compared to wild-type mice. Furthermore, lack of Nr4a1 in mice results in exacerbated fibrosis in two model of skin fibrosis. The use of small molecules that function as NR4A1 agonists can restore its activity, re-activating an endogenous negative regulation of TGF-β signalling. Hence, they can be used as potential treatment to inhibit fibrosis (Palumbo-Zerr *et al*., 2015). Importantly, cytosporone-B is a small molecule that acts as a selective agonist for NR4A1 (Zhan *et al*., 2008). Cytosporone-B increases the nuclear retention of NR4A1 in cultured fibroblasts. In wild-type mice with a constitutively active TGF-β-R type I, the use of Cytosporone-B results in a down-regulation of TGF-β target genes, reduces collagen production and inhibits myofibroblast differentiation. Nr4A1-null mice are not responsive to Cytosporone-B. Moreover, it also has anti-fibrotic effects, as exemplified by its therapeutical effects in TGF-β-R type I-induced skin fibrosis and bleomycin-induced pulmonary fibrosis (Palumbo-Zerr *et al*., 2015). Hence, it would be interesting to test if cytosporone-B could either replace or synergise with A83-01 to enhance expansion of eMSCs in prolonged culture.

Taken together, TF binding motif discovery and mining of the RNA-seq data revealed enrichment and depletion of putative TFs likely to be involved in the regulation of chromatin configuration underlying the wholesale transcriptomic reprogramming. Interestingly, this exercise yielded a potential novel pharmacological target that might be used enhance *in vitro* expansion of eMSCs.

Chapter 6

Discussion

Discussion

Cell-specific responses to a given cue, whether hormones, growth factors, cytokines, chemokines or stress signals, are not only determined by the level of expression and activation status of relevant receptors, signal transduction pathways and downstream TFs but also by the organisation of the chromatin on which TFs act in conjunction with interacting partners, such as co-activators, co-repressors, histone-modifying protein complexes and the basal transcriptional machinery (Chen & Dent, 2014).

The structural subunit of chromatin is the nucleosome. It contains approximately 147 bp of DNA wrapped almost twice around a central octamer composed of two molecules each of the four core histones: H2A, H2B, H3 and H4. Generally, the compact structure of the nucleosome prevents TF binding (Kornberg, 1974). Upon chromatin remodelling, active promoters are often depleted of nucleosomes, forming 'nucleosome-depleted regions' that are flanked by relatively unstable nucleosomes containing the histone variants H2A.Z and H3.3 (Jin & Felsenfeld, 2007). Similarly, enhancers, which are regulatory elements typically located far from their target promoters, are often associated with nucleosomes containing H2A.Z and H3.3, and specific histone modifications. Further, high-throughput chromosome conformation capture (3C)-derived (Dekker *et al*. 2002) methods have revealed that chromatin is organised in open and closed compartments that tend to be spatially segregated depending on their transcriptional activity (Lieberman-Aiden *et al*. 2009). At a local level, functionally related genes have been shown to be brought close in space to be transcribed in a correlated fashion during cell differentiation. These genes, which may map to different chromosomes, are organized in spatial clusters that sometimes referred to as transcriptional "factories" (Osborne *et al*. 2004; Cavalli 2007).

Modulation of chromatin architecture regulates differential exposure of DNA to binding of transcriptional regulators and hence dictates activation or repression of transcription (Voss & Hager, 2014). 'Initiating factors' localize chromatin remodelling proteins and histone modifiers at specific *cis*-regulatory elements of

the genome, partly due to the fact that they share common features with histone linkers and hence exhibit the ability of binding nucleosomes and chromatin (Zaret & Caroll, 2011). Pioneers factors, including FoxA and GATA proteins (Bossard & Zaret, 1998; Gualdi *et al.,* 1996; Cirillo *et al*., 1998; Cirillo & Zaret, 1999), steroid receptors (Swinstead *et al*., 2016), are a special category of proteins capable to penetrate and open highly compacted DNA structures in coordination with ATP-dependent chromatin remodelling complexes, allowing other TF binding (Zaret & Caroll, 2011). Single-molecule tracking (SMT) experiments showed that pioneer factors have highly transient genomic interactions, displaying a DNA residence time of about 9 sec. This suggests that highly dynamic chromatin/factor interactions initiate regulatory events that modulate chromatin accessibility and ultimately regulate gene expression (Swinstead *et al*., 2016).

Genome-wide chromatin accessibility mapping assays, including DNase-seq (Thurman *et al*., 2012; Piper *et al*., 2013, Tsompana &Buck, 2014), FAIRE-seq (Giresi *et al*., 2007; Simon *et al*., 2012) and the recently identified ATAC-seq (Buenrostro *et al*., 2013; Buenrostro *et al*., 2015) directly probe accessible chromatin regions that contain *cis*-regulatory elements, such promoters, enhancers and other regulatory elements (Valouev *et al.*, 2011; Consortium, 2012; Thurman *et al*., 2012, Myong *et al*., 2016). Global identification of DNA-protein interactions in the genome can be studied using 'digital genomic footprinting' (Hesselberth *et al*., 2009), where short sequence motifs refractory to nuclease digestion infer factor occupancy (Thurman *et al*., 2012; Baek *et al*., 2012). This approach provides a good alternative to ChIP-seq, providing higher resolution and avoiding antibody issues (Sung *et al*., 2016).

ATAC-seq is an advanced genome-wide analysis method that enables mapping of chromatin accessibility and regulatory networks through footprinting analysis and can be applied to rare populations of cells (Buenrostro *et al*., 2013). Hence, in this work, I applied ATAC-seq to identify dynamic changes in the *cis*-regulatory DNA landscape underpinning decidualization of EnSCs and in the maintenance of a stem-like phenotype of eMSCs in prolonged cultures.

Mapping of dynamic chromatin changes in decidualizing EnSCs

Decidualization is a profound transformation of EnSCs from fibroblast-like to secretory decidual cells that occurs 'spontaneously' in menstruating species (Brosens *et al*., 2006). Decidual transformation involves large-scale gene expression changes (Gellersen & Brosens, 2014; Takano *et al*., 2007). Genome-wide remodeling of the chromatin architecture underlies the wholesale transcriptomic reprogramming upon decidualization (Munro *et al*., 2010; Zelenko *et al*., 2012). Gene expression profiling studies revealed that genes coding for epigenetic modulators are up-regulated during decidualization, and they include histone-modifiers and binding proteins, DNA methyltransferases and CpG-binding proteins. This suggests that a dynamic epigenetic code operates on the chromatin landscape of the EnSCs during decidualization and is responsible of the acquisition of the decidual identity (Grimaldi *et al*., 2012). Specifically, an example is provided by declining expression level for the histone methyltransferase enhancer of Zeste homolog 2 (EZH2) during decidualization. This results in a gradual loss of trimethylation of histone 3 on lysine 27 (H3K27me3) within the proximal promoters *PRL* and *IGFBP1*. A coordinated loss of methylation and gain of acetylation at the same loci results in increased accessibility of the chromatin, which is indicative of a positive regulation fo the transcription. This chromatin remodelling underpins the acquisition of decidual phenotype (Grimaldi *et al*., 2011). Also, another study indicates that the use of the DNA methylation inhibitor 5-aza-2'-deoxycytidine in human EnSCs alters genomic conformation and results, amongst others, in the up-regulation fo decidual genes involved in cellular properties that feature decidual cells, for example ECM organization and cell adhesion (Logan *et al*., 2010). Conversely, inhibition of methylation prior to and after implantation in the mouse impairs decidualization and correlates with pregnancy failure (Gao *et al.,* 2012). These observations suggest that a dynamic epigenetic code operates on the chromatin structure as decidualization unfolds.

In this work, I first optimised ATAC-seq and applied the technique to primary EnSCs to map the genome-wide changes in chromatin landscape upon decidualization, a process critical for embryo implantation and placenta formation (Gellersen & Brosens, 2014; Salker *et al*., 2011). I reasoned that this differentiation model would be informative as several lines of evidence showed that a dynamic epigenetic code operates atop the *cis*-regulatory landscape in decidualizing cells (Grimaldi *et al*., 2012; Zelenko *et al*., 2012; Munro *et al*., 2010).

A total of 185,084 regions of accessible chromatin were mapped in EnSCs and, based on a stringent criterion (Bonferroni adjusted $p < 0.05$), 1,225 and 278 loci opened or closed upon decidualization, respectively. Approximately 27 % of dynamic loci located within 10 kb upstream of TSSs. Changes in genomic accessibility at major decidual genes, such as *PRL* and *IGFBP1*, confirmed the ability of ATAC-seq to accurately map changes in the *cis-regulatory* elements of the chromatin. Independent primary cultures, either undifferentiated or decidualized for 4 days, were subjected to RNA-seq. In line with previous studies (Gellersen & Brosens, 2014; Kuroda *et al*., 2013; Brar *et al*., 2001; Giudice, 2004; Lu *et al*., 2008; Takano *et al*., 2012), RNA-seq revealed that decidualization is associated with wholesale reprogramming of EnSC functions, exemplified by the induction and repression of 1,432 and 1,499 genes, respectively. Although different cultures were used, integrated ATAC-seq and RNA-seq analyses revealed a strong association between changes in DNA accessibility within 10 kb of the promoter and in gene expression.

De novo binding motif discovery using HOMER (Heinz *et al*., 2010) revealed that decidualization of EnSCs is associated with enrichment and depletion of 17 and 7 short sequence motifs, respectively. Analysis of footprints confirmed protein occupancy in 22 out of 24 binding motifs, suggesting TF binding in the majority of the biding sites. Highly enriched motifs in the opening ATAC-seq peaks included high affinity binding sites for known decidual TFs, including CEBPB/CEBPD, FOSL2, FOXO1, PGR, and STAT3/STAT5 (Gellersen & Brosens, 2014; Mazur *et al*., 2015; Kaya *et al*., 2015; Jiang et al., 2015; Kim *et al*., 2005). Previous studies reported that interaction between TFs can differently modify chromatin accessibility (Christian *et al*., 2002; Christian *et al*., 2002; Lynch

et al., 2009). Evidence of TF cooperation in regulating decidual gene expression was also apparent in the footprint analysis. For example, cross-referencing of ATAC-seq data with published ChIP-seq data showed that enrichment for both FOXO1 and PGR binding sites correlate opening chromatin (Mazur *et al*., 2015; Vasquet *et al*., 2015). However, binding sites with high affinity for FOSL2 in the absence of PGR were enriched in closing chromatin regions. These observations fit well with the fact that FOSL2 physically interacts with PGR in decidualizing cells, making it a member of the growing family of PGR co-activators (Mazur *et al*., 2015).

Cross-referencing the binding motifs in the ATAC-seq data with RNA-seq data revealed putative TFs not yet implicated in decidualization. For example, transcript levels of *RORA*, *ARNTL*, and *MEIS1* increase upon decidualization in parallel with enrichment of high-affinity binding sites for these TFs in opening ATAC-seq peaks. Conversely, down-regulation *RUNX1*, *RUNX2*, *SOX12*, *TCF3* and *ETS1* upon decidualization correlated with depletion of high affinity binding sites.

The role of these putative novel transcriptional regulators in decidual transformation of EnSCs requires further investigation. Time limitations prevented me of pursuing this line of investigation any further, although a graduate student subsequently demonstrated that siRNA-mediated knockdown of *ARNTL, TCF3 and NFE2L1* perturbed the induction of *PRL* and I*GFBP1* in decidualizing cultures. Knockdown of *RUNX1* had little impact on the expression of decidual marker genes, although this does not necessarily preclude a role for this TF in other processes.

The ATAC-seq analysis of undifferentiated and decidualizing EnSCs is important on multiple levels. First, it provides an important resource to analyse chromatin changes associated with differential gene expression at specific loci. The footprint analysis provides insight into the transcriptional drivers of genes of interests, although confirmation still requires ChIP-PCR or cross-referencing with existing ChIP-seq data sets. Nevertheless, the ATAC-seq data will greatly facilitate mechanistic analysis of the pathways and downstream TFs that regulate specific

genes or gene networks. Second, although beyond the scope of my investigations, additional bioinformatics analysis yielded important insights into the emergence of 'spontaneous' decidualization in evolution (Gellersen & Brosens, 2014). In most mammals, decidualization is triggered by the implanting embryo. However, in menstruating species, i.e. higher primates, four species of bats, the elephant shrew and the common (Cairo) spiny mouse, decidualization is 'spontaneous', meaning that it is initiated during the mid-luteal phase of each cycle, independently of an implanting embryo. It is thought that spontaneous decidualization in primates and other species evolved independently (Bellofiore *et al*., 2017; Emera *et al*., 2012). In keeping with this model, ATAC-seq analysis revealed overrepresentation of primate-specific transposable elements, especially *Alu* repeats, in opening chromatin loci in decidualizing cells. The overrepresented Alu elements are conserved in menstruating but not in non-menstruating primates, suggesting that this transposable element was co-opted in the *cis*-regulatory landscape that drives spontaneous decidualization (Norris *et al*., 1995; Mason *et al*., 2010). Finally, my analysis provided proof of principle that ATAC-seq is a powerful tool to screen rapidly for dynamic chromatin changes in human endometrial cells. I envisage that applying this technique to various reproductive disorders associated with aberrant endometrial function, such as endometriosis, endometrial cancer, infertility and recurrent miscarriage, will yield important mechanistic insights into the underlying pathological pathways.

Integrated ATAC-seq/RNA-seq analysis of eMSCs expanded in culture

I spent the second half of my PhD in the laboratory of Professor Caroline Gargett where I explored strategies to improve our understanding of the therapeutic potential of eMSCs in regenerative medicine.

The endometrium offers a new, readily available source of MSCs for cell-based therapy for women with reproductive health disorders, including Asherman's syndrome and POP (Patel *et al*., 2008; Bockeria *et al*., 2013; Darzi *et al*., 2016). For example, it has been recently shown that eMSCs seeded on

polyamide/gelatin meshes could improve clinical outcomes for POP treatment. They promoted angiogenesis, showed anti-infallmatory properties and differentiated into smooth cells and fibroblasts, when transplanted in an immunocompromised mouse. Based on these promising findings, a large animal model, such as ovine, has been developing as new system to explore if autologous transplanted eMSCs function through paracrine effect or if they differentiated themselves into epithelial and muscle cells of the vagina (Gargett *et al*., 2016). However, as in the case for adult MSCs from other tissues, the relative scarcity of eMSCs necessitates significant expansion of cells in culture for clinical applications (Baxter *et al*., 2004; Ulrich *et al*., 2013). eMSCs spontaneously differentiate during prolonged culture (Zhu *et al*., 2011; Ulrich *et al*., 2014; Gargett *et al*., 2016), lose their clonogenicity as well as their ability to reconstitute tissue *in vivo* (Baxter *et al*., 2004; Banfi *et al*., 2002).

A recent study showed that selective inhibition of TGF-β-R signalling using a small molecule, A83-01, increases proliferative potential and maintains the functional properties of eMSCs during prolonged culture (Gurung *et al*., 2015). For clinical application, it is of paramount importance to understand the mechanisms underlying pharmacological expansion of eMSCs in culture. My study was predicated on the observation that A83-01 can be used as chemical approach to modulate cell identity (Li *et al*., 2013). My aim was to map the genome-wide changes in chromatin landscape and gene expression in response to A83-01 treatment of eMSCs and to provide insights into the mechanisms of action of this compound.

First, I validated the effect of A83-01-induced TGF-β-R inhibition on the proliferative ability of eMSCs and expression of stem cell markers during prolonged culture. A83-01 conferred a clear proliferative advantage as demonstrated by cumulative population doubling. However, as freshly eMSCs are highly proliferative, the effect was only apparent after 22 or more days in culture. Next, flow cytometry analysis was used to assess expression of phenotypic markers. This analysis revealed that A83-01 treatment increases the percentage of CD140b- and SUSD2- positive cells as well as the MFI for the indicated markers. Hence, A83-01 maintains the surface phenotype of eMSCs

during prolonged culture. However, despite this effect of A83-01 on the expression of surface markers being consistent between different primary cultures, changes were not significantly difference. This underlies the intrinsic differences between different primary cultures, which should be taken into account for therapeutic use. Finally, CFU-F assays revealed that A83-01 treatment increases clonal efficiency, thus attenuating loss of clonogenicity during culture expansion. Again, the magnitude of the effect of treatment varied between primary cultures. A recent study showed that the abundance of eMSCs correlates inversely with increased body mass index (Murakami *et al*., 2014). In addition, eMSC deficiency has also been associated with recurrent pregnancy loss (Lucas *et al*., 2016). These observations raise the possibility that clinical variables determine the ability of eMSCs to be expanded in culture as well as the responsiveness of the cells to TGF-β-R inhibition. Hence, additional studies are required to determine the factors that determine the proliferative capacity of eMSCs *in vitro*.

Next, I hypothesized that TGF-β-R blockade with A83-01 induced a reprogramming of gene expression responsible for the resulting undifferentiated state. Hence, to explore the effect of A83-01 on the genome-wide expression profile of expanded eMSCs, I performed RNA-seq. PCA revealed that TGF-β-R blockade results in a differential gene expression and, interestingly, underscored intrinsic variability between different primary cultures. Transcriptomic analysis of the differentially expressed genes showed, amongst others, that genes implicated in regulation of cell growth and cell fate commitment were induced and repressed, respectively. These observations supported the results generated from the functional analyses, demonstrating that A83-01 increases proliferative potential and prevents differentiation of expanded eMSCs. *SUSD2* transcript levels were upregulated in response to A83-01 treatment in accordance with the flow cytometry data. However, the RNA-seq analysis did not confirm an increase in transcript levels of genes encoding either CD140b (PDGFRB) or other perivascular markers (Murakami *et al*., 2014), such as *MCAM, ELN* and *MYH11*.

Mining of the data revealed that TGF-β-R inhibition repressed the expression of numerous genes encoding for ECM components, including *COL1A1*, *COL1A2*

and *SPARC*. ECM production is a well characterized response to injury and TGF-β signalling is master regulator. More accurately, in the case of tissue damage, fibroblasts transit from a quiescent to an activated state, where TGF-β signalling, amongst others signalling pathways, activates genes encoding for ECM proteins and cytoskeletal remodelling (Nakerakanti and Trojanowska, 2012; Biernacka, A., *et al,* 2011). Hence, this suggests that the effect of TGF-β-R blockade in maintaining eMSCs in a less differentiated state might be mediated by preventing fibroblast activation and limiting ECM deposition in prolonged culture.

To determine if A83-01 induces a stem cell signature, I compared the transcriptome profile of A83-01 treated and untreated eMSCs with the RNA-seq data obtained from another dataset, comparing clonal eMSCs to time-matched unselected PVCs. Concordant and discordant differentially expressed genes were extracted from these data sets. This analysis revealed that TGF-β-R inhibition only partly recapitulates the transcriptional profile of clonal eMSCs. Interesting, attenuated expression of genes encoding for ECM constituents was both a feature of A83-01 treated eMSCs in prolonged cultures and clonal cells in CFU-F assays. These observations underscore my assumption that the effect of A83-01 on eMSCs in prolonged culture relate, at least in part, to the inhibition of genes coding ECM components.

Transcriptional profiling revealed that A83-01 partly maintains the expression of some genes associated with stemness (e.g. SUSD2) and, importantly, inhibits genes associated with fibroblast activation. However, RNA-seq analysis does not provide insight into the TF network that mediates the cellular responses to A83-01 treatment. ATAC-seq analysis provided unbiased analysis of the changes in the *cis*-regulatory landscape that underpin the cellular responses to A83-01 treatment. I hypothesized that the responsiveness to A83-01-induced TGF-β-R blockade was dependent upon genome-wide remodelling of the chromatin architecture, which in turn enables recruitment or release of TFs likely responsible of maintaining eMSCs in an undifferentiated state during culture.

ATAC-seq revealed a wholesale remodelling of chromatin landscape and mapped genomic regions that dynamically change in response to the treatment.

Chromatin remodelling at specific loci alters binding of TFs and thus gene expression and because TFs can both activate and repress transcription, the correlation between dynamic changes in chromatin landscape and gene expression is not necessarily linear (Chen & Dent, 2014). Nevertheless, analysis of 200 genes associated with open and closed chromatin regions revealed a strong statistical correlation between changes in gene expression and differentially organized chromatin. There was ample evidence of the importance of chromatin remodelling at specific loci in modulating expression of nearby genes. For example, induction of *RARB*, *TGFBR3* and *SUSD2* correlated with increased chromatin accessibility at, and upstream, of their promoters. Conversely, down-regulation of *CADM1*, *CLO1A1* and *WNT5A* was associated with loss of chromatin accessibility at proximal promoters and distal enhancers.

De novo short sequence binding motifs using HOMER revealed enrichment and depletion of TF binding motifs upon opening or closing of chromatin. Combining ATAC-seq and RNA-seq identified several putative TFs likely to be involved in chromatin remodelling. Some of the most highly enriched *cis*-regulatory motifs showed high affinity for TFs implicated in eMSC differentiation, for example CEBPB and RORA (Frith & Genever, 2008; Miyamoto *et al*., 2012). Hence, their role in maintaining cultured eMSCs in an undifferentiated state merits further investigation. Interestingly, footprint analysis also yielded some novel putative pharmacological targets that ultimately may enhance *in vitro* expansion of eMSCs even further. For example, RNA-seq data showed that A83-01 markedly increases *NR4A1* expression, which in the ATAC-seq data was paralleled by genome-wide enrichment for NR4A1 binding site in A83-01 treated eMSCs. NR4A1, perhaps better known as NUR77, is nuclear receptor that negatively regulates TGF-β signalling and prevents prolonged fibroblast activation, thereby limiting fibrosis (Palumbo-Zerr *et al*., 2015). These intriguing findings suggest that up-regulation of *NR4A1* in A83-01 treated eMSCs functions as an endogenous inhibitor of TGF-β signalling. Further, Palumbo-Zerr *et al*. (2005) showed that NR4A1 reduces collagen production, which again is in accordance with the A83-01 responses in prolonged cultures. Interestingly, NR4A1 is an orphan nuclear receptor and its transcriptional activity can be enhanced using small molecules such as cytosporone-B (Zhan *et al*., 2008). Hence, it would be interesting to test

if cytosporone-B, alone and in synergy with A83-01, promotes *in vitro* expansion of eMSCs.

A83-01 treatment of cultured eMSCs exemplifies of how the use of small molecules can be an effective alternative to genetic approaches to regulate cellular states. In comparison to genetic manipulations, i.e. overexpression or silencing of specific TFs or signalling intermediates, reversibility is perceived as a major advantage of the use of chemically defined culture medium for MSC expansion (Li *et al*., 2013). However, in view of the extensive chromatin remodelling induced by A83-01, questions are raised regarding the degree of reversibility upon withdrawal of this inhibitor. Again, combined ATAC-seq and RNA-seq analyses provide a robust tool to answer these questions in exquisite detail. Arguably, total or near-total reversibility of the A83-01 effects is likely an important step in overcoming the regulatory hurdles associated with clinical translation.

In summary, by integrating advanced genome-wide expression and DNA accessibility profiling techniques, my work has advanced our understanding of the dynamic changes in the *cis*-regulatory DNA landscape underpinning decidualization of primary endometrial cells and maintenance of a stem-like phenotype of eMSCs in prolonged cultures. Analyses of these two large data sets revealed novel transcriptional regulators in cycling endometrium and putative new targets that could be exploited to accelerate clinical translation of autologous endometrial stem cell therapies for a variety of reproductive disorders. Furthermore, the data sets generated during the course of my investigations constitute an important resource to interrogate fundamental molecular questions pertaining to human endometrial cell biology.

Future work

Analysis of dynamic chromatin changes in human decidualizing endometrial stromal cells revealed novel transcriptional regulators that might play a role in licencing specific genomic regions for chromatin remodelling upon decidualization.

The role of these putative transcriptional regulators in decidual transformation of EnSCs requires further investigation. Experimentally, Real Time quantitative PCR (RT-qPCR) and western blot could be applied to validate the induction of TFs of interest at a transcript and protein level. ChIP-qRT-PCR or cross-referencing with available ChIP-seq data (e.g. ENCODE database), would provide confidence in the transcriptional regulation of genes of interest by specific TFs. Furthermore, silencing of the most highly ranked conserved TFs by siRNA-mediated gene silencing could be performed to validate their role upon decidualization. Time limitations prevented me of persuing this line of investigation even further, although a graduate student subsequently demonstrated that siRNA-mediated knockdown of *ARNTL*, *NFE2L1* and *TFC3* perturbated the induction of *PRL* and *IGFBP1* in decidualizing cultures.

Furthermore, my analysis provided proof of principle that ATAC-seq is a powerful toll to screen rapidly for dynamic chromatin changes in human endometrial stromal cells. I envisage that applying this assay to various reproductive disorders associated with aberrant endometrial function, such as endometriosis, endometrial cancer, infertility and recurrent miscarriage, will yield important mechanistic insights into the underlying pathological pathways.

As part of my Warwick-Monash alliance studentship, I then joined the laboratory of Professor Caroline Gargett in Melbourne, Australia, where I applied RNA-seq and ATAC-seq analyses to study the impact of TGF-β-R signalling inhibition on eMSCs maintained in prolonged culture. Amongst others, a consistent and prominent gene signature in the RNA-seq data involves down-regulation of genes involved in ECM deposition and metabolism. Furthermoe, my analysis indicated, amongst others, the induction of Nur77 that may be an important TF that mediate

the repression of ECM genes in response to A83-01 treatment. Hence, it would be interesting to focus on these results and validate the induction of Nur77 at mRNA and protein level through RT-qPCR and westeren blot, respectively. As next step, it would be then interesting to test if the selective Nur77 agoinist cytosporone B, alone or in synergy with A83-01 promotes in *vitro* expansion and clonogenicity.

Time limitations prevented me of persuing this line of investigations, although these experiments are ongoing in our laboratory.

Appendices

Appendix 1. Opening Motifs coupled to high affinity TFs

Opening Motifs	*P*	Matches to Known Motifs
Motif1	1E-140	CEBPE/CEBPB/CEBPD/CEBPG/CEBPA/HLF/DBP/TEF
Motif2	1E-83	AP-1/BATF/JDP2/FOS-JUN/FOSL2/Jun-AP1/Atf3/Fos/Junb/
Motif3	1E-64	Isgf3g/Foxj3/Foxo1/Foxd2/Foxp2/Foxp1/Foxp3/Foxl1/Foxo4
Motif4	1E-45	Pgr/Gre/PR/ARE/NR3C2/NR3C1/AR/Sox13
Motif5	1E-28	Bcl6/Stat5a/Stat4/Stat1/Stat3/Stat5/Stat6
Motif6	1E-28	CREB/Atf1/Crem/Atf3/Creb1Creb3/Xbp1
Motif7	1E-25	Egr2/Egr1/Panc1-Rbpj1/Egr4/Egr3/E2F6/Znf263
Motif8	1E-25	CEBP-Ap1/Chop/Atf4/Foxk1/Foxj1/Zbtb12/Rhox11/Runx2
Motif9	1E-25	Foxj1/Cdx1/Mafg-NFE2L1/Foxj3/Cdx2/Rxra/RORA/Hoxc10
Motif10	1E-24	Irx5/Forkhead/Irx4/Foxg1/Foxa1/Foxo3/Foxd2/Foxd1/Foxj2
Motif11	1E-24	NF1/NFIA/NFIX/NFIC/Nkx3.1/Stat5a-Stat5b/Hic1/Stat3/Rfx5
Motif12	1E-23	Hmbox1/Hoxc9/Foxl2/Hoxa9/FoxL1/Foxq1/Foxk1
Motif13	1E-18	Nanog?/Zic1/DCE/Zic3/Ap4/Zic2/MyoG
Motif14	1E-16	TFEB/TFEC/TFE3/MITF/USF1/Arntl/BHLHE41/USF2/bHLH/Nkx2.3
Motif15	1E-15	Znf322/Spdef/Smad3/Zfx/Zfp691/Runx1/PR/DCE/Klf1
Motif16	1E-14	Tgif2/Pax3-Fkhr/Jund/Meis1/nr1f2/Tgif1/Esrra
Motif17	1E-12	Myc/NeuroD1/NPAS2/Max-myc/Usf2/Olig2/Bhlhe23/TFEC/NeuroD2/Atoh1

Appendix 2. Closing Motifs coupled to high affinity TFs

Closing Motifs	***P***	**Matches to Known Motifs**
Motif1	1E-32	Tead1/Tead3/Tead4/Tead2/Spib/Nfatc1/Sox17/Nfatc3
Motif2	1E-26	Runx1/Runx2/Runx3/Znf354c/Foxk1/foxh1
Motif3	1E-18	Sox8/Sox17/Tead2/Tead4/Tead3/Stat6/Sox5
Motif4	1E-15	Sox5/Sry/Sox18/Sox30/Sox9/Sox12/HMG/Sox5/Sox13/Sox8
Motif5	1E-14	Zbtb18/Tcfe2a/Tal1-Tcf3/Ascl1/Scl/Ascl2/Atoh1/Scl/Tcf3
Motif6	1E-12	Pu.1/Sfpi1/Ets1/SpiB/Etv6/EHF/Etv2/Erg/Elf5
Motif7	1E-12	Hand1-Tcf3/Tead3/Tead4/Zbtb3/Tead2/Smad3/Tead1/Zfp410

Appendix 3. Up-regulated genes upon decidualization: Log2-fold change ≥ 1

Gene Symbol	log2-fold change	*q*
SST	10.47197586	1.96E-126
IGFBP1	10.04965709	5.32E-98
LRRC15	7.385318639	7.45E-63
PRL	7.248956321	2.6E-93
PROK1	7.113095846	1.15E-61
PTPN5	7.065324986	2.51E-39
RP11-480G7.1	6.849292565	2.78E-38
CGA	6.83131967	1.57E-30
NTRK1	6.787199825	2.4E-46
TMEM132C	6.435175832	1.32E-48
WNT4	6.31380214	1.26E-53
SH2D2A	6.267299957	1.17E-55
MYLK3	6.13304507	1.16E-39
TREM1	6.079634179	2.96E-37
RP11-162I7.1	6.028422193	2.4E-21
SORCS1	5.983804669	2.72E-48
ALOX15B	5.981615407	1.09E-24
ZBTB16	5.94979952	5.95E-32
GPBAR1	5.895475533	1.39E-27
RP11-1260E13.4	5.833965583	2.31E-25
PRIMA1	5.814874592	3.33E-33
LEFTY2	5.780800776	5.28E-28
ACTBP8	5.722620317	3E-17
TRABD2B	5.69109739	1.46E-35
SLC46A2	5.640934147	1.13E-16
ADORA2BP	5.529117037	6.96E-16
CXCL14	5.527608904	1.36E-26

IL1RL1	5.387245456	9.52E-15
EDNRB	5.246106726	1.04E-25
CHI3L2	5.207649519	2.61E-25
OMD	5.192877801	1.27E-30
SIGLEC7	5.180944105	1.95E-15
RP11-362F19.1	5.120734832	8.85E-38
PCDH20	5.08386358	5.62E-13
IGHV3-74	5.081227525	6.92E-14
DKK1	5.077616084	2.51E-29
LINC00473	5.067759137	4.52E-34
LGI2	5.059443021	3.64E-32
TRIM67	5.057619226	1.32E-19
MAOA	5.00976758	6.86E-35
SLC7A8	4.977745742	2.57E-61
TH	4.973070729	5.46E-19
KLK4	4.963728367	1.18E-20
KCNA4	4.909844379	2.26E-15
EREG	4.806409039	4.43E-17
ENHO	4.802584573	1.85E-24
AADAC	4.746973747	8.61E-12
FST	4.68077209	7.1E-17
MAOB	4.649769044	8.78E-28
CHST7	4.623372379	5.4E-45
P2RY14	4.593757874	1.9E-18
HSD17B13	4.55893132	5.61E-15
BRINP2	4.479677862	4.8E-12
RAMP3	4.459563596	3.88E-15
SERPINA6	4.452100099	3.61E-10
WNT10B	4.437798811	9.96E-12
C11orf86	4.419743714	1.85E-09
ABLIM2	4.416528841	9.3E-31
HSD11B1	4.384625956	5.92E-09
ENPP1	4.338704044	1.42E-19

RP11-342I1.2	4.336124752	5.26E-14
GSG1L	4.291571606	4.37E-10
CNR1	4.264000519	2.96E-08
SDIM1	4.214860169	4.26E-11
RP11-269G24.6	4.206309114	4.17E-09
NKAIN1	4.194596227	5.71E-43
GAL	4.188934357	3.03E-11
PLXNA4	4.168853569	6.87E-16
ACE2	4.167646567	1.44E-10
CDKN1C	4.146119667	6.3E-46
WNT1	4.120520939	4.02E-08
LINC00924	4.11595963	1.36E-17
RP11-752D24.2	4.106050485	3.31E-16
TUBA3D	4.096919147	4.42E-08
RP11-81H14.2	4.059016933	7.55E-10
FKBP5	4.046394029	4.76E-23
THSD7A	4.04610117	1.27E-18
ABI3BP	4.033320059	2.95E-62
GADD45G	4.027072616	7.19E-18
MLC1	4.025057181	4.17E-16
INSRR	4.022887424	3.54E-13
GALNT15	4.012815118	4E-18
CD38	4.003343934	1.94E-16
RP11-7F17.3	3.990978778	2.26E-12
SV2C	3.986096842	3.55E-09
PENK	3.965407511	1.36E-65
SAT1	3.937351564	1.29E-71
P4HA3	3.934212991	2.81E-41
RP11-466P24.7	3.927154372	3.96E-09
RHOU	3.893028986	1.48E-22
IL15	3.875560637	8.26E-25
PODNL1	3.863771751	8.48E-26
IL1R2	3.852387638	1.13E-10

GLB1L2	3.845927613	6.61E-31
CRLF1	3.843238288	1.78E-08
GAPT	3.806082812	0.000000525
RBP4	3.796940024	1.41E-17
CD226	3.796832247	3.88E-22
RP11-138H11.1	3.791000196	0.000000207
GPX3	3.780658286	9.52E-08
RP11-443C10.1	3.763515959	0.000000267
APOO	3.752184168	7.76E-32
MACC1-AS1	3.730832627	0.000000029
MYOCD	3.717760099	9.39E-30
CSF3R	3.7149218	2.25E-11
WNT3A	3.69559305	0.000000365
MGST1	3.675309148	1.09E-24
EML6	3.673224722	3.12E-16
ADAMTSL4	3.641957335	2.12E-23
SYNDIG1	3.636533583	1.06E-08
RAB3C	3.630927248	0.00000106
ENPEP	3.618983138	2.75E-13
KLF15	3.617987956	1.64E-27
STAR	3.612420463	1.09E-10
RP11-161D15.3	3.606012286	0.00000036
REM1	3.600479027	2.86E-08
FAM89A	3.592188823	2.1E-37
FAM167A	3.590414973	5.8E-13
ATOH8	3.552550157	2.67E-28
Z98256.1	3.545890643	3.89E-16
CPB1	3.544468175	0.000000789
SLC7A2	3.544204907	2.72E-41
PPAP2B	3.533435906	1.63E-59
COL23A1	3.532051246	4.2E-09
RP11-459O1.2	3.527095274	0.00000484
ELOVL3	3.525162464	3.77E-19

RP11-820L6.1	3.519510796	2.09E-09
EFEMP1	3.519048676	8.71E-18
ELMOD1	3.517731118	7.07E-14
SLC10A6	3.514596188	0.00000027
ACSM5	3.50622087	5.21E-09
KAL1	3.47408889	7.87E-11
IL1B	3.461104128	0.00000578
HAND2	3.444476979	7.08E-67
PLCL1	3.444370106	1.3E-11
TREML3P	3.441577235	0.00000198
INHA	3.439702925	5.96E-17
SEC14L4	3.425292886	1.64E-08
C5AR2	3.415752326	9.68E-14
RORB	3.41035228	8.64E-32
ENPP2	3.402811339	1.14E-12
LPAR1	3.389651636	1.59E-25
ST8SIA4	3.37203793	6.03E-15
ADRA2C	3.371863689	1.19E-16
SRGN	3.367673477	2.76E-18
RP11-454P21.1	3.361843853	0.00000863
ATP8A2	3.360169117	1.04E-17
CACNB2	3.358547479	6.61E-14
ABCA8	3.345991159	1.62E-24
DNAAF1	3.339761375	1.05E-09
PC	3.338982996	7.53E-14
WNT16	3.332264686	1.65E-09
INSC	3.320834882	0.00000994
RBKS	3.316594539	6.57E-24
TM4SF1	3.315899528	5.7E-12
RP11-486P11.1	3.308412128	2.06E-09
C1QTNF1-AS1	3.305754084	2.34E-11
TMEM132B	3.30338227	2.63E-24
LINC00707	3.280406585	5.29E-09

CHRDL1	3.26318667	0.000033
IL1R1	3.241932375	1.22E-19
RASL10B	3.205076262	2.82E-18
LMO3	3.202778655	0.00000301
PYGM	3.198443738	9.95E-10
LINC00890	3.193117675	1.59E-09
CRISPLD2	3.165844721	7.12E-34
ANGPTL1	3.16250368	0.0000488
ADAMTS15	3.153578985	0.0000241
MFSD2A	3.153369393	1.51E-10
C2orf72	3.146692749	6.48E-10
TLE6	3.142154285	7.37E-21
CRYAB	3.110478952	2.1E-21
PRRG4	3.110099954	7.89E-11
AKR1C1	3.108742974	3.72E-23
MUM1L1	3.102059793	1.51E-21
SIPA1L2	3.101856044	1.65E-09
SPARCL1	3.096592976	1.95E-11
IRS2	3.094442587	4.65E-31
AGXT2	3.080450666	0.000000124
TMEM37	3.075127651	2.47E-20
SYN3	3.06806329	7.85E-09
CFD	3.065334389	0.000000734
CAB39L	3.059760683	3.69E-27
LGR4	3.044146457	3.44E-15
AADACL4	3.01738113	1.68E-11
PRR15	3.01124917	8.02E-11
AC010132.11	3.006613955	0.0000526
ADAMTS8	3.003929252	0.000000222
ADAMTS3	2.978378146	2.02E-09
INSR	2.977190024	5.88E-22
ING1	2.976650207	8.75E-29
KDR	2.965615013	2.89E-09

NDP	2.963382526	0.000130516
IGFBP4	2.940146489	2.03E-38
PILRA	2.936989746	0.000000566
CST11	2.935149754	0.0001852
KCNB1	2.928654945	1.31E-08
HTR2A	2.92617072	0.00000013
NELL2	2.926070602	0.0000687
CXXC4	2.924649199	1.97E-08
PRKG1-AS1	2.91779531	8.38E-08
RASL11B	2.914775361	1.17E-11
FAM134B	2.896450418	4.66E-21
SERPINB10	2.893105567	0.000231385
IL18R1	2.890806163	0.00000025
AOC3	2.889639667	5.68E-10
APOA1	2.885217443	0.000178052
STAC2	2.879099091	0.000000811
PTPRN	2.872427964	0.000000507
ALDH1L1	2.869849601	0.000000044
TVP23A	2.865081508	0.00000448
RP11-43F13.3	2.863221451	0.000000478
C11orf96	2.859237683	1.21E-18
RSPO3	2.858672778	3.53E-10
RP3-525N10.2	2.856645664	0.000000508
IGFBP2	2.856103162	5.1E-30
GRM7	2.854978585	0.00000614
TEX26-AS1	2.852671601	0.00000549
DNER	2.848200953	0.00000124
PRLR	2.845442089	3.34E-10
RP11-158M2.3	2.845380187	0.00000828
IL2RA	2.844781241	0.000237571
CLEC2D	2.839847872	3.96E-18
APOD	2.838841917	3.39E-13
PHEX	2.821222499	7.29E-10

RHOB	2.814733046	1.97E-44
MRAP2	2.80267586	0.00000249
RP11-475B2.1	2.798291701	2.74E-13
KCNK3	2.795808362	0.000322205
PAEP	2.794514812	0.000000011
RNF182	2.792860966	8.13E-21
C3	2.790729345	6.54E-23
STON2	2.789767743	0.0000668
PRG2	2.773214417	0.000319426
PPAPDC1A	2.769183665	2.48E-10
COMP	2.768723069	0.0000123
NPR1	2.762976252	2.98E-22
C7	2.76245137	0.00011759
RP11-184M15.1	2.750717579	0.000325432
RP11-38P22.2	2.75052607	0.000335178
LSAMP	2.748235961	1.2E-15
KCTD12	2.737422484	0.000093
SLC25A19	2.735331871	1.29E-11
RP11-563P16.1	2.727282533	0.000206247
CRYGN	2.726571973	0.000000836
SPP1	2.716754871	4.27E-17
TNFRSF1B	2.715807943	2.83E-15
GCOM1	2.715404443	0.00019947
SAMD11	2.710910451	0.000000173
RYR2	2.710310834	0.000156131
AC005083.1	2.708454535	0.000139211
TPPP	2.696915146	0.000104982
ADCY1	2.694803009	1.53E-27
FLVCR2	2.69338035	3.01E-10
PLA2G7	2.690407858	1.67E-24
40238	2.688579507	0.000000162
CD83	2.686105539	1.07E-11

GGT5	2.684981133	3.28E-10
COL15A1	2.684593456	4.86E-18
RP1-78O14.1	2.679184464	8.48E-21
CELF2	2.676156704	1.66E-08
DPEP2	2.6748813	0.000440448
CILP	2.672173371	0.000698901
CSF3	2.669556077	0.000645905
RAI2	2.662377305	3.29E-37
RP11-356I2.4	2.662027825	6.64E-08
IGHG1	2.652351567	0.000769645
RP11-148L24.1	2.649836952	0.000000609
FERMT2	2.648561372	2.12E-16
DEPTOR	2.647989253	1.4E-33
EVA1C	2.644197411	2.06E-23
HAND2-AS1	2.642678371	4.18E-30
ESYT3	2.642156739	2.38E-08
DRP2	2.641028267	0.00000434
SLC31A2	2.637895279	3.54E-10
RASGRP2	2.635932977	9.19E-32
MAPK10	2.631828365	1.03E-20
LYPD3	2.62605081	0.000000817
RGCC	2.62132235	1.08E-24
WDR86-AS1	2.620810486	1.18E-10
PARM1	2.620266216	0.000413056
BTC	2.617570287	0.0000013
RP11-284M14.1	2.613587544	0.000163051
RP11-75L1.2	2.610696583	1.53E-09
LTBP1	2.607729433	1.96E-15
DEFB124	2.606719017	0.000883572
SIX2	2.604723908	0.000000556
HSPB6	2.600882898	3.58E-43
COLEC11	2.595650866	0.000000307

PLAGL1	2.59564667	1.87E-21
ARC	2.593991507	0.000000027
NEBL	2.589869208	0.00000131
CD14	2.582180472	0.000000126
PCBP3	2.579244858	9.55E-15
ANXA13	2.570330787	0.00078588
ADAMTS4	2.569027716	4.72E-11
CEBPD	2.563077238	9.36E-12
RP11-54O7.3	2.554464595	0.00000106
SERPINB2	2.548866248	0.000000807
ABCC8	2.545736678	0.000104418
TSC22D3	2.535616042	2.72E-17
LRPAP1	2.526904008	2.2E-27
ABTB2	2.525198788	2.58E-11
FRMD3	2.522767179	0.00000141
CA8	2.513865233	0.0000149
TIE1	2.512235185	0.00011046
XCR1	2.509119598	0.001357846
DCN	2.499266014	1.58E-16
TIMP4	2.495714827	0.0000136
PPP1R14C	2.495483138	6.67E-09
SLC39A2	2.495180019	0.001439967
HOMER2	2.494956053	0.0000204
CORO2A	2.494323166	0.00000166
CD1D	2.493559325	0.0000142
AKR1C2	2.490894824	8.21E-08
AC034110.1	2.490438497	0.00080321
GNG4	2.484601337	4.17E-27
HPD	2.482700042	0.001288565
OR7E36P	2.480785938	0.000829077
CTSL	2.479685275	8.3E-24
DUSP1	2.462416802	2.95E-16
SIGLEC9	2.462303779	0.0000001

TNFAIP8L3	2.458394417	0.000127388
TMEM150C	2.457997935	1.24E-24
PRKAG2-AS1	2.456612888	0.000120325
AC040977.1	2.454376245	0.000100875
CCDC73	2.448777583	0.000234999
IL1RL2	2.442517108	0.00000201
AC003984.1	2.439700733	0.000542473
CTB-167B5.2	2.439122346	0.001846684
RP11-390N6.1	2.438909681	0.000979772
OSBPL10	2.438501607	6.11E-10
RP11-130L8.2	2.43741056	0.000253823
PCK1	2.433837924	0.002036516
TAGAP	2.427664836	0.000570617
MEDAG	2.425650406	3.07E-10
AVPI1	2.4252814	7.65E-15
U82695.10	2.425079441	1.01E-13
GLUL	2.421411466	2E-16
RP11-680A11.5	2.420874788	1.16E-09
RASD1	2.420521067	3.73E-08
LONRF2	2.418382933	7.19E-14
ENPP3	2.417256681	0.002047524
PI15	2.414129026	0.001075189
TNS4	2.410350541	0.00000114
JPH1	2.402800382	7.82E-16
G0S2	2.400494118	1.96E-14
TLE2	2.400376262	1.81E-34
RGL3	2.398752517	6.29E-08
MDM1	2.392601339	8.77E-09
TMC1	2.391852491	0.000148206
HSD17B6	2.388527772	0.000000487
CTD-2210P24.4	2.377240419	0.000340802
RP11-215H22.1	2.373707017	0.00259798
RPH3AL	2.370824395	3.04E-08

GABRG3	2.370145799	0.002580067
ATP2B3	2.369738076	0.00052022
HIST1H1C	2.366281484	2.48E-19
RP11-61L23.2	2.364445583	1.33E-10
RP11-697N18.3	2.361958674	0.0000126
SNAP91	2.355707318	3.27E-09
RGS2	2.354410205	5.35E-20
AC007255.8	2.353412025	0.001155953
CRB2	2.347608039	0.00049717
HS1BP3-IT1	2.342234466	0.000268151
CTB-138E5.1	2.335562954	0.002362833
GPR155	2.33281371	1.15E-08
FAM153B	2.331627823	0.001907821
FAM19A4	2.331457076	0.002832473
UBE2QL1	2.331382166	0.0000197
FAM124B	2.330030574	0.003056648
COLEC10	2.328770807	0.000329714
RP11-705C15.2	2.321890003	0.000000019
KALRN	2.318371634	0.00000332
TMEM108	2.318105619	2.66E-11
RP11-362F19.3	2.31421067	0.003328399
PID1	2.312728893	6.37E-27
KCNS2	2.298862356	0.000516423
ITPR1	2.297806922	3.79E-09
RP11-4F5.2	2.295799972	0.000218614
FAM49A	2.292906065	0.00000869
SPTSSA	2.292202464	8.74E-13
AGTR1	2.290032473	0.001302367
RP11-43F13.4	2.289750124	0.000879877
NNMT	2.288165237	6.46E-13
SIK1	2.286956222	1.24E-13
PKP2	2.280055316	0.0000102
ACVR1C	2.279449767	0.000476169

JAKMIP2	2.277582668	0.0000106
ELN	2.273805159	3.62E-08
GREB1	2.272390023	1.24E-19
UPK1B	2.266062608	0.00000207
LCN1	2.265784964	0.001734054
ALOX15	2.264961647	0.003175063
POM121L9P	2.264273284	0.00132285
UNC5C	2.26426601	0.0000427
SMIM5	2.252498077	0.0000939
ITIH1	2.250628731	0.003338434
CHSY1	2.250285829	0.00000373
GAB3	2.247477377	1.39E-08
CD68	2.245477199	0.000000206
ANO7P1	2.243657194	0.000000252
REN	2.237425659	0.002234535
SCUBE1	2.236842716	0.000666088
KERA	2.236254819	0.001365505
NKD1	2.234971396	0.0000429
RP11-535A5.1	2.228661376	0.004733873
CHN2	2.227420853	0.000634549
EPB41L3	2.225909541	5.1E-15
SDK1	2.219434722	0.000000318
AL133318.1	2.219204853	0.000110788
SYT12	2.217747168	0.001504721
HTRA3	2.21761786	0.00000195
PTPRZ1	2.215653588	0.004984428
TUBA3E	2.214177314	0.004665039
LUM	2.209702707	5.61E-24
PRR24	2.208212708	6.21E-25
RP1-124C6.1	2.208053259	0.002597368
SFMBT2	2.204194415	3.01E-14
C1orf21	2.200876433	1.81E-20
NFIL3	2.198490269	2.09E-16

HIST1H3D	2.194272965	0.000899822
RP11-401P9.4	2.188285263	0.0000629
RP11-13K12.1	2.188218935	0.00000352
RET	2.187829337	0.000000303
CLMN	2.183000541	0.0000919
RP11-65J21.3	2.180237304	0.000564445
MYO16	2.180044816	7.66E-08
NRCAM	2.178276846	0.00000232
EFHC2	2.176542188	0.00000322
C13orf45	2.172724027	0.005845543
COL4A3	2.172668376	0.0000263
TNFRSF8	2.172233323	1.53E-13
RP11-760H22.2	2.168167014	5.21E-11
KIAA1210	2.168049027	0.005790341
XYLT1	2.166358022	2.28E-08
PPARGC1A	2.165189242	0.00029744
RAET1G	2.164096611	0.000245
CYP11A1	2.159513621	0.00000672
KIAA1217	2.157664837	0.00000249
PAK3	2.155893909	2.14E-10
CHST2	2.154306465	9.38E-15
RP11-505E24.3	2.142569561	0.005656615
TAC1	2.139274229	0.004920471
P2RY1	2.136230043	0.00675812
AC002398.12	2.136029005	0.000398873
SPHK1	2.135284513	1.11E-23
SPATA41	2.131942923	0.000293665
CCL8	2.131914903	0.006339395
BAIAP2L2	2.13033707	0.00001
MAPT	2.129695095	0.000001
CCDC151	2.124020051	0.000149908
CCR7	2.122817938	0.006578185
MAATS1	2.120692129	0.002638941

ADAMTS2	2.11871963	1.6E-15
LY6K	2.117537003	0.0000177
RP11-705C15.3	2.116297986	2.41E-08
FXYD1	2.116193253	0.0000646
COL4A5	2.110105923	0.0000181
SBSN	2.109422264	0.000824308
CHGA	2.103326957	0.005978988
MT2A	2.103281735	7.14E-12
C1orf132	2.102418278	0.00000665
CORIN	2.09938667	0.0000264
SYTL4	2.097476589	3.49E-13
AC023469.2	2.091220996	0.00803818
IGF1	2.090521567	0.00000923
PPM1H	2.090144719	0.0000295
LL22NC03-104C7.1	2.087453779	0.007810831
CCDC68	2.0842616	6.94E-11
HIST1H2BJ	2.083320525	0.00000108
GAS1	2.082295339	1.12E-12
RBP1	2.081228961	1.02E-24
RP11-259O2.1	2.074070945	0.004680329
SLC1A1	2.074045157	0.000000102
AOX1	2.073108244	0.008424756
MMP8	2.068261756	0.001212226
C2orf50	2.067329017	0.008570288
KLK2	2.065638443	0.005862767
WNT9A	2.062857151	0.00000864
IGSF10	2.061919325	0.008710527
KRT5	2.060907211	0.00000459
RP11-1096D5.1	2.059360494	0.008518375
ADAMTS1	2.056140475	1.98E-08
AGFG2	2.056113598	2.16E-12
SERPINE1	2.053751819	4.04E-11

AC021016.6	2.052891805	0.002761976
PTGS1	2.052170591	1.59E-20
SLC22A31	2.051427789	0.005500795
PRODH	2.044665118	0.00920311
BTBD3	2.035726596	0.0000041
CTD-3064M3.3	2.031334734	0.004084508
COL4A6	2.030235736	0.009343875
COL5A3	2.029621976	5.94E-08
SOAT2	2.027392275	0.000248683
KCNC4	2.02668866	0.000000156
CREG1	2.022620709	1.37E-20
CCDC69	2.022407114	0.0000462
MFSD2B	2.021896922	0.001906507
ERBB3	2.020747714	0.000000356
OGN	2.01958994	0.0000175
AC104695.3	2.019102385	0.000182034
CTD-2263F21.1	2.014421207	0.002644507
TGM2	2.00792395	4.23E-15
CISH	2.005385314	0.000000103
RAMP1	2.003008678	8.32E-21
VIT	1.999971405	0.010723755
RP11-403A21.1	1.999659057	0.010586459
MAFB	1.997339799	8.21E-08
GATA3	1.99698369	0.009645591
RP11-318G21.4	1.993980894	0.011504047
TSHZ2	1.990682737	0.0000102
MYPN	1.987516609	0.002779504
HPGD	1.987356041	0.010165714
LARGE	1.986554184	0.00000248
PDE7B	1.986513789	0.000000502
KCNK12	1.983299149	0.003518403
ROCK2	1.981263416	1.23E-12
SLC37A3	1.978529431	3.81E-23

NFASC	1.975384731	0.0000384
PTGIR	1.972686301	0.000000551
GALNT13	1.972123613	0.001246076
COL4A4	1.970745129	0.00000455
CCL26	1.969888091	0.005154014
CAMKK1	1.968219824	1.29E-11
TNFSF14	1.966836794	0.009623982
CCL20	1.959350787	0.000140337
RP11-492E3.2	1.957865964	0.000000241
PISD	1.957106281	1.56E-17
RBM20	1.954980734	0.003829148
RP11-95H3.1	1.953969952	0.012635101
KIAA0040	1.949622444	0.000231995
FAM9B	1.948850389	0.013512975
C20orf141	1.942305568	0.012955415
STEAP4	1.940362848	0.004162187
SLC40A1	1.939938727	0.0000146
TIMP3	1.939849224	0.013136
KRT23	1.939149223	0.0000351
IRAK3	1.936990101	1.48E-13
AC002456.2	1.936343361	0.00104619
AC023115.2	1.933376326	0.006371318
LINC00856	1.932641266	0.008792996
TRIM29	1.927215802	0.000000862
STON1-GTF2A1L	1.927197856	0.000998425
ACTN2	1.927076728	0.005455629
SH3BP5	1.925701435	5.01E-17
KCNJ8	1.925143998	2.02E-14
F12	1.924108811	0.000226775
AC073316.2	1.922991348	0.013395198
MATN2	1.921985407	0.000000216
RP11-254F19.2	1.921483868	0.012502595

TPRG1	1.92136212	0.001407885
PCDP1	1.91982718	0.001454165
AOX3P	1.919674922	0.013603004
NR4A3	1.917690487	0.0000013
MEI1	1.915401143	0.0000639
C1QTNF1	1.913636436	6.98E-14
TPBGL	1.910544645	0.000884532
MTR	1.906553989	2.83E-10
SLC47A1	1.905851936	1.04E-09
KLF4	1.904560124	0.000000134
NKAIN3	1.902323233	0.001257516
RP11-172E9.2	1.902068442	0.015588671
IL1A	1.899164372	0.012537653
PER1	1.898010231	0.000000136
HLX	1.895989367	2.64E-19
RP13-514E23.1	1.894852892	0.009881734
MERTK	1.89313357	0.00010487
WNT6	1.892755782	0.0000383
ZFP92	1.891622936	0.002812272
CALN1	1.891562619	0.016236978
METTL7A	1.886246963	5.43E-10
TSKU	1.885993751	5.31E-21
SMOC2	1.878740166	8.28E-08
C6orf57	1.878546301	1E-10
LGI4	1.876874199	0.003255434
RADIL	1.875149293	0.0000284
APCDD1	1.873749193	0.017034396
ZNF189	1.873721399	7.67E-12
RGS11	1.873253138	0.000713082
RP11-589N15.2	1.870856561	0.00000211
VCAN-AS1	1.867604186	0.007415789
CPEB1	1.862006049	0.000000882
WNT9B	1.858748798	0.015433069

PEMT	1.854793196	2.49E-13
STX11	1.854551223	0.000238949
ALOX5AP	1.851394435	0.000666266
ABHD5	1.849316202	2.35E-18
IL11	1.843390865	0.013007385
EPYC	1.840906121	0.0000142
RGS22	1.840527825	6.21E-08
FAM213A	1.839803701	3.56E-10
LINC00570	1.837915645	0.017650363
ACPL2	1.835315234	2.74E-08
ANKFN1	1.834611466	0.01183427
RP11-98L5.2	1.834519099	0.012934036
C20orf27	1.834273441	0.00000392
PDLIM1	1.833971231	0.000000597
PPP2R1B	1.833026894	1.62E-21
CD248	1.824289986	0.0000797
RGS16	1.820778907	0.00160499
ST6GALNAC2	1.818607774	6.54E-12
TMEM151A	1.81822051	0.016750963
MFI2	1.817968231	0.000273208
CTD-2201G3.1	1.813813525	0.008704196
ZNF804A	1.810780044	1.49E-08
AJAP1	1.799153204	0.0000303
RP11-384O8.1	1.798691159	0.011446084
NAP1L5	1.797648526	0.00000019
COL26A1	1.797353634	0.0000112
ADHFE1	1.796066604	0.000000155
CXCR2	1.794334901	0.020731383
CHEK2	1.789958181	4.56E-09
CXCR4	1.789755917	0.001670891
CD82	1.785162508	0.000111714
AL844165.1	1.783815882	0.021682345
ITPKC	1.783487945	2.34E-12

AC010987.6	1.78311582	0.02192402
OR1H1P	1.782993215	0.018584907
NLGN4X	1.782387072	8.71E-10
RHCG	1.781995295	0.022834498
FBXO32	1.780183556	0.00000014
RP11-64P14.7	1.776846853	0.024332074
WBSCR27	1.776565994	0.00006
IL1RN	1.774281653	0.002173131
ZC2HC1B	1.772896981	0.024320223
GLP2R	1.772077833	0.019740582
NKX6-1	1.768071386	0.0000702
RP3-428L16.1	1.767523648	0.015726924
ASIP	1.765477802	0.025123389
SNAP25	1.760054563	7.81E-08
ELMO1	1.756964765	0.002760171
MCOLN1	1.756296259	1.28E-19
RP11-466P24.2	1.756043789	2.2E-11
WIPF1	1.753366802	2.75E-11
LEPREL1-AS1	1.750027705	0.008100875
RNF144A-AS1	1.74832355	0.0000162
POM121L10P	1.747269944	0.017806299
HSPB1	1.747140722	1.84E-10
ADA	1.744586526	0.00000124
DANCR	1.742322963	5.45E-12
FGD5	1.740369034	0.0000127
RP11-124N19.3	1.740274582	0.003454559
NID2	1.738702228	1.67E-08
APBB1IP	1.736386863	0.000530101
DNM1P46	1.73613965	0.002540208
COL24A1	1.735862504	0.0000395
NYAP1	1.73429676	0.00000255
TNMD	1.733655175	0.024283951
RP11-75L1.1	1.732850603	0.024374358

PLAC9	1.72953624	0.008836331
RP1-117B12.4	1.728497752	0.014902217
SLC2A8	1.726320172	1.69E-09
LDLR	1.72622817	0.00000218
GCG	1.723711344	0.028784311
TMEM66	1.721824023	5.58E-16
WT1	1.72049256	5.83E-19
NCCRP1	1.720305891	0.010505177
38961	1.719607231	0.00000742
OSTF1	1.717724792	3.88E-09
ABLIM3	1.717264558	0.020766155
TPST1	1.713417372	1.02E-19
SYT13	1.713398126	0.000255464
POPDC3	1.712196651	5.77E-08
PCSK5	1.711378409	0.0000023
RP11-767I20.1	1.709168416	0.026049032
LINC01140	1.70856529	0.018680581
CYP26B1	1.708023792	0.00000178
SERPING1	1.707873409	2.63E-15
RNU6-813P	1.704833427	0.02681177
RP11-505E24.2	1.703192519	0.0307661
HIST1H2BD	1.700164415	8.41E-10
RP11-488C13.1	1.699200951	0.028593049
C11orf70	1.698889993	0.00000347
RGS17	1.697438316	0.000784159
HIST1H2BG	1.696512206	0.009016291
BASP1	1.69620046	7.06E-19
RP11-736N17.4	1.695575058	0.002659976
TYMP	1.693888538	3.81E-09
KLKP1	1.692543439	0.02460159
LONRF3	1.689769019	0.003489262
ZNF330	1.688357006	7.29E-14
HIST1H2BC	1.687774239	0.0000569

USP46	1.687347195	4.38E-13
OACYLP	1.686805448	0.027035782
RP4-625H18.2	1.686773694	0.010259982
SNX10	1.686037378	0.00000188
ANG	1.685816479	3.51E-08
RPL21P13	1.684696804	0.031863424
AC141928.1	1.676633419	0.00034053
BMPER	1.675722565	0.0000084
RP13-39P12.3	1.674333915	0.027045492
UBE2Q2L	1.672800102	0.030681582
KLHL13	1.672596827	0.00000174
ABCC9	1.671842525	4.69E-13
PIR	1.670779854	0.0000099
ENTPD3	1.669963206	0.005952935
KREMEN1	1.669576469	0.0000187
TNFRSF11B	1.669087811	5.04E-10
SOCS3	1.666623686	5.22E-10
ROR2	1.665399798	6.38E-10
IGDCC3	1.664417176	0.00311271
DLG5	1.664370397	0.000000435
RP3-368B9.2	1.664116756	0.02325028
AC091878.1	1.663586543	0.001139514
snoU13	1.663328265	0.021162639
SLC22A3	1.662044393	0.002322128
CA12	1.660847596	0.00000295
RP1-86C11.7	1.660828799	0.00541163
HHIPL2	1.659767391	0.028485885
SGSH	1.658077114	1.05E-15
RP11-524F11.2	1.654601666	0.034211082
RP3-428L16.2	1.653925646	0.002114019
AC068610.3	1.653865983	0.034798177
MTHFS	1.653573936	0.0000153
RP1-27K12.4	1.651833478	0.03489139

CACNA2D3	1.650800325	7.63E-08
COL28A1	1.65051731	0.000492613
SLC24A2	1.64819369	0.001424714
CLEC4E	1.646774198	0.011191716
TMEM27	1.646544729	0.015264134
RP11-65J21.4	1.645604782	0.036865029
CDC20P1	1.645287576	0.003656146
CAMK1G	1.642954507	0.000000491
DNAI1	1.642363529	0.03729037
CLU	1.641978526	0.000186221
SEC14L6	1.640842312	0.012982143
COX7A1	1.640274229	1.72E-09
ZSCAN1	1.63694011	0.003418033
RAP1B	1.636197865	1.1E-12
SRD5A3	1.635740359	0.00000044
TFPI	1.635194284	4.11E-09
RP11-342M1.3	1.634220063	0.00398794
C19orf10	1.633841339	1.01E-08
PNKD	1.633838961	1.52E-10
RP11-248N22.1	1.63298903	0.037490823
EXOC3L4	1.632363523	0.010325967
RP11-384F7.2	1.631701599	0.038485189
IGHV3-72	1.630171214	0.032691356
EOGT	1.6295511	2.45E-08
ARMC12	1.627348028	0.039184315
TBC1D2B	1.625926927	0.000000041
ST3GAL5	1.625897913	0.000000017
ADAMTS9	1.625787113	0.0002449
TNNC2	1.625090415	0.019506203
RDH12	1.622732926	0.038568852
STON1	1.616073961	1.06E-10
MAMLD1	1.614312048	2.1E-15
LEPREL1	1.614124441	0.0000024

RP11-710C12.1	1.613666115	0.023506195
ADAMTS7P4	1.612778158	0.000014
KANK3	1.612630342	0.016232277
HIST1H2AE	1.611269219	0.023532348
RBBP6	1.60876236	1.17E-12
SLC11A1	1.608284831	0.010478563
RP11-281O15.7	1.608019876	0.040832526
SCNN1A	1.60754268	0.0000135
CKMT2	1.607521118	0.014536029
RNF13	1.606093863	3.79E-12
IGFBPL1	1.604253103	0.015963401
RLTPR	1.60362865	0.017066229
BCO2	1.603121085	0.006769537
PLCD4	1.600238354	0.0191573
LINC-PINT	1.599573226	5.72E-09
LINC00957	1.599358467	0.000616252
GTF2A1L	1.598458585	0.024285248
ANGPTL4	1.59731217	0.0000629
DFNB31	1.597018101	0.000896154
MOB3B	1.596380282	0.000240263
LRRC3DN	1.596173696	0.0000155
ARHGEF19	1.596127579	3.61E-13
AP3B2	1.595354852	0.001627958
OXCT2	1.594057127	0.018644895
FSTL3	1.593781986	5.44E-10
RPGRIP1	1.592865683	0.03327251
RP5-888M10.2	1.592687536	0.041885066
GAREM	1.592587623	0.000000986
MCC	1.591880799	0.000000236
LMTK3	1.590443351	0.013137435
LRFN4	1.589321593	0.00000403
RP11-196O16.1	1.588302246	0.002904708
RP11-363E7.4	1.586750388	0.000172838

FIGF	1.58525248	0.039413035
SLAIN1	1.583717188	0.001888544
CHPT1	1.583200479	7.05E-14
PRUNE2	1.582732391	0.000245256
MAP7	1.579863615	0.00000107
CCDC114	1.579862528	0.009497506
RP11-64C1.1	1.579200313	0.005526407
MT1M	1.578739236	0.009431561
RP1-137D17.2	1.574821354	0.045364381
PTPN13	1.574816901	0.000123539
RP11-582J16.4	1.574799524	0.023554159
GATA6-AS1	1.574098702	0.013731044
NR4A2	1.573138579	0.005924375
GP5	1.572238002	0.037532608
C10orf10	1.572166039	0.001085919
DIRAS2	1.571677416	0.0000572
SIL1	1.571586585	0.000000142
AC079776.2	1.570458348	0.002371618
RAB11FIP1	1.568670572	0.002107324
ZCCHC6	1.566955241	0.0000015
FAM115C	1.566952217	0.0000679
ARHGEF26	1.563564522	0.00000798
C1QL1	1.561827045	0.012838042
C5orf49	1.56146304	0.025887626
SLC24A3	1.561041983	0.000000323
AC073109.2	1.559576645	0.047673981
ASL	1.558861005	8.75E-08
RP11-115D19.1	1.558407574	0.0414802
SLC2A1	1.557620333	8.16E-15
SPAG4	1.557050513	0.000136086
KYNU	1.556276415	0.006397526
MT1G	1.555203894	0.045381796
CEP44	1.552662608	0.000000776

SULF2	1.552028489	1.05E-09
ATP6V0E1	1.550412077	2.06E-16
ELTD1	1.54968019	0.0000467
GPR20	1.54863589	0.030300081
KCNE3	1.544742485	0.000980098
SPON1	1.544152812	0.0000886
LRRC8A	1.543991023	2.23E-12
PLAUR	1.543870838	3.03E-08
CPM	1.543241518	6E-11
TAF7L	1.542923194	0.004583988
ADARB1	1.541344467	4.28E-12
TNNT3	1.54132338	0.042359958
MIR1282	1.539102129	0.019627946
RP11-439M11.1	1.539074351	0.016950237
USP15	1.536410307	0.0000264
RP11-314M24.1	1.534050221	0.034746251
PSD	1.52902121	5.89E-10
MAGI3	1.528545516	0.001024342
PKDCC	1.528247274	0.001690803
SLC9A9	1.526601414	0.0000126
AC003090.1	1.526189808	0.0399755
C3AR1	1.526117698	0.04987714
KRT6A	1.524559881	0.021305023
SOAT1	1.522022355	0.0000646
LINC01134	1.521115425	0.01609066
CYP7B1	1.520247808	0.001005873
AC078941.1	1.51983426	0.015792855
PNP	1.516108577	0.0000218
DACT2	1.514763275	0.023362928
SIGLEC17P	1.512311602	0.04914162
FYN	1.511574626	4.44E-08

NRXN1	1.50989091	0.020737872
C20orf24	1.508467653	8.6E-11
TMEM45A	1.508108084	0.0000205
H6PD	1.505643192	0.000207274
ISPD	1.505548604	0.000390502
CXorf57	1.505513872	0.008164725
TBXA2R	1.50004816	0.0000062
CEACAM1	1.499161192	0.002135964
USP46-AS1	1.497633219	0.0000398
SSR4P1	1.496857921	0.01509914
RP11-21L23.2	1.496215125	0.000000645
RP11-529E10.6	1.49479655	0.000354197
TGFBR3	1.494637718	0.0000717
KCND3	1.493084562	0.000307979
FAM105A	1.492336751	0.000000056
PKD1L2	1.491889325	0.001083178
RNF219-AS1	1.491583365	0.048429215
RP11-544M22.8	1.49150246	0.048369196
TNFAIP3	1.490937278	1.69E-12
RNF39	1.488020406	0.038550035
DBI	1.485287975	2.37E-08
LINC00035	1.483278542	0.016091548
ALDOC	1.479917132	0.001599301
ZEB1	1.479761554	0.0000384
LIX1	1.478230106	0.042768273
VSIG1	1.474631676	0.026666768
HIST2H2BE	1.474322655	2.89E-09
TRPM3	1.473365361	0.017972519
ALDH3B1	1.47297686	1.82E-12
CEND1	1.470511117	0.016121718
IL13RA2	1.469481579	0.0000506
C5orf27	1.469106373	0.034572032

SLCO2B1	1.468948414	0.011963602
SMAD6	1.468230888	0.0000179
NEAT1	1.467005994	7.57E-08
MCTP2	1.466771906	0.014329288
MANF	1.46663456	5.47E-10
VCAN	1.466100429	0.04511107
HTRA4	1.465842465	0.029091124
SQRDL	1.461878155	2.91E-08
LCP2	1.461629571	0.034354988
CD59	1.460756118	0.000000704
HYAL1	1.459088453	0.021557352
FOSL2	1.458755469	2.29E-14
ASPA	1.458483612	0.027939425
CDA	1.458277475	0.001678315
DLG5-AS1	1.457393131	0.016290274
BAI3	1.455138585	0.012653458
GATA6	1.454197069	0.000465182
SLCO2A1	1.453544417	0.005358179
ID4	1.452831194	0.003692418
MT1X	1.451121118	0.0000838
KIAA0408	1.450783709	0.047788576
TMEM35	1.446889048	7.17E-08
RP11-327F22.2	1.446574396	0.018073007
LYNX1	1.445602485	0.0000007
HAP1	1.443033689	0.006199729
AC013271.3	1.442320568	0.001928964
LINC00632	1.440860512	0.009511506
ADIRF	1.439550752	0.009264352
EPOR	1.439285116	0.000106005
SAMD13	1.438726946	0.021623122
FZD10	1.436688703	0.003435848
BEAN1	1.436675839	0.005832434
COX6C	1.436021586	2.07E-08

FBXO10	1.435682872	0.000000259
GPRIN3	1.434384641	0.000765065
IRF6	1.433724422	0.004734422
TCTA	1.430327145	0.00000505
GPR150	1.428831498	0.041682211
RP11-421L10.1	1.423575454	0.049827201
LPCAT3	1.423422388	0.000207204
ULBP2	1.421868856	0.000168362
SUMF2	1.421258984	0.000000988
TYW1B	1.420644504	0.001393554
METRN	1.418983303	1.91E-10
RBPMS-AS1	1.416660203	0.010841539
CERS6	1.416448818	0.0000161
CMC1	1.415341835	8.92E-09
RP11-438B23.2	1.415024648	0.029928611
DNASE1L1	1.412293872	0.00000579
FBXO8	1.411753372	2.82E-08
ANKRD37	1.410710427	0.000986198
HIST1H2AC	1.410230783	6.54E-12
HIST1H3E	1.409730536	0.002508901
SLC10A3	1.40882265	0.0000604
SPTBN4	1.40808218	0.001729987
APOC1	1.407565958	0.002643187
FAM207A	1.407539558	0.000000208
SMCO3	1.406063313	0.020874443
FAM155A	1.405522768	0.000002
ZNF331	1.402020257	0.0000244
EMC7	1.402004748	2.78E-10
FAM86HP	1.401575643	0.001584282
LINC01006	1.401196189	0.020120663
PPM1L	1.39991773	0.001222086
COQ2	1.399719062	3.27E-08
LGALS3	1.399174101	0.000000419

IL8	1.398747448	0.000590745
PAQR7	1.398646515	0.000503643
C1QTNF6	1.397303553	0.0000108
DIRC2	1.39428555	8.75E-09
LHFP	1.394162847	1.19E-08
OLFM1	1.392928998	0.000000235
GAB2	1.391926782	5.28E-12
CPAMD8	1.391475682	0.002240131
USP35	1.391421686	0.00000285
CHSY3	1.391273656	0.001819096
TMBIM1	1.390735086	3.05E-12
TMEM150A	1.390392103	0.000000279
WDR86	1.38967353	0.0000011
TMEM120A	1.388859928	0.00000304
TRMT44	1.386992255	5.29E-10
CASC10	1.384272681	0.003761494
RAB31	1.382513674	5.39E-12
RND2	1.379724864	0.000630811
SFTPB	1.378650159	0.030301595
CHRD	1.375684447	1.73E-09
TMTC2	1.372589383	0.003510207
MGAT3	1.371716582	0.000351618
CYP1B1	1.371400515	0.001045482
CDH20	1.37102203	0.030526128
EMILIN2	1.368081944	3.52E-10
TRPM6	1.367518421	0.019820343
FAM46C	1.3674966	0.002103078
FKBP1B	1.366564116	0.000496295
HIST1H2BK	1.366012737	0.00000104
FASN	1.364699132	0.004083817
RP11-137H2.6	1.362079998	0.000000616
RILP	1.361963089	0.000555303
TCEAL3	1.360373706	0.000000605

AC002467.7	1.359700497	0.013158584
PDK4	1.358889257	0.003350472
CTTNBP2	1.35843633	0.000126656
C11orf53	1.356336166	0.018004508
ECHDC3	1.354543531	0.004479087
IMPA2	1.35400468	0.000000183
MAF	1.353907966	0.000273758
TTPAL	1.353380987	0.000318663
MAP3K5	1.352009231	0.000000591
ATP8A1	1.351691881	0.001169042
ELFN1	1.350464908	0.002316701
RP13-884E18.4	1.35037637	0.022862038
FAM198A	1.348377853	0.002174158
TCF21	1.346746771	0.025763122
S100A4	1.346744457	0.001228556
WIPI1	1.344698084	6.94E-11
KIAA1377	1.342698955	0.000000373
KIAA1045	1.34171414	0.020950697
RCBTB1	1.339667844	0.0000298
ZMYM6NB	1.339617642	0.0000259
CTD-3065J16.9	1.337747697	0.00693657
NINJ2	1.335897348	0.036048508
RP11-800A3.7	1.334510219	0.00245172
DNAJC12	1.33424849	0.000125904
FADS1	1.333672002	0.0002311
RPRM	1.332483764	0.010019141
MAP3K14-AS1	1.331983179	0.045630792
EPHB6	1.331793856	0.00000158
IP6K3	1.328476968	0.0000188
KLHL26	1.328137764	0.000105201
NPTX2	1.32775582	0.007794316
SEC11C	1.323893725	1.59E-09
DPM3	1.322717179	0.00000159

ATG9B	1.319763776	0.00608322
CTB-92J24.3	1.31795796	0.000000146
SNX22	1.317803828	0.00615265
EPDR1	1.314627754	0.00000131
SMPD1	1.314419474	3.82E-09
JOSD2	1.310415416	0.00000209
SMOX	1.308640382	0.000000283
IFI35	1.308251454	0.000000158
RELT	1.306211133	0.0000484
CYB5R1	1.305883499	1.47E-11
C6orf211	1.30571037	0.00000388
SHBG	1.303051858	0.017237628
CLDN23	1.302384729	0.013292533
SLC3A2	1.299915147	2.6E-10
NR4A1	1.299631832	3.8E-09
FAH	1.29847521	0.000000617
GHR	1.296999405	0.0000221
CD151	1.29678032	5.32E-08
KLF9	1.295996019	2.23E-11
CCDC102B	1.295810211	0.004830063
C9orf72	1.295808257	0.000000036
TGFBR1	1.293281366	0.000000705
HLA-E	1.292392162	0.000000019
HPSE	1.292324872	0.0000395
SNX21	1.290839163	0.000024
TNFAIP2	1.290202033	3.78E-08
GCKR	1.289470995	0.031424088
CNTN3	1.28855765	0.000026
PYGL	1.288448149	2.89E-11
GNG2	1.2884176	0.000357985
MAPK14	1.288316698	0.000000531
TMED8	1.287783342	0.00000196
DERL1	1.287308042	0.0000209

A1BG-AS1	1.287277746	0.0000102
NOL3	1.285863101	5.32E-09
FOXO1	1.285107969	1.15E-08
TMEM179B	1.285095955	2.88E-08
GPR115	1.284627328	0.007461423
NUDT16	1.28294248	0.000288912
BRE	1.282485258	3.5E-10
FAM46A	1.282418667	0.0000841
MFSD12	1.281400275	0.00000497
NPC2	1.281239099	7.42E-10
CCDC170	1.279231176	0.00000558
ABHD14A	1.277011673	0.000355965
RAB6C-AS1	1.276021885	0.008766651
IDI1	1.274859033	0.0000853
ZC3H12A	1.274687054	0.000881729
STYK1	1.272989573	0.037332184
WT1-AS	1.271103024	0.000000147
B3GAT3	1.268622331	2.22E-09
NMNAT2	1.268451853	0.001568904
FKBP2	1.267970084	5.27E-09
PLCD1	1.267306988	0.000242223
DOK6	1.265312429	0.000816392
RMDN2	1.26521307	0.000000939
LINC01160	1.264672265	0.018029252
B4GALT3	1.263924166	7.83E-08
MXRA7	1.263780533	2.48E-11
GPRC5B	1.263221078	0.0000235
UBAC2-AS1	1.263076139	0.037019624
MAP1B	1.263056365	0.002011341
SOD2	1.262059337	0.0000103
HSD17B14	1.261929502	9.83E-08
GPD1L	1.261911037	0.002706501
STRBP	1.261279705	0.000539641

ZDHHC12	1.259602536	0.0000173
RP11-175K6.1	1.259537873	0.016555734
HDAC4	1.258952843	1.54E-08
DNAJC1	1.258678785	0.00000117
DCTN6	1.256819127	3.61E-08
LRRC3	1.255557677	0.001962805
STOM	1.25469557	0.00000115
CTD-2127H9.1	1.254528088	0.042689981
SORBS1	1.254525583	0.001645484
NR1D1	1.254266487	0.0000159
SAA1	1.25338875	0.000542707
CCDC85A	1.252674254	0.013916287
ALDH1A3	1.24982956	0.000578113
SCD5	1.249791289	2.14E-08
DIAPH2	1.24888199	0.002277153
AHCY	1.248670538	0.000412846
CXCL1	1.247635794	0.004064576
RP11-712B9.2	1.247343978	0.018917079
SESTD1	1.247321262	4.66E-09
RP1-239B22.5	1.246964135	0.000226932
ST20	1.246879908	0.007907312
GLB1	1.245698287	0.0000152
SLC19A2	1.245342785	0.00000423
PCDH9	1.245329204	0.017244738
FXYD5	1.244872787	0.001609889
TAP1	1.244827201	0.000240871
SLC6A8	1.243453477	1.3E-09
ST6GALNAC1	1.243087397	0.03429316
STARD8	1.243003102	0.018229593
IL15RA	1.242412492	0.00151752
CDH11	1.241379801	0.00000827
NDRG1	1.238357806	3.47E-08
ZNF860	1.235799005	0.022143863

CD302	1.235618669	2.42E-09
DLEC1	1.235075075	0.037560565
FZD4	1.23490267	0.002761287
CERK	1.233889305	0.00000421
ROM1	1.232505182	0.001030049
HEXIM2	1.232219654	0.000497571
AQP8	1.231886586	0.042964808
RP11-395B7.4	1.23171644	0.00257345
XG	1.228759824	0.00247024
LYN	1.227065704	0.000285928
GCNT1	1.226682078	0.0000384
SH3RF3-AS1	1.224889304	0.004522612
RORA	1.22485908	0.00000172
OSTM1	1.224069459	1.11E-09
CTU1	1.22269609	0.000696148
TGFBR3L	1.222214776	0.033970237
FAM174A	1.221909323	0.0000155
USP38	1.221693262	2.91E-08
HSD17B7	1.219710188	0.000550366
GLA	1.218623478	0.0000048
LYSMD1	1.218352878	0.00000288
GALNT18	1.218334521	0.000000437
SNX24	1.218037675	4.67E-08
ITGBL1	1.217328556	0.01226742
IFNGR1	1.217122247	0.000000721
ATP13A3	1.216529843	0.000210655
PRADC1	1.216449479	0.0000397
TMEM208	1.215824357	0.000000112
SLC39A11	1.21563409	0.000172798
PDE10A	1.214474895	0.00000159
ARNTL	1.2133024	0.000086
SEMA3A	1.211066047	2.98E-10
SLC2A1-AS1	1.210349071	0.004628834

HIST1H2BN	1.210343217	0.006716039
H2AFJ	1.20993956	0.00000212
EMR2	1.208429212	0.000510335
ENPP4	1.20729261	0.0000542
FAM199X	1.205435892	0.001030161
PPIB	1.203821728	0.00000661
AIM1L	1.20300416	0.031512518
CRADD	1.20218002	0.000327568
MBNL1-AS1	1.200289053	0.0000179
TSPAN7	1.200002248	0.019546689
IFITM10	1.198074205	0.0000858
ACER3	1.197363472	0.000155574
IZUMO4	1.196846022	0.010854237
ADORA2B	1.196364629	0.006427161
NCK1	1.195343596	0.00000319
RCAN1	1.195233177	0.000488797
PTRH1	1.194113953	0.000434252
NOG	1.193321521	0.025116592
LGMN	1.192056583	4.46E-08
CDH26	1.191933177	0.037468574
PON2	1.190572726	8.79E-10
POLE4	1.189544017	0.000000217
LAYN	1.188554042	3.05E-09
MICA	1.187727177	0.000000487
CLIC2	1.187028864	0.004015933
BEST1	1.186467376	0.000000472
PNCK	1.186379202	0.032430098
SRPX	1.183474638	0.00000421
ACAT1	1.183019365	0.0000745
GPR157	1.182808523	0.00000994
HS1BP3	1.182768399	0.0000718
MAPRE3	1.182657498	0.0000326
38596	1.181907447	0.000484278

IFI27L1	1.178090648	0.00000339
RRAS	1.177197916	0.000107884
AC112229.4	1.176825588	0.0000212
CMIP	1.175257753	4.44E-08
SCML1	1.174274018	0.001463986
AGTRAP	1.17386477	0.000000806
RP11-434C1.1	1.173791422	0.029360349
LMAN2	1.172597157	0.00000268
DHRS3	1.172355047	0.004174565
WBSCR17	1.171885818	0.033031134
SPOCK2	1.171220013	0.022798557
ARL4D	1.170340526	0.000857494
MRPL33	1.170297073	3.98E-08
ACTC1	1.169702054	0.039587383
GNA15	1.169174741	0.045421767
ERGIC1	1.168125626	0.0000528
SEMA3B	1.166835892	0.00000827
LSS	1.163226847	0.0000447
PNPLA2	1.162722023	0.00000127
CTC-786C10.1	1.162665543	0.005085051
TMCC3	1.161419458	0.001242724
KLK10	1.161365029	0.000241134
ITGB8	1.159011565	0.000180976
CTA-217C2.1	1.158754747	0.0000329
AC011242.6	1.158571335	0.00203434
FTL	1.157893814	6.79E-08
FBLN5	1.157737789	5.62E-08
CTD-3184A7.4	1.157106714	0.005691721
SLC2A12	1.155757066	0.011829383
SUSD2	1.154675518	0.0000139
ATG4A	1.154148901	0.000168345
RP11-112L6.4	1.153956918	0.044218449
NUS1P2	1.153687326	0.021613466

RPGR	1.152777611	0.0000447
LINC00467	1.151137456	0.011178493
TMEM38B	1.150365957	0.0000149
CPEB4	1.150134818	0.0000585
ARSG	1.149769753	0.003486197
EMP3	1.149069292	0.000366223
HLA-DMA	1.148560465	0.0288779
CLDND1	1.148239127	0.00000116
OSMR	1.147305836	0.001019215
LAMA2	1.147294857	0.007928491
SASH1	1.145390577	0.002081366
ALDH2	1.143446789	0.005064371
TSPAN12	1.142079552	0.0000269
AKAP13	1.141915461	0.000105697
ADCY2	1.140664286	0.000307863
ERVMER34-1	1.140009351	0.000806253
RAB4B	1.139526825	0.0000119
HSD17B1	1.138711158	0.000504733
LAMC3	1.135712506	0.008801155
RP11-498C9.2	1.134756112	0.017917543
MFAP3L	1.133653452	0.003814681
RP11-218E20.3	1.133452662	0.013084946
STC1	1.130187335	0.006859142
PTPRN2	1.130121597	0.000551775
CLTB	1.12990164	0.000000352
CRELD2	1.129622723	0.0000123
UNG	1.128873806	0.00000026
BRF2	1.12881169	0.0000033
REXO2	1.128109716	0.000000113
NCOA4	1.128104318	2.52E-08
EML2	1.127891242	0.000896832
CSPG4P12	1.127719537	0.000323929
ABCA3	1.12601281	0.004207433

CFH	1.125513997	0.023063893
DPP6	1.12512603	0.022958441
SGCB	1.125100737	0.0000357
HYAL3	1.124332532	0.001510463
SLC35D1	1.12409496	0.00188802
CCDC86	1.123854357	0.000000667
GLRX	1.122144237	0.00000182
TEX2	1.121391505	0.0000838
EIF2AK3	1.120640933	0.000196224
FGGY	1.120616967	0.008607184
C20orf195	1.120132272	0.043057855
RNASEK-C17orf49	1.119505385	0.047665906
CTSB	1.119490921	4.21E-08
TSC22D4	1.117333849	0.00000288
C1R	1.116118394	0.000000253
METAP2	1.115278155	2.27E-09
ACYP2	1.11510513	0.0000072
VWA1	1.114449057	0.006665227
CYSTM1	1.111146641	0.00000146
RAB18	1.109395178	0.000000311
AIFM2	1.109168787	0.000000505
ANKRD2	1.109100566	0.047686368
HIST1H4H	1.108581316	0.002599349
RNASEL	1.108375965	0.0000147
FZD10-AS1	1.107655936	0.018088072
SRCRB4D	1.107554489	0.02815255
WNT5B	1.105209566	0.001966888
BAMBI	1.10448095	0.000429173
RABAC1	1.103687875	0.00000571
RP11-54A9.1	1.101367812	0.019773213
ZNF438	1.101027807	0.001593901
MMP19	1.100638915	4.34E-08

PRDX4	1.100284028	0.000262322
ERO1L	1.09986748	4.45E-09
UGT2B7	1.09955948	0.003858595
HDAC9	1.097980161	0.028944414
TPGS1	1.097876466	0.000496634
TMED3	1.097415666	0.0000927
LINC00598	1.096882326	0.021424385
LINC00968	1.096546168	0.009986394
CES1	1.096413808	0.0000925
SLC44A1	1.094877748	0.0000226
TLR4	1.094767652	0.000458681
LITAF	1.094359256	0.000000107
LINC00683	1.093369924	0.035135295
POLD4	1.093267027	0.0000151
KCNK1	1.090654211	0.00000588
IL18	1.087905837	0.002964625
CTD-2013N24.2	1.08524189	0.043466414
NEU1	1.084860955	0.000000274
KL	1.084734946	0.013388252
TXN	1.084233524	0.000637565
SIK2	1.083300841	0.000000849
GLUD2	1.082624907	0.006571167
MFAP5	1.082565062	0.004334919
LNX1	1.081700054	0.012808709
CITED4	1.081315899	0.00042852
TMEM154	1.081304161	0.000413826
SLC1A2	1.080374367	0.011505658
RP11-67L2.2	1.080280522	0.000895536
CA5BP1	1.080052759	0.00249785
WDFY3-AS2	1.080039528	0.003623417
AIM1	1.07831128	0.026465849
RP5-1065J22.8	1.076864223	0.034352436

TRPC4	1.075830934	0.000280234
C3orf58	1.075553155	0.0000772
COPZ2	1.075328977	0.000491879
RP11-395A13.2	1.075151917	0.007246924
TMEM147	1.074745146	2.46E-08
SGK1	1.073660651	0.001509197
MZT2B	1.073244429	0.000492024
MXRA8	1.07318014	0.000000104
CCDC53	1.071789047	0.00000298
PROSER2	1.071060963	0.000102915
RBMS1	1.070952322	2.11E-08
TXNDC15	1.070442219	0.00000038
TSPO	1.070130726	0.0000994
GCNT3	1.069924285	0.022182992
ZBTB11-AS1	1.069815225	0.001269856
LRP8	1.068148352	0.010331958
ATRAID	1.067975336	0.0000143
DCXR	1.066736824	0.000136486
VKORC1	1.066147276	0.000331091
ABHD17B	1.065401919	0.000000662
PHYH	1.064819543	0.000000407
PGD	1.06426437	0.001787192
TSPAN13	1.06421385	0.001140606
GPR108	1.06366209	0.000000379
FAM53B	1.063583415	0.0000125
RNF152	1.063388689	0.000446698
BLVRB	1.062577827	0.00000779
RP11-295K3.1	1.059631591	0.046623711
STAT3	1.058100669	0.000732367
ALDH1A2	1.057537351	0.000177704
RIOK3	1.056642824	0.000000374
SLC30A1	1.055558017	0.0000162
PGM2	1.053528289	0.000483417

SSC5D	1.053368668	0.000293832
QPRT	1.052884567	0.00000552
MDFIC	1.052005221	0.000000345
RP11-465B22.3	1.051661615	0.038711172
C19orf24	1.05054259	0.000013
ADAP1	1.05048429	0.024833042
TMEM53	1.050082701	0.002478145
GREB1L	1.049227112	0.000000236
SLC35E3	1.049176373	0.0000837
SLC35G2	1.048578471	0.0000498
EDN2	1.048532984	0.01820462
ABCA1	1.048038249	0.00209095
OLFML2B	1.047582624	0.010152895
NUDT16P1	1.047532401	0.046368792
ITPK1	1.046675966	0.000000176
EDEM2	1.045872576	0.000184636
SDF4	1.044939581	0.0000149
CCDC159	1.044571961	0.0000765
GBA	1.043412178	4.64E-08
C9orf89	1.043302115	0.000000669
DOCK8	1.041661138	0.009860664
CA2	1.041220254	0.047874404
MCTP1	1.041116503	0.000805821
B3GNT2	1.040310437	0.000253715
ABAT	1.039645799	0.006275146
HLA-F	1.038637278	0.003970509
C1orf85	1.038408754	0.00000661
NAP1L3	1.037426698	0.00040181
DDRGK1	1.037251581	0.00000206
ADCY3	1.036446955	0.01131106
AP1S2	1.036411698	0.003273882
ITFG3	1.036073912	0.0000103
ADD3	1.03509132	0.0000191

ABCB8	1.032737998	0.000832048
SLC7A11	1.031990316	0.002992049
TM7SF2	1.031621121	0.000254867
C4orf48	1.031587345	0.000824828
SERPINB9	1.031164729	0.004860422
RCN3	1.030229938	0.000243447
SELM	1.02887497	0.00000632
OAT	1.026786509	0.00000689
LINC01003	1.026754129	0.01870097
PDIA5	1.026426732	0.002507018
CTD-2536I1.1	1.026226694	0.030369919
CLYBL	1.026125059	0.006889708
SCPEP1	1.023603378	0.000000126
MCUR1	1.023052194	0.000000693
RP11-295G20.2	1.022734904	0.012459688
PBLD	1.021956036	0.000477084
PLXND1	1.021697621	0.015850715
KCNMB4	1.021311641	0.008571318
AIMP2	1.020502087	0.0000388
PIGP	1.020279812	0.0000367
PDCD5	1.020179948	0.000024
MASP1	1.019252126	0.006980522
DHCR7	1.019192468	0.009869387
RNF14	1.018986653	0.000000758
UNC79	1.01895397	0.047009399
EMP2	1.018911752	0.00000251
TBC1D1	1.01847604	0.005795156
ATP6V0B	1.016839267	0.000000122
ARL4A	1.015746742	0.000219986
KIAA1549	1.015659147	0.0000788
EPHX1	1.015589478	0.0000965
CD63	1.014066646	0.00000684
RN7SL3	1.014007665	0.028904959

GPX7	1.013373015	0.000231373
TAF13	1.01314447	0.00000085
CASP9	1.012774883	0.000106155
MIEN1	1.012570652	0.00011376
SELPLG	1.012549218	0.006583901
RP11-355B11.2	1.011113976	0.021816117
RP11-334C17.5	1.010745856	0.008119996
IL10RB	1.01021324	0.0000429
FBLN1	1.010003497	0.0000108
SPRYD4	1.009926545	0.000520667
MOV10L1	1.00957762	0.0000115
C19orf70	1.009104463	0.0000114
SUSD3	1.00889758	0.0031879
BNIP3P1	1.008148531	0.000943918
HMGN3	1.007320653	0.0000904
SERF2	1.006651206	0.0000427
ACE	1.006264416	0.029982176
SNX25	1.005917218	0.000000648
MVD	1.005663721	0.000700055
FKBP11	1.005568114	0.001894719
LIMS3	1.005411808	0.000306247
TIMP1	1.004995052	0.000281971
SMAP1	1.003187967	0.0000773
RP11-135L13.4	1.002763049	0.011294848
UCP2	1.002259488	0.025851129
UBE2D1	1.001839468	0.000000447
C5AR1	1.001532007	0.023904805
LINC00116	1.000665521	0.000792991

Appendix 4. Down-regulated genes upon decidualization: Log2-fold change ≤ -1

Gene Symbol	log2-fold change	q
TNFSF18	-6.478964402	3.23E-32
INHBE	-5.884321704	1.04E-18
EGR2	-5.274229596	2.66E-17
SERTAD4	-4.999475267	3.27E-26
TNFRSF19	-4.891775017	7.89E-76
SSTR1	-4.890083317	6.37E-43
MXRA5	-4.489495577	6.63E-33
PHGDH	-4.430202293	1.18E-36
SYTL5	-4.419102984	5.6E-41
DKK2	-4.32675239	7.69E-10
CALB2	-4.12458001	1.54E-15
TNFSF4	-3.960684243	2.01E-20
SLC6A9	-3.93819276	1.72E-19
TNNT2	-3.937206526	1.03E-14
COL12A1	-3.882128111	4.95E-59
ADRA1D	-3.876341209	4.89E-13
TMEM130	-3.693861991	5.32E-11
FAM196B	-3.676870569	5.26E-15
GLI1	-3.665220372	2.01E-12
SBF2-AS1	-3.665135925	4.97E-41
HTR1D	-3.645204857	4.07E-09
MYBL2	-3.633644884	2.51E-33
LRP2	-3.62009864	0.000000285
PSAT1	-3.607758077	3.74E-13
SULT1C4	-3.604581401	2.17E-11
CNTN5	-3.602621883	6.06E-09
ADM2	-3.594698793	4.29E-14

ITIH3	-3.558075628	2.49E-16
38047	-3.501007808	9.45E-15
MXRA5P1	-3.484783246	0.000000478
NCKAP5	-3.480388334	3.33E-15
OLFML2A	-3.478998768	1.26E-16
MKI67	-3.462861154	3.93E-27
FAM111B	-3.399998921	1.94E-14
MEOX1	-3.39852901	9.06E-11
SORCS3	-3.386384818	0.0000109
DOCK2	-3.354057658	2.13E-08
BUB1B	-3.341101433	3.11E-28
CACNG4	-3.334648774	0.00000049
NEIL3	-3.332498259	1.01E-13
GBP4	-3.319460316	9.71E-26
RASGRP3	-3.317088224	6.91E-11
LINC00643	-3.309890415	0.00000919
CHRM2	-3.304274792	1.37E-12
RP11-284N8.3	-3.281040135	0.000000128
FMN2	-3.259599217	2.21E-24
DTL	-3.249761598	1.04E-15
TNFSF15	-3.235616735	1.3E-10
WNT2	-3.233514586	3.2E-12
KCNA3	-3.230462217	0.000000201
ZNF365	-3.221292117	4.35E-15
MIR143HG	-3.219573115	1.2E-22
DPY19L2P1	-3.184966903	2.09E-11
BRIP1	-3.182414237	9.4E-22
NCAPG	-3.175300379	1.49E-24
CCNE2	-3.15732126	1.15E-12
RP11-709B3.2	-3.149127291	7.58E-09
IQGAP3	-3.143042706	2.84E-27

RIBC2	-3.139096696	0.0000338
AL121578.2	-3.108761843	0.0000427
SKA3	-3.103322449	1.55E-14
RP11-554D15.1	-3.102458777	0.0000226
HJURP	-3.088061719	1.18E-18
NES	-3.087777528	1.05E-16
DIO2	-3.054472453	1.66E-18
SYT1	-3.043178477	8.65E-11
E2F7	-3.036895256	4.6E-12
C1QTNF7	-3.033298963	7.4E-12
TYMS	-3.030154902	3.81E-20
HUNK	-3.027191731	4.3E-22
PDE5A	-3.02220806	2.22E-13
RASGRP1	-2.983978379	3.88E-10
LINC00617	-2.983070033	0.000000274
ASF1B	-2.981733991	1.83E-15
MIR145	-2.979353524	4.42E-20
FJX1	-2.969208172	1.91E-08
ZNF469	-2.959950264	1.2E-12
CPA4	-2.949856419	3.22E-14
KIF20A	-2.942080275	2.07E-17
ADAMTS16	-2.933999798	1.93E-11
LRRC17	-2.922721978	4.15E-08
CAND2	-2.921606653	7.74E-15
IGFBP5	-2.915642343	0.000121201
CAMK1D	-2.910196942	6.16E-13
GINS2	-2.901039018	1.94E-10
AC131025.8	-2.894287997	0.00000318
CENPU	-2.883437441	8.25E-15
RP11-426C22.4	-2.882712369	0.000000176

RP11-588K22.2	-2.880159074	0.0000338
FAM64A	-2.87355014	1.29E-16
KIT	-2.866737402	4.62E-10
BUB1	-2.865749724	1.88E-18
RAD54L	-2.865290807	1.75E-10
ANLN	-2.86244239	4.2E-24
MAP3K7CL	-2.862418319	5.03E-14
TENM4	-2.856956301	2.64E-08
MRVI1	-2.85019438	1.65E-18
RRM2	-2.848489188	9.54E-30
DPY19L2	-2.84835008	2.48E-10
NUF2	-2.845470417	1.19E-14
EGR1	-2.844014529	7.5E-38
RAB3B	-2.837069233	1.61E-10
UHRF1	-2.832300717	1.39E-23
NRP2	-2.828769535	8.91E-10
E2F8	-2.825564432	0.000000236
FOXM1	-2.8222335	6.49E-23
POSTN	-2.818605362	3.66E-16
CNTN1	-2.815799532	0.000000013
VASH2	-2.812041267	3.44E-08
NREP	-2.808165496	2.52E-14
CDC25C	-2.8075364	1.52E-10
COL8A1	-2.799157262	3.44E-17
DPYSL3	-2.79466439	0.0000738
E2F2	-2.787418993	0.000000584
CASC5	-2.784711854	7.48E-23
EXO1	-2.767062159	3.62E-08
TROAP	-2.766756916	1.67E-14
PLCB1	-2.763230911	3.95E-09
NCAPH	-2.762443973	1.44E-14
ERCC6L	-2.761729534	0.000000849

GTSE1	-2.760317869	1.27E-18
GUCY1A3	-2.755576835	0.00000929
FAM83D	-2.749806384	2.23E-15
CEP55	-2.744744396	7.72E-24
CAMK2A	-2.741106867	0.0000221
TICRR	-2.737970191	4.97E-10
CLSPN	-2.725606992	7.14E-12
PKNOX2	-2.723249265	0.00000012
MCM10	-2.71105548	1.48E-10
LINC00327	-2.70742165	8.32E-09
PRELP	-2.695510256	4.41E-11
NTF3	-2.692058007	0.00000034
HRK	-2.69176817	0.000405801
RP1-140K8.5	-2.687139142	0.000055
CDK1	-2.686430719	2.02E-20
TNXB	-2.684158515	4.75E-13
TMPO-AS1	-2.683801139	0.000000782
RASSF2	-2.680154098	1.55E-19
PRRG3	-2.667713698	0.0000693
KIF18B	-2.66690852	1.22E-11
HEPACAM	-2.6613203	0.000604723
LBH	-2.660207214	4.02E-13
FNDC1	-2.658126877	4.24E-10
LANCL3	-2.658075168	0.00000202
SGCD	-2.655198295	1.47E-08
ITM2A	-2.655176184	0.0000152
ATP8B1	-2.651453703	8.94E-12
FRMD4A	-2.648969956	9.57E-08
SPAG5	-2.647535803	4.59E-19
C6orf141	-2.646631398	0.000157089
KB-1410C5.2	-2.645960662	0.000784577
DLGAP5	-2.641384938	2.29E-18
MYLK	-2.641246354	4.84E-16

SHCBP1	-2.63963268	8.77E-21
MBOAT1	-2.63852621	1.92E-14
ZNF367	-2.634271598	1.77E-12
CBLN2	-2.632933831	0.000382016
CDT1	-2.623787024	3.06E-11
ESCO2	-2.621971973	4.9E-11
SAPCD2	-2.620799777	0.000000066
TTK	-2.615696129	1.34E-15
PLEKHA4	-2.607120201	2.27E-13
RGS4	-2.605585551	1.75E-11
DUSP6	-2.604070472	3.73E-10
FBXL22	-2.598403388	0.00028374
AURKB	-2.590395231	9.71E-09
AFF3	-2.589586994	1.19E-34
TOP2A	-2.586289371	1.68E-33
NCAM1	-2.584530914	7.2E-10
RNF165	-2.582138394	0.00000829
COL16A1	-2.58096138	1.19E-09
TCF19	-2.580803063	7.8E-15
FAT3	-2.578357579	0.0000308
SLC7A3	-2.577730974	0.00000297
C17orf107	-2.575776026	8.91E-08
ZNF711	-2.573121138	2.81E-13
ATP8B4	-2.570764748	0.00000244
KCNA6	-2.57030129	0.000222132
SLC4A4	-2.56674004	0.000111146
RCOR2	-2.559210209	6.46E-08
BIRC5	-2.557153182	2.94E-23
GRIN2A	-2.556971109	0.0000493
SH3BP1	-2.556666562	1.13E-11
CLDN11	-2.555386995	0.00000469
PLK1	-2.555312528	2.04E-23
KIAA0101	-2.552340448	3.08E-14

CNGA1	-2.545374806	0.0000828
FIBIN	-2.545311685	0.00000125
ARHGDIB	-2.544881595	1.54E-17
CTD-2297D10.2	-2.540334518	0.001277033
PGM5	-2.537295676	0.000000001
KIF11	-2.52217967	2.29E-22
RCAN2	-2.52103494	0.00000024
SETBP1	-2.518417714	8.06E-08
PREX2	-2.518168046	0.00000114
FLRT1	-2.513214045	0.001269368
CDC20	-2.513119746	3E-13
JPH4	-2.511447318	3.61E-11
LGR5	-2.51028343	0.00000695
LPAR4	-2.506172281	0.000628627
KIF18A	-2.50579416	2.86E-09
B3GALT2	-2.504062616	0.000022
CDC6	-2.503426398	7.23E-15
SCHIP1	-2.500726907	0.0000562
MIR143	-2.497194546	0.001384495
ROBO3	-2.494197514	0.00000238
PKMYT1	-2.493300237	1.07E-08
FHOD3	-2.49218599	0.000584822
PTCHD4	-2.492171895	7.97E-08
INPP5J	-2.490575513	0.0000725
PLK4	-2.490068687	2.03E-12
CTD-2269F5.1	-2.488974041	0.000692397
PTHLH	-2.488465151	0.00000259
LMNB1	-2.487120932	2.53E-12
CDCA5	-2.484806913	2.04E-17
DEPDC1	-2.482434201	2.36E-18
CDCA2	-2.480510691	1.02E-10

POLQ	-2.478629246	9.35E-11
IGDCC4	-2.477579509	7.25E-11
FGF9	-2.475103095	0.00000694
RHOJ	-2.473712537	7.16E-12
AC010890.1	-2.464496393	0.000437394
RPS6KA6	-2.460063483	1.55E-08
SYPL2	-2.458308889	1.96E-22
SULF1	-2.456466359	2.53E-15
ASPM	-2.453593354	2.4E-11
KIAA0754	-2.451906867	1.16E-09
ARMC4	-2.449780727	0.000063
PALM2	-2.44869371	1.66E-08
PAPPA2	-2.44733788	0.001173298
KIF2C	-2.44468025	1.04E-15
CENPF	-2.444601607	1.91E-22
CDCA3	-2.438101079	1.03E-14
RP11-344E13.3	-2.434641194	1.42E-08
PALM2-AKAP2	-2.422229159	0.000516258
PLXDC1	-2.419288127	3.01E-10
NUSAP1	-2.418966479	5.58E-23
NTM	-2.40698604	0.00000339
BAI2	-2.40556779	1.16E-09
KIF14	-2.405385085	1.61E-12
AC007362.1	-2.404446376	0.000022
CR1	-2.404385258	0.000609959
CSRP2	-2.396168646	0.000000398
CENPA	-2.395279822	1.08E-10
PRC1	-2.393201969	9.64E-27
EBF3	-2.385871027	0.00010583
USP53	-2.375775592	1.33E-14
SFRP1	-2.373884818	2.48E-10

FMNL3	-2.36835175	1.11E-13
ADCY4	-2.365269932	9.32E-12
WEE1	-2.363762306	4.54E-09
MIR503HG	-2.361276121	4.77E-10
GREM2	-2.360653989	0.000021
C11orf82	-2.356432581	1.12E-08
NBEAP1	-2.352763347	0.0000966
ZFHX4	-2.346937544	0.00000142
RP11-354P17.15	-2.344879178	0.002773462
AKAP5	-2.343047438	0.00000581
LOXL1-AS1	-2.342058003	9.76E-08
IL17RB	-2.34034	0.00011532
LINC01085	-2.34002086	0.00049182
BLM	-2.339699519	5.76E-08
SMAD3	-2.334169554	0.000000077
FMO2	-2.333362191	0.00176912
RP11-693N9.2	-2.332496978	0.002923398
NPM2	-2.3252047	0.000108454
HOXD-AS1	-2.324000374	0.000784553
SHROOM3	-2.322535646	2.03E-11
CLEC14A	-2.321131034	0.002076507
FOXS1	-2.315029325	0.001130009
ERP27	-2.313765088	0.00088978
CDCA8	-2.312390941	1.77E-15
KIFC1	-2.309665067	1.12E-14
DIAPH3	-2.309176469	4.44E-15
TPX2	-2.308886563	1.14E-13
HTR7P1	-2.307756798	0.00000197
GRIP2	-2.307248529	0.000037
TOX	-2.307052786	0.000490731
KIF4A	-2.30619643	3.81E-15

TGM1	-2.305425486	0.0000488
RP11-554A11.4	-2.300902559	0.000226492
ATP2B1	-2.29889117	7.23E-18
ANK2	-2.296192964	4.98E-10
PAG1	-2.288607519	5.24E-10
TLL1	-2.287836422	0.001528438
PLCE1-AS1	-2.282682834	0.001052457
SPC25	-2.28171544	1.37E-08
HMCN1	-2.276924021	5.22E-11
MYH11	-2.274267171	2.89E-09
MBNL3	-2.27078741	0.0000401
PTGES3P1	-2.268376082	0.001190105
GUCY1B3	-2.264289242	0.00000402
RP11-548O1.3	-2.262507875	8.85E-17
ATAD5	-2.262433242	0.000000182
ZBTB12	-2.262034795	4.73E-08
NUP210	-2.261351567	0.00000243
SYT16	-2.261269077	0.003037695
LRRC4B	-2.258836845	5.62E-12
TK1	-2.258657083	4.01E-14
AC092667.2	-2.257244242	0.003425463
BMF	-2.249544411	0.00000549
OIP5	-2.245650261	0.00000897
PTX3	-2.242238557	0.00083907
C2CD4C	-2.241011406	0.004468727
CCDC81	-2.238508096	1.07E-14
B4GALNT4	-2.23530012	0.0000855
UBE2C	-2.231986792	4.89E-11
ITGA4	-2.229440966	1.25E-15
TSPAN18	-2.227738862	0.0000136
MCM5	-2.224744937	8.52E-19

PCDH10	-2.223533616	2.07E-08
CCNB2	-2.223365716	2.11E-13
DNM1	-2.221740562	2.87E-08
CCDC15	-2.221575275	0.00000555
GABRA5	-2.220025516	0.000000793
ARHGAP11A	-2.213086477	5.31E-16
CDKN3	-2.212165792	8.25E-11
RAD51AP1	-2.211759963	5.06E-10
RASGRF1	-2.208316027	0.000215123
WNK4	-2.20704619	0.0000174
SYT7	-2.199943493	0.000017
TRHDE	-2.199250495	0.0000365
PBK	-2.198957613	2.16E-13
RP11-297M9.2	-2.197234193	0.000877263
DOCK10	-2.196527424	0.00000403
COLGALT2	-2.196303717	0.005259501
ADAM12	-2.19588053	2.74E-11
RHOBTB1	-2.191464427	9.24E-09
LZTS1	-2.186449047	0.000148225
ITGA11	-2.182456477	0.000000341
PPP1R12B	-2.180127579	2.25E-11
CENPH	-2.179755794	2.02E-09
CSDC2	-2.179361742	2.45E-09
OSR1	-2.179180435	0.001112401
OBSCN	-2.176311888	6.09E-19
MELK	-2.168342884	5.24E-09
GPSM2	-2.166053494	1.03E-08
ZNF521	-2.164815144	0.000000164
TRERF1	-2.164382967	1.28E-16
STC2	-2.1608153	0.0000266
SAMD3	-2.159316299	0.000165789
PRRT2	-2.158451148	0.00000353

NDUFA4L2	-2.156744044	0.000713615
LINC00312	-2.155708559	0.0000223
ISM1	-2.153585758	0.00000129
ADCYAP1R1	-2.151627836	0.006264154
ZNF488	-2.149789834	0.0000227
CD200	-2.144906872	0.001651094
ROBO2	-2.144216146	9.29E-12
F2RL1	-2.143275499	0.00000698
OSBPL7	-2.143185956	6.21E-11
HOXA2	-2.14255104	0.000412025
NXPH4	-2.142039282	0.002332883
FAM69B	-2.140775781	0.001713747
KIF23	-2.140582139	7.71E-20
B3GALNT1	-2.139120409	0.0000287
KIF15	-2.138303801	5.13E-08
RASSF5	-2.131736287	0.002741549
C1orf198	-2.129769249	2.66E-12
DNMT3B	-2.12767501	0.000000222
CMAHP	-2.124354981	4.92E-08
IL34	-2.122671452	0.000666157
DNAH10OS	-2.122568844	0.0000143
NEK2	-2.118321753	1.11E-08
FLI1	-2.115576482	0.000559807
EZH2	-2.112994951	0.000000043
ITGA8	-2.11227624	0.0000365
PCP4	-2.107991382	0.007378635
BRCA2	-2.107489482	0.00000021
CDH4	-2.10742278	0.000241856
PRR11	-2.106322877	9.22E-13
ABCA10	-2.105732423	0.000426767
RP11-9G1.3	-2.103722901	0.007149446
PDGFC	-2.101487497	2.57E-10
ANO1	-2.098828435	9.93E-08

SDPR	-2.09717574	6.85E-09
CTD-2267D19.6	-2.096782618	0.007809255
IQCA1	-2.096128559	0.000150256
NPAS4	-2.094531787	0.006848542
37865	-2.093158918	0.000132505
DIRC3	-2.093027873	0.001195316
MYH10	-2.092442709	9.72E-19
PRR5L	-2.086056771	0.00000301
TSPAN8	-2.082310376	0.00016909
ETV4	-2.080386428	0.0000317
SLC35F3	-2.079776176	0.0000322
CRABP2	-2.078102979	0.000116978
KCNMA1	-2.076545277	0.000403127
AC109642.1	-2.076026426	0.006765439
ATCAY	-2.075964004	0.000000517
SGOL1	-2.074550197	0.000000774
FBXO43	-2.072747461	0.006625009
TMEM119	-2.072428559	2.37E-08
RP11-686D22.3	-2.07237848	0.000616602
NFIX	-2.071397297	1.35E-17
MRGPRF	-2.071241264	0.00000345
LOXL4	-2.069725536	2.22E-08
CREB5	-2.067509004	0.000000489
CIT	-2.066646783	0.00000578
RP11-597D13.7	-2.065650849	0.001883486
MIAT	-2.059690778	0.000617955
MCM7	-2.058242981	2.88E-10
PLCH1	-2.055381194	0.00000456
NUAK1	-2.054327639	1.33E-11
CADPS	-2.05376396	0.000255413

GINS4	-2.053727295	2.19E-09
IL17RD	-2.051129968	0.00000859
ACBD7	-2.047215239	0.002613015
SSPN	-2.046301304	9.86E-08
APOL3	-2.042176051	0.000000533
HELLS	-2.041555355	8.21E-14
NFE2L3	-2.037530469	1.31E-09
C8orf34	-2.034864051	0.00135787
CDC45	-2.033516062	0.000000179
RECQL4	-2.03291442	3.65E-08
SYNPO2	-2.030453525	4.65E-15
FGF17	-2.021140331	0.003960524
TRIP13	-2.017705266	1.16E-12
MPPED2	-2.014741891	0.005830251
RP11-567M16.1	-2.001347621	0.002749451
PREX1	-2.001048423	3.69E-12
LIG1	-2.000529633	0.00000242
WFDC1	-2.000035491	4E-10
RP11-355I22.7	-1.996607518	0.006327423
SLC7A4	-1.995333838	0.000742676
CASS4	-1.995056326	0.011440371
GRIA1	-1.991944274	3.42E-10
HYDIN	-1.991895351	0.000000325
MEX3A	-1.990570326	0.0000426
DPY19L2P4	-1.988655744	0.011700205
MMP11	-1.988604124	0.008111229
CCNA2	-1.987248522	3.72E-16
ADAMTS6	-1.982030154	1.76E-12
LINC00865	-1.978518562	1.74E-08
ACTG2	-1.977661141	1.87E-10
FAT1	-1.976684522	7.1E-10

JPH2	-1.97536599	1.53E-11
DIRAS1	-1.97253106	0.0000004
ZNF853	-1.970571751	0.000000255
PMAIP1	-1.968399362	0.0000352
MARK1	-1.967200641	9.12E-08
TRAC	-1.964563894	0.011549905
LINC00920	-1.961645081	0.009086035
RP11-253E3.3	-1.961549871	0.0000268
BBC3	-1.96118209	0.000136263
RP11-268J15.5	-1.960057795	0.000000696
WTAPP1	-1.959000805	0.008175978
KIF20B	-1.956395893	3.97E-13
KIAA1524	-1.954749061	8.52E-12
RP11-617D20.1	-1.953872057	0.003194924
PABPC4L	-1.951433807	0.000000993
ARL4C	-1.950777366	0.000219631
MSC	-1.950485075	0.000000603
MKX	-1.949885089	0.001232259
VANGL2	-1.946924773	0.00000282
FZD7	-1.946408213	0.0000182
RUNX2	-1.943965268	0.0000449
PDZD4	-1.938897662	0.0000647
HMMR	-1.937881597	1.23E-10
ZSWIM4	-1.93670169	0.00000027
DYRK2	-1.936550813	3.31E-14
RAC2	-1.935924562	0.001116274
CAV1	-1.933403705	1.3E-11
SPEG	-1.929911132	0.000000015
XRCC2	-1.929316382	0.0000064
E2F1	-1.927780115	0.000000683

CENPM	-1.927533499	0.0000194
GBP2	-1.926595108	2.98E-09
VEGFC	-1.923791131	7.53E-16
TRAIP	-1.923010562	0.0000257
HCAR1	-1.922036067	0.010227421
FANCA	-1.920729548	6.66E-09
SCN5A	-1.919804766	0.0000123
GAL3ST4	-1.917511439	0.000139598
SERTAD4-AS1	-1.916954057	0.014866845
FAR2	-1.916097097	1.47E-11
EPB41	-1.915412376	0.000350185
PSG1	-1.914284258	0.007666882
AC096677.1	-1.913395871	0.009081171
RP11-60L3.1	-1.912369603	0.004841773
CTC-301O7.4	-1.91190995	0.000913528
LIN7A	-1.911016772	8.54E-09
KIAA1683	-1.910892544	1.75E-09
THSD1	-1.91031867	0.005677119
TGFB3	-1.899001275	0.00024946
FMO3	-1.897878764	0.013304985
RP11-141M1.3	-1.897824076	0.013176646
ACKR4	-1.892517339	0.003298757
AC112721.2	-1.892371892	0.014249004
GREM1	-1.891026865	0.012176514
NEFL	-1.890870589	0.004033896
FAM211A	-1.887511971	0.000000643
SLC9A7	-1.88685015	0.00000236
FRMD6	-1.885244063	1.25E-10
GINS1	-1.883473084	0.000000022
CCDC14	-1.883381565	5.6E-10
FGL2	-1.882812898	0.006620856

RNU2-52P	-1.881230061	0.017129922
F2RL2	-1.881214195	8.97E-14
LRRC8C	-1.880597303	0.0000472
DAPK2	-1.878658283	0.0000672
DCAF12L2	-1.878595921	0.005014279
NXPH3	-1.878055992	0.000115543
SCN9A	-1.876730197	0.001504701
CCDC144CP	-1.876193306	0.002903279
HMGA2	-1.875666932	0.000366307
C10orf105	-1.873162701	0.010336008
SCN8A	-1.872845873	4.08E-08
PSRC1	-1.869171472	0.000000739
SLC26A10	-1.868488027	0.0000221
CENPK	-1.868265253	0.00000107
PCK2	-1.867643111	0.00000247
PPARGC1B	-1.867139173	0.0000738
GPR137C	-1.866199668	0.000761738
LYPD6B	-1.866192927	0.018022636
ROR1	-1.864768542	4.54E-11
CCDC3	-1.863388399	0.0000358
DES	-1.863220615	0.000000801
OLR1	-1.862006401	5.07E-08
CEACAM19	-1.859660433	5.15E-14
ARHGAP11B	-1.857594156	0.000000084
RP11-286H15.1	-1.856248991	0.010777556
RP11-247C2.2	-1.851388426	0.005193945
CHAF1B	-1.849703914	0.000000285
TMEM179	-1.848532038	0.001975116
MPZ	-1.848497285	0.000572506
CCNB1	-1.846246557	1.05E-11
TUBB8P4	-1.846232372	0.0192896

XKR5	-1.845863187	0.007856124
NEURL1B	-1.845803546	0.0000355
USP32P1	-1.842980926	0.00253844
PLN	-1.841838937	0.004614065
SFRP4	-1.83788442	0.00000304
IFNA6	-1.837880757	0.014739652
GBP3	-1.836634573	2.07E-10
PALLD	-1.83603568	5.02E-16
SEMA3D	-1.835610768	0.000045
PPFIA4	-1.832693756	0.000129416
WDR62	-1.832325732	0.00000234
AMOT	-1.830689368	0.0000063
PKD1L1	-1.829997864	0.000204581
LOXL1	-1.829891462	9.89E-18
C21orf58	-1.828221021	0.000000459
DOCK11	-1.828123864	1.57E-16
APOBEC3B	-1.828029048	0.0000472
MAD2L1	-1.827297765	3.99E-10
ARSI	-1.826719383	0.0000179
MMP9	-1.825552403	0.006680274
KIF26A	-1.82432201	4.2E-14
RP11-181G12.2	-1.823513942	0.000814228
GOLGA2P7	-1.822313694	7.79E-08
C18orf54	-1.821578505	0.000000036
AP000349.1	-1.820473363	0.011836815
DMC1	-1.817454667	0.00955226
MCM2	-1.817325909	2.87E-14
FAM198B	-1.812823038	0.0000663
CTD-2231H16.1	-1.811141353	0.01817454
TMSB15A	-1.810943725	0.000245525
CCL7	-1.808403526	0.017448233

MTMR9LP	-1.807722446	0.00000544
GRIK5	-1.807200573	0.0000954
MYOM1	-1.807114506	0.004974024
TMPO	-1.80215813	3.75E-10
FLNC	-1.800326892	3.69E-09
KLK6	-1.800322448	0.005601325
USP44	-1.800303636	0.000218816
CCDC74A	-1.800080301	0.0000435
MDGA1	-1.799728979	3.33E-09
SRPK3	-1.798510852	0.019341211
FGF1	-1.798010233	0.000127062
AK5	-1.795712273	0.022826358
C11orf87	-1.792200284	0.00245873
POLE2	-1.78977476	0.000611249
PTPLAD2	-1.789772284	3.11E-10
RP11-685N10.1	-1.789116808	0.017994533
RP11-32B5.1	-1.788454011	0.003113509
CPE	-1.788442486	0.0000931
ANGPTL2	-1.788043611	0.0000544
SKA1	-1.787536914	0.00000324
RP11-527D7.1	-1.786571949	0.011006191
KLF2	-1.786497626	0.008051672
NRIP2	-1.785762169	0.017728445
SLA	-1.78573073	0.000963978
VSTM5	-1.78295722	0.012060274
GAS2L3	-1.780834517	1.99E-08
RP11-222A11.1	-1.77961457	0.004799796
AC073046.25	-1.775118993	0.022348384
RNU6-26P	-1.770551692	0.023113799
PCDH7	-1.769437795	2.91E-10

APLN	-1.76830577	0.011371444
RP11-448G15.3	-1.765052435	0.00000581
CASKIN1	-1.763247907	0.01465852
FANCI	-1.762243699	3.3E-14
HS3ST5	-1.759193538	0.007741988
SNORD116-20	-1.758500296	0.001794279
TRIM22	-1.758085411	0.000000388
PSD2	-1.7580503	0.003981133
RP1-122P22.2	-1.755253269	0.004110115
DRAXIN	-1.750505849	0.017223147
MOXD1	-1.749189103	0.0000388
TSPAN11	-1.749101725	0.000292461
RTKN2	-1.745749387	4.32E-09
RMI2	-1.742682343	0.00000566
PRICKLE1	-1.741837149	5.62E-13
ARHGAP29	-1.74020055	0.000856342
PEAK1	-1.73650316	5.91E-11
SHF	-1.73510917	0.000565903
NIPAL1	-1.733802347	0.000360891
ADORA1	-1.7330717	0.001408875
ANK1	-1.732827685	0.0000497
NPBWR1	-1.732286575	0.017906909
GJC2	-1.731255805	0.005167043
EPHB3	-1.729023239	0.000000112
C7orf57	-1.727852627	0.02798049
TMEM132E	-1.724620555	0.027000018
TRIM59	-1.723766706	0.00000592
ACTA2-AS1	-1.723561158	0.000576473
TRIB2	-1.720899286	0.000000473
ZWINT	-1.720865007	4.32E-08

LRFN5	-1.72045189	0.0000335
RAB39B	-1.718522805	0.019316687
C9orf106	-1.715869013	0.02573332
GRIP1	-1.715550214	0.000021
NHSL2	-1.715119581	0.005966732
SH2B3	-1.713784046	1.1E-12
CADM4	-1.712784048	0.00000455
DCHS1	-1.712332019	1.82E-09
MCM4	-1.712241941	9.61E-12
CAMK2B	-1.711896429	0.029812243
PTTG1	-1.711786302	9.11E-10
FLNB	-1.70698703	1.48E-08
CAMK4	-1.706056633	0.003752318
CHDH	-1.705938677	0.006003894
MICAL3	-1.705415896	6.98E-11
GSG2	-1.704088815	0.000358196
ARHGAP25	-1.703116022	0.001647108
XK	-1.700723436	0.004310226
ITGA7	-1.699735264	0.000225809
ADRA2A	-1.697015859	0.03129121
NEDD4L	-1.696593454	0.0000699
CTD-2078B5.2	-1.695415144	0.03020842
RP11-20I23.8	-1.695195966	0.000132832
DLEU2	-1.695185218	0.003959935
ISLR2	-1.694964387	0.0000102
AP001476.2	-1.692425771	0.023398745
SH2D5	-1.692328473	0.003513456
PCDH18	-1.687480488	1.31E-14
MIR181A2HG	-1.68612028	0.002150866
GPC2	-1.685960472	0.000176234
TMEM215	-1.68435687	0.015310482
NAV1	-1.682993442	2.47E-08

NMT2	-1.682722095	1.43E-13
RP1-170O19.14	-1.681957207	0.011076567
CST1	-1.680962328	0.000000707
ADAM19	-1.679805175	1.46E-14
RFC3	-1.677535287	6.56E-10
ADAMTS10	-1.676892793	0.000077
AGAP2	-1.676820528	0.015685399
AC004893.11	-1.676005119	0.001306439
HSD17B2	-1.673541288	0.001598932
KRT34	-1.672966874	0.00000264
FZD8	-1.672653261	0.000288208
RP11-87H9.3	-1.669927259	0.033915922
PTGFRN	-1.66891837	8.25E-10
MIR503	-1.667480753	0.034518011
SGCG	-1.6671746	0.008964827
CHRNA1	-1.664578872	0.034382718
ALDH1L2	-1.6640022	5E-10
PPP2R2B	-1.663594296	0.030800635
ETV5	-1.662293651	7.94E-08
GXYLT2	-1.661920008	0.0000332
MB21D2	-1.661652215	0.00000785
BMP6	-1.661616821	0.019514548
GPC4	-1.659712398	0.001158888
TMEM173	-1.659445151	0.0000017
ZNF385D	-1.659345827	0.030099417
SPTBN2	-1.657973416	0.000246614
PDE6G	-1.657513675	0.029238427
SYNJ2	-1.657025058	0.0000401
MTHFD2	-1.657005597	0.00000154
MND1	-1.654556269	0.012990893
PGM5P2	-1.654345356	0.032709851
HBEGF	-1.652849402	0.000326046

CEP78	-1.651638587	2.45E-08
MGARP	-1.651068213	0.000490408
SBK1	-1.650711437	0.01443076
RGMA	-1.650670414	0.000233774
NUDT10	-1.650532493	0.000555501
RP11-597D13.9	-1.649734998	0.0000145
POC1A	-1.649302087	0.0000042
ZFP69B	-1.647691096	0.000165893
WNT2B	-1.643244118	0.003507653
DLG3	-1.642546546	0.000000472
DCLK2	-1.64215165	0.00000578
EPPK1	-1.640091166	0.008732266
UNC5B	-1.639755011	3.81E-13
SOX8	-1.639634415	0.027135821
PHC1P1	-1.639267514	0.002762733
TCF7	-1.638917029	0.0000158
ATP10A	-1.638372307	0.000669216
CNIH2	-1.633551762	0.01485785
ETV1	-1.629130871	0.034298246
SYDE2	-1.628796786	0.000000843
TANC1	-1.628720787	1.22E-11
AC006115.3	-1.628635998	0.030546688
ENAH	-1.628162787	7.57E-16
EDA2R	-1.628104984	0.00000153
LINC00862	-1.627814807	0.020210732
LINC00993	-1.62771216	0.032728566
KLHL4	-1.624113303	0.034556089
DRAM1	-1.623083633	7.95E-12
LEF1	-1.622431864	0.002807537
FAIM3	-1.621839898	0.010769048
FILIP1L	-1.621673448	3.62E-17
SOX6	-1.621643913	1.04E-08

TNFRSF10C	-1.620792639	0.00046929
FAM19A2	-1.620424387	0.0000537
RP11-445H22.4	-1.620026123	0.039458475
TCF7L1	-1.61946676	4.43E-09
KCNG1	-1.618699124	0.0000123
SH3D21	-1.617139599	0.0000585
FAXC	-1.615432034	0.004641804
IQCJ-SCHIP1	-1.614815648	0.00052
RP11-383H13.1	-1.613844065	7.24E-09
GLYATL2	-1.613412372	0.035711589
RP4-791M13.3	-1.613360452	0.017968122
CDC42EP3	-1.612880145	7.11E-17
RP11-283G6.3	-1.610943626	0.035752558
NRGN	-1.608963903	0.012337824
AF186192.5	-1.608240507	0.041270455
CDH10	-1.607421759	0.026555053
ASB2	-1.606319826	0.008580819
LINC00900	-1.603852562	0.036317376
SACS	-1.603313133	6.4E-13
PRSS12	-1.601901593	0.0000158
RP11-381E24.1	-1.601390758	0.036337694
HPSE2	-1.601310901	0.000560421
KIF24	-1.599637473	0.0000323
RP11-1109F11.3	-1.598207404	0.023406044
GLIS3	-1.597753021	0.000488311
BMP7	-1.595226462	0.020270206
CACNA2D2	-1.593408508	0.016975389

RP11-424C20.2	-1.593126561	0.016866107
FABP4	-1.591296184	0.000334233
STOX1	-1.589855479	0.01674256
RP11-404P21.5	-1.589551131	0.042512851
MCOLN3	-1.589424601	0.000323894
TRHDE-AS1	-1.586109168	0.031898047
ELOVL2	-1.584624849	0.04365474
TACC1P1	-1.583128231	0.038693541
GALNT16	-1.581054592	0.038396279
LINGO1	-1.577672542	0.018662404
HMGA1	-1.577583927	0.000118675
THBS1	-1.574846823	0.029258293
FHL3	-1.574142333	9.21E-08
TGIF2	-1.57305238	0.0000247
OSBPL6	-1.572264764	0.00072271
DHRS11	-1.571941918	0.00025779
OLFML1	-1.571686967	0.0000211
ZNF93	-1.569930194	0.00000462
NPAS3	-1.569767814	0.002551559
AJUBA	-1.569338449	0.000489331
COL11A1	-1.5690582	0.04657872
PPME1	-1.568702433	4.95E-11
RP1-170O19.20	-1.568621785	0.011669399
AHRR	-1.566767297	2.98E-10
ACVRL1	-1.566358766	0.0000223
RP11-540A21.2	-1.566175208	0.001503159
ARHGAP28	-1.566013388	0.002403906
PTGIS	-1.565773143	0.044445264
LRRC2	-1.565291004	0.000187532

RP11-366L5.1	-1.565010378	0.041578717
BACH2	-1.56464702	0.003266105
PTCH2	-1.562532006	0.001493651
RSPO2	-1.562079473	0.037414751
DBF4B	-1.559554259	0.00000539
IFNA2	-1.557574195	0.041383462
SLC25A37	-1.557547739	3.48E-11
CELSR2	-1.557132312	0.002582317
RP5-858B6.3	-1.555412204	0.045521957
ARHGEF39	-1.555198987	0.000835335
CENPO	-1.554432965	0.000000026
RHEBL1	-1.554310536	0.003494227
RAPGEFL1	-1.551184821	0.0000733
LINC00908	-1.547372287	0.000518881
CDHR3	-1.54708137	0.002321191
SLC1A4	-1.544842525	0.00000172
PTN	-1.543314208	0.0000777
CDH2	-1.542189852	0.000000891
PYROXD2	-1.541948398	3.32E-10
ESPL1	-1.53843873	0.000000927
CDC25A	-1.538318341	0.000268729
DOK3	-1.538023688	0.004585771
SGK223	-1.536944578	0.00000141
AKNA	-1.536347406	7.27E-11
PKN3	-1.535201427	0.000142514
EVA1A	-1.535121079	0.001162841
GPR63	-1.531917986	0.033571953
HOXA13	-1.531695757	0.0000459
LPHN2	-1.530283137	0.0000163
RAD51	-1.529349107	0.00000752
CPEB2	-1.52866417	8.21E-12
ST5	-1.527230275	9.08E-11

CCDC144A	-1.525566948	0.013772522
RP11-695J4.2	-1.525560188	0.001883518
NOTCH1	-1.524473055	6.7E-12
CALML4	-1.523222336	0.00036323
CEP128	-1.521449918	0.000279471
TCEA1P2	-1.521375356	0.004219699
TCL6	-1.521346383	0.001589244
CTD-2015H6.3	-1.520943546	0.002244243
RP11-177H13.2	-1.520113457	0.007780136
AURKA	-1.516774841	2.49E-09
SGIP1	-1.514044604	0.0000532
IRF2BPL	-1.513709401	0.000000496
EDIL3	-1.511913965	0.000000447
RP11-713M15.2	-1.511847203	0.033965571
FLT1	-1.511017259	0.001144879
HDAC5	-1.509721703	5.29E-08
DSCC1	-1.509211651	0.0000372
MEX3B	-1.508899987	0.000585966
NBPF3	-1.50874211	0.0000195
CLIC3	-1.508697785	0.008345039
CRNDE	-1.508655047	0.006539222
PDGFB	-1.508436245	0.002761168
FZD2	-1.507952885	4.02E-11
PTOV1-AS1	-1.507338916	0.004084377
RP11-757G1.6	-1.505462904	0.008346365
CSMD2	-1.505175463	0.000121291
C1RL-AS1	-1.504551821	0.0000493
N4BP2L1	-1.504444466	0.003234086

AMOTL1	-1.504166592	0.00000541
PARD3B	-1.501648786	0.0000151
ABCA9	-1.501594696	0.047124647
ZNF33B	-1.501374816	0.000857743
CDKL5	-1.50120498	0.002536277
FBXO5	-1.501190079	9.37E-08
CTD-2033D15.1	-1.500321745	0.026432252
GDPD3	-1.50011567	0.005445737
UHRF1BP1	-1.499366112	1.29E-08
STRIP2	-1.498181069	0.002095304
KLHL29	-1.49683536	0.0000136
DENND2A	-1.493973043	0.000000295
PELI2	-1.491003595	3.37E-08
EME1	-1.490200542	0.004004551
ANKRD34A	-1.489963569	0.001567841
B4GALT6	-1.489196358	0.000002
NACAD	-1.488933234	0.000000052
WI2-3658N16.1	-1.487581685	0.000469256
HS6ST2	-1.486934847	0.039265471
RP11-863P13.3	-1.486474033	0.037961376
GCNT4	-1.486113463	3.51E-09
KLF12	-1.485180198	0.0000334
ASXL3	-1.484982554	0.042502922
RAB15	-1.48420716	0.0000291
TNFRSF4	-1.482660614	0.023299639
GNB3	-1.478152688	0.000556614
MEST	-1.478132602	1.67E-10
USP32P3	-1.477547429	0.001497884
TAGLN	-1.476697993	9.79E-16
GRM4	-1.476624635	0.039242738

PHLPP1	-1.472823683	0.0000137
CENPE	-1.471859128	8.45E-08
RP11-125B21.2	-1.469309114	0.041027316
GABRQ	-1.468021248	0.018465657
LINC00622	-1.467128794	0.032413276
RP11-309G3.3	-1.46624281	0.00519144
ICA1L	-1.465032203	0.0000092
FIGNL1	-1.463965944	0.00000692
PLEKHG4B	-1.463618555	0.013027632
UBA7	-1.463494723	0.000000808
APOL2	-1.463335989	0.0000591
FANCB	-1.462948376	0.001861117
DNM3OS	-1.459711421	3.6E-09
ZNF496	-1.4596419	0.000000187
SPRED2	-1.459300317	6.11E-10
SMAGP	-1.458484637	0.004253701
SLC8A1	-1.457421675	0.000806803
KIRREL	-1.455398426	0.000000038
MMS22L	-1.454439087	0.000000986
IKBKE	-1.454407118	0.000000139
KCND1	-1.453802555	0.000585458
RP11-2E11.9	-1.451197904	0.021900292
GOLGA2P5	-1.449698402	0.026338865
MYH9	-1.44952182	5.03E-14
LPPR3	-1.449283547	0.036930063
RIMS1	-1.449156673	0.004452538
SLC4A8	-1.447910891	0.001883194
C1QTNF9B-AS1	-1.44761888	0.000245651
MSH2	-1.446372951	0.00000156
SPDL1	-1.446133877	6.44E-09

HEG1	-1.445109492	3.96E-08
RGS10	-1.442616314	0.000000709
ARHGEF6	-1.441579487	0.000000472
KAZN	-1.440779098	0.0000752
C18orf56	-1.440184479	0.0357386
SLC9A7P1	-1.438320261	0.026467991
HAS2	-1.437163925	0.001614362
BMP4	-1.43679476	0.0020705
CASP12	-1.434917743	0.038100334
LRRC37A4P	-1.434687205	0.010096788
IFIT2	-1.433534172	0.001930176
CKAP2L	-1.432096109	0.00108021
TNC	-1.431099019	0.005179574
THBS2	-1.430939208	0.000846517
DGKI	-1.429954503	0.00000151
SLC23A3	-1.429947864	0.011215685
CTGF	-1.428736105	0.0000218
ARHGAP18	-1.428434511	0.000000153
PDCD1LG2	-1.42840129	0.0000194
NR2F1	-1.427948689	2.07E-10
LOXL2	-1.425555377	4.31E-15
RP11-395P17.3	-1.425157991	0.001939848
FABP3	-1.423115615	0.001106293
AF001548.5	-1.422515756	0.003754984
TACC3	-1.421840234	0.00001
ICOSLG	-1.421497291	0.004166209
CMKLR1	-1.421460554	0.037647857
TENM3	-1.420721855	0.000000552
MIR4442	-1.420698902	0.030211827
MAP3K14	-1.420159166	0.000328164
GSDMB	-1.419359195	0.0000061
TMEM144	-1.418295588	0.00047431

ABCB4	-1.418088052	0.029839818
RFX2	-1.41724588	0.0000607
ZNF300	-1.416859975	0.0000289
KRT15	-1.416079386	0.019112937
RUNX1	-1.415714938	1.72E-08
CECR2	-1.415476101	0.038795867
RP11-474B16.1	-1.415295468	0.026658804
PHC1	-1.414574124	1.58E-08
SLFN13	-1.410978498	0.00365457
TCEA3	-1.410908569	0.00117969
IL18BP	-1.41076464	0.000893833
PABPC1L	-1.408430963	0.000000276
MTL5	-1.408308299	0.041261491
MCF2L2	-1.404201856	0.007681263
PPFIBP2	-1.403062534	0.000966173
RP5-1043L13.1	-1.402221832	0.002468038
ST8SIA1	-1.401944478	0.00379539
DACH1	-1.401449425	0.003641002
PDLIM7	-1.400273022	0.00000007
LINC01116	-1.398624739	0.004634583
RP11-134G8.8	-1.398412559	0.00946113
C9orf47	-1.39788861	0.00175172
TRANK1	-1.396248833	0.00000262
ARHGAP26	-1.39601779	0.005866679
UGCG	-1.395370101	0.000151035
AC144831.1	-1.391720847	0.032485191
ORC1	-1.391151079	0.005251692
SLC27A6	-1.389706612	0.025406767
WARS	-1.3890727	1.79E-08

RP11-999E24.3	-1.388110775	0.006519942
AMH	-1.387829199	0.035640527
CACNA1H	-1.387353784	0.00000485
CEBPG	-1.385313748	0.0000341
NEU3	-1.385192963	0.002907857
WHSC1	-1.383451572	2.84E-12
AC093642.5	-1.383274301	0.0324671
PFKP	-1.382357607	0.000132586
NBPF11	-1.382007525	0.045654275
AIF1L	-1.381769163	0.000000379
SIX4	-1.381323772	0.00000063
KRT18	-1.380679015	0.005576733
CCNF	-1.378582938	0.0000113
GPR124	-1.377223148	0.000190463
CCND1	-1.37716183	6.45E-08
FAM13A-AS1	-1.376423268	0.006727188
RP11-748H22.1	-1.37609713	0.045883769
FAM169A	-1.374336434	0.000483395
RP11-696N14.1	-1.37424795	0.0000449
IER5	-1.372717668	0.000275909
KLF5	-1.372644618	0.000193684
MAP6D1	-1.372566507	0.003773796
HMGB3	-1.372565209	0.000670635
NEXN	-1.37244988	0.000210982
BCL7A	-1.371382297	0.003200792
RP1-152L7.5	-1.369927388	0.00000747
SPRY2	-1.368542649	8.61E-08
EGR3	-1.367644087	0.003896868
DEPDC1B	-1.367602077	0.020088487
INCA1	-1.365761935	0.008794831

KLRAP1	-1.363849765	0.003203857
ACVR2B-AS1	-1.362625786	0.028123354
FOXF1	-1.361150196	0.012797529
WDR76	-1.360826551	0.00000107
CCDC85C	-1.360488229	0.001147627
C19orf57	-1.358467595	0.03643936
RP11-686D22.7	-1.357858612	0.000137443
ANKRD53	-1.35718578	0.037592942
ATXN7L2	-1.357013386	0.0000316
HIC1	-1.356934547	0.00000133
C5	-1.356634098	0.001018251
MYBL1	-1.354916666	0.0000453
ST7-AS1	-1.354765876	0.008404221
RPLP0P2	-1.354762699	0.045941518
TIMELESS	-1.354621517	2.26E-08
RARB	-1.354122753	0.000812739
BDNF	-1.353318959	0.027321426
AC005943.5	-1.352821697	0.001470724
RPL29P19	-1.351839076	0.023303643
CNNM1	-1.351611465	0.000319195
IFFO2	-1.350890869	0.0000019
RP11-259N19.1	-1.350836638	0.03810824
CYFIP2	-1.35040911	0.001206655
ZNF286B	-1.350212494	0.00726741
PRIM1	-1.350204058	0.003679031
AC092835.2	-1.350146741	0.044676665
LINC00672	-1.349764696	0.002540465
RP1-257A7.4	-1.347023943	0.03668313
KIAA1211	-1.346071862	8.38E-08
STK33	-1.343589083	0.003483176
FANCD2	-1.343104279	0.0000463

BFSP1	-1.342897594	0.003460643
LYPD1	-1.342252746	0.041775836
USP49	-1.341580539	0.0000168
HECW2	-1.341348177	0.000175352
CADPS2	-1.340707699	0.0000705
ZNF827	-1.340037943	0.000000105
FAM71F2	-1.339806201	0.045628603
MACF1	-1.339753711	6.76E-09
TMEM71	-1.338834002	0.034175419
FAM65B	-1.336256072	0.000000145
SPRY1	-1.33584203	0.0000138
SMO	-1.333723159	0.00000352
CKAP2	-1.332369307	1.27E-09
ISYNA1	-1.332040107	0.000258123
PITX1	-1.331338935	0.007692095
RP11-1008C21.2	-1.330357666	0.014045892
TET3	-1.329941703	6.18E-09
CCDC64	-1.329586714	0.013825691
FOXN3	-1.327862597	0.000000346
CHML	-1.324585194	0.000246822
SCN2A	-1.324165815	0.017296074
TET1	-1.322807534	0.000427172
RIMS3	-1.322523985	0.00361921
ZNF608	-1.321452426	0.000736313
KIAA1432	-1.319601877	5.84E-11
ZCCHC18	-1.318769341	0.030482525
SGMS2	-1.317147487	0.000000204
HHAT	-1.314926443	0.000603718
APOBEC3G	-1.314633808	0.0000449
NTRK3	-1.314235669	0.008806112
GAB1	-1.313106911	0.000000884
DDC8	-1.312874091	0.01960377

RGS5	-1.311276071	0.039685962
VAT1L	-1.310036148	0.000873878
LRRC61	-1.309825088	0.018511246
BNC2	-1.309372636	0.00000004
EPHA2	-1.308849479	0.001233901
GBP5	-1.308549383	0.024648043
CADM1	-1.307999772	0.00000787
PMEL	-1.307930346	0.023560355
RP1-151F17.2	-1.307181309	0.003705242
MMP16	-1.30675356	0.000000776
ASGR1	-1.305923369	0.046656859
SALL2	-1.301874564	0.000097
MAST4	-1.300613225	0.0000123
BZRAP1	-1.299439401	0.000172928
DTX4	-1.29941053	4.37E-09
RP11-582J16.5	-1.296898943	0.00165944
RP11-1055B8.7	-1.2955117	6.66E-08
NXNL2	-1.295055803	0.031650643
VPS9D1-AS1	-1.293581345	0.04504517
RASL12	-1.29341841	0.015329661
ICAM1	-1.293004511	0.003339837
RP11-1002K11.1	-1.292929214	0.018167233
CDK18	-1.292276068	0.001210027
KLHL30	-1.289754203	0.034954266
PARP8	-1.288721083	0.000346266
TRIB3	-1.288698562	5.07E-08
AQP1	-1.288168612	0.011936472
BCL9	-1.288133048	0.000000673

JMJD7-PLA2G4B	-1.285279094	0.004440277
GUCY1A2	-1.284711172	0.004677331
NYNRIN	-1.28281794	1.24E-09
MSI1	-1.282314558	0.038941442
ZNF775	-1.282186599	7.49E-09
CCDC150	-1.282052888	0.006883051
ARNT2	-1.282029008	0.001209619
MMP12	-1.281947583	0.014790328
MIR27B	-1.281717895	0.017963223
PAFAH1B3	-1.280966127	0.008133925
ATP1B1	-1.279398008	0.01087965
ASPHD2	-1.279136494	0.004020732
PELI1	-1.27838413	0.000316336
NRG1	-1.278381265	0.022806281
MCM3	-1.275950981	0.000000022
CCDC136	-1.274472965	0.000332754
RP11-20I23.13	-1.272799847	0.002492598
RP11-46C24.7	-1.272744149	0.008852312
ZSWIM5	-1.272448361	0.00000648
IL27RA	-1.272439903	0.000412407
COLQ	-1.272304382	0.001688806
MMP24	-1.271650554	0.013837135
POPDC2	-1.268847442	0.030102315
ITGA6	-1.26742873	0.00000624
CYYR1	-1.267062719	0.008161676
CST4	-1.266736469	0.041667649
RNF125	-1.265724986	0.041162094
BRCA1	-1.265580225	0.000342491
TRO	-1.264666369	0.000000298
KHDC1	-1.264064983	0.004452443

AC005003.1	-1.263231569	0.041498759
HIVEP1	-1.263218425	6.02E-08
ZNF724P	-1.262153826	0.035350892
RUNX1T1	-1.261671785	0.00000433
ARHGAP31	-1.261247783	8.28E-08
DNMBP	-1.260468962	0.000000071
PSIP1	-1.259244255	1.16E-08
CHAF1A	-1.259175501	0.00000789
DSP	-1.258532061	0.01521903
RP11-617F23.1	-1.257323171	0.021249836
COL13A1	-1.257164646	0.001820769
TP53I11	-1.256929021	1.71E-10
SH3BP2	-1.256763985	0.0000303
PRPH2	-1.256359897	0.000208766
ANKRD36B	-1.256006666	0.04171958
BATF3	-1.255831028	0.032629743
PDE8B	-1.255361587	0.0000868
BGN	-1.254766465	0.000000143
ULBP1	-1.254751994	0.000703645
TBKBP1	-1.254476186	0.000362882
EPHA7	-1.254305005	0.007281265
USP13	-1.254159866	0.00000131
PXN	-1.252664994	5.61E-09
RP11-161M6.2	-1.251649977	0.039368971
DCSTAMP	-1.251072992	0.044230629
ACTA2	-1.250267253	9.69E-10
BAIAP2L1	-1.25026024	0.010162158
ASNS	-1.250156095	0.000396643
N4BP2	-1.249501652	0.00000165
TRIO	-1.248223273	9.72E-09
SHMT2	-1.244973596	0.000000256

ZBED6CL	-1.243997819	0.007270446
SMC4	-1.243749591	0.000000059
BCOR	-1.243461553	0.000132493
HSPA12A	-1.243247109	0.000000014
POLD1	-1.241167874	0.0000041
CTD-2619J13.9	-1.240320373	0.026825674
ZNF215	-1.240159927	0.000543632
ZNF852	-1.240128069	0.007244884
SRGAP1	-1.239092114	1.26E-08
ARHGEF2	-1.238822621	0.00000421
GBP1	-1.238549292	0.000000995
CYR61	-1.236688785	0.0000641
RAPGEF3	-1.234718363	0.027599553
USP54	-1.233596006	0.0000159
PKD1P6	-1.232384788	0.002691457
JAG1	-1.231969043	0.002603744
FBXL19-AS1	-1.230754245	0.002392063
ABCG4	-1.230717413	0.049710396
LINC00936	-1.230712171	0.009335723
KIF17	-1.229970623	0.019337875
KLHL5	-1.228753766	0.00000574
PASK	-1.228655189	0.000822771
MAMDC4	-1.227735197	0.001482269
LEPR	-1.227457599	0.0014979
ZNF248	-1.227348411	0.000855433
PCYT1B	-1.226050466	0.001189274
FAM132B	-1.223946207	0.036557682
GEM	-1.223537932	0.002393337
ANKRD36	-1.222302848	0.000997695
PER2	-1.221153884	0.0000723
TRIM6	-1.220915865	0.005346217
ZNF33A	-1.220035558	0.001259881

TIFA	-1.219918591	0.002271154
FAM129A	-1.219714458	0.020853258
SATB1	-1.218988401	0.000000442
RP11-1114A5.4	-1.218117599	0.025719132
PHTF2	-1.217394833	3.6E-09
A2M-AS1	-1.215887657	0.02475154
TNS3	-1.215704937	7.16E-08
SPRY4	-1.214394363	0.000195127
DLC1	-1.214003512	7.79E-09
TNFRSF12A	-1.213588332	0.010382058
MXD3	-1.212415208	0.000118109
TNFRSF10B	-1.212130053	0.0000676
CAMK2N2	-1.212046787	0.034775701
NNAT	-1.211327206	0.020136036
ZWILCH	-1.211298793	0.000000164
ITPRIP	-1.210954843	0.00436897
GNPTAB	-1.208103696	0.0000077
TMED10P2	-1.207201996	0.031449302
TMEM25	-1.207070023	0.003699968
FAM78A	-1.20673162	0.00235961
SVEP1	-1.20609739	0.0000751
HOXD9	-1.205121715	0.000000837
NBPF1	-1.202410191	0.00000575
CTD-3099C6.9	-1.202402345	0.042359789
CDK2	-1.202346531	0.0000232
C3orf67	-1.201197551	0.04394658
MFAP2	-1.200760549	0.007426188
INA	-1.200573942	0.005243267
TRAM2	-1.19988506	0.00000996
ADCY10P1	-1.199523472	0.004912362
SLC7A1	-1.198908375	0.000000023

ALS2CL	-1.198898665	0.000676618
COL27A1	-1.198196469	0.000117795
GRIK2	-1.196124247	0.004661553
FRAS1	-1.196097325	0.007292314
FRY	-1.194695455	8.74E-08
CCDC18	-1.19319172	0.00136731
CHRNA5	-1.192585393	0.035349048
ZNF730	-1.192411318	0.04248736
RBFOX2	-1.19156249	2.92E-08
TMEM158	-1.190050638	0.001028084
RP4-565E6.1	-1.188834088	0.007002391
HMGB2	-1.188083083	0.0000283
TMEM26	-1.187967834	0.001608951
CNN1	-1.187600711	5.46E-08
FEN1	-1.185363088	0.00000222
ARNTL2	-1.184756554	0.0000894
SAMD12	-1.184094847	0.015165964
GSG1	-1.182493827	0.041906944
ASTN2	-1.181508543	0.000187494
KCNT2	-1.181294189	0.026462531
GPT2	-1.181247427	0.0000239
FAM227A	-1.180568971	0.003229582
RP1-228H13.5	-1.18049339	0.000914576
LMO2	-1.179274689	0.046212397
RP11-958N24.1	-1.178708581	0.008778984
FHDC1	-1.176484991	0.004009785
NFIC	-1.176299496	6.68E-10
NAV2	-1.176141023	0.001325734
PIK3CD	-1.17578646	5.25E-08
COL11A2	-1.175487692	0.01278411
CCNJL	-1.175304048	0.000937345

NBPF12	-1.175210868	0.000106911
CAP2	-1.173834003	0.0000795
CACNA1A	-1.172747402	0.019831595
CBX2	-1.172361832	0.001279255
FAM171B	-1.172228479	0.0000892
NEO1	-1.171679324	0.00000324
MEGF6	-1.171088032	0.029066928
TPBG	-1.169710891	0.000046
ACTN4	-1.16933254	7.86E-10
DUSP5	-1.168872929	0.017884078
BARD1	-1.168756381	0.000330992
AC105020.1	-1.168504116	0.011744936
RBPMS2	-1.167331814	0.005624776
RNASEH2A	-1.167312265	0.0000272
CAPRIN2	-1.166670893	0.000340705
RNF207	-1.165624358	0.000101921
LASP1	-1.164899278	4.83E-09
LIMD2	-1.164429599	0.001468516
MIR214	-1.163749117	0.002512846
RUSC2	-1.162448379	0.00013797
SLC7A5	-1.161171942	0.007277869
MURC	-1.160791269	0.042593277
MTURN	-1.160462397	0.002683384
ARHGEF40	-1.160227042	0.00000176
TRIM46	-1.159917132	0.002186828
PAK1	-1.159200941	0.000000215
FSD1	-1.159140883	0.002731373
PLEKHG2	-1.15833448	0.00000155
MET	-1.158082501	0.000904674
TRBC2	-1.157901293	0.02421002
NLGN3	-1.157543335	0.014477848
DDB2	-1.156902967	0.0000628
MCM6	-1.15647677	0.000000765

LAMA4	-1.156117037	0.0000143
RP11-88I18.2	-1.155714697	0.004523915
STK32A	-1.154681504	0.017149707
KCNH2	-1.154462815	0.0000759
LIMD1	-1.151760338	0.00000107
MYO18A	-1.151596884	0.000216553
SLFN11	-1.151305948	0.000201634
DNMT3A	-1.151176722	0.000201881
KCNS3	-1.150539956	0.007992634
GLIPR2	-1.150053564	0.0000431
FAM171A1	-1.149574216	0.000187138
SOX4	-1.149336469	0.004819044
CDK19	-1.149102806	0.000163662
FHL2	-1.147455887	0.0000203
TBC1D30	-1.147334755	0.036874908
CRIM1	-1.14632882	0.000000996
BRD3	-1.146323963	0.000217186
RP4-756G23.5	-1.145620627	0.02899806
AVPR1A	-1.14558315	0.042924433
KDM2B	-1.145391141	0.00000984
EPHB4	-1.145128178	0.0000967
HLA-F-AS1	-1.144806493	0.026798598
CDRT4	-1.144411844	0.029473413
CHTF18	-1.143637249	0.001046377
C2CD3	-1.143618031	0.00000821
PACRG	-1.14268526	0.04806388
DPYSL4	-1.142324224	0.001954333
SOGA2	-1.142110616	0.0005771
MAP3K1	-1.142056498	0.000131048
RP11-566E18.3	-1.139559136	0.0000132
SGOL2	-1.13856315	0.0000673

FCHSD2	-1.136947724	0.00000256
RGS3	-1.136728252	0.000691761
COCH	-1.136336287	0.000210805
DCLRE1B	-1.136326494	0.0000753
TMEM194A	-1.135987087	0.00000132
NDC80	-1.133264214	0.000528023
TSPY26P	-1.132794286	0.00000618
FKBP9L	-1.132598536	0.008770517
FUT8	-1.131481078	0.000000031
MTBP	-1.130793374	0.004034171
VAMP5	-1.130348407	0.001671023
ZFYVE9	-1.130163167	0.000000622
ZNF782	-1.129429792	0.006484064
ZCCHC14	-1.129015541	0.000178437
RGS9	-1.127668401	0.001287474
SLC35F2	-1.1274915	0.009890064
FANCG	-1.127206437	0.00000925
CDC42EP1	-1.126939861	0.0000139
RP11-1212A22.1	-1.12637014	0.014428195
TRAF5	-1.12615709	0.00000122
TCF3	-1.125987962	0.0000207
ITPR3	-1.125381357	0.006595103
PTPRK	-1.124575805	0.00010066
SHROOM4	-1.123698357	0.001523654
RP11-296I10.6	-1.123204973	0.011902392
SLC16A14	-1.12305411	0.024420571
RBL1	-1.120857967	0.000223393
PARD6G	-1.119906733	0.001832317
CCDC30	-1.119838674	0.034166279
BHLHE40	-1.119562055	0.000509249
POLA1	-1.119230156	0.000137117

HECTD2	-1.118400746	0.0000471
NETO1	-1.118370929	0.022795101
FIGN	-1.118048206	0.006588892
NCAM2	-1.117642603	0.013016414
PIEZO2	-1.117292343	0.021631813
LCAT	-1.116548998	0.000165121
TRIM45	-1.115564355	0.000691792
PEAR1	-1.114158279	0.000101171
GDF15	-1.113507891	0.000956236
ZFP36L2	-1.113390402	0.000537559
CCSAP	-1.113342087	0.000315921
ADAM11	-1.113293802	0.018978886
CORO1A	-1.113148222	0.033034266
MIS18BP1	-1.111946643	0.000108432
H19	-1.111927919	0.007002939
CLUHP3	-1.111855306	0.002292928
PYGO1	-1.111729829	0.000104343
PDLIM5	-1.1111692	0.000000174
PLEKHG1	-1.107771827	0.000462877
FBLIM1	-1.107267039	0.0000315
ZNF362	-1.106521037	0.0000242
CYP1A1	-1.105117456	0.036382833
SLCO5A1	-1.104476093	0.003502238
RHBDF2	-1.102277061	0.000221406
PLCG1	-1.100655673	0.00000816
DDX12P	-1.100158962	0.04442761
FARP1	-1.099517358	0.000000308
ANKRD36C	-1.099027922	0.014551052
XPOT	-1.097821686	0.000000468
TRIM47	-1.09671528	0.00122602
LYPD6	-1.095956724	0.013743517
ACTN1	-1.095724246	0.000000221
MPV17L	-1.095403014	0.033015631

OXTR	-1.092966776	0.000253825
TNS1	-1.091593815	0.000104661
RP11-686D22.8	-1.091565644	0.004280014
ZMYM3	-1.09134313	0.000000266
ZNF280B	-1.090307584	0.006611919
TRPC6	-1.090008016	0.000170223
SOGA1	-1.089100901	0.000000604
FAM131B	-1.088371863	0.001147764
GJC1	-1.086945128	0.0000166
DNHD1	-1.085850664	0.000999064
CDH24	-1.085471588	0.00063774
GDPD5	-1.085316602	0.0000881
UBE2T	-1.083656822	0.00055181
SMAD1	-1.083448681	0.0000419
RP3-510D11.2	-1.083002007	0.030356321
YPEL2	-1.082020462	0.000261445
FAM85A	-1.081126968	0.00416424
GALNT6	-1.079665834	0.02079754
HOXB3	-1.078524862	0.004159137
RCC2	-1.078410247	0.000221127
CIDEB	-1.077703057	0.010893043
KIF22	-1.077530502	0.0000321
AL591479.1	-1.077245961	0.047467226
PRDM5	-1.077062464	0.000444282
PURG	-1.076499021	0.019667026
SPOCD1	-1.07615664	0.000865401
ARVCF	-1.076021018	0.008718021
PPP1R13L	-1.073884195	0.00056412
ZNF792	-1.07346174	0.009850432
NFIA	-1.073217031	0.000927542
C2orf27A	-1.072596429	0.015164259

SYNE2	-1.071817445	0.004954913
C1orf112	-1.071608884	0.000521399
POLE	-1.071491013	0.0000252
RP11-686D22.4	-1.071088793	0.022300192
MARS	-1.070559287	0.0000106
PATZ1	-1.070350184	0.00022409
LAMA5	-1.068415884	0.00000763
CTD-2303H24.2	-1.06825393	0.023749188
ADSSL1	-1.068134386	0.017556951
SH3RF1	-1.067707252	0.003837991
CNN2	-1.067168107	0.000021
XRCC3	-1.067148837	0.007830883
LRRC8B	-1.066998618	0.026574184
LMNB2	-1.066982083	0.00000131
NCAPD2	-1.06564098	0.0000175
FZD6	-1.064960017	0.006317521
ZNF70	-1.064625932	0.002823639
ZNF445	-1.063563221	0.000000843
PTRF	-1.062217321	0.000000208
RP11-91J19.4	-1.061550638	0.001343376
LMCD1	-1.060824527	0.010656084
SAMD14	-1.060594928	0.000277312
CNIH3	-1.059999208	0.00161139
SPIN4	-1.059910487	0.001089481
HSPA12B	-1.059907076	0.046093692
KLF11	-1.059002361	0.003192926
PSMC3IP	-1.058918079	0.000876837
PHLDA3	-1.05884121	0.014958181
C21orf91	-1.058435687	0.0000126
EPHA5	-1.058120727	0.049076699

MAP4K5	-1.057689861	0.000685563
PYCARD	-1.057394783	0.008368763
NLRP1	-1.057087943	0.004626271
PAXIP1-AS2	-1.056366963	0.020182769
AMER1	-1.056357344	0.003338261
DPY19L2P2	-1.056285919	0.043705353
KIF9-AS1	-1.056015301	0.002864436
ANO4	-1.054962156	0.043909459
SLC38A1	-1.054542409	0.0000221
NEFM	-1.054399395	0.010933198
PLGLA	-1.054238932	0.031392285
PCNA	-1.053805502	0.0000641
FLNA	-1.052600437	0.000018
AC159540.1	-1.05248918	0.000946731
EHD3	-1.052361776	0.00000519
ZMAT3	-1.051328292	0.000659477
DBN1	-1.051250456	0.006786884
ANKRD13A	-1.049319429	0.0000119
TMSB15B	-1.048266108	0.017438993
KIAA1324L	-1.045780736	0.005726442
CYTH3	-1.042887749	0.0000029
NFKBIE	-1.042709036	0.000465455
ZNF714	-1.042557684	0.00097083
FN1	-1.042443407	0.00000465
SWAP70	-1.042209844	0.000218875
PTPRJ	-1.04088043	0.002124488
C1QTNF2	-1.040029004	0.029836025
NPTXR	-1.039890396	0.0000183
TMEM237	-1.039523543	0.0000502
CARS	-1.038009484	0.00000751
ZNF217	-1.037858153	0.000123553
ABCC4	-1.037046174	0.00000132
MKL2	-1.036164386	0.000590451

CENPI	-1.035135797	0.002979761
RP11-383J24.6	-1.033508827	0.022425999
SPECC1	-1.032669097	0.002102084
RMI1	-1.032629472	0.000789099
TCEAL7	-1.030782692	0.001443588
ORC2	-1.029965812	0.000621963
AFAP1L1	-1.029704346	0.001150282
PKD1P5	-1.028832348	0.014916348
HCP5	-1.028130342	0.004647442
PAMR1	-1.027187906	0.003150013
AC125232.1	-1.025722079	0.019999514
FGD1	-1.02545259	0.00000238
SASS6	-1.024865472	0.003211091
NF1	-1.024856454	0.00000063
INCENP	-1.023891448	0.0000346
NANOS1	-1.023429121	0.018366556
KMT2A	-1.023277883	0.00000403
ERF	-1.02158642	0.00000674
B3GALTL	-1.021576433	0.001747701
PMEPA1	-1.021213655	0.033085669
KMT2E	-1.020986328	0.000162622
PIWIL4	-1.019412275	0.023999684
EHMT2	-1.019251802	0.0000293
CDKN1A	-1.018002509	0.001996708
PARD3	-1.017132589	0.002210396
LDB2	-1.01570263	0.000293129
GOLGA6L20	-1.015062286	0.01785534
CDKL1	-1.014635336	0.004629265
RP11-698N11.4	-1.014210345	0.03245145
PCDHGC3	-1.014021254	0.013081356
GLI3	-1.013396565	0.00000598

SLC20A2	-1.012381853	0.002983501
NR2F1-AS1	-1.011226759	0.0000174
TMEM200A	-1.010061958	0.000609005
ATXN7L1	-1.008790677	0.00018566
ANKRD50	-1.008685596	0.000104994
CNTRL	-1.008494808	0.001884598
EXT1	-1.008457345	0.000000223
TCF4	-1.00806519	0.00000344
SV2A	-1.007973786	0.0000065
AEBP1	-1.007722692	0.0000203
EXTL1	-1.007362086	0.021566498
C10orf12	-1.00600794	0.015777561
TFAP4	-1.005799915	0.006620903
SLC22A15	-1.005227405	0.012762106
DTWD2	-1.003067569	0.001348091
ERCC2	-1.00148498	0.0000251
ZNF436	-1.000559927	0.000662032
SPEF2	-1.000452891	0.038311373

Appendix 5. Up-regulated genes upon A83-01 treatment: Log2-fold change ≥ 1

Gene Symbol	log2-fold change	*q*
DMKN	4.523963536	8.27978E-28
DPP6	4.447884761	1.34849E-19
CPVL	4.250279449	4.08576E-18
STAR	3.999001852	7.5428E-28
WDR86-AS1	3.988012684	6.38718E-13
INSC	3.972614236	8.65087E-14
THBD	3.897921319	6.06721E-14
NPR1	3.863393913	1.1083E-22
PLA2G7	3.83005198	1.16967E-22
CEACAM1	3.641867474	2.00749E-12
GDF7	3.614411536	3.05962E-18
CDK18	3.60803325	1.2436E-25
WNK2	3.506100657	1.04066E-13
KDR	3.494189986	3.48995E-11
PDE3B	3.456980678	7.73737E-21
RRAGD	3.346332525	4.66204E-15
WDR86	3.33783044	2.72936E-09
STAC	3.32618256	5.3289E-16
SCARA5	3.265194702	2.71209E-07
NR0B1	3.254839379	1.25831E-08
RARB	3.254517463	1.05697E-33
EPB41L3	3.24712539	8.10396E-08
SNX10	3.234557287	1.66061E-18
ASPA	3.206758651	4.74258E-21
WISP2	3.203273617	1.35691E-11
NFIB	3.188784186	1.2835E-14
PTGES	3.175727149	5.01326E-18
SLC25A18	3.166413619	1.13659E-23
TLR3	3.126577806	1.616E-20
AC012065.7	3.110767063	9.18381E-10
SPTLC3	3.105330742	1.21654E-10
AK4	3.067240747	3.21233E-16
COLEC12	3.050666458	5.93249E-17
RARRES1	3.034939537	1.27095E-08
IRAK3	3.024529749	1.58869E-15
ADORA2B	2.991345949	1.12806E-13
TMEM132D	2.985047005	5.61955E-06

MFI2	2.97843671	1.07552E-22
SUSD3	2.973538383	1.36158E-11
HEYL	2.965177293	2.2063E-10
DOCK8	2.939295355	4.26296E-10
IL18R1	2.897917158	1.14773E-05
BIRC7	2.859490391	3.05314E-05
CARD11	2.84867975	4.68215E-09
TNFRSF1B	2.834311013	1.09547E-11
ENPP2	2.806957931	5.55734E-14
LCP1	2.781189271	1.51376E-06
CYP1B1	2.772837679	6.77781E-10
KIAA1199	2.767241795	1.41034E-08
COL4A3	2.753078616	5.95851E-05
EMILIN2	2.747028523	9.09765E-17
SHANK2	2.745602509	2.12864E-05
RP11-676J15.1	2.727317276	5.52855E-05
FCGR2A	2.726253335	1.27801E-08
SLC6A12	2.709309964	3.83362E-05
MALL	2.702227732	4.54745E-14
EYA4	2.701854815	1.92203E-07
PCBP3	2.690009113	2.49393E-13
A2M	2.685826988	4.58496E-10
IGFBP2	2.682062571	4.16842E-21
FGF12	2.66710222	1.30051E-05
ANXA9	2.662632645	3.19569E-08
CLUL1	2.646851668	0.000143838
PCDH15	2.6378804	0.000146101
EPB41L4A	2.626440236	9.83805E-07
GPM6B	2.612022103	8.16355E-09
HPSE	2.605262634	3.66991E-09
HAP1	2.600477197	2.27683E-16
JAG1	2.599824365	6.096E-13
WWC1	2.589294338	2.2207E-05
BEAN1	2.58898313	6.74382E-08
PKDCC	2.586019047	3.90644E-09
SLC29A2	2.581876316	6.18842E-08
ITGAX	2.566678816	2.60427E-05
CD1D	2.565439561	5.83812E-05
NKX3-1	2.563516505	3.90031E-07
GALNT14	2.562490981	5.90425E-05
FAM134B	2.560937864	3.56057E-10
PHYHIP	2.543511954	5.18379E-13
MOB3B	2.520525723	2.07946E-08
TMEM132B	2.51333156	4.03316E-10

HS3ST1	2.504067064	0.000430696
NUP210	2.496907546	4.98953E-05
SEC14L6	2.495839368	2.98825E-06
IGSF10	2.493264337	6.50805E-15
C12orf68	2.491911348	2.07946E-08
CRISPLD2	2.486811635	4.2032E-16
GALNT12	2.479525817	4.00894E-09
WNK4	2.478640235	1.06225E-15
SLIT2	2.473951358	7.35122E-15
IRX6	2.469015342	0.00040394
GPRIN3	2.468411206	2.51111E-09
FAM53B-AS1	2.461353726	0.000700851
GRB7	2.456059026	1.15263E-06
CA12	2.453152357	4.21463E-05
ALDH1L1	2.452772946	3.65219E-07
OVCH1	2.442647096	2.84701E-05
FOXQ1	2.43845721	0.000213923
ALDH1A1	2.436511865	6.06834E-07
RASD1	2.430125164	3.52987E-07
TGFBR3	2.430091326	1.23317E-22
ST6GALNAC2	2.428743255	1.46198E-12
TMTC1	2.426034584	5.84608E-13
LPAR3	2.420949228	2.67461E-05
RAB37	2.418521654	0.000304863
EFEMP1	2.414959522	0.000125276
SPARCL1	2.411961701	0.000188828
SNAP25	2.402941015	2.22317E-06
FAM49A	2.397166601	1.00266E-07
EVA1C	2.394314513	5.06751E-11
KCNS2	2.393600715	2.28935E-05
CLIC6	2.392098494	2.0434E-08
SLC47A1	2.387770364	1.11859E-07
PPP2R2B	2.387676432	0.000411282
STX11	2.374666889	5.4405E-05
LCN1	2.361756013	0.001356513
VNN2	2.357695437	0.001097313
TNK1	2.355294234	1.83822E-05
ACSL5	2.347195501	2.04579E-18
PTGS2	2.345045543	0.000358164
MTSS1	2.345028166	0.000229975
PRUNE2	2.338687402	2.63245E-07
GSTA3	2.338421156	0.0003586
CSF1	2.32912662	8.26615E-21
LINC00173	2.324517303	0.001089943
PTPRH	2.323339268	7.69833E-13

BAALC	2.314032091	1.73447E-07
HSD11B1	2.299083588	0.000420319
TACSTD2	2.292031066	6.06834E-07
WBSCR27	2.290034976	2.11262E-08
KRT19	2.289988397	9.44957E-08
IL1R1	2.286786853	1.55004E-18
MBP	2.281683096	9.11926E-13
PRRG4	2.280315786	6.06834E-07
CEBPD	2.279009202	2.65443E-13
CHRNA7	2.2722242	0.001131056
ITGA8	2.265306779	7.06923E-06
KCP	2.263149919	1.4024E-06
SEMA3E	2.257695697	0.000327788
KLHL13	2.250326334	3.61727E-07
BZRAP1	2.247542371	7.96642E-13
SYT7	2.245343485	1.83595E-05
FAM131C	2.239988227	0.000970877
C2	2.239522183	1.40224E-06
IGSF9B	2.237634849	0.00296644
IL22RA1	2.22014095	0.003286968
TMEM179	2.218808786	0.001967934
RASL11A	2.218642102	1.52336E-06
SIGLEC9	2.217268398	0.000204675
WT1	2.205052539	4.94047E-16
AC003092.1	2.197358563	0.000229894
SOD3	2.195734142	1.07211E-08
AC114730.2	2.194370162	0.00353063
HAAO	2.192090932	2.82808E-06
MGAT3	2.191976493	2.40669E-08
DDO	2.19159744	2.17449E-05
GAS7	2.189862499	6.28562E-18
RXFP1	2.173700497	1.95337E-13
ADIRF	2.167450623	0.000125276
CCDC64	2.165715653	0.002803297
ENPEP	2.161418536	4.02974E-11
SLCO2A1	2.149658578	0.003995374
VWA1	2.148738069	2.7777E-14
LLGL2	2.143426419	3.18206E-05
IGFBP6	2.141735288	3.52079E-11
CX3CL1	2.135027985	7.06923E-06
EPHX2	2.130591807	2.60273E-05
C10orf10	2.130463137	3.59575E-15
FMNL1	2.128784066	4.84454E-07
SLC27A2	2.126684912	0.003752742

RP11-359E10.1	2.122916908	0.000301592
TTC39A	2.116888593	1.41735E-05
CELF2	2.116112463	9.24492E-07
RHBDL3	2.114921136	0.00109169
CCRL2	2.111913494	0.001371502
TNXB	2.110264254	9.77476E-06
RP11-720L2.3	2.110186858	0.003408966
KCNMA1	2.10729627	1.39426E-09
TMCC3	2.101051662	0.000261671
CD68	2.097302317	0.000398317
GGT5	2.093313077	2.16403E-06
KIAA1644	2.090563642	0.000317106
BHLHE41	2.076202399	3.8026E-06
PCSK1	2.075156712	0.005072554
RASGRP2	2.060568562	1.09781E-08
NR4A2	2.059908396	4.42847E-06
TNFSF10	2.055611403	0.000430696
CNGA1	2.047774018	0.000726675
ADRA2C	2.039742228	7.11175E-06
PPARGC1A	2.039072568	4.18599E-07
CD40	2.03335826	0.000825255
AQP3	2.032532679	2.34409E-05
NEFM	2.023641263	2.4806E-06
RAI2	2.021674816	0.001985238
ST8SIA4	2.013057439	0.001922268
FAM81A	2.009167347	8.94335E-05
CD22	2.007740113	0.002567913
CCL26	1.990041559	0.004564531
SFRP1	1.9883606	0.000453217
MTUS2	1.988131651	0.004882914
BCAM	1.987940233	2.91416E-07
RBM11	1.985564415	0.010870819
RIPPLY3	1.98266121	0.00470003
SIGLEC17P	1.982431716	0.005998417
LIFR	1.979845235	2.01342E-10
STK32B	1.974266625	1.91354E-05
GPR126	1.973104203	2.60436E-09
RAB27B	1.971163404	0.001460373
SCN5A	1.968503563	2.1737E-06
FGD5	1.96654739	0.01260517
RP11-445H22.4	1.964153348	0.006115711
KCNK15	1.96241556	0.002204983
ANK1	1.958808226	1.97632E-05
KIAA1671	1.957076721	6.90508E-10

AIM1	1.95604009	5.60674E-08
LPPR5	1.954591765	0.01402222
ARHGAP20	1.954432836	2.82808E-06
SORL1	1.953170741	4.04745E-06
COL4A4	1.952375834	0.00333102
AC073621.2	1.947334368	0.009692452
FYB	1.945720617	0.01468672
FAIM2	1.944773608	3.97606E-06
IL15RA	1.942579999	4.50291E-05
CLCN1	1.941902813	0.010441548
DDIT4L	1.93980802	5.93878E-08
LINC00341	1.931266954	6.32514E-07
PBX4	1.928398759	0.001506052
CRYGN	1.924223059	0.013040332
PPP1R14A	1.919632954	2.91201E-06
CSF3R	1.91938153	0.007025045
FAM162B	1.917912872	0.000303997
FAM65B	1.916883734	0.000144225
CTD-2135D7.5	1.913329928	0.015543126
CAMK1G	1.910271099	1.26221E-09
CTD-2020K17.1	1.909588466	2.79705E-06
TMEM150C	1.899790525	4.70718E-05
CLDN23	1.897888265	6.69316E-05
RBP7	1.896386936	0.012293622
SOD2	1.896275782	3.84895E-13
GPR133	1.883512898	0.000873841
PRDM6	1.876969623	6.22772E-05
PRRX2	1.87332607	9.11352E-05
SDK1	1.868196907	1.27369E-09
WT1-AS	1.859541701	7.62226E-05
HTRA3	1.857444656	1.74216E-05
CLMN	1.855458502	0.021223295
KRT18	1.84966319	6.84516E-10
NETO1	1.849658017	0.003031901
KB-1517D11.4	1.845777402	0.010663211
L1CAM	1.840736089	8.86643E-07
RP11-752D24.2	1.840493452	0.01611129
CHRD	1.840030848	1.53076E-08
C1orf21	1.839820231	1.55285E-05
RARRES3	1.837329367	0.000231354
ANKRD33	1.835770256	0.015456307
CYP26B1	1.835511141	0.002356232
TNFRSF21	1.834795607	1.25831E-08

RP11-598F7.5	1.833651375	0.025151608
C1orf226	1.826696728	0.00109169
KRT36	1.823564063	0.026798346
GIPC3	1.820024903	2.18119E-05
FAM89A	1.818275949	2.50964E-06
FAM149A	1.816691743	1.1658E-06
AQP8	1.813109165	0.000205496
AGPAT9	1.805893901	0.000432837
TSHZ2	1.805310743	0.00109169
NKAIN3	1.801582145	0.025936388
HOXB-AS3	1.799948725	5.17495E-06
PLEKHG1	1.793390244	1.26686E-11
PZP	1.782568147	0.03082676
STEAP4	1.781518692	0.032899001
RUNX3	1.777179975	0.033530971
GUCY1A3	1.776166189	0.000265919
IL1RL1	1.769501192	0.021118209
DLL4	1.768041165	0.001883777
LZTS1	1.764682053	0.015221302
ACVRL1	1.764650886	3.21036E-06
AC141928.1	1.762500738	1.01773E-07
IL6R	1.761348952	1.65336E-06
AOX1	1.757923896	0.001478439
TRPC3	1.751912591	0.000202698
ZC3H12D	1.751761725	0.004257433
ASS1	1.748304032	2.09204E-07
TRIM54	1.748233372	0.035384371
RGL3	1.746918249	6.90517E-05
SNCA	1.744003674	5.6389E-05
ADAMTSL4	1.739635622	0.000357704
ANKRD30A	1.737203339	0.04047545
TMEM54	1.733808631	2.05321E-06
ANKRD6	1.733063398	4.95358E-06
RP4-647C14.2	1.73215444	0.001151843
TNFSF13B	1.729353708	0.000899094
NDNF	1.729300438	0.009254167
LINC00944	1.728920623	0.03332757
APOC1	1.726457981	0.00561843
LAG3	1.722711494	1.6558E-05
MTL5	1.722319621	0.00308804
GUCY1B3	1.721334515	7.62226E-05
VWA7	1.716909972	0.004393848
FAM124A	1.714595229	1.0725E-05
LY75	1.711691279	0.032146864
EYA1	1.709760525	0.001624348

AGT	1.708283288	0.00586709
APOBEC3H	1.707550314	0.041563844
HCAR1	1.702847111	3.93872E-05
FGF13	1.70217859	0.008135816
ANKRD29	1.701871102	0.006739214
LXN	1.697707304	2.39674E-05
AL512428.1	1.69738468	0.035912336
ZNF536	1.695833179	0.047067663
SNCG	1.694735372	0.016040854
LINC01140	1.693137092	0.01917327
RP11-151D14.1	1.692546093	0.042028167
WNT2B	1.692447913	0.005746005
CELSR1	1.688147127	1.19057E-06
LAPTM5	1.686789244	0.044921489
KIAA0040	1.68605153	0.025251802
LINGO2	1.685412258	0.000538878
KCND3	1.68306562	0.028276098
GMFG	1.680649595	0.014080865
RP11-173M11.2	1.680326244	0.025251802
GS1-72M22.1	1.679163915	0.006279484
OAF	1.674403747	2.47584E-09
CRABP2	1.669425218	0.00693407
GPR150	1.665151428	0.012051353
CGN	1.664064218	0.029499099
RP11-432J24.5	1.660024916	0.044071243
ADH1C	1.659787099	0.006225331
APOL1	1.658247568	2.43688E-06
PSG4	1.657846522	0.003296631
SCIN	1.655170655	0.036084131
GRIN2A	1.654360276	0.024309705
MAN1C1	1.654323616	0.000234311
TRIM29	1.653541594	0.042028167
OSR2	1.653345632	9.77476E-06
RAC2	1.653345399	6.92963E-06
LAMA3	1.651664455	0.003226389
ABCC3	1.650547965	0.003138053
CD14	1.64814649	0.016257208
BRINP1	1.648118019	0.015375891
TM4SF1	1.646736937	0.011232018
RP11-713C5.1	1.646262938	0.017609351
PARM1	1.645774083	0.005721504
LAMB3	1.642943186	0.0109364
TMEM255B	1.64060797	0.015491297

GPRC5C	1.640099608	0.001093143
NOV	1.639269298	3.33823E-05
EBF3	1.636274319	0.003076395
CMKLR1	1.634792833	0.035389921
PLA2G4A	1.626903412	0.000800598
CFD	1.625732726	0.028343057
MAP3K5	1.619323813	1.10872E-09
NR4A3	1.61795794	0.042991452
MYL3	1.613585655	0.006644119
ADH1B	1.61186906	0.027826811
SYNPO	1.610739375	1.59543E-05
SH3GL2	1.609013909	0.006078516
IL2RB	1.597459461	0.000661427
CCBE1	1.595626984	0.009869886
ADRA2A	1.59513277	0.016211049
RP4-555D20.2	1.592825663	0.044540924
ADRA1D	1.585888458	0.001430055
KCNC4	1.584437737	0.002693654
ANKEF1	1.582988106	0.006271271
PRSS21	1.582238863	0.000165226
UNC13D	1.578590633	0.000166431
ABCC6P2	1.577734092	0.041605335
ASPHD1	1.576820627	0.006644119
ERVMER34-1	1.576663805	0.006111317
NIPAL1	1.574220669	0.007420398
MBNL3	1.573338718	1.41432E-05
IGJ	1.572530241	0.041950636
NYAP1	1.57093959	0.003840841
PTER	1.570038425	0.000393474
TPD52	1.564382943	0.002227432
AK7	1.560029048	0.014740148
ZNF204P	1.559283703	0.049542875
ADAP2	1.555993019	0.012299707
NAV2	1.553840141	0.000914577
PTPRU	1.551596041	0.00437233
RP11-549B18.1	1.550805053	0.007004965
B4GALT6	1.550671888	3.76252E-05
PYGM	1.54689077	0.002527125
MAMDC2	1.542290814	0.007347731
RNF125	1.538223848	0.003212115
TMEM100	1.536019281	0.048801662
CFB	1.535984209	0.032906323
SPIRE2	1.534775469	1.73447E-07
TIMP4	1.534583902	0.019821074

GRTP1	1.529418482	0.001655179
SDC4	1.529115886	1.34414E-05
RP11-49I11.1	1.528205636	0.002117165
DHRS13	1.527301594	8.41752E-05
AC005481.5	1.526944868	0.038938096
LINC00939	1.525755982	0.021167122
TWIST1	1.523062967	6.06834E-07
PDE10A	1.519513962	0.005683109
PTH1R	1.519333506	0.008339494
SBSN	1.513657833	0.047067663
ACE	1.512927923	4.08035E-05
HSPB6	1.507190644	7.9336E-09
BATF2	1.502972086	3.43693E-05
LIMCH1	1.502886463	0.001486947
CHST1	1.502046824	0.02172337
PLXND1	1.501729376	8.06006E-09
DAPK2	1.501296834	1.54492E-05
HYAL1	1.499989246	0.001412677
NOS3	1.493074484	0.009657902
SYNE3	1.491809312	0.000917734
RCSD1	1.485676051	0.039891499
TINAGL1	1.485465059	0.033495137
APOL3	1.48333261	1.25077E-06
C11orf96	1.476891495	0.00599711
NPR3	1.47445021	0.030609329
IL33	1.474274344	5.4405E-05
CAMK2A	1.47084691	0.040949429
BACH2	1.47036775	0.003408966
NRG1	1.467271357	0.002083118
RTN4R	1.461587321	0.014050753
PTX3	1.460529681	8.94335E-05
NR4A1	1.458169973	0.001726673
CLDN7	1.457785205	0.000777721
EGFLAM	1.457025475	0.027320913
SCN1B	1.454941628	0.001001161
S100A3	1.453367855	0.005651751
MRGPRF	1.451845167	0.001600468
SUSD2	1.451695217	2.71674E-05
PSG2	1.443829899	0.007602201
COL4A6	1.44380629	0.000937182
CDCP1	1.440790459	0.009925089
IL20RA	1.440441521	0.007121537
KCNQ3	1.439756561	0.018525025
MCOLN2	1.437923395	0.003225921
METRN	1.437009089	2.34409E-05

RFX8	1.436750574	0.014652461
HLA-F	1.436053771	1.07393E-05
NDRG1	1.435817461	6.66947E-06
PRKAA2	1.431110912	0.003650729
NOD1	1.429575348	5.6389E-05
RP11-554A11.4	1.42909879	0.00109169
BAIAP2	1.429078737	9.29958E-07
TFAP2C	1.428792702	1.18899E-05
DUSP5	1.427846146	0.010950435
CDCA7	1.427786342	0.0007725
ALDH3B1	1.425976588	0.000124743
STEAP3	1.418049433	0.004666912
CARD9	1.414073277	7.63135E-06
ITPR3	1.408630292	9.01351E-05
FBLN1	1.408265903	3.25267E-05
TGFB3	1.407106045	0.000825285
PTPRN2	1.405428247	0.002747605
DKK1	1.404919246	0.012761395
TMC6	1.397746214	0.002986748
IL17RE	1.396969013	0.029357578
CDH13	1.392151414	0.001655179
SYNM	1.391171769	0.001471107
ERBB3	1.385790779	0.047383084
SLC40A1	1.384537885	0.006050549
FCRLB	1.383434547	0.024804674
EMX2OS	1.382595206	0.000762315
OLFM1	1.3819068	0.032196461
CSDC2	1.380703895	0.000229245
CCDC109B	1.380272393	1.18585E-05
MLPH	1.380252655	0.000281469
TGFBR3L	1.372084197	0.044869396
TPPP3	1.37036954	0.000385163
DAAM2	1.370317619	8.84796E-06
PITPNM2	1.370052987	4.6018E-05
MARK1	1.368896386	0.00394273
CKB	1.365744984	0.012088881
RGS16	1.365646483	0.02071941
CHST15	1.36382792	6.7843E-05
TIMP3	1.363798957	4.19014E-05
FAM47E-STBD1	1.361033246	0.032906323
MCOLN3	1.359154944	0.000188828
PODXL	1.352028996	0.032553511
MME	1.351383141	0.016663228
CTSD	1.351377983	7.42898E-05

TRIM7	1.350681127	0.03082676
TJP2	1.349469533	0.001499913
C10orf54	1.347600265	0.001143401
GJD3	1.346549024	0.006160294
SEMA4D	1.344491513	0.001804856
TNIK	1.343289275	0.001572324
BZRAP1-AS1	1.342638446	0.029983115
NANOS1	1.341674036	0.031661553
RPS6KA1	1.340729147	0.006078516
THRB	1.336690973	0.003580244
POU2F3	1.335924891	0.035951111
ELOVL2	1.331747314	0.020730963
DSG2	1.326258114	0.008074757
USP53	1.324271227	0.042613412
TEC	1.320295003	0.042864515
GPX3	1.318845405	0.002384039
PLD1	1.312467124	4.84454E-07
STXBP2	1.310721317	0.000876848
IFITM1	1.308812993	0.003237857
CCDC69	1.308649799	0.001827044
BAIAP3	1.308331353	0.019005565
PLIN2	1.306614061	6.71354E-06
KIAA1456	1.30657947	0.000486965
ARID5A	1.300386354	0.000813092
VAMP5	1.298555392	2.66866E-05
FAM167B	1.295742354	0.005240048
ISG20	1.292668926	0.003092007
EFCAB1	1.285779815	0.032637814
CCDC102B	1.285618971	0.024865899
PEG10	1.283229825	0.009542099
GCK	1.280194206	0.028459154
ALS2CL	1.277219617	0.005679358
PRELP	1.275467478	0.002554584
NEURL1B	1.274111575	0.000633865
RP11-1002K11.1	1.273994642	0.01015546
TENC1	1.271881699	0.001351068
TCEA3	1.271684069	4.19407E-05
FBLN7	1.270609949	0.000140301
C6orf141	1.266773931	0.002060293
NHS	1.258263736	0.006378622
ETV7	1.25819009	0.011905589
HRH1	1.257633362	0.001649238
SLC35G2	1.254994576	0.012059008
FCHO1	1.254257562	0.012761395

ICAM4	1.252307872	0.032005769
GGT1	1.251732276	0.011806992
SH2D4A	1.25051618	0.00125498
PIM3	1.249157991	0.000281705
DBNDD2	1.247155985	0.041804588
LITAF	1.247145832	0.000847011
FOXP2	1.246752195	0.001048841
FXYD5	1.24598431	0.014793522
P2RX4	1.24390261	0.009060811
HHEX	1.24243162	0.024036631
NOTCH1	1.241351473	0.000229975
HLA-DPB1	1.239268154	0.003384651
HMSD	1.236778624	0.040774626
APLP2	1.234153469	0.029511801
RAB3IL1	1.234066073	0.000180262
DPP4	1.232574345	0.021880853
GCNT1	1.230093595	0.014626339
FAM83H	1.228624522	0.030940891
ITGB8	1.227647718	6.44376E-05
NR1H3	1.223999107	0.013648987
TCL6	1.223044046	0.009939553
DIRAS1	1.220036294	0.047068973
ABCA6	1.217429856	0.009647418
MEIS3P2	1.217253701	0.001336329
MOCOS	1.215936801	0.015369103
RADIL	1.215884982	0.00696336
SCARA3	1.214674204	0.004093897
PSG5	1.213017996	0.033946007
FLT1	1.2130058	0.038627879
NAMPTL	1.212624022	0.014793522
ABHD17C	1.212385815	0.015277797
BOC	1.206289516	5.17495E-06
SH2D5	1.203824676	0.045697933
HOXB3	1.200178066	0.001881039
GNAL	1.193791036	0.015534194
ADARB1	1.19346543	0.00071735
ACOT4	1.191418345	0.041130536
PSG1	1.189668647	0.037080325
RIN1	1.189415677	0.001336329
TMOD1	1.188562866	0.048712928
LINC00346	1.185953254	0.004856198
OSMR	1.185644885	0.000158044
CEBPB	1.185191119	0.000490638
S100A4	1.18154356	0.035116313
USP44	1.177821879	0.021123504

ZFP36	1.175490795	0.000552164
KRT8	1.175072805	0.002561479
ATCAY	1.173446416	0.046574328
HMGB2	1.172832857	0.003953641
FAM174B	1.170811811	0.018390492
LAMA4	1.170238057	0.007146069
PLA2G16	1.169842557	0.008089805
SMIM10	1.16734237	0.001001481
CLGN	1.165518837	0.006437564
SNED1	1.163689746	0.017609351
MFSD6	1.157255583	0.009132511
TPCN1	1.155667732	0.001777491
AVPI1	1.152689668	0.009060811
ADCY1	1.149872228	0.012663968
EPDR1	1.148877891	0.044675384
MTMR10	1.148295798	0.003408966
EPAS1	1.147139127	0.002526727
FRAS1	1.146654177	0.033168116
THPO	1.14593051	0.041937297
CYGB	1.142345734	0.029983115
KCNIP3	1.140362619	0.032213465
PC	1.132900465	0.001558976
HSPB8	1.131874496	0.029983115
VAT1L	1.130569703	0.009789871
GPRC5A	1.128236542	0.000140947
ALDOC	1.127243299	0.0066582
AFAP1L2	1.124755159	0.000700851
COL18A1	1.119668778	0.000534247
GLUL	1.118551849	0.002150489
ROR2	1.115151721	0.000653496
BDKRB2	1.11124515	0.00014157
TAPSAR1	1.109356942	0.001641384
ADCY4	1.10654184	0.007039999
CORO2B	1.105766585	0.004551005
MAP7	1.103051669	0.03082676
MPV17L	1.10009602	0.040563078
SIGIRR	1.094363208	0.000970877
TOX2	1.086051217	0.018909858
CDC42EP4	1.084500411	0.000273656
HNMT	1.080154102	0.003104592
HLA-DPA1	1.075685283	0.007979228
DUSP1	1.07275888	0.021880853
CHCHD10	1.072486169	0.005046582
DMTN	1.071717369	0.042402279
ADPRH	1.070568468	0.041605335

FLI1	1.066356976	0.005753723
ST6GALNAC6	1.060895452	8.08985E-05
SLC37A1	1.058678612	0.006113425
AGFG2	1.057885166	0.012232955
PCK2	1.056623505	0.030609329
CNTNAP1	1.054960024	0.000315922
ANXA11	1.054392449	8.94028E-05
CTSH	1.053912196	0.008971679
F10	1.053837078	0.000216637
STOM	1.053687356	0.000928467
CCR10	1.052157152	0.014538748
SMAD3	1.050685388	0.014024537
ECHDC3	1.049695467	0.01839861
NFIL3	1.046759285	0.008043276
TBC1D8	1.046047397	0.023201167
KREMEN1	1.045257026	0.033530971
MAP3K8	1.042897362	0.015167486
ECE1	1.037655876	0.009605174
SLC9A3R1	1.037511759	0.002886058
CNKSR3	1.034133864	0.000861636
SFMBT1	1.032669129	0.01084408
CBX7	1.028514082	0.02995244
PLCL2	1.027016713	0.00241592
NAMPT	1.025073603	0.018802824
BCL3	1.021382376	0.010765852
EFNB2	1.020425232	0.002204983
SAV1	1.018245629	0.000586984
CTNNAL1	1.018163363	0.009254167
PLA2R1	1.017670146	0.000243211
ENOSF1	1.013115315	0.000308971
EFNA5	1.011668295	0.008133989
TMCO4	1.008810151	0.002342093
APOE	1.007265735	0.034935787
C16orf45	1.00642347	0.043682696
SECTM1	1.002140968	0.01714322
IL6ST	1.001329341	0.000548785
PLEKHF1	1.000538546	0.017802588

Appendix 6. Down-regulated genes upon A83-01 treatment: Log2-fold change < -1

Gene Symbol	Log2-fold change	q
KCNE4	-1.003149166	0.023400333
CASK	-1.004025572	0.005004505
PTPRD	-1.006076373	0.003879865
APCDD1	-1.007142571	0.030585672
DOCK9	-1.007263856	0.000459728
TGIF2	-1.007503321	0.044798066
THAP2	-1.007929303	0.041605335
KIAA1217	-1.02636513	0.041950636
NNAT	-1.027689615	0.006998066
ZNF804A	-1.03050877	0.00350631
CLCN4	-1.035221971	0.020775617
FHDC1	-1.036443976	0.040638383
PDCD1LG2	-1.037729473	0.039346794
NR2F1-AS1	-1.03927625	0.006102824
EPHA5	-1.04291727	0.001794243
DRP2	-1.043467631	0.041499829
FKBP7	-1.043502863	0.000635843
MMP16	-1.044806272	0.001181136
SH3BGRL2	-1.045457829	0.006748617
ANTXR1	-1.050840211	0.000134035
PDE4B	-1.053041202	0.005679358
COL4A2	-1.0537044	0.013599398
MRAS	-1.056193934	0.000554393
PCDHGA4	-1.056737862	0.012655969
SLC9A7	-1.061226157	0.037812983
LINC00936	-1.067703727	0.002384039

MCAM	-1.07241098	0.039707804
LNX2	-1.072814049	0.004246079
PRDM1	-1.074108008	0.031863329
AGPS	-1.074231581	0.001309704
GOLGA2P7	-1.079265479	0.010740254
CAMK1D	-1.080119378	0.006476974
MAST4	-1.080595166	0.001120906
TMEM132A	-1.084946743	0.007557099
ITGB5	-1.086350007	0.000442129
PTGFR	-1.086879014	0.021073957
OPN3	-1.091174654	0.000265656
CCNJL	-1.092917669	0.009673355
STK38L	-1.096948485	9.07075E-05
ITGA4	-1.098594161	0.010849903
WISP1	-1.101516718	0.005787411
PDGFC	-1.105000744	0.017427635
HUS1	-1.108211886	0.002943876
TLN2	-1.109650392	0.001437035
SPRY2	-1.110911261	0.015816043
F2R	-1.113998498	0.005985014
SSTR1	-1.115747394	0.007261605
SLC41A2	-1.119065717	0.01887024
COL7A1	-1.119540585	0.013738984
DDHD1	-1.124079887	0.0061883
TGFBI	-1.124128147	0.00897028

COL5A2	-1.127308874	0.004459059
MIR29A	-1.129449339	0.001122534
ZNF117	-1.131753719	0.003036148
MMP11	-1.135015314	0.006751631
MEX3B	-1.137225808	0.023213668
LANCL3	-1.137507206	0.019093473
OSBPL10	-1.137865244	0.000495968
SEMA3F	-1.138236678	0.019188062
ITGA1	-1.139799575	0.045531016
LIMS1	-1.141557877	0.011025236
LAMC1	-1.141837269	0.001222061
TTYH3	-1.144267757	4.94212E-05
C14orf37	-1.149887062	0.000229894
SNHG14	-1.150003734	0.016893762
RBM24	-1.157266358	0.001175412
SPARC	-1.164087614	0.000842631
FGFRL1	-1.164484984	3.44974E-05
FAM101B	-1.168483087	0.001889011
LAMA2	-1.169086526	0.040949429
C16orf87	-1.169351706	0.000180681
COTL1	-1.170453619	0.001804856
COL1A2	-1.172149664	0.001443097
ANO8	-1.173091179	0.007300823
FOXP4	-1.174786281	2.49822E-05
NR2F1	-1.17673198	0.001857707

LOX	-1.178259568	0.003076992
PXDN	-1.187066842	1.72344E-05
ZFP69B	-1.187253556	0.0017013
RP1-228H13.5	-1.188399244	0.001991292
RHOBTB1	-1.188776082	0.000796754
SAT1	-1.194987128	0.000497223
ZNF219	-1.196247338	0.009254167
MMP15	-1.198106652	0.000495968
SMO	-1.198732661	0.029357578
ADSSL1	-1.19926368	0.04601717
SERINC5	-1.201607473	0.001160839
HMGA2	-1.204896222	0.020159737
FBN1	-1.206465317	0.000284386
RP1-152L7.5	-1.21041747	0.001275461
BNC2	-1.212704769	1.11255E-05
PCDHGA3	-1.214480147	0.040949429
TES	-1.219858226	0.006578619
IKZF2	-1.220414426	0.017161504
KLHL4	-1.225259106	0.035073566
PABPC4L	-1.226571518	0.001244734
JAM2	-1.227277766	0.007854584
MGAT5	-1.238116822	0.000547369
FRY	-1.241011031	0.001727492
ADAM19	-1.246014971	0.009516703
SLC2A1	-1.248094746	0.013289106
KIAA1549	-1.250277587	6.164E-06

TOX	-1.251902577	0.048712928
TET3	-1.252089565	0.000805929
LMBR1	-1.25311301	0.000654643
PSD3	-1.257862165	2.41624E-05
ABTB2	-1.25796413	0.000359178
FNBP1L	-1.25812032	0.001386618
C8orf4	-1.264007616	0.006768668
SLC22A23	-1.264259341	0.01132718
FRK	-1.26443841	0.006522989
NRIP2	-1.267076433	0.035079594
RP11-686D22.8	-1.270115707	0.004654208
EFNA4	-1.270949937	0.000213923
FANK1	-1.275628938	0.02068082
MAP3K7CL	-1.283530009	0.018451985
PCDHB3	-1.283864339	0.037786411
ENC1	-1.285030612	6.70829E-06
CLDN1	-1.290732138	0.008421189
TRPA1	-1.292388207	0.00676838
CREB5	-1.29338688	0.027572656
L3MBTL3	-1.297024981	2.06522E-05
NTN4	-1.29914414	0.005325635
GLIS1	-1.30747925	0.027358655
AP001062.7	-1.30900451	0.004523561
CCDC144A	-1.309756847	0.028644374
CASP12	-1.311001491	0.037432615
CDK5R1	-1.314336233	0.000100564
IGFBP7	-1.319145465	0.000621772
TSPAN6	-1.319288866	1.77497E-05

ABCC9	-1.322317937	0.03082676
SLC38A5	-1.32285975	0.001842652
DCHS1	-1.325317729	0.000849285
PYCR1	-1.330892276	6.12745E-06
RNF182	-1.341012926	0.002763086
AMPD3	-1.346627957	0.000265397
PCDHGB1	-1.349929566	0.015393363
MFAP2	-1.355247718	3.33823E-05
ALDH1B1	-1.356180747	0.001246048
KIAA1324	-1.357008409	0.028797227
GAD1	-1.358593458	0.01973426
TMEM206	-1.362198323	1.56787E-05
FAM227A	-1.370965522	0.005850622
THBS1	-1.371079975	0.032672691
ADAMTS7	-1.372188293	7.7583E-05
PHEX	-1.372874097	0.0149599
C1orf51	-1.374624865	4.6018E-05
FAM26E	-1.377731044	0.029115663
CD163L1	-1.378619683	0.003172064
AF131217.1	-1.382223554	0.023213668
ZSWIM4	-1.383558111	1.40224E-06
ENAH	-1.386617794	1.4965E-06
RP11-119F7.5	-1.387767464	0.024141061
ATP2B1	-1.388464409	1.55267E-05
LOXL2	-1.389164896	0.000380555

SLC2A11	-1.391924448	0.000159286
GPT2	-1.392727847	2.08771E-05
ADCY10P1	-1.396532475	0.017237376
IL16	-1.398390325	0.025258388
GDPD1	-1.401964189	0.001135726
TNFSF4	-1.402163045	0.001267358
TMEM2	-1.403966675	0.000155569
PNMAL1	-1.408520236	0.005634212
PDGFD	-1.410703296	0.00339235
ESYT3	-1.411181232	0.043750738
PLCB4	-1.411219979	0.026820317
BAMBI	-1.411853181	1.85693E-05
CACNG8	-1.412146447	0.024309705
NCKAP5	-1.413899184	2.59287E-05
H2BFM	-1.414542706	0.033701805
MARCKS	-1.416283968	1.14773E-05
DOK6	-1.419033544	3.33823E-05
SHANK1	-1.421431465	0.000400802
SORBS1	-1.422419026	0.005544643
RASGRP3	-1.428881558	0.022005216
RNF122	-1.429753738	0.000660983
SPECC1	-1.4366618	8.23588E-07
HECW1	-1.440795498	1.68787E-06
HIST1H2BG	-1.443212222	0.041866862
ADAMTS17	-1.446770911	0.027826811
TTC3P1	-1.4477692	0.010617819

BCAT1	-1.447927052	9.98812E-06
HK2	-1.450353498	0.008830174
PDE3A	-1.458311355	0.000825255
INPP5F	-1.460886265	4.12816E-05
COL12A1	-1.469260357	0.000166257
SHROOM2	-1.474328076	0.000213923
SEMA5A	-1.474500872	0.000381306
PURG	-1.475279704	0.043377258
SOX6	-1.477099608	1.08454E-05
RP11-395N3.1	-1.483508707	0.02306876
ARVCF	-1.4837121	4.57545E-06
PPP1R3C	-1.484019939	0.002731269
TFAP2A-AS1	-1.485280498	0.040125482
PWAR6	-1.485836086	0.011781972
SRPX2	-1.488479386	0.000136313
RP11-686D22.4	-1.489184837	0.019869472
MB21D2	-1.490246593	3.33823E-05
COL16A1	-1.497024556	5.07311E-06
COL24A1	-1.498617123	0.000125842
OSR1	-1.500672423	3.18028E-05
COL5A1	-1.503160529	2.34409E-05
TSC22D3	-1.507345225	4.99372E-05
HIST1H4E	-1.511785965	0.026988238
FBLN5	-1.515640932	4.69642E-06
TRO	-1.51692688	0.002281829
ACTR3C	-1.517474916	0.00566621

PCDH19	-1.518343602	0.006953228
PODXL2	-1.518730208	0.016864566
TENM3	-1.524353939	0.000308121
SH3D19	-1.528917744	1.02405E-05
KBTBD11	-1.529607402	0.002336982
ANGPT2	-1.531015922	0.037080325
WNT7B	-1.533691952	0.047454216
PGM5	-1.534794535	0.005980265
NTF3	-1.535110115	1.15377E-05
PARD6G	-1.535480587	0.000498801
PRLR	-1.539551628	0.013508143
GPR155	-1.539953129	5.46935E-06
PCDHA4	-1.540860516	0.027630666
RHOJ	-1.544526966	1.00154E-07
LMO3	-1.545548621	0.004551005
CSRNP3	-1.548603444	0.003584309
SBF2-AS1	-1.549928484	7.91267E-05
BPGM	-1.561932566	4.77212E-06
FMNL2	-1.571927714	1.27904E-05
LPPR3	-1.574643815	0.040949429
GNA14	-1.579398062	0.005157507
GALNT5	-1.584237721	0.003552645
UPP1	-1.593358504	4.19014E-05
NANOS3	-1.594091298	0.037665144
HIST1H4H	-1.599534715	0.000824108

PDPN	-1.600446433	9.9702E-08
SPSB1	-1.605025244	2.6791E-07
RP1-193H18.2	-1.609181398	0.035190579
ST6GALNAC3	-1.61226093	1.09888E-05
MYH11	-1.61349125	0.044305347
NAP1L2	-1.614649932	0.011755049
RP11-87H9.3	-1.615292441	0.01956656
SEMA3C	-1.61577532	7.31795E-09
SLCO5A1	-1.619284633	0.026284186
XIRP2	-1.621276141	0.037295553
COL4A1	-1.621504462	4.87212E-05
ANGPTL1	-1.622425104	0.043661089
SCUBE3	-1.622757257	2.12396E-05
MIR199A2	-1.625092927	0.008069264
ADAMTSL2	-1.628121765	0.011483887
SHF	-1.631137764	0.002317168
HAS2-AS1	-1.631192461	0.02975416
ACTG2	-1.634381075	0.011025236
LMCD1	-1.639124472	0.000552164
EPYC	-1.644425141	0.001335308
IRS1	-1.646936353	2.46447E-06
ECM2	-1.653077895	0.006815095
SLC4A4	-1.659243729	0.025041723
SEMA6D	-1.659755959	0.002851451
LEF1	-1.660127734	0.000747302
AC004538.3	-1.660866504	0.04729791

P4HA3	-1.663550791	9.45778E-05
LRRC61	-1.663691362	0.000653496
PIK3R3	-1.671560077	2.74875E-05
PXDNL	-1.680036286	0.044451674
PCDHB2	-1.683913875	0.006717169
LINC00519	-1.684341972	0.012761395
SOBP	-1.684519558	0.000255061
RP11-524D16__A.3	-1.685089113	2.4806E-06
AJ006998.2	-1.693964008	0.008938635
FBXL22	-1.699466273	0.012223654
PADI1	-1.700826383	0.017098404
CSF2RB	-1.706529007	1.17292E-05
KCNN2	-1.707053902	0.043377258
DPYSL4	-1.710701553	8.44023E-06
BMP3	-1.711521652	0.033495137
LNX1	-1.711534267	0.010975419
ESRP1	-1.714575875	0.043750738
MMP2	-1.717831326	2.02679E-12
SOX4	-1.720659977	1.89129E-09
KCNMB4	-1.722101657	1.48268E-05
GLI1	-1.722653907	0.002628812
NRXN3	-1.723792538	6.29253E-05
SLC29A4	-1.725642473	0.000593291
ISM1	-1.731069475	0.00010277
SYNE1	-1.732383285	7.41093E-09

CCDC170	-1.732680173	8.73345E-05
PCSK1N	-1.732995374	0.006620563
MSC	-1.733359878	0.003591872
SIPA1L2	-1.736737869	0.000111656
BMF	-1.736775691	0.000105355
C8orf34	-1.741338599	0.006955252
ST6GAL1	-1.74270831	1.85949E-06
RP11-344E13.3	-1.745093794	0.001743546
KIAA1755	-1.745286778	0.001335599
MAP2K6	-1.75008688	0.000425727
PCDHB15	-1.753361409	0.021688801
PLCXD2	-1.754012476	0.022708116
RP11-999E24.3	-1.757371818	0.000816311
NIPAL4	-1.760066575	0.008832518
SLA	-1.764507261	0.001504071
ABCA10	-1.767574885	0.004609152
RP11-395N3.2	-1.768553061	0.001077919
PALLD	-1.768929957	1.96057E-05
ALOX5AP	-1.770102664	0.013892233
SERTAD4	-1.775632289	0.000182362
LUZP2	-1.786071731	0.008339494
ANGPT1	-1.789041681	4.02869E-06
FGFR2	-1.800175494	0.030031761
AC112721.2	-1.806036677	0.024909504
PKNOX2	-1.808554295	8.45414E-05
RP11-383H13.1	-1.809784162	0.000376712

ZNF556	-1.813232902	0.00038131
SBK1	-1.814995582	0.004920988
SLC38A4	-1.818133548	1.03868E-05
ADAM12	-1.821092874	4.5738E-05
COL1A1	-1.821888216	1.37122E-09
CDKN2B	-1.828118795	1.9991E-05
SNCAIP	-1.837460177	5.07311E-06
DNAJC12	-1.838496715	0.003442091
RP11-64C1.1	-1.841637234	0.024424023
DIRAS3	-1.844292306	1.34221E-05
ARHGEF37	-1.852600692	6.0002E-07
ASXL3	-1.854011793	0.023213668
CTB-92J24.3	-1.85508656	7.06923E-06
IGF1	-1.856528567	0.011722464
SLIT3	-1.859527234	0.005852752
TP53I3	-1.860572775	1.86186E-08
GRIK2	-1.861757438	2.01288E-11
PCDHB16	-1.862425516	0.000649431
S1PR1	-1.866720885	0.001300327
GDPD4	-1.875445416	0.020856394
PCDHB14	-1.878082461	0.005817001
OLFM2	-1.879542171	0.002660167
C3orf80	-1.881880926	0.000651633
CDK6	-1.882687652	1.01967E-09
PCDHB5	-1.883891519	0.005634212

MIAT	-1.888796323	0.002790803
GFRA1	-1.89538925	0.002353612
PCDHB13	-1.896723764	0.00586709
37226	-1.896946291	0.013725437
PCDHB7	-1.897147537	0.002497579
GSG1	-1.900783444	0.001437689
RASGRF2	-1.906070575	2.35792E-05
SCN7A	-1.908018363	0.002010818
GRIA4	-1.910300625	0.000136306
TMEFF1	-1.913425936	0.011613234
SKIL	-1.915778883	2.42406E-11
RP11-521J24.1	-1.923299875	0.016411465
CXXC4	-1.928185525	0.009127827
SGCG	-1.929804786	0.015760477
FAM133A	-1.932333981	0.015742101
CDH3	-1.935500276	0.007854584
CASC15	-1.936042809	2.60866E-05
BMP6	-1.941438062	0.01501158
BGN	-1.942471854	7.7583E-05
ZBED6CL	-1.942767625	5.58625E-06
RP11-396O20.2	-1.948523049	0.013190197
GPC2	-1.957790243	2.99335E-05
TCF21	-1.957847136	0.006330892
HR	-1.959784299	0.000732708
MLLT11	-1.960333104	1.56379E-06

ADAMTS6	-1.965858384	5.34313E-08
PDE1A	-1.983061604	0.000647074
RP11-33A14.1	-1.985375604	0.00927709
ZCCHC18	-1.985654204	7.63135E-06
LPCAT2	-1.986084239	5.2384E-07
SYTL2	-1.989465333	1.06372E-05
INHBA	-1.991681265	4.48737E-06
TSPAN33	-1.998348802	1.99148E-05
VCAN	-2.000872024	2.7168E-07
ZSWIM5	-2.002110149	2.76986E-07
PALM2	-2.008745712	4.19407E-05
AC093850.2	-2.019469294	0.009528213
TNC	-2.019688856	0.009906615
FN1	-2.030019716	2.34691E-08
PCDH9	-2.038941333	1.64866E-05
ABCA4	-2.044160168	0.000543869
PID1	-2.04577043	1.46269E-08
HSD17B2	-2.046792065	0.000141109
PRSS12	-2.047138713	8.83331E-09
POU2F2	-2.047781744	6.64233E-10
KCNIP4	-2.051655215	0.006373718
DNM3OS	-2.056635784	6.64692E-12
PGM2L1	-2.058903908	3.68887E-12
ZNF853	-2.059176282	0.00116375
MIR214	-2.077086281	2.10176E-07
ELFN2	-2.07761603	0.000254485

NRG4	-2.077785815	0.006637224
ACTC1	-2.077868744	0.005623645
CILP	-2.083974109	0.001646899
CBX2	-2.08534355	1.41801E-07
NRP2	-2.08881767	9.54412E-12
PCDHB10	-2.089264836	0.000495968
FAT4	-2.090498953	4.62532E-09
KCNAB1	-2.09215729	0.006030614
LINC00607	-2.092652766	0.00214605
LINC00704	-2.098788964	0.00566621
TPRG1	-2.104058143	0.0010915
CHN1	-2.110348483	6.33932E-18
PCDH10	-2.110894338	6.96592E-18
RP11-259N19.1	-2.114475572	7.06923E-06
RP3-512B11.3	-2.114966522	0.001292137
PIEZO2	-2.116217993	0.000225883
COMP	-2.11700877	0.00595781
PCYT1B	-2.118240967	0.000149493
AL163953.3	-2.122136092	4.00854E-06
WNT11	-2.125401916	0.005349686
KMO	-2.132484737	0.002679196
ATP10A	-2.132586423	0.003408966
ADCY2	-2.133326866	0.000189456
MDFI	-2.137221049	0.005121291
IGDCC4	-2.137547393	2.92181E-06
RP1-212P9.2	-2.138702321	0.00486077

RARRES2	-2.140130773	4.57586E-07
PADI2	-2.144327327	0.004504975
F2RL2	-2.147575246	2.06025E-05
CTTNBP2	-2.158318266	1.54362E-09
NEGR1	-2.159862065	4.02974E-11
AFF3	-2.190235275	1.26447E-08
CDH2	-2.193611787	1.03483E-19
VANGL2	-2.206635944	0.000784123
NOX4	-2.220046417	1.24764E-05
MXRA5P1	-2.249008056	0.000256989
ISLR2	-2.249123842	8.64341E-05
KCNA3	-2.249408613	0.001697363
LINC00900	-2.264860417	0.000935529
HPGD	-2.270325101	7.94326E-06
METTL21C	-2.270517404	0.002361551
CAPN6	-2.28554698	2.5647E-08
C7orf57	-2.285945053	0.001953313
AC090954.5	-2.294486951	0.002037008
LRRC4	-2.296541943	0.000157283
RP11-664D7.4	-2.301500146	0.001990311
SPOCK1	-2.302065838	6.80844E-14
NTM	-2.302989034	7.62015E-05
NEDD9	-2.307341468	9.18381E-10
CTD-2319I12.1	-2.318731887	0.00109352
EMB	-2.3198147	0.00114359
PCDHB11	-2.33218444	0.000559367

RP11-356J5.12	-2.348906194	2.80777E-07
ITIH3	-2.353078942	2.54561E-14
LPAR4	-2.358580512	3.34022E-06
ENTPD1	-2.362963218	3.59017E-07
EYA2	-2.386555528	0.00116375
AC007362.1	-2.392631785	6.50233E-10
RP11-247C2.2	-2.402232247	5.79095E-05
MIR181A2HG	-2.404314535	4.05952E-05
LYPD1	-2.405967201	1.45035E-08
ZFHX2	-2.417346378	1.56379E-06
IGF2	-2.43232945	4.95358E-06
NELL2	-2.437755324	0.00033082
ATRNL1	-2.439154069	2.99645E-10
PLN	-2.441706135	1.2446E-05
ICOSLG	-2.451293011	3.20588E-05
CHRDL2	-2.456564271	0.000687626
NREP	-2.457605771	1.47961E-13
TC2N	-2.47261367	3.98997E-07
CALB2	-2.482153596	7.63135E-06
NAP1L3	-2.489862215	3.21884E-10
TYRP1	-2.492135907	0.000571964
HAS2	-2.502709898	3.98997E-07
C1QTNF7	-2.514075758	1.58884E-09
LRIG1	-2.516046911	1.37558E-06
EPHA3	-2.526027008	0.000339918
ZNF711	-2.532562333	2.24528E-07

SAMD11	-2.569954012	1.71666E-05
SPON2	-2.570959665	7.73188E-11
COL11A1	-2.582648258	1.42922E-14
ABCB1	-2.59211482	2.24791E-06
TFAP2A	-2.610557762	4.67241E-15
ZPLD1	-2.620526229	0.000177111
OMD	-2.625436366	1.19181E-05
IGFBP5	-2.631341953	3.49489E-06
LRRC17	-2.635369491	7.17366E-07
DSP	-2.643963469	4.65973E-17
F2RL1	-2.657762185	1.98857E-09
KANK4	-2.658604239	0.000100564
RP11-817J15.3	-2.681678672	0.000152405
LRP1B	-2.687776713	2.53746E-09
LRRTM3	-2.692726315	0.00014002
FAM150B	-2.696500954	0.000119098
FRMPD4	-2.699785495	5.43443E-07
FAM196B	-2.708649168	5.96792E-12
TSPAN2	-2.719526283	1.75464E-05
PLXDC1	-2.721731043	3.90681E-06
C7	-2.725249371	1.04659E-05
KCNS1	-2.758504959	1.14968E-06
MFAP5	-2.76710485	1.07393E-05
RPRM	-2.771648594	2.41624E-05
COL6A6	-2.788141942	2.52776E-06
KIF26B	-2.791833575	6.36016E-19

DGKI	-2.828958785	3.67936E-10
SEMA3D	-2.83683745	5.4236E-11
PDE1C	-2.855529834	3.08091E-05
CACNA2D3	-2.885658644	5.3376E-08
PLXDC2	-2.888677529	1.16369E-15
TSPAN11	-2.90836048	4.48737E-06
SCXA	-2.932908207	3.45263E-09
ST6GAL2	-2.943521012	1.59405E-26
B3GALT1	-2.945703352	7.18904E-13
FIBIN	-2.953214283	7.29682E-07
RP11-284N8.3	-2.962164216	8.10658E-06
GPR68	-2.962568733	3.20797E-06
ROBO2	-2.982732036	5.16738E-18
PRR5L	-2.993391908	1.7856E-13
APCDD1L	-3.000400747	5.50638E-09
SLC14A1	-3.001994959	7.06923E-06
GRIA3	-3.016047443	6.18385E-15
NRK	-3.02929229	1.85949E-06
FGF10	-3.065540603	1.48849E-06
EFHD1	-3.068058255	3.46431E-14
CCDC88C	-3.078824502	1.06751E-06
LDLRAD4	-3.082221409	1.9009E-07
MXRA5	-3.083071792	3.1317E-16
SULT1C4	-3.08329137	1.45394E-06
MEX3A	-3.098310067	1.88422E-10
AL121578.2	-3.103729147	2.81945E-07

PKD1L1	-3.111127904	1.16495E-11
CHRM2	-3.135166063	3.01436E-12
RP11-567M16.1	-3.161690977	6.51053E-10
FIGF	-3.179697294	1.27095E-08
CTGF	-3.182807582	2.60982E-27
COCH	-3.254932222	2.59236E-09
PKIA	-3.255853823	8.46252E-11
COL8A1	-3.295080925	2.46596E-11
RP11-355I22.7	-3.296662383	5.44243E-09
DLX5	-3.299609446	1.45035E-08
SGCD	-3.313037252	6.52922E-13
SIK1	-3.315847491	9.70607E-25
RFTN2	-3.3711162	4.41541E-24
CXCR4	-3.376829738	1.52624E-09
DIO2	-3.400051234	9.37958E-41
TEK	-3.403354152	2.55349E-35
OSGIN2	-3.426117412	6.52168E-35
CORIN	-3.433010421	2.29708E-13
HEPH	-3.433775639	1.88631E-18
MKX	-3.442720859	1.00524E-25
SYT16	-3.458110791	1.88977E-09
MMP7	-3.476306817	8.0129E-12
PREX2	-3.479914644	5.60209E-11
SERPINE2	-3.487519343	8.71652E-22
TMEM215	-3.495134405	6.90297E-08

CSMD3	-3.512134402	2.64262E-09
EGR2	-3.522310021	6.58807E-11
EDNRB	-3.522936121	1.89129E-09
HUNK	-3.528167826	4.16842E-21
WNT5A	-3.540337265	4.99808E-30
TNFSF18	-3.548948163	6.41625E-14
NPBWR1	-3.554439652	3.17381E-08
ALPL	-3.554476968	2.26167E-09
WNT2	-3.602851955	4.33008E-14
CCND2	-3.616496445	4.4211E-10
SYTL5	-3.636929333	3.74035E-31
ESR1	-3.664376545	7.03795E-29
TENM4	-3.67136597	7.45585E-28
EPHA7	-3.690076245	8.93497E-11
NCAM1	-3.724242248	5.16738E-18
KCNMB2	-3.736265991	1.43528E-22
NKD2	-3.743045934	4.14815E-10
HMCN1	-3.745331708	2.24101E-19
DIRC3	-3.881284809	7.73959E-19
CLSTN2	-3.933863047	2.42606E-26
PTHLH	-3.935931394	8.31702E-15
COL25A1	-3.980171784	4.59105E-18
TNFSF15	-4.036151947	4.20505E-25
CST4	-4.04063998	2.17525E-11
MEOX1	-4.131813768	1.05628E-12
RASSF2	-4.227649306	2.83959E-32

CHRNA1	-4.244059875	1.50826E-16
ELN	-4.266666039	7.82622E-15
COL10A1	-4.317286369	7.16832E-19
KCNC1	-4.338936901	7.79828E-15
CST2	-4.382294904	2.86349E-14
C11orf87	-4.435728175	3.13546E-19
KCNH1	-4.48977746	2.03115E-18
PLCH1	-4.508772564	2.57512E-44
VASH2	-4.563993386	3.13504E-40
MMP10	-4.578072389	1.19757E-17
HTRA1	-4.673379334	3.54806E-30
HTR1D	-5.583471612	2.37595E-28
CADM1	-5.817100237	1.92958E-46
LINC00643	-6.236143291	7.07665E-37
PMEPA1	-6.743359183	1.67117E-57
CST1	-6.771958173	2.80323E-64

Appendix 7. A83-01 Up-regulated GO categories

Go Term	Term	*P*
GO:0005886	plasma membrane	9.26E-10
GO:0019838	growth factor binding	3.83E-05
GO:0004896	cytokine receptor activity	0.000271
GO:0030522	intracellular receptor signaling pathway	0.000454
GO:0043034	costamere	0.000458
GO:0004016	adenylate cyclase activity	0.000476
GO:0004016	adenylate cyclase activity	0.000476
GO:0004016	adenylate cyclase activity	0.000476
GO:0001558	regulation of cell growth	0.000776
GO:0003707	steroid hormone receptor activity	0.00089
GO:0017080	sodium channel regulator activity	0.000913
GO:0017080	sodium channel regulator activity	0.000913
GO:0043401	steroid hormone mediated signaling pathway	0.001199
GO:0004879	RNA polymerase II transcription factor activity, ligand-activated sequence-specific DNA binding	0.001734
GO:0030054	cell junction	0.002582
GO:0007169	transmembrane receptor protein tyrosine kinase signaling pathway	0.003122
GO:0004924	oncostatin-M receptor activity	0.003867
GO:0002003	angiotensin maturation	0.00686
GO:0004897	ciliary neurotrophic factor receptor activity	0.007547
GO:0038165	oncostatin-M-mediated signaling pathway	0.007968
GO:0043565	sequence-specific DNA binding	0.00842

GO:0016021	integral component of membrane	0.00853
GO:0006069	ethanol oxidation	0.008895
GO:0009190	cyclic nucleotide biosynthetic process	0.008895
GO:0009190	cyclic nucleotide biosynthetic process	0.008895
GO:0005201	extracellular matrix structural constituent	0.010719
GO:0006367	transcription initiation from RNA polymerase II promoter	0.01183
GO:0070120	ciliary neurotrophic factor-mediated signaling pathway	0.012953
GO:0001657	ureteric bud development	0.013026
GO:0008076	voltage-gated potassium channel complex	0.014011
GO:0010951	negative regulation of endopeptidase activity	0.015361
GO:0014069	postsynaptic density	0.016133
GO:0005587	collagen type IV trimer	0.017675
GO:0001665	alpha-N-acetylgalactosaminide alpha-2,6-sialyltransferase activity	0.017974
GO:0008191	metalloendopeptidase inhibitor activity	0.018828
GO:0003081	regulation of systemic arterial blood pressure by renin-angiotensin	0.018951
GO:0071376	cellular response to corticotropin-releasing hormone stimulus	0.018951
GO:0006869	lipid transport	0.023361
GO:0004908	interleukin-1 receptor activity	0.024563
GO:0019221	cytokine-mediated signaling pathway	0.025252
GO:0032755	positive regulation of interleukin-6 production	0.025647
GO:0005112	Notch binding	0.026002
GO:0001574	ganglioside biosynthetic process	0.027945
GO:0005044	scavenger receptor activity	0.029617

GO:0032760	positive regulation of tumor necrosis factor production	0.030316
GO:0050700	CARD domain binding	0.031971
GO:0010765	positive regulation of sodium ion transport	0.032286
GO:0045747	positive regulation of Notch signaling pathway	0.033592
GO:0014068	positive regulation of phosphatidylinositol 3-kinase signaling	0.034247
GO:0097503	sialylation	0.036956
GO:0007189	adenylate cyclase-activating G-protein coupled receptor signaling pathway	0.038265
GO:0008074	guanylate cyclase complex, soluble	0.039487
GO:0004383	guanylate cyclase activity	0.04013
GO:0001822	kidney development	0.041942
GO:0051894	positive regulation of focal adhesion assembly	0.041952
GO:0003208	cardiac ventricle morphogenesis	0.042225
GO:0061314	Notch signaling involved in heart development	0.042225
GO:0034097	response to cytokine	0.044208
GO:0005581	collagen trimer	0.048347
GO:0001223	transcription coactivator binding	0.048976
GO:0004716	receptor signaling protein tyrosine kinase activity	0.048976

Appendix 8. A83-01 Down-regulated GO categories

GO Term	Term	P
GO:0005578	proteinaceous extracellular matrix	4.31E-22

GO:0030574	collagen catabolic process	1.73E-13
GO:0007156	homophilic cell adhesion via plasma membrane adhesion molecules	1.17E-10
GO:0005509	calcium ion binding	4E-10
GO:0005201	extracellular matrix structural constituent	4.17E-09
GO:0005886	plasma membrane	4.74E-09
GO:0005788	endoplasmic reticulum lumen	2.27E-08
GO:0016339	calcium-dependent cell-cell adhesion via plasma membrane cell adhesion molecules	2.08E-07
GO:0030199	collagen fibril organization	4.59E-06
GO:0005581	collagen trimer	9.99E-06
GO:0050919	negative chemotaxis	1.34E-05
GO:0050919	negative chemotaxis	1.34E-05
GO:0007416	synapse assembly	3.4E-05
GO:0001755	neural crest cell migration	0.000115
GO:0001837	epithelial to mesenchymal transition	0.000117
GO:0048843	negative regulation of axon extension involved in axon guidance	0.000187

GO:0045499	chemorepellent activity	0.00022
GO:0022617	extracellular matrix disassembly	0.000229
GO:0004222	metalloendopeptidase activity	0.000395
GO:0048846	axon extension involved in axon guidance	0.000513
GO:0030215	semaphorin receptor binding	0.000835
GO:0060070	canonical Wnt signaling pathway	0.001909
GO:0021612	facial nerve structural organization	0.002762
GO:0070493	thrombin receptor signaling pathway	0.002762
GO:0045165	cell fate commitment	0.004291
GO:0045211	postsynaptic membrane	0.004509
GO:0071526	semaphorin-plexin signaling pathway	0.004678
GO:0048407	platelet-derived growth factor binding	0.005008
GO:0005088	Ras guanyl-nucleotide exchange factor activity	0.005171
GO:0050918	positive chemotaxis	0.006055
GO:0003873	6-phosphofructo-2-kinase activity	0.006393
GO:0006813	potassium ion transport	0.006409

GO:0036486	ventral trunk neural crest cell migration	0.006527
GO:0097490	sympathetic neuron projection extension	0.006527
GO:0097491	sympathetic neuron projection guidance	0.006527
GO:1902285	semaphorin-plexin signaling pathway involved in neuron projection guidance	0.006527
GO:0005109	frizzled binding	0.006547
GO:0071805	potassium ion transmembrane transport	0.007899
GO:0008076	voltage-gated potassium channel complex	0.008582
GO:0071300	cellular response to retinoic acid	0.009208
GO:0015459	potassium channel regulator activity	0.010249
GO:0004331	fructose-2,6-bisphosphate 2-phosphatase activity	0.01042
GO:0015057	thrombin receptor activity	0.01042
GO:0006003	fructose 2,6-bisphosphate metabolic process	0.010635
GO:1901166	neural crest cell migration involved in autonomic nervous system development	0.010635

GO:0016021	integral component of membrane	0.011279
GO:0005161	platelet-derived growth factor receptor binding	0.012505
GO:0005161	platelet-derived growth factor receptor binding	0.012505
GO:0038191	neuropilin binding	0.012505
GO:0007215	glutamate receptor signaling pathway	0.012868
GO:0045725	positive regulation of glycogen biosynthetic process	0.012868
GO:0050930	induction of positive chemotaxis	0.012868
GO:0040007	growth	0.013837
GO:0051482	positive regulation of cytosolic calcium ion concentration involved in phospholipase C-activating G-protein coupled signaling pathway	0.013837
GO:0030182	neuron differentiation	0.014985
GO:0048341	paraxial mesoderm formation	0.015598
GO:0005158	insulin receptor binding	0.018974
GO:0005520	insulin-like growth factor binding	0.020827

GO:0005004	GPI-linked ephrin receptor activity	0.02093
GO:0008373	sialyltransferase activity	0.024131
GO:0016055	Wnt signaling pathway	0.025146
GO:0048015	phosphatidylinositol-mediated signaling	0.027072
GO:0097503	sialylation	0.028468
GO:0007160	cell-matrix adhesion	0.032473
GO:0070700	BMP receptor binding	0.034329
GO:0021675	nerve development	0.035006
GO:0061549	sympathetic ganglion development	0.035006
GO:0001568	blood vessel development	0.038366
GO:0005796	Golgi lumen	0.039666
GO:0046835	carbohydrate phosphorylation	0.041067
GO:0006000	fructose metabolic process	0.042795
GO:0035235	ionotropic glutamate receptor signaling pathway	0.045793

References

Accili, D. & Arden, K. C. (2004) FoxOs at the crossroads of cellular metabolism, differentiation, and transformation. *Cell*, 117 (4): 421-426.

Acharya, A., Baek, S. T., Huang, G., Eskiocak, B., Goetsch, S., Sung, C. Y., Banfi, S., Sauer, M. F., Olsen, G. S., Duffield, J. S., Olson, E. N. & Tallquist, M. D. (2012) The bHLH transcription factor Tcf21 is required for lineage-specific EMT of cardiac fibroblast progenitors. *Development*, 139 (12): 2139-2149.

Al-Sabbagh, M., Fusi, L., Higham, J., Lee, Y., Lei, K., Hanyaloglu, A. C., Lam, E. W., Christian, M. & Brosens, J. J. (2011) NADPH oxidase-derived reactive oxygen species mediate decidualization of human endometrial stromal cells in response to cyclic AMP signaling. *Endocrinology*, 152 (2): 730-740.

Anon (2012) An integrated encyclopedia of DNA elements in the human genome. *Nature*, 489 (7414): 57-74.

Aplin, J. D., Charlton, A. K. & Ayad, S. (1988) An immunohistochemical study of human endometrial extracellular matrix during the menstrual cycle and first trimester of pregnancy. *Cell Tissue Res*, 253 (1): 231-240.

Baek, S., Sung, M. H. & Hager, G. L. (2012) Quantitative analysis of genome-wide chromatin remodeling. *Methods Mol Biol*, 833 433-441.

Banfi, A., Bianchi, G., Notaro, R., Luzzatto, L., Cancedda, R. & Quarto, R. (2002) Replicative aging and gene expression in long-term cultures of human bone marrow stromal cells. *Tissue Eng*, 8 (6): 901-910.

Barragan, F., Irwin, J. C., Balayan, S., Erikson, D. W., Chen, J. C., Houshdaran, S., Piltonen, T. T., Spitzer, T. L., George, A., Rabban, J. T., Nezhat, C. & Giudice, L. C. (2016) Human Endometrial Fibroblasts Derived from Mesenchymal Progenitors Inherit Progesterone Resistance and Acquire an Inflammatory Phenotype in the Endometrial Niche in Endometriosis. *Biol Reprod*, 94 (5): 118.

Baxter, M. A., Wynn, R. F., Jowitt, S. N., Wraith, J. E., Fairbairn, L. J. & Bellantuono, I. (2004) Study of telomere length reveals rapid aging of human marrow stromal cells following in vitro expansion. *Stem Cells*, 22 (5): 675-682.

Bell, O., Tiwari, V. K., Thoma, N. H. & Schubeler, D. (2011) Determinants and dynamics of genome accessibility. *Nat Rev Genet*, 12 (8): 554-564.

Bellofiore, N., Ellery, S. J., Mamrot, J., Walker, D. W., Temple-Smith, P. & Dickinson, H. (2017) First evidence of a menstruating rodent: the spiny mouse (Acomys cahirinus). *Am J Obstet Gynecol*, 216 (1): 40.e41-40.e11.

Biernacka, A., Dobaczewski, M. & Frangogiannis, N. G. (2011) TGF-beta signaling in fibrosis. *Growth Factors*, 29 (5): 196-202.

Bockeria, L., Bogin, V., Bockeria, O., Le, T., Alekyan, B., Woods, E. J., Brown, A. A., Ichim, T. E. & Patel, A. N. (2013) Endometrial regenerative cells for treatment of heart failure: a new stem cell enters the clinic. *J Transl Med*, 11 56.

Bossard, P. & Zaret, K. S. (1998) GATA transcription factors as potentiators of gut endoderm differentiation. *Development*, 125 (24): 4909-4917.

Brar, A. K., Frank, G. R., Kessler, C. A., Cedars, M. I. & Handwerger, S. (1997) Progesterone-dependent decidualization of the human endometrium is mediated by cAMP. *Endocrine*, 6 (3): 301-307.

Brar, A. K., Handwerger, S., Kessler, C. A. & Aronow, B. J. (2001a) Gene induction and categorical reprogramming during in vitro human endometrial fibroblast decidualization. *Physiol Genomics*, 7 (2): 135-148.

Brar, A. K., Handwerger, S., Kessler, C. A. & Aronow, B. J. (2001b) Gene induction and categorical reprogramming during in vitro human endometrial fibroblast decidualization. *Physiol Genomics*, 7 (2): 135-148.

Brosens, J. J. & Gellersen, B. (2006) Death or survival--progesterone-dependent cell fate decisions in the human endometrial stroma. *J Mol Endocrinol*, 36 (3): 389-398.

Brosens, J. J., Pijnenborg, R. & Brosens, I. A. (2002) The myometrial junctional zone spiral arteries in normal and abnormal pregnancies: a review of the literature. *Am J Obstet Gynecol*, 187 (5): 1416-1423.

Brosens, J. J., Salker, M. S., Teklenburg, G., Nautiyal, J., Salter, S., Lucas, E. S., Steel, J. H., Christian, M., Chan, Y. W., Boomsma, C. M., Moore, J. D., Hartshorne, G. M., Sucurovic, S., Mulac-Jericevic, B., Heijnen, C. J., Quenby, S., Koerkamp, M. J., Holstege, F. C., Shmygol, A. & Macklon, N. S. (2014) Uterine selection of human embryos at implantation. *Sci Rep*, 4 3894.

Buenrostro, J. D., Giresi, P. G., Zaba, L. C., Chang, H. Y. & Greenleaf, W. J. (2013) Transposition of native chromatin for fast and sensitive epigenomic profiling of open chromatin, DNA-binding proteins and nucleosome position. *Nat Methods*, 10 (12): 1213-1218.

Cao, X., Li, Y., Luo, R. Z., Zhang, L., Zhang, S. L., Zeng, J., Han, Y. J. & Wen, Z. S. (2015) Expression of Cystatin SN significantly correlates with recurrence, metastasis, and survival duration in surgically resected non-small cell lung cancer patients. *Sci Rep*, 5 8230.

Cavalli, G. (2007) Chromosome kissing. *Curr Opin Genet Dev*, 17 (5): 443-450.

Chan, R. W., Schwab, K. E. & Gargett, C. E. (2004a) Clonogenicity of human endometrial epithelial and stromal cells. *Biol Reprod*, 70 (6): 1738-1750.
Chan, R. W., Schwab, K. E. & Gargett, C. E. (2004b) Clonogenicity of human endometrial epithelial and stromal cells. *Biol Reprod*, 70 (6): 1738-1750.

Chen, T. & Dent, S. Y. (2014) Chromatin modifiers and remodellers: regulators of cellular differentiation. *Nat Rev Genet*, 15 (2): 93-106.

Christian, M., Pohnke, Y., Kempf, R., Gellersen, B. & Brosens, J. J. (2002a) Functional association of PR and CCAAT/enhancer-binding protein beta isoforms: promoter-dependent cooperation between PR-B and liver-enriched inhibitory protein, or liver-enriched activatory protein and PR-A in human

endometrial stromal cells. *Mol Endocrinol*, 16 (1): 141-154.

Christian, M., Zhang, X., Schneider-Merck, T., Unterman, T. G., Gellersen, B., White, J. O. & Brosens, J. J. (2002b) Cyclic AMP-induced forkhead transcription factor, FKHR, cooperates with CCAAT/enhancer-binding protein beta in differentiating human endometrial stromal cells. *J Biol Chem*, 277 (23): 20825-20832.

Cirillo, L. A., McPherson, C. E., Bossard, P., Stevens, K., Cherian, S., Shim, E. Y., Clark, K. L., Burley, S. K. & Zaret, K. S. (1998) Binding of the winged-helix transcription factor HNF3 to a linker histone site on the nucleosome. *Embo j*, 17 (1): 244-254.

Cirillo, L. A. & Zaret, K. S. (1999) An early developmental transcription factor complex that is more stable on nucleosome core particles than on free DNA. *Mol Cell*, 4 (6): 961-969.

Cloke, B., Huhtinen, K., Fusi, L., Kajihara, T., Yliheikkila, M., Ho, K. K., Teklenburg, G., Lavery, S., Jones, M. C., Trew, G., Kim, J. J., Lam, E. W., Cartwright, J. E., Poutanen, M. & Brosens, J. J. (2008) The androgen and progesterone receptors regulate distinct gene networks and cellular functions in decidualizing endometrium. *Endocrinology*, 149 (9): 4462-4474.

Cornillie, F. J., Lauweryns, J. M. & Brosens, I. A. (1985) Normal human endometrium. An ultrastructural survey. *Gynecol Obstet Invest*, 20 (3): 113-129.

Darzi, S., Werkmeister, J. A., Deane, J. A. & Gargett, C. E. (2016) Identification and Characterization of Human Endometrial Mesenchymal Stem/Stromal Cells and Their Potential for Cellular Therapy. *Stem Cells Transl Med*, 5 (9): 1127-1132.

Dekker, J., Rippe, K., Dekker, M. & Kleckner, N. (2002) Capturing chromosome conformation. *Science*, 295 (5558): 1306-1311.

DiMattia, G. E., Gellersen, B., Duckworth, M. L. & Friesen, H. G. (1990) Human prolactin gene expression. The use of an alternative noncoding exon in decidua and the IM-9-P3 lymphoblast cell line. *J Biol Chem*, 265 (27): 16412-16421.

Dimitriadis, E., White, C. A., Jones, R. L. & Salamonsen, L. A. (2005) Cytokines, chemokines and growth factors in endometrium related to implantation. *Hum Reprod Update*, 11 (6): 613-630.

Emera, D., Romero, R. & Wagner, G. (2012) The evolution of menstruation: a new model for genetic assimilation: explaining molecular origins of maternal responses to fetal invasiveness. *Bioessays*, 34 (1): 26-35.

Emmerson, S. J. & Gargett, C. E. (2016) Endometrial mesenchymal stem cells as a cell based therapy for pelvic organ prolapse. *World J Stem Cells*, 8 (5): 202-215.

Evans, J., Salamonsen, L. A., Winship, A., Menkhorst, E., Nie, G., Gargett, C. E.

& Dimitriadis, E. (2016) Fertile ground: human endometrial programming and lessons in health and disease. *Nat Rev Endocrinol*, 12 (11): 654-667.

Evers, J. L. (2002) Female subfertility. *Lancet*, 360 (9327): 151-159.

Favier, B. & Dolle, P. (1997) Developmental functions of mammalian Hox genes. *Mol Hum Reprod*, 3 (2): 115-131.

Fedoroff, N. V. (2012) Presidential address. Transposable elements, epigenetics, and genome evolution. *Science*, 338 (6108): 758-767.

Fraser, J. D., Irving, B. A., Crabtree, G. R. & Weiss, A. (1991) Regulation of interleukin-2 gene enhancer activity by the T cell accessory molecule CD28. *Science*, 251 (4991): 313-316.

Frith, J. & Genever, P. (2008) Transcriptional control of mesenchymal stem cell differentiation. *Transfus Med Hemother*, 35 (3): 216-227.

Gao, F., Ma, X., Rusie, A., Hemingway, J., Ostmann, A. B., Chung, D. & Das, S. K. (2012) Epigenetic changes through DNA methylation contribute to uterine stromal cell decidualization. *Endocrinology*, 153 (12): 6078-6090.

Gargett, C. E. (2007) Uterine stem cells: what is the evidence? *Hum Reprod Update*, 13 (1): 87-101.

Gargett, C. E. & Healy, D. L. (2011) Generating receptive endometrium in

Asherman's syndrome. *J Hum Reprod Sci*, 4 (1): 49-52.

Gargett, C. E., Nguyen, H. P. & Ye, L. (2012a) Endometrial regeneration and endometrial stem/progenitor cells. *Rev Endocr Metab Disord*, 13 (4): 235-251.

Gargett, C. E., Nguyen, H. P. & Ye, L. (2012b) Endometrial regeneration and endometrial stem/progenitor cells. *Rev Endocr Metab Disord*, 13 (4): 235-251.

Gargett, C. E., Schwab, K. E. & Deane, J. A. (2016a) Endometrial stem/progenitor cells: the first 10 years. *Hum Reprod Update*, 22 (2): 137-163.

Gargett, C. E., Schwab, K. E. & Deane, J. A. (2016b) Endometrial stem/progenitor cells: the first 10 years. *Hum Reprod Update*, 22 (2): 137-163.

Gargett, C. E., Schwab, K. E., Zillwood, R. M., Nguyen, H. P. & Wu, D. (2009a) Isolation and culture of epithelial progenitors and mesenchymal stem cells from human endometrium. *Biol Reprod*, 80 (6): 1136-1145.

Gargett, C. E., Schwab, K. E., Zillwood, R. M., Nguyen, H. P. & Wu, D. (2009b) Isolation and culture of epithelial progenitors and mesenchymal stem cells from human endometrium. *Biol Reprod*, 80 (6): 1136-1145.

Gargett, C. E. & Ye, L. (2012) Endometrial reconstruction from stem cells. *Fertil Steril*, 98 (1): 11-20.

Gellersen, B., Brosens, I. A. & Brosens, J. J. (2007) Decidualization of the human

endometrium: mechanisms, functions, and clinical perspectives. *Semin Reprod Med*, 25 (6): 445-453.

Gellersen, B. & Brosens, J. (2003) Cyclic AMP and progesterone receptor cross-talk in human endometrium: a decidualizing affair. *J Endocrinol*, 178 (3): 357-372.

Gellersen, B. & Brosens, J. J. (2014) Cyclic decidualization of the human endometrium in reproductive health and failure. *Endocr Rev*, 35 (6): 851-905.

Gellersen, B., DiMattia, G. E., Friesen, H. G. & Bohnet, H. G. (1989) Prolactin (PRL) mRNA from human decidua differs from pituitary PRL mRNA but resembles the IM-9-P3 lymphoblast PRL transcript. *Mol Cell Endocrinol*, 64 (1): 127-130.

Ghirlando, R., Litt, M. D., Prioleau, M. N., Recillas-Targa, F. & Felsenfeld, G. (2004) Physical properties of a genomic condensed chromatin fragment. *J Mol Biol*, 336 (3): 597-605.

Giresi, P. G., Kim, J., McDaniell, R. M., Iyer, V. R. & Lieb, J. D. (2007) FAIRE (Formaldehyde-Assisted Isolation of Regulatory Elements) isolates active regulatory elements from human chromatin. *Genome Res*, 17 (6): 877-885.

Giudice, L. C. (2004a) Microarray expression profiling reveals candidate genes for human uterine receptivity. *Am J Pharmacogenomics*, 4 (5): 299-312.

Giudice, L. C. (2004b) Microarray expression profiling reveals candidate genes

for human uterine receptivity. *Am J Pharmacogenomics*, 4 (5): 299-312.

Godbole, G. & Modi, D. (2010) Regulation of decidualization, interleukin-11 and interleukin-15 by homeobox A 10 in endometrial stromal cells. *J Reprod Immunol*, 85 (2): 130-139.

Gray, C. A., Bartol, F. F., Tarleton, B. J., Wiley, A. A., Johnson, G. A., Bazer, F. W. & Spencer, T. E. (2001) Developmental biology of uterine glands. *Biol Reprod*, 65 (5): 1311-1323.

Grimaldi, G., Christian, M., Quenby, S. & Brosens, J. J. (2012a) Expression of epigenetic effectors in decidualizing human endometrial stromal cells. *Mol Hum Reprod*, 18 (9): 451-458.

Grimaldi, G., Christian, M., Quenby, S. & Brosens, J. J. (2012b) Expression of epigenetic effectors in decidualizing human endometrial stromal cells. *Mol Hum Reprod*, 18 (9): 451-458.

Grimaldi, G., Christian, M., Steel, J. H., Henriet, P., Poutanen, M. & Brosens, J. J. (2011) Down-regulation of the histone methyltransferase EZH2 contributes to the epigenetic programming of decidualizing human endometrial stromal cells. *Mol Endocrinol*, 25 (11): 1892-1903.

Gross, D. S. & Garrard, W. T. (1988) Nuclease hypersensitive sites in chromatin. *Annu Rev Biochem*, 57 159-197.

Gualdi, R., Bossard, P., Zheng, M., Hamada, Y., Coleman, J. R. & Zaret, K. S. (1996) Hepatic specification of the gut endoderm in vitro: cell signaling and transcriptional control. *Genes Dev*, 10 (13): 1670-1682.

Gurung, S., Werkmeister, J. A. & Gargett, C. E. (2015) Inhibition of Transforming Growth Factor-beta Receptor signaling promotes culture expansion of undifferentiated human Endometrial Mesenchymal Stem/stromal Cells. *Sci Rep*, 5 15042.

Hanna, J., Goldman-Wohl, D., Hamani, Y., Avraham, I., Greenfield, C., Natanson-Yaron, S., Prus, D., Cohen-Daniel, L., Arnon, T. I., Manaster, I., Gazit, R., Yutkin, V., Benharroch, D., Porgador, A., Keshet, E., Yagel, S. & Mandelboim, O. (2006) Decidual NK cells regulate key developmental processes at the human fetal-maternal interface. *Nat Med*, 12 (9): 1065-1074.

Heinz, S., Benner, C., Spann, N., Bertolino, E., Lin, Y. C., Laslo, P., Cheng, J. X., Murre, C., Singh, H. & Glass, C. K. (2010) Simple combinations of lineage-determining transcription factors prime cis-regulatory elements required for macrophage and B cell identities. *Mol Cell*, 38 (4): 576-589.

Herlofsen, S. R., Bryne, J. C., Hoiby, T., Wang, L., Issner, R., Zhang, X., Coyne, M. J., Boyle, P., Gu, H., Meza-Zepeda, L. A., Collas, P., Mikkelsen, T. S. & Brinchmann, J. E. (2013) Genome-wide map of quantified epigenetic changes during in vitro chondrogenic differentiation of primary human mesenchymal stem cells. *BMC Genomics*, 14 105.

Hesselberth, J. R., Chen, X., Zhang, Z., Sabo, P. J., Sandstrom, R., Reynolds, A. P., Thurman, R. E., Neph, S., Kuehn, M. S., Noble, W. S., Fields, S. & Stamatoyannopoulos, J. A. (2009) Global mapping of protein-DNA interactions in vivo by digital genomic footprinting. *Nat Methods*, 6 (4): 283-289.

Jiang, Y., Liao, Y., He, H., Xin, Q., Tu, Z., Kong, S., Cui, T., Wang, B., Quan, S., Li, B., Zhang, S. & Wang, H. (2015) FoxM1 Directs STAT3 Expression Essential for Human Endometrial Stromal Decidualization. *Sci Rep*, 5 13735.

Jin, C. & Felsenfeld, G. (2007) Nucleosome stability mediated by histone variants H3.3 and H2A.Z. *Genes Dev*, 21 (12): 1519-1529.

Jones, M. C., Fusi, L., Higham, J. H., Abdel-Hafiz, H., Horwitz, K. B., Lam, E. W. & Brosens, J. J. (2006) Regulation of the SUMO pathway sensitizes differentiating human endometrial stromal cells to progesterone. *Proc Natl Acad Sci U S A*, 103 (44): 16272-16277.

Kaya, H. S., Hantak, A. M., Stubbs, L. J., Taylor, R. N., Bagchi, I. C. & Bagchi, M. K. (2015) Roles of progesterone receptor A and B isoforms during human endometrial decidualization. *Mol Endocrinol*, 29 (6): 882-895.

Kessler, C. A., Bachurski, C. J., Schroeder, J., Stanek, J. & Handwerger, S. (2008) TEAD1 inhibits prolactin gene expression in cultured human uterine decidual cells. *Mol Cell Endocrinol*, 295 (1-2): 32-38.

Kim, M. R., Park, D. W., Lee, J. H., Choi, D. S., Hwang, K. J., Ryu, H. S. & Min,

C. K. (2005) Progesterone-dependent release of transforming growth factor-beta1 from epithelial cells enhances the endometrial decidualization by turning on the Smad signalling in stromal cells. *Mol Hum Reprod*, 11 (11): 801-808.

Koido, M., Sakurai, J., Tsukahara, S., Tani, Y. & Tomida, A. (2016) PMEPA1, a TGF-beta- and hypoxia-inducible gene that participates in hypoxic gene expression networks in solid tumors. *Biochem Biophys Res Commun*, 479 (4): 615-621.

Kouzarides, T. (2007) Chromatin modifications and their function. *Cell*, 128 (4): 693-705.

Labied, S., Kajihara, T., Madureira, P. A., Fusi, L., Jones, M. C., Higham, J. M., Varshochi, R., Francis, J. M., Zoumpoulidou, G., Essafi, A., Fernandez de Mattos, S., Lam, E. W. & Brosens, J. J. (2006) Progestins regulate the expression and activity of the forkhead transcription factor FOXO1 in differentiating human endometrium. *Mol Endocrinol*, 20 (1): 35-44.

Lalmansingh, A. S., Karmakar, S., Jin, Y. & Nagaich, A. K. (2012) Multiple modes of chromatin remodeling by Forkhead box proteins. *Biochim Biophys Acta*, 1819 (7): 707-715.

Lekstrom-Himes, J. & Xanthopoulos, K. G. (1998) Biological role of the CCAAT/enhancer-binding protein family of transcription factors. *J Biol Chem*, 273 (44): 28545-28548.

Li, L. & Xie, T. (2005a) Stem cell niche: structure and function. *Annu Rev Cell Dev Biol*, 21 605-631.

Li, L. & Xie, T. (2005b) Stem cell niche: structure and function. *Annu Rev Cell Dev Biol*, 21 605-631.

Li, W. & Ding, S. (2010) Generation of novel rat and human pluripotent stem cells by reprogramming and chemical approaches. *Methods Mol Biol*, 636 293-300.

Li, W., Jiang, K. & Ding, S. (2012) Concise review: A chemical approach to control cell fate and function. *Stem Cells*, 30 (1): 61-68.

Li, W., Li, K., Wei, W. & Ding, S. (2013) Chemical approaches to stem cell biology and therapeutics. *Cell Stem Cell*, 13 (3): 270-283.

Li, W., Zhou, H., Abujarour, R., Zhu, S., Young Joo, J., Lin, T., Hao, E., Scholer, H. R., Hayek, A. & Ding, S. (2009) Generation of human-induced pluripotent stem cells in the absence of exogenous Sox2. *Stem Cells*, 27 (12): 2992-3000.

Li, Z., Liu, C., Xie, Z., Song, P., Zhao, R. C., Guo, L., Liu, Z. & Wu, Y. (2011) Epigenetic dysregulation in mesenchymal stem cell aging and spontaneous differentiation. *PLoS One*, 6 (6): e20526.

Lieberman-Aiden, E., van Berkum, N. L., Williams, L., Imakaev, M., Ragoczy, T., Telling, A., Amit, I., Lajoie, B. R., Sabo, P. J., Dorschner, M. O., Sandstrom, R., Bernstein, B., Bender, M. A., Groudine, M., Gnirke, A., Stamatoyannopoulos, J.,

Mirny, L. A., Lander, E. S. & Dekker, J. (2009) Comprehensive mapping of long-range interactions reveals folding principles of the human genome. *Science*, 326 (5950): 289-293.

Logan, P. C., Ponnampalam, A. P., Rahnama, F., Lobie, P. E. & Mitchell, M. D. (2010) The effect of DNA methylation inhibitor 5-Aza-2'-deoxycytidine on human endometrial stromal cells. *Hum Reprod*, 25 (11): 2859-2869.

Lu, Z., Hardt, J. & Kim, J. J. (2008a) Global analysis of genes regulated by HOXA10 in decidualization reveals a role in cell proliferation. *Mol Hum Reprod*, 14 (6): 357-366.

Lu, Z., Hardt, J. & Kim, J. J. (2008b) Global analysis of genes regulated by HOXA10 in decidualization reveals a role in cell proliferation. *Mol Hum Reprod*, 14 (6): 357-366.

Lucas, E. S., Dyer, N. P., Murakami, K., Lee, Y. H., Chan, Y. W., Grimaldi, G., Muter, J., Brighton, P. J., Moore, J. D., Patel, G., Chan, J. K., Takeda, S., Lam, E. W., Quenby, S., Ott, S. & Brosens, J. J. (2016) Loss of Endometrial Plasticity in Recurrent Pregnancy Loss. *Stem Cells*, 34 (2): 346-356.

Lynch, V. J., Brayer, K., Gellersen, B. & Wagner, G. P. (2009) HoxA-11 and FOXO1A cooperate to regulate decidual prolactin expression: towards inferring the core transcriptional regulators of decidual genes. *PLoS One*, 4 (9): e6845.

Lynch, V. J., Leclerc, R. D., May, G. & Wagner, G. P. (2011) Transposon-

mediated rewiring of gene regulatory networks contributed to the evolution of pregnancy in mammals. *Nat Genet*, 43 (11): 1154-1159.

Lynch, V. J., Nnamani, M. C., Kapusta, A., Brayer, K., Plaza, S. L., Mazur, E. C., Emera, D., Sheikh, S. Z., Grutzner, F., Bauersachs, S., Graf, A., Young, S. L., Lieb, J. D., DeMayo, F. J., Feschotte, C. & Wagner, G. P. (2015) Ancient transposable elements transformed the uterine regulatory landscape and transcriptome during the evolution of mammalian pregnancy. *Cell Rep*, 10 (4): 551-561.

Mahoney, J. A., Ntolosi, B., DaSilva, R. P., Gordon, S. & McKnight, A. J. (2001) Cloning and characterization of CPVL, a novel serine carboxypeptidase, from human macrophages. *Genomics*, 72 (3): 243-251.

Mantena, S. R., Kannan, A., Cheon, Y. P., Li, Q., Johnson, P. F., Bagchi, I. C. & Bagchi, M. K. (2006) C/EBPbeta is a critical mediator of steroid hormone-regulated cell proliferation and differentiation in the uterine epithelium and stroma. *Proc Natl Acad Sci U S A*, 103 (6): 1870-1875.

Maruyama, T. & Yoshimura, Y. (2008) Molecular and cellular mechanisms for differentiation and regeneration of the uterine endometrium. *Endocr J*, 55 (5): 795-810.

Mason, C. E., Shu, F. J., Wang, C., Session, R. M., Kallen, R. G., Sidell, N., Yu, T., Liu, M. H., Cheung, E. & Kallen, C. B. (2010) Location analysis for the estrogen receptor-alpha reveals binding to diverse ERE sequences and widespread

binding within repetitive DNA elements. *Nucleic Acids Res*, 38 (7): 2355-2368.

Masuda, H., Anwar, S. S., Buhring, H. J., Rao, J. R. & Gargett, C. E. (2012a) A novel marker of human endometrial mesenchymal stem-like cells. *Cell Transplant*, 21 (10): 2201-2214.

Masuda, H., Anwar, S. S., Buhring, H. J., Rao, J. R. & Gargett, C. E. (2012b) A novel marker of human endometrial mesenchymal stem-like cells. *Cell Transplant*, 21 (10): 2201-2214.

Mazur, E. C., Vasquez, Y. M., Li, X., Kommagani, R., Jiang, L., Chen, R., Lanz, R. B., Kovanci, E., Gibbons, W. E. & DeMayo, F. J. (2015) Progesterone receptor transcriptome and cistrome in decidualized human endometrial stromal cells. *Endocrinology*, 156 (6): 2239-2253.

McGinty, R. K. & Tan, S. (2015) Nucleosome structure and function. *Chem Rev*, 115 (6): 2255-2273.

Miyamoto, S., Cooper, L., Watanabe, K., Yamamoto, S., Inoue, H., Mishima, K. & Saito, I. (2010) Role of retinoic acid-related orphan receptor-alpha in differentiation of human mesenchymal stem cells along with osteoblastic lineage. *Pathobiology*, 77 (1): 28-37.

Miyazaki, K., Maruyama, T., Masuda, H., Yamasaki, A., Uchida, S., Oda, H., Uchida, H. & Yoshimura, Y. (2012) Stem cell-like differentiation potentials of endometrial side population cells as revealed by a newly developed in vivo

endometrial stem cell assay. *PLoS One*, 7 (12): e50749.

Mulac-Jericevic, B. & Conneely, O. M. (2004) Reproductive tissue selective actions of progesterone receptors. *Reproduction*, 128 (2): 139-146.

Munro, S. K., Farquhar, C. M., Mitchell, M. D. & Ponnampalam, A. P. (2010) Epigenetic regulation of endometrium during the menstrual cycle. *Mol Hum Reprod*, 16 (5): 297-310.

Murakami, K., Lee, Y. H., Lucas, E. S., Chan, Y. W., Durairaj, R. P., Takeda, S., Moore, J. D., Tan, B. K., Quenby, S., Chan, J. K., Gargett, C. E. & Brosens, J. J. (2014) Decidualization induces a secretome switch in perivascular niche cells of the human endometrium. *Endocrinology*, 155 (11): 4542-4553.

Nair, R. R., Jain, M. & Singh, K. (2011) Reduced expression of gap junction gene connexin 43 in recurrent early pregnancy loss patients. *Placenta*, 32 (8): 619-621.

Nakerakanti, S. & Trojanowska, M. (2012) The Role of TGF-beta Receptors in Fibrosis. *Open Rheumatol J*, 6 156-162.

Naso, M. F., Liang, B., Huang, C. C., Song, X. Y., Shahied-Arruda, L., Belkowski, S. M., D'Andrea, M. R., Polkovitch, D. A., Lawrence, D. R., Griswold, D. E., Sweet, R. W. & Amegadzie, B. Y. (2007) Dermokine: an extensively differentially spliced gene expressed in epithelial cells. *J Invest Dermatol*, 127 (7): 1622-1631.

Norris, J., Fan, D., Aleman, C., Marks, J. R., Futreal, P. A., Wiseman, R. W.,

Iglehart, J. D., Deininger, P. L. & McDonnell, D. P. (1995) Identification of a new subclass of Alu DNA repeats which can function as estrogen receptor-dependent transcriptional enhancers. *J Biol Chem*, 270 (39): 22777-22782.

Osborne, C. S., Chakalova, L., Brown, K. E., Carter, D., Horton, A., Debrand, E., Goyenechea, B., Mitchell, J. A., Lopes, S., Reik, W. & Fraser, P. (2004) Active genes dynamically colocalize to shared sites of ongoing transcription. *Nat Genet*, 36 (10): 1065-1071.

Padykula, H. A. (1991) Regeneration in the primate uterus: the role of stem cells. *Ann N Y Acad Sci*, 622 47-56.

Palumbo-Zerr, K., Zerr, P., Distler, A., Fliehr, J., Mancuso, R., Huang, J., Mielenz, D., Tomcik, M., Furnrohr, B. G., Scholtysek, C., Dees, C., Beyer, C., Kronke, G., Metzger, D., Distler, O., Schett, G. & Distler, J. H. (2015) Orphan nuclear receptor NR4A1 regulates transforming growth factor-beta signaling and fibrosis. *Nat Med*, 21 (2): 150-158.

Patel, A. N., Park, E., Kuzman, M., Benetti, F., Silva, F. J. & Allickson, J. G. (2008) Multipotent menstrual blood stromal stem cells: isolation, characterization, and differentiation. *Cell Transplant*, 17 (3): 303-311.

Piper, J., Elze, M. C., Cauchy, P., Cockerill, P. N., Bonifer, C. & Ott, S. (2013) Wellington: a novel method for the accurate identification of digital genomic footprints from DNase-seq data. *Nucleic Acids Res*, 41 (21): e201.

Plante, B. J., Kannan, A., Bagchi, M. K., Yuan, L. & Young, S. L. (2009) Cyclic regulation of transcription factor C/EBP beta in human endometrium. *Reprod Biol Endocrinol*, 7 15.

Pohnke, Y., Kempf, R. & Gellersen, B. (1999) CCAAT/enhancer-binding proteins are mediators in the protein kinase A-dependent activation of the decidual prolactin promoter. *J Biol Chem*, 274 (35): 24808-24818.

Richer, J. K., Jacobsen, B. M., Manning, N. G., Abel, M. G., Wolf, D. M. & Horwitz, K. B. (2002) Differential gene regulation by the two progesterone receptor isoforms in human breast cancer cells. *J Biol Chem*, 277 (7): 5209-5218.

Schwab, K. E. & Gargett, C. E. (2007a) Co-expression of two perivascular cell markers isolates mesenchymal stem-like cells from human endometrium. *Hum Reprod*, 22 (11): 2903-2911.

Schwab, K. E. & Gargett, C. E. (2007b) Co-expression of two perivascular cell markers isolates mesenchymal stem-like cells from human endometrium. *Hum Reprod*, 22 (11): 2903-2911.

Simon, J. M., Giresi, P. G., Davis, I. J. & Lieb, J. D. (2012) Using formaldehyde-assisted isolation of regulatory elements (FAIRE) to isolate active regulatory DNA. *Nat Protoc*, 7 (2): 256-267.

Sivasubramaniyan, K., Harichandan, A., Schumann, S., Sobiesiak, M., Lengerke, C., Maurer, A., Kalbacher, H. & Buhring, H. J. (2013) Prospective isolation of

mesenchymal stem cells from human bone marrow using novel antibodies directed against Sushi domain containing 2. *Stem Cells Dev*, 22 (13): 1944-1954.

Song, L. & Crawford, G. E. (2010) DNase-seq: a high-resolution technique for mapping active gene regulatory elements across the genome from mammalian cells. *Cold Spring Harb Protoc*, 2010 (2): pdb.prot5384.

Spitzer, T. L., Rojas, A., Zelenko, Z., Aghajanova, L., Erikson, D. W., Barragan, F., Meyer, M., Tamaresis, J. S., Hamilton, A. E., Irwin, J. C. & Giudice, L. C. (2012) Perivascular human endometrial mesenchymal stem cells express pathways relevant to self-renewal, lineage specification, and functional phenotype. *Biol Reprod*, 86 (2): 58.

Sung, M. H., Baek, S. & Hager, G. L. (2016) Genome-wide footprinting: ready for prime time? *Nat Methods*, 13 (3): 222-228.

Swinstead, E. E., Miranda, T. B., Paakinaho, V., Baek, S., Goldstein, I., Hawkins, M., Karpova, T. S., Ball, D., Mazza, D., Lavis, L. D., Grimm, J. B., Morisaki, T., Grontved, L., Presman, D. M. & Hager, G. L. (2016) Steroid Receptors Reprogram FoxA1 Occupancy through Dynamic Chromatin Transitions. *Cell*, 165 (3): 593-605.

Takahashi, K. & Yamanaka, S. (2006) Induction of pluripotent stem cells from mouse embryonic and adult fibroblast cultures by defined factors. *Cell*, 126 (4): 663-676.

Takano, M., Lu, Z., Goto, T., Fusi, L., Higham, J., Francis, J., Withey, A., Hardt, J., Cloke, B., Stavropoulou, A. V., Ishihara, O., Lam, E. W., Unterman, T. G., Brosens, J. J. & Kim, J. J. (2007a) Transcriptional cross talk between the forkhead transcription factor forkhead box O1A and the progesterone receptor coordinates cell cycle regulation and differentiation in human endometrial stromal cells. *Mol Endocrinol*, 21 (10): 2334-2349.

Takano, M., Lu, Z., Goto, T., Fusi, L., Higham, J., Francis, J., Withey, A., Hardt, J., Cloke, B., Stavropoulou, A. V., Ishihara, O., Lam, E. W., Unterman, T. G., Brosens, J. J. & Kim, J. J. (2007b) Transcriptional cross talk between the forkhead transcription factor forkhead box O1A and the progesterone receptor coordinates cell cycle regulation and differentiation in human endometrial stromal cells. *Mol Endocrinol*, 21 (10): 2334-2349.

Taylor, H. S., Igarashi, P., Olive, D. L. & Arici, A. (1999) Sex steroids mediate HOXA11 expression in the human peri-implantation endometrium. *J Clin Endocrinol Metab*, 84 (3): 1129-1135.

Telgmann, R. & Gellersen, B. (1998) Marker genes of decidualization: activation of the decidual prolactin gene. *Hum Reprod Update*, 4 (5): 472-479.

Telgmann, R., Maronde, E., Tasken, K. & Gellersen, B. (1997) Activated protein kinase A is required for differentiation-dependent transcription of the decidual prolactin gene in human endometrial stromal cells. *Endocrinology*, 138 (3): 929-937.

Thurman, R. E., Rynes, E., Humbert, R., Vierstra, J., Maurano, M. T., Haugen, E., Sheffield, N. C., Stergachis, A. B., Wang, H., Vernot, B., Garg, K., John, S., Sandstrom, R., Bates, D., Boatman, L., Canfield, T. K., Diegel, M., Dunn, D., Ebersol, A. K., Frum, T., Giste, E., Johnson, A. K., Johnson, E. M., Kutyavin, T., Lajoie, B., Lee, B. K., Lee, K., London, D., Lotakis, D., Neph, S., Neri, F., Nguyen, E. D., Qu, H., Reynolds, A. P., Roach, V., Safi, A., Sanchez, M. E., Sanyal, A., Shafer, A., Simon, J. M., Song, L., Vong, S., Weaver, M., Yan, Y., Zhang, Z., Lenhard, B., Tewari, M., Dorschner, M. O., Hansen, R. S., Navas, P. A., Stamatoyannopoulos, G., Iyer, V. R., Lieb, J. D., Sunyaev, S. R., Akey, J. M., Sabo, P. J., Kaul, R., Furey, T. S., Dekker, J., Crawford, G. E. & Stamatoyannopoulos, J. A. (2012) The accessible chromatin landscape of the human genome. *Nature*, 489 (7414): 75-82.

Tsompana, M. & Buck, M. J. (2014) Chromatin accessibility: a window into the genome. *Epigenetics Chromatin*, 7 (1): 33.

Uhlen, M., Fagerberg, L., Hallstrom, B. M., Lindskog, C., Oksvold, P., Mardinoglu, A., Sivertsson, A., Kampf, C., Sjostedt, E., Asplund, A., Olsson, I., Edlund, K., Lundberg, E., Navani, S., Szigyarto, C. A., Odeberg, J., Djureinovic, D., Takanen, J. O., Hober, S., Alm, T., Edqvist, P. H., Berling, H., Tegel, H., Mulder, J., Rockberg, J., Nilsson, P., Schwenk, J. M., Hamsten, M., von Feilitzen, K., Forsberg, M., Persson, L., Johansson, F., Zwahlen, M., von Heijne, G., Nielsen, J. & Ponten, F. (2015) Proteomics. Tissue-based map of the human proteome. *Science*, 347 (6220): 1260419.

Ulrich, D., Muralitharan, R. & Gargett, C. E. (2013) Toward the use of endometrial

and menstrual blood mesenchymal stem cells for cell-based therapies. *Expert Opin Biol Ther*, 13 (10): 1387-1400.

Uysal, G., Acmaz, G., Madendag, Y., Cagli, F., Akkaya, H., Madendag, I. & Karakilic, E. U. (2017) The Efficacy of Dienogest in the Treatment of Simple Endometrial Hyperplasia without Atypia. *Gynecol Obstet Invest*,

Valouev, A., Johnson, S. M., Boyd, S. D., Smith, C. L., Fire, A. Z. & Sidow, A. (2011) Determinants of nucleosome organization in primary human cells. *Nature*, 474 (7352): 516-520.

van Es, M. A., van Vught, P. W., Blauw, H. M., Franke, L., Saris, C. G., Van den Bosch, L., de Jong, S. W., de Jong, V., Baas, F., van't Slot, R., Lemmens, R., Schelhaas, H. J., Birve, A., Sleegers, K., Van Broeckhoven, C., Schymick, J. C., Traynor, B. J., Wokke, J. H., Wijmenga, C., Robberecht, W., Andersen, P. M., Veldink, J. H., Ophoff, R. A. & van den Berg, L. H. (2008) Genetic variation in DPP6 is associated with susceptibility to amyotrophic lateral sclerosis. *Nat Genet*, 40 (1): 29-31.

Vasquez, Y. M., Mazur, E. C., Li, X., Kommagani, R., Jiang, L., Chen, R., Lanz, R. B., Kovanci, E., Gibbons, W. E. & DeMayo, F. J. (2015) FOXO1 is required for binding of PR on IRF4, novel transcriptional regulator of endometrial stromal decidualization. *Mol Endocrinol*, 29 (3): 421-433.

Verrecchia, F. & Mauviel, A. (2002) Transforming growth factor-beta signaling through the Smad pathway: role in extracellular matrix gene expression and

regulation. *J Invest Dermatol*, 118 (2): 211-215.

Voss, T. C. & Hager, G. L. (2014) Dynamic regulation of transcriptional states by chromatin and transcription factors. *Nat Rev Genet*, 15 (2): 69-81.

Wang, W., Taylor, R. N., Bagchi, I. C. & Bagchi, M. K. (2012) Regulation of human endometrial stromal proliferation and differentiation by C/EBPbeta involves cyclin E-cdk2 and STAT3. *Mol Endocrinol*, 26 (12): 2016-2030.

Wolff, E. F., Wolff, A. B., Hongling, D. & Taylor, H. S. (2007) Demonstration of multipotent stem cells in the adult human endometrium by in vitro chondrogenesis. *Reprod Sci*, 14 (6): 524-533.

Ying, Q. L., Wray, J., Nichols, J., Batlle-Morera, L., Doble, B., Woodgett, J., Cohen, P. & Smith, A. (2008) The ground state of embryonic stem cell self-renewal. *Nature*, 453 (7194): 519-523.

Yu, C., Liu, K., Tang, S. & Ding, S. (2014) Chemical approaches to cell reprogramming. *Curr Opin Genet Dev*, 28 50-56.

Zaret, K. S. & Carroll, J. S. (2011) Pioneer transcription factors: establishing competence for gene expression. *Genes Dev*, 25 (21): 2227-2241.

Zelenko, Z., Aghajanova, L., Irwin, J. C. & Giudice, L. C. (2012) Nuclear receptor, coregulator signaling, and chromatin remodeling pathways suggest involvement of the epigenome in the steroid hormone response of endometrium and

abnormalities in endometriosis. *Reprod Sci*, 19 (2): 152-162.

Zhan, Y., Du, X., Chen, H., Liu, J., Zhao, B., Huang, D., Li, G., Xu, Q., Zhang, M., Weimer, B. C., Chen, D., Cheng, Z., Zhang, L., Li, Q., Li, S., Zheng, Z., Song, S., Huang, Y., Ye, Z., Su, W., Lin, S. C., Shen, Y. & Wu, Q. (2008) Cytosporone B is an agonist for nuclear orphan receptor Nur77. *Nat Chem Biol*, 4 (9): 548-556.

Zhu, S., Wei, W. & Ding, S. (2011) Chemical strategies for stem cell biology and regenerative medicine. *Annu Rev Biomed Eng*, 13 73-90.

Publications

Pavle Vrljicak*, Emma S. Lucas*, Lauren Lansdowne*, **Raffaella Lucciola***, Joanne Muter, Nigel P. Dyer, Jan J. Brosens, Sascha Ott (2017). Analysis of chromatin accessibility in decidualizing human endometrial stromal cells. In press *The FASEB Journal*.

* These authors contributed equally to this work.

Raffaella Lucciola, Pavle Vrljicak, Sascha Ott, Jan J Brosens, Caroline Gargett (2017). Genome-wide mapping of regulatory transcriptional networks in human endometrial mesenchymal stem/stromal cells by ATAC-seq and RNA-seq. Abstract in press *Gene Medicine*.

Paul J. Brighton, Yojiro Maruyama, Katherine Fishwick, Pavle Vrljicak, Shreeya Tewary, Risa Fujihara, Joanne Muter, Emma S. Lucas, Taihei Yamada, Laura Woods, **Raffaella Lucciola**, Yie Hou Lee, Satoru Takeda, Sascha Ott, Myriam Hemberger, Siobhan Quenby, Jan J. Brosens (2017). Clearance of senescent decidual cells by uterine natural killer cells drives endometrial remodeling during the window of implantation. In press *eLife.*